Durham E-Theses

Frequency and triggering mechanisms of submarine mass movements and their geohazard implications

POPE, EDWARD,LEONARD

How to cite:

Use policy

Frequency and triggering mechanisms of submarine mass movements and their geohazard implications

By

Ed L. Pope

Thesis submitted for the degree of Doctor of Philosophy

July 2017

Department of Geography

Durham University

ABSTRACT

DEPARTMENT OF GEOGRAPHY

UNIVERSITY OF DURHAM

Doctor of Philosophy

Frequency and triggering mechanisms of submarine mass movements and their geohazard implications

By **Ed Pope**

Submarine mass movements are one of the most important processes for moving sediment across our planet. They represent the dominant process for moving sediment in many parts of the world's oceans, freshwater lakes and reservoirs. These flows also represent a significant geohazard. They can generate damaging tsunami and have the potential to damage strategically important seafloor infrastructure. It is therefore important to understand the frequency and triggering mechanisms of these events. This thesis aims to further our understanding using a variety of different data types (artificial data, deposits found in cores, seismic stratigraphy and submarine cable breaks) across different spatial scales.

First, artificial data is used to analyse the impacts of large age uncertainties on identifying a triggering mechanism for large (>1 km^3) landslides in a global database. It is shown that the size of age uncertainties, the small number of landslides within the database and the combination of multiple different settings into one dataset will likely result in landslides appearing to occur randomly. As a result it is suggested that it is prudent to focus on well-dated landslides from one setting with similar triggers rather than having a poorly calibrated understanding of landslide ages in multiple settings which may prevent a trigger being identified.

Second, a global database of subsea fibre optic cable breaks is used to investigate the triggering of submarine mass movements by earthquakes and tropical cyclones. Globally earthquakes between M_w 3 and M_w 9.2 are shown to trigger mass movements. However, in contrast to previous assertions it is shown that there is not a specific earthquake magnitude that will systematically trigger mass movements capable of breaking a cable. The susceptibility of slopes to fail as a consequence of large and small earthquakes is dependent on the average seismicity of the region and the volume of sediment supplied annually to the continental shelf.

The frequency of damaging tropical cyclone triggered submarine mass movements is lower than earthquake triggered mass movements. Analysis of the cable break database reveals three mechanisms by which mass movements are triggered. First, tropical cyclones trigger flows directly, synchronous to their passage due to dynamic loading of the seabed. Second, flows are triggered indirectly, as a consequence of peak flood discharges delivering large volumes of sediment to the continental shelf. Third, flows are triggered indirectly following a delay as a consequence of the large volumes of rapidly deposited sediment that occurs after the passage of a tropical cyclone. No clear global relationship between future climate change and flow frequency is shown, however, changes to cyclone activity in specific regions appears likely to increase damaging flow frequency.

Third, using a new piston core dataset, the timing and frequency of glacigenic debris-flows on the Bear Island Trough-Mouth Fan is investigated. The timing of glacigenic debris-flows over the last 140,000 years is shown to be controlled by the presence of an ice stream close to the shelf edge. Moreover, it is shown that the frequency and volumes of these flows is controlled by the overall dynamics of the Barents Sea Ice Sheet which vary significantly over the 140,000 year time period.

Last, a review of the relationship between ice sheets and submarine mass movements around the Nordic Seas over the Quaternary is presented using published seismic and sediment core datasets. From these data sources, the growth and decay histories of the Greenland, Barents Sea and Scandinavian Ice Sheets are tracked relative to the different types of submarine mass movements identified on their margins. The type and frequency of submarine mass movement is shown to be highly variable as a consequence of variable ice sheet extent, rates of sediment transport and meltwater export of sediment. These records have allowed the identification of first order controls on sediment delivery to continental margins at ice sheet scales. It has also enabled updated conceptual models of trough-mouth fan processes, glaciated margin development and submarine landslide occurrence to be developed.

Table of Contents

List of Tables

List of Figures

DECLARATION OF AUTHORSHIP

I, Ed Pope, declare that this thesis entitled

"Frequency and triggering mechanism of submarine mass movements and their geohazard implications"

and the work presented in it is my own and has been generated by me as the result of my own original research.

I confirm that:

1. This work was done wholly or mainly while in candidature for a research degree at this University;

2. Where any part of this thesis has previously been submitted for a degree or any other qualification at this University or any other institution, this has been clearly stated;

3. Where I have consulted the published work of others, this is always clearly attributed;

4. Where I have quoted from the work of others, the source is always given. With the exception of such quotations, this thesis is entirely my own work;

5. I have acknowledged all main sources of help;

6. Where the thesis is based on work done by myself jointly with others, I have made clear exactly what was done by others and what I have contributed myself;

7. Parts of this work have been published as:

   Pope, E. L., Talling, P. J., Urlaub, M., Clare, M. A., Hunt, J. E., Challenor, P. 2015. Are large submarine landslides temporally random or do uncertainties in available age constraints make it impossible to tell? Marine Geology, 369, 19 – 23.

   Pope, E. L., Talling, P. J., Carter, L. 2017. Which earthquakes trigger damaging submarine mass movements: insights from a global record of submarine cable breaks? Marine Geology, 384, 131 – 146.

   Pope, E. L., Talling, P. J., Carter, L., Clare, M. A., Hunt, J. E. 2017. Damaging sediment density flows triggered by tropical cyclones. Earth and Planetary Science Letters, 458, 161 – 169.

   Pope, E. L., Talling, P. J., Hunt, J. E., Dowdeswell, J. A., Allin, J. R., Cartigny, M. J. B., Long, D., Mozzato, A., Stanford, J. D., Tappin, D. R., Watts, M. 2016. Long-term record of Barents Sea

Ice Sheet advance to shelf edge from 140,000 year record. Quaternary Science Reviews, 150, 55 – 66.

Parts of this work have been submitted as:

Pope, E. L., Talling, P. J., Ó Cofaigh, C. (*Submitted)*. The relationship between ice sheets and submarine mass movements in the Nordic Seas during the Quaternary. Earth-Science Reviews.

Work during preparation of this thesis has also contributed to:

Gavey, R., Carter, L., Liu, J., Talling, P. J., Hsu, R., **Pope, E.**, Evans, G. 2017. Frequent sediment gravity flows formed by different triggering mechanisms: observations from subsea cable breaks in the Gaoping Canyon-Manila Trench, Taiwan. Marine Geology, 384, 147 - 158.

Talling, P. J., Clare, M. A., Urlaub, M., Hunt, J. E., **Pope, E.** 2014. Large submarine landslides on continental slopes: Geohazards, Methane Release and climate change. Oceanography, 27, 32 – 45.

Other papers that I have contributed to during my doctoral studies, but are not detailed within this thesis, include:

Allin, J. R., Hunt, J. E., Clare, M. A., **Pope, E. L.**, Talling, P. J., Masson, D. G. 2016. Different frequencies and triggers of canyon filling and flushing events in Nazaré Canyon, offshore Portugal. Marine Geology, 371, 89 – 105.

Allin, J. R., Mozzato, A., Talling, P. J., Hunt, J. E., Tappin, D. R., Cartigny, M. J. B., **Pope, E. L.**, Watts, M., Clare, M. A., Haflidason, H., Baeten, N. J. (*Submitted*)*.* A new view of large (>100 km^3 submarine landslides: triggered from the top down, weakly tsunamigenic, and occurring twice in a glacial cycle.

Azpiroz-Zabala, M., Cartigny, M. J. B., Talling, P. J., Parsons, D. R., Sumner, E. J., Clare, M. A., Simmons, S. M., Cooper, C., **Pope, E. L.** (2017). Newly recognised turbidity current structure can explain prolonged flushing of submarine canyons. Science Advances 3, e1700200.

Pope, E. L., Jutzeler, M., Cartigny, M. J. B., Shreeve, J., Talling, P. J., Wright, I. C., Wysoczanski, R. J. (*Submitted*)*.* Large eruption and landslides shape volcanic island submarine slopes. Earth and Planetary Science Letters.

Pope, E. L., Cartigny, M. J. B., Hage, S., Clare, M. A., Talling, P. J., *et al.* (*In Prep*). Signal Shredding: evidence from a Canadian fjord turbidity current system.

Pope, E. L., Willis, I. C., Pope, A., Miles, E. S., Arnold, N. S., Rees, W. G. S. 2016. Contrasting snow and ice albedo derived from MODIS, Landsat ETM+ and airborne data from Langjökull, Iceland. Remote Sensing of Environment, 175, 183 – 195.

Talling, P. J., **Pope, E. L.** et al. 2015. Key future directions for research on turbidity currents and their deposits. Journal of Sedimentary Research, 85, 153 – 169.

Watts, M., Talling, P. J., Hunt, J. E., Davies, S., Xuan, C., Van Peer, T., Taylor, V., Tappin, D. R., Haflidason, H., **Pope, E. L.,** Pelagia Scientific Party. (*In Prep*). Two huge tsunamigenic landslides occurred offshore Norway in the last 52,000 years.

Willis, I. C., **Pope, E. L.**, Arnold, N. S., Leysinger-Vieli, G., Long, S. 2016. Drainage networks, lakes and water fluxes beneath the Antarctic Ice Sheet. Annals of Glaciology 57, 96 – 108.

Work related to this thesis has been presented at the following conferences:

Pope, E. L., Talling, P. J., Urlaub, M., Clare, M. A., Hunt, J. E., Challenor, P. 2014 Are large submarine landslide in Polar Regions temporally random or do uncertainties in available age constraints make it impossible to tell? Geophysical Research Abstracts, Vol. 16, EGU2014-7818.

Pope, E. L., Talling, P. J., Hunt, J. E. 2015. Tming and frequency of glacigenic debris flows on the Bear Island Fan. Geophysical Research Abstracts, Vol. 17, EGU2015-3095.

Pope, E. L., Willis, I. C., Pope, A., Miles, E. S., Arnold, N. S., Rees, W. G. S. 2015. Contrasting snow and ice albedos derived from MODIS, Landsat ETM+ and airborne data from Langjökull, Iceland. Geophysical Research Abstracts, Vol. 17, EGU2015-3079.

Pope, E. L., Talling, P. J., Carter, L. 2015. Can universal principles for earthquake triggering of turbidity currents be applied: insights from a global record of submarine cable breaks? 7th International Symposium on Submarine Mass Movements and Their Consequences, Wellington, NZ, 1 – 4 November 2015.

Pope, E. L., Talling, P. J., Carter, L., Clare, M. A., Hunt, J. E. 2016. Where do submarine landslides and turbidity currents pose the biggest hazard to subsea cables? ICPC Plenary Meeting, Hamburg, Germany, 12 – 14 April 2016.

Pope, E. L., Talling, P. J., Hunt, J. E., Dowdeswell, J. A. 2016. Timing and frequency of glacigenic-debris flows on the Bear Island Fan – implications for the growth and decay of the Barents Sea Ice Sheet. PAST Gateways, Trondheim, Norway, 23 – 27 May 2016.

Pope, E. L., Talling, P. J., Carter, L., Clare, M. A., Hunt, J. E. 2016. Where do submarine sediment density flows pose the biggest hazard to subsea infrastructure? Industry-Academia Workshop on Geohazards for Marine Infrastructure. National Oceanography Centre Southampton, 27 June, 2016.

I have also provided contributions to the following work presented at conferences:

Allin, J. R., Talling, P. J., Hunt, J. E., Clare, M. A., **Pope, E. L.** 2014. Variabillity in turbidity current frequency within a central Portuguese margin canyon. British Sedimentological Research Group Annual Meeting, Nottingham, December 2014.

Allin, J. R., Talling, P. J., Hunt, J. E., Clare, M. A., **Pope, E. L.** 2015. Variability in turbidity current frequency within a central Portuguese margin canyon. Geophysical Research Abstracts, Vol. 17, EGU2015-2298.

Allin, J. R., Mozzato, A., Talling, P. J., Hunt, J. E., Tappin, D., Bondevik, S., Haflidason, H., Baeten, N., Cartigny, M. J. B., Dowdeswell, J. A., Long, D., **Pope, E. L.**, Stanford, J. D., Watts, C. 2016. Was the Traenadjupet Slide tsunamigenic? Geophysical Research Abstracts, Vol. 17, EGU2016-2144.

Azpiroz, M., Cartigny, M. J. B., Talling, P. J., Clare, M. A., Cooper, C., Parsons, D., Sumner, E. J., Simmons, S., **Pope, E. L.** 2015. Direct observations of turbidity currents in the Congo Canyon reveals a new flow structure. 31st IAS Meeting of Sedimentology, 22 – 25 June, Poland.

Azpiroz, M., Cartigny, M. J. B., Talling, P. J., Clare, M. A., Parsons, D., Sumner, E., Simmons, S., Cooper, C., **Pope, E. L.** 2016. New model of turbidity current suggested after direction observation of turbidity currents in the Congo Canyon. AAPG, Calgary, Alberta, Canada, 19 – 22 June.

Azpiroz, M., Cartigny, M. J. B., Talling, P. J., Clare, M. A., Parsons, D., Sumner, E., Simmons, S., **Pope, E. L.** 2016. New turbidity current model based on high-resolution monitoring of the longest flow ever measured. Geophysical Research Abstracts, Vol. 18, EGU2016-4532.

Carter, L., Talling, P. J., Gavey, R., Liu, J., **Pope, E. L.** 2015. Climate vs Tectonics: mass flows detected by repeated telecommunication cable breaks off Taiwan. 7th International Symposium on Submarine Mass Movements and Their Consequences, Wellington, NZ, 1 – 4 November 2015.

Cartigny, M. J. B., Azpiroz, M., Talling, P. J., Clare, M. A., Parsons, D., Sumner, E., Simmons, S., **Pope, E. L.** 2016. Novel structure of turbidity currents in the Congo Canyon based on the best

time-resolution acoustic measurements ever taken: implications for submarine cable hazards. ICPC Plenary Meeting, Hamburg, Germany, 12 – 14 April 2016.

Cartigny, M. J. B., Azpiroz, M., Symons, W. O., Sumner, E., Talling, P. J., Clare, M. A., Parsons, D., Simmons, S., **Pope, E. L.** 2016. How direct observations change our view of turbidity currents and their deposits. 32nd IAS International Meeting of Sedimentology, 23 – 25 May, Morocco.

Clare, M. A., **Pope, E. L.**, Talling, P. J., Hunt, J. E., Carter, L. 2016. What threat do turbidity currents and submarine landslides pose to submarine telecommunications cable infrastructure? Geophysical Research Abstracts, Vol. 18, EGU2016-4347.

Mozzato, A., Tappin, D., Talling, P. J., Cartigny, M. J. B., Long, J., Hunt, J. E., Watts, C., **Pope, E. L.**, Allin, J. R., Stanford, J., Dowdeswell, J. A. 2015. Insights from new high resolution data from the Traenadjupet Slide on the Norwegian Margin. Geophysical Research Abstracts, Vol. 17, EGU2015-5455.

Talling, P. J., **Pope, E. L.**, Hunt, J. E., Allin, J. R., Cartigny, M. J. B., Long, D., Mozzato, A., Stanford, J., Tappin, D., Watts, C. 2015. New insights into the timing, triggers and emplacement of prodigious submarine landslides in the Nordic Seas. Geophysical Research Abstracts, Vol. 17, EGI2015-2231.

Talling, P. J., Watts, C., Mozzato, A., Allin, J. R., Bondevik, S., Haflidason, H., Tappin, D., **Pope, E. L.**, Hunt, J. E., Cartigny, M. J. B., Dowdeswell, J. A., Long, D., Beaten, N., Stanford, J. 2016 How are large (>400 km^3) submarine landslides related to the growth and decay of Arctic ice-sheets? PAST Gateways, Trondheim, Norway, 23 – 27 May 2016.

Talling, P. J., Watts, C., Mozzato, A., Allin, J. R., **Pope, E. L.,** Hunt. J. E., Tappin, D., Cartigny, M. J. B., Dowdeswell, J. A., Haflidason, H., Long, D., Stanford, J. 2016. What is the relationship between glacial cycles and large (>500 km^3) submarine landslides and associated tsunami? William Smith Meeting 2016; Glaciated Margins: The Sedimentary and Geophsyical Archive, London, UK, 2 – 3 June 2016.

Watts, C., Hunt, J. E., Talling, P. J., Allin, J. R., **Pope, E. L.** 2015. Geochemical insights into the provenance of large scale North Atlantic turbidites. Geophysical Research Abstracts, Vol. 17, EGU2015-8711.

Willis, I. C., **Pope, E. L.**, Pope, A., Arnold, N. S., Rees, W. G. S. 2013. Biases in surface albedo derived from MODIS and ETM+ data and implications for energy balance and melt. AGU Fall Meeting Abstracts, Vol. 1, 0616.

Willis, I. C., **Pope, E. L.,**Leysinger-Vieli, G., Long. S. 2015. Drainage networks, lakes and water fluxes beneath the Antarctic Ice Sheet. IGS Symposium on the Hydrology of Glaciers and Ice Sheets. June 2015.

Signed: *E. Pope*

Statement of Copyright

Acknowledgements

First, I would like to thank my supervisors, James Hunt, and especially Pete Talling. Thank-you for providing me with the opportunity to do the PhD, and the help and support you have provided during the four years. I am also indebted to you for allowing me the freedom to do such a large variety of things and travel to as many places as I have been able to as part of the research. Your relaxed attitude and willingness to allow ever greater freedom of study has undoubtedly helped make the the PhD as enjoyable as it has been. I would also like to thank Colm Ó Cofaigh for making my transition to Durham very smooth and providing excellent advice and guidance on the work that I have undertaken while at Durham but also advice for future projects.

In addition to my supervisors many others have contributed greatly to my work in the last four years. Mike 'the Commodore' Clare has been a great sounding board for ideas and an ever reliable fieldwork and conference companion. I have benefitted from Matthieu Cartigny's clear and insightful analysis as well as his determination to move discussions to a more social setting wherever possible. I would also like to thank Lionel Carter and Julian Dowdeswell for their input into different parts of this thesis, which greatly helped the work, but also for their wider advice. I always enjoy our time together discussing everything from science to failings of New Zealand Cricket culture.

Many others, both in Southampton and in Durham have of course contributed to my time as a PhD and this thesis. Thank you all very much, it has been a pleasure and wouldn't have been the same without you!

Last, but not least, I would like to thank my family for putting up with 8 years of unintelligible ramblings and the age old question of 'What is he actually doing? and 'What is he going to do once he leaves university?'. Science communication clearly has a long way to go, but that is for another time....

Chapter 1:   Why do we need to understand the frequency and triggering mechanisms for submarine mass movements?

1.1   Rationale

Submarine mass movements, such as submarine landslides, debris flows and turbidity currents, are one of the most important flow processes for moving sediment across our planet (Hampton et al., 1996; Hühnerbach and Masson, 2004; Masson et al., 2011; Korup, 2012; Talling et al., 2012). Indeed they dominate sediment transport budgets in many areas of the World's oceans, freshwater lakes and reservoirs (Korup, 2012; Einsele, 2013). Individual flows can be far larger than terrestrial landslides, involving the transport of hundreds or even several thousand cubic kilometres of sand and mud (Hampton et al., 1996; Masson et al., 2002; Haflidason et al., 2004; Maslin et al., 2004; Hjelstuen et al., 2005; Chaytor et al., 2009; Talling et al., 2012). These flows present a major hazard. Individual flows have the potential to damage or destroy seafloor infrastructure (Carter et al., 2009; Parker et al., 2009). They also have the potential to generate damaging tsunami (Haflidason et al., 2005; Løvholt et al., 2005; 2008) and contribute significantly to tsunami generated by earthquakes (Tappin et al., 2001; 2014). Despite the clear societal importance of submarine mass movements and the numerous locations worldwide where they have been identified, we still have relatively little understanding of the frequency and triggering mechanisms of these flows. With limited appreciation of the characteristic frequency of these events or the likelihood that their frequency may change in the future it is extremely different to make appropriate hazard assessments for nearby communities (Thomas et al., 2010). Principally, these uncertainties are the result of few events being directly witnessed as a consequence of their occurrence underwater or the lack of application of appropriate technologies (Inman et al., 1976; Talling et al., 2015). The aim of this thesis is to try to address some of these issues.

Submarine mass movements take a variety of forms and occur in a large range of environments. At the largest scale, large submarine landslides can contain volumes in excess of 3,000 km^3 of sediment (see Fig. 1; Paull et al., 1996; Haflidason et al., 2004) whilst at the smallest scale, delta lip failures, have volumes of ~10,000 m^3 (Hill, 2012). The frequency of these flows also varies by six orders of magnitude (Masson et al., 2006). Deposits from these flows have been found in a range of locations from fjords to open continental slopes and abyssal plains (Krause et al., 1970; Piper and Aksu, 1987; Piper and Savoye, 1993; Dowdeswell and Elverhøi, 2002; Piper and

Normark, 2009; Urlaub et al., 2013; Clare et al., 2014; Hughes Clarke et al., 2014). The variability of these flows in terms of volume, frequency and setting provides major challenges to understanding submarine mass movements. Inferences can be made from the geological record and proposed physical processes can be modelled; however, both techniques need to be constrained using direct measurements.
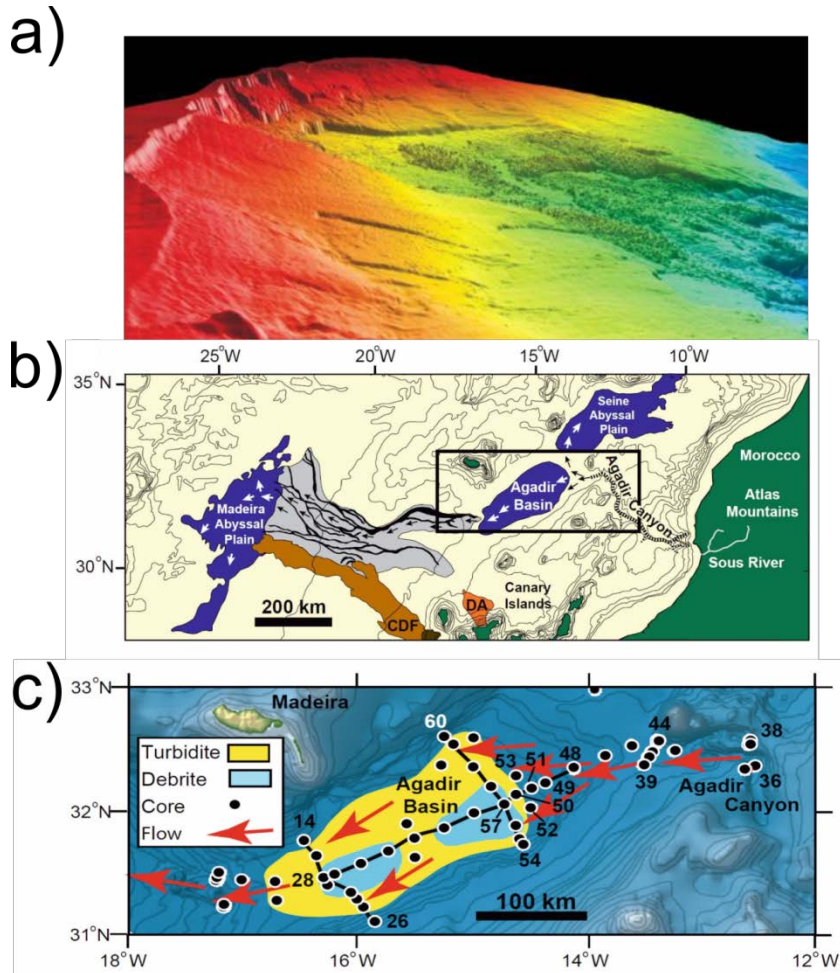
Figure 1.1 Illustration of the potentially large volumes of sediment which can be transported by submarine mass movements. a) View from the north of the Storegga Slide, the headwall of the landslide is up to 500 m high and contained in excess of 3000 km^3 (Image from Christian Berndt, GEOMAR). b) The Moroccan turbidite system offshore NW Africa. The system contains the Agadir Canyon (stippled); Agadir basin, Seine and Madeira abyssal plains; channel network between Agadir basin and Madeira abyssal plain (grey shade); Canary Debris Flow (CDF; shaded brown); Debris Avalanche (DA) from Canary Islands. Individual flows can be correlated over 1500 km through this system. One such flow which occurred approximately 60,000 years ago is shown in c). The location of sediment cores and the extent of the correlated turbidite sand (yellow) and cohesive debris flow (blue) are shown. Figure modified from Talling et al. (2007).

1.2   Project aims

The overarching aim of this thesis is to improve our understanding of the frequency and triggering mechanisms of submarine mass movements and their governing processes across the World's oceans. Submarine mass movements are highly variable in terms of their form (e.g. debris flows vs turbidity currents), frequency and triggering mechanisms in different settings around the World (Piper and Normark, 2009). This variability makes analysis of their frequency and triggering mechanisms through a single methodology challenging. For example, frequent (>10 per year) small volume flows can be directly monitored at a single location using a suite of different instruments including Acoustic Doppler Current Profilers and repeat multibeam bathymetric surveys (Hughes Clarke et al., 2012; Cooper et al., 2013; Clare et al., 2016). However, using these methods to analyse large volume infrequent events (1 per 1000 years) is extremely difficult (Talling et al., 2014). It is therefore necessary to design studies appropriate for the mass movement type being considered. This study attempts to achieve this through the use of four different datasets across different spatial scales.

At the largest scale, this study attempts to understand the frequency and triggering mechanisms of large submarine landslides globally. Due to the relatively small number of known events of this scale and their poorly constrained ages, this is achieved using statistical tests. Statistics are used here as they allow an unbiased, robust method for analysing recurrence times in relatively small datasets.

At regional scales, this study then uses a global database of subsea cable breaks to analyse the triggering mechanisms for more high frequency events. The use of a global dataset of cable breaks enables the first analyses of earthquake and tropical cyclone triggering of mass movements at global and regional scales from direct measurements.

At a local scale, this study attempts to analyse the triggering mechanism behind a single type of flow in one location, namely glacigenic debris-flows on the Bear Island Trough-Mouth Fan. Focussing on a single flow type and in one location enables the use of traditional piston coring and dating methods to understand flow frequency over 140,000 years in a single location.

Last, drawing on results from these and other studies, a review of known submarine mass movements around the Nordic Seas is carried out. This allows the role that ice sheets play in submarine mass movement occurrence to be assessed. Using these different dataset types and varying geographical scales enables this study to analyse specific triggering and frequency regimes for submarine mass movements that has not been possible in previous studies.

1.3   Thesis outline and key science questions posed

Each chapter focusses on answering a specific science question and has been submitted for publication. This is noted ahead of each chapter's abstract. At the time of submission, four lead-authored papers arising from this thesis have been accepted and published (**Chapters 2** and **3** – Marine Geology, **Chapter 4** – Earth and Planetary Science Letters, **Chapter 5** – Quaternary Science Reviews). One chapter has been submitted for publication and is currently in review (**Chapter 6** – Earth Science Reviews). The main questions addressed in this thesis are listed below:

Chapter 2: Are large submarine landslides temporally random or do uncertainties in available
**   age constraints make it impossible to tell?**

A wide variety of hypothesised mechanisms have been proposed for how large submarine landslides are triggered. It is difficult to test these proposed mechanisms due to how infrequent these events are and our inability to know precisely where these events will happen before they occur (Talling et al., 2014). Very few large submarine landslides are also dated precisely (Urlaub et al., 2013). It is therefore difficult to relate their occurrence to environmental factors that may have triggered the slope failure.

In spite of these problems, previous studies have inferred that factors such as global sea level provide a first order control on large submarine landslide frequency (Owen et al., 2007; Lee, 2009). If such a signal exists on a global extent then it should be possible to statistically link landslide frequency changes to sea level changes. Previous work has attempted to identify such a link using a global database of submarine landslides (Urlaub et al., 2013). However, this work concluded that the frequency of large submarine landslides could not be discerned from a Poisson (temporally random) distribution and thus no significant link with sea level could be identified.

Many of the large submarine landslides in the Urlaub et al. (2013) database had ages with relatively large uncertainties (error bars). It is therefore important to understand whether a possible relationship between sea level change and landslide frequency had been obscured by the dating uncertainties, and thus what the potential impact of future climate and sea level change may be on slide frequency. **Chapter 2** attempts to answer these questions using simulated datasets of landslide ages to investigate the possible impacts of age uncertainties on statistical analyses. By using artificial datasets of landslide ages we are able to test the sensitivity of statistical methodologies to specific variables, i.e. age error bar size and number of events. By doing this, we are able to suggest possible future strategies for understanding landslide triggering and the appropriateness of statistical techniques for analysing event datasets.

Chapter 3: Which earthquakes trigger damaging submarine mass movements?

Earthquakes are often cited as common triggers for submarine mass movements (Adams, 1990; Goldfinger et al., 2012; Gràcia et al., 2013). Specifically, large earthquakes (i.e. >M_w 7) are believed by some to always generate mass movements along specific continental margins (Nelson et al., 1995; Goldfinger et al., 2012). Using this assumption, records of turbidites have been used to reconstruct earthquake histories for different plate margins around the world (Goldfinger et al., 2003; Pouderoux et al., 2012; Moernaut et al., 2014; 2015). These earthquake histories have then been used to inform hazard assessments.

Turbidite palaeoseismology reconstructions of earthquake histories have proved controversial (see **Chapter 3** for a full discussion). This stems from two factors. First, a robust reconstruction requires understanding and constraint of key variables such as the sedimentary regime of the region in question and precise dating of deposits (Atwater and Griggs, 2012; Atwater et al., 2014). Second, there have been few direct observations of submarine mass movement occurrence during or after specific earthquakes with which assumptions can be tested. These two factors mean that there remains a great deal of uncertainty in terms of the relationship between turbidite deposits and large earthquakes.

Increasing our understanding of earthquake triggering of submarine mass movements requires long term monitoring data of submarine slope stability during and after specific earthquakes. To help achieve this, a global database of subsea fibre-optic cable breaks is used to analyse which earthquake do (and do not) trigger submarine mass movements which were sufficiently powerful to break cables over 25 years. Without the dating uncertainties identified in **Chapter 2**, these indirect measurements of submarine mass movement occurrence triggered by earthquakes allow us to explore and identify which environmental parameters need to be assessed and constrained in order to reconstruct earthquake triggering of submarine mass movements in the geological record. Identification of these parameters and the likelihood of an earthquake triggering a mass movement in a specific location can also help inform reconstructions of earthquake histories which use mass movement deposits.

Chapter 4: How do tropical cyclones trigger damaging sediment density flows?

While earthquakes are cited as the main triggers for submarine mass movements, there is increasing evidence that tropical cyclones play a prominent role in triggering mass flow events (Bea et al., 1983; Carter et al., 2009; Liu et al., 2012; Gavey et al., 2017). However, as with earthquakes, our understanding of the frequency and importance of these mass flows for the transport of sediment, heat, fresh or ultra-saline water and organic carbon to the deep ocean is

constrained by the limited number of observations (Kao et al., 2010). Tropical cyclone triggering of mass movements have primarily been identified based on the impacts of the mass movement on seafloor infrastructure. It is unclear from these observations alone how frequently tropical cyclones trigger submarine mass movements around the world due to the temporal and spatial limitations of these observations (Patterson, 1974; Frenkel et al., 2006; Sugi et al., 2009; Peduzzi et al., 2012). As a result there is a large amount of uncertainty surrounding the possible impacts of projected climate change on tropical cyclone triggering of submarine mass movements and thus what the corresponding geohazard implications would be.

Chapter 4 attempts to reduce the limitations of previous studies in terms of identifying submarine mass movements triggered by tropical cyclones. To achieve this, the global database of subsea fibre-optic cable breaks over 25 years is used to identify submarine mass movements triggered by tropical cyclones. These indirect measurements enable us to identify where and how frequently tropical cyclones trigger submarine mass movements but also the mechanisms by which they are triggered by this meteorological phenomenon. From these measurements it is possible to analyse the geohazard potential of these flows for different areas of the world in the near future.

Chapter 5: How do glacigenic debris-flows relate to ice sheet processes?

While **Chapter 2** focussed on methodologies for identifying triggering mechanisms for submarine mass movements and **Chapters 3** and **4** focussed on submarine mass movements triggered by specific mechanisms, **Chapter 5** focusses on the triggering of a specific type of submarine mass movement. Glacigenic debris-flows have been identified in the geological record with ages ranging from Snowball Earth glaciations (Hoffman et al., 1998; Martin, 1999; Nelson et al., 2009) up to those associated with Quaternary glaciations (Vorren and Laberg, 1997; King et al., 1998; Wilken and Mienert, 2006). Glacigenic debris-flows can contain volumes of up 20 km^3 of sediment and are therefore one of the most important mechanisms for transporting sediment on high-latitude continental margins (Ottesen et al., 2005). Deposits from these flows are also one of the major components building trough-mouth fans (Taylor et al., 2002a). Understanding the frequency of these flows is therefore crucial to understanding polar continental margin evolution (Taylor et al., 2002b).

Previous studies have asserted that the occurrence of glacigenic debris-flows are indicative of ice being present at or close to the shelf edge of major cross-shelf troughs (Laberg and Vorren, 1995; Ó Cofaigh et al., 2003). However, no study has been able to date more than a single debris-flow deposit due to the thickness of the deposits. Using methods identified in **Chapter 2**, **Chapter 5** identifies the possible triggering mechanisms for glacigenic debris-flows from core deposits on the

Bear Island Trough-Mouth Fan. Using multiple (>40) distal glacigenic debris-flow deposits in multiple cores, the frequency and timing of flows is identified in order to assess the control of ice sheet processes on the occurrence of the flows and whether it is possible to reconstruct ice sheet histories from the sedimentary deposits found on trough-mouth fans.

Chapter 6: What is the relationship between ice sheet histories and submarine mass movements?

Chapter 6 brings together many of the themes explored in previous chapters, but particularly those in **Chapter 2** and **Chapter 5**. Ice sheets and submarine mass movmements are the most significant phenomena governing sediment transport on glaciated continental margins as well as their resulting sedimentary architecture (Vorren et al., 1998; Ó Cofaigh et al., 2003). The rapid delivery of sediment by ice sheets to glaciated margins has been inferred to be a major contributing factor to glacigenic debris-flow (see **Chapter 5**) and submarine landslide occurrence (Laberg and Vorren, 1995; Haflidason et al., 2005). However, rates of ice sheet sediment delivery are not constant but are a function of climatic variability, internal dynamics and the substrate over which the ice is moving. Understanding the relationship between ice sheet processes and submarine mass movements is therefore crucial, both to reconstructing ice sheet histories from the sedimentary record but also to understanding glaciated margin evolution.

Previous studies which have linked large-scale sedimentation on glaciated margins with former ice sheet behaviour have been based on observations around the Nordic Seas (Dowdeswell et al., 1996; Bryn et al., 2003). These studies have produced models linking sedimentary architecture (i.e. submarine channels, glacigenic debris-flows, etc.) to the presence/velocity of ice delivering sediment to the shelf break and in the case of large submarine landslides the fluctuations between glacial and interglacial sedimentation (Dowdeswell et al., 1996; Dowdeswell and Siegert, 1999; Bryn et al., 2005). However, since the inception of these models, studies have been able to identify how sedimentation has changed over time on specific sections of continental margins beyond the last glacial period and our understanding of the frequency of large submarine landslides has improved (Nygård et al., 2005; Watts et al., 2016). The goal of **Chapter 6** is therefore to review the advance and retreat histories of the Greenland, Barents Sea and Scandinavian Ice Sheets around the Nordic Seas during the Quaternary and the related record of submarine mass movements. By comparing these records with those from other margins around the world, **Chapter 6** assesses whether we are able to derive a set of general models for ice sheet driven sedimentary processes and landform formation. Moreover, it also provides as assessment of large submarine landslide frequency and recurrence on glaciated continental margins and thus better constrains the relationship between submarine mass movements and ice sheet processes.

1.4   Research motivation

The following section outlines the key motivations for this thesis, with respect to submarine mass movements as geohazards and their related triggering mechanisms.

1.4.1   Submarine mass movements as geohazards

1.4.1.1   Tsunami triggered by submarine mass movements

Submarine mass movements can generate destructive tsunami that can damage coastal infrastructure and cause large numbers of fatalities (Tappin et al., 2001; Bondevik et al., 2005). The main controls on landslide-generated tsunami are the potential volumes, initial acceleration and speed of the mass movement (Geist, 2000; Tappin et al., 2001; Waythomas and Watts, 2003; Waythomas et al., 2006; Harbitz et al., 2014). If the mass movement is of sufficient volume and accelerates quickly enough, the mass movement can generate a tsunami or contribute to a tsunami triggered independently by an alternative mechanism, i.e. an earthquake (Tappin et al., 2008; 2014).

1.4.1.2   Submarine mass movements contributing to earthquake initiated tsunami

The Papua New Guinea tsunami of 17 July 1998 demonstrates the value of understanding submarine mass movements. A tsunami that was 10 – 15 m high hit the coast of Sissano Lagoon, Papua New Guinea (Fig. 1.2) following a M_w 7.1 earthquake resulting in over 2,200 fatalities (Tappin et al., 2008). Analysis of the earthquake revealed that it did not possess the correct characteristics with which to generate the observed tsunami (Synolakis et al., 2002; Tappin et al., 2008). Instead, field observations, survivor accounts and modelling studies indicated that the tsunami had been generated by a small and relatively deep water submarine slump (Geist, 2000; Tappin et al., 2001; Synolakis et al., 2002; Matsumoto et al., 2003). Recognition of the tsunami generation potential for relatively small mass movements following earthquakes demonstrates the need to understand submarine mass movement frequency in order to inform future hazard assessment for at risk coastal communities.
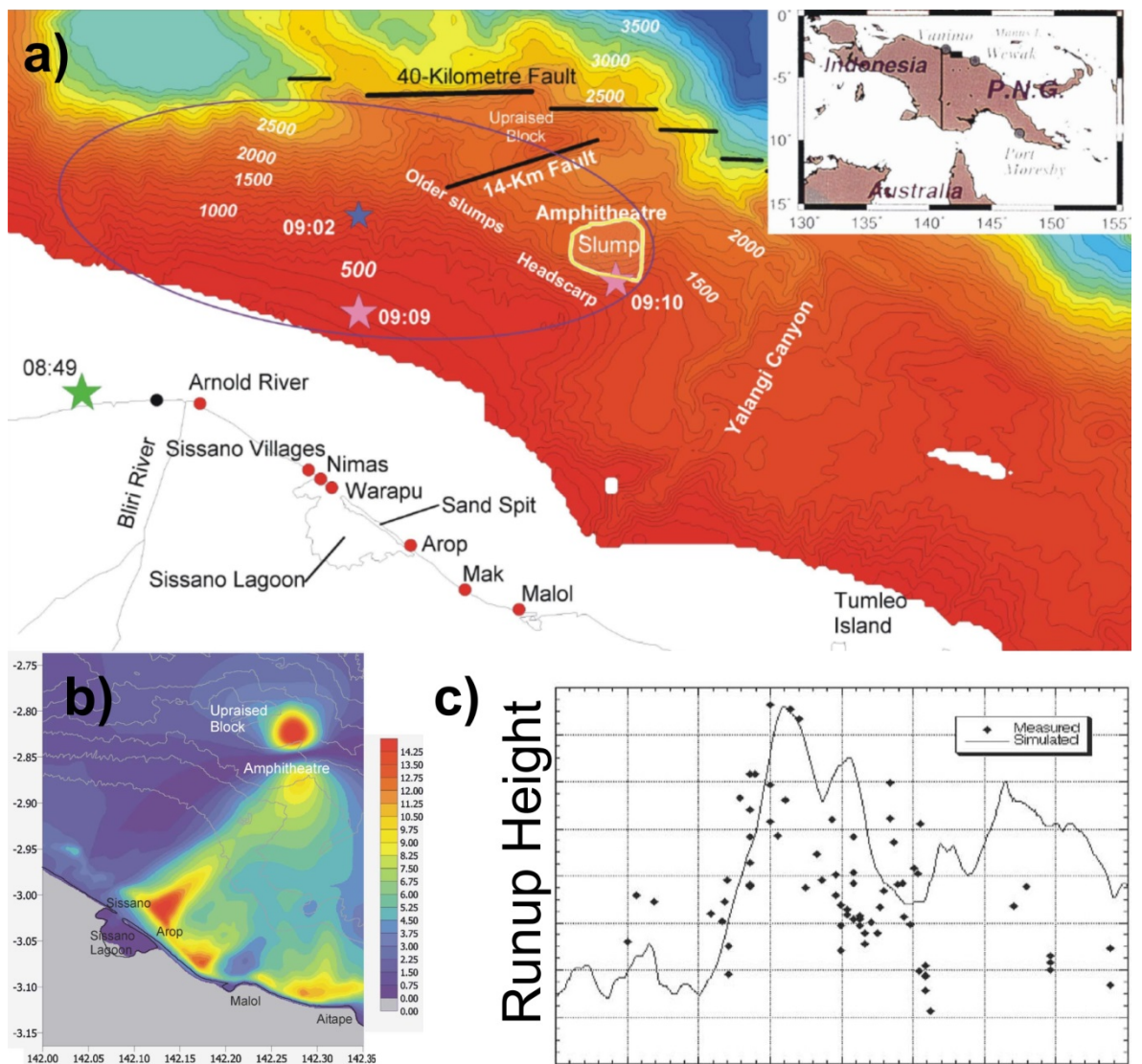
Figure 1.2 Papua New Guinea tsunami generation of 17 July 1998. a) Location map of the northern Papua New Guinea coast struck by the tsunami of July 1998 and bathymetry from the 1999 Kairei survey. Also shown is the earthquake epicentre (green star), the aftershocks (pink stars), the slump signal (blue star – with error ellipse in blue from Synolakis et al. (2002), the main villages destroyed (red dots), the slump area, and main seabed features. b) Time-lapse images of the maximum wave elevation in metres within the simulation domain of a 130 m grid. Wave focussing and shoaling by bathymetric features is evident. Depth contours are in 500 m intervals. c) Simulated wave maxima agree quite well with maximum water elevations measured onshore (modified from Tappin et al., 2001; 2008).

1.4.1.3   Submarine mass movement triggering of tsunami in isolation

Recognition of the possible cause of the Papua New Guinea tsunami resulted in a re-evaluation of global tsunami risk and in particular where observed earthquake magnitudes have not correlated with measured tsunami run-up heights. Specific interest as part of this re-evaluation was directed

towards the Storegga Slide. The largest known submarine landslide, the Storegga Slide volume is estimated to be more than 3,000 km^3, while runout from this slide affected an area of 90,000 km^2 (Solheim et al., 2005a). The Storegga Slide occurred about 8,100 years ago and generated a tsunami whose deposits have been found in Scotland (Dawson et al., 1988), Norway (Bondevik et al., 1997), the Faroe Islands (Grauert et al., 2001) and the Shetland Islands (Bondevik et al., 2003) at heights in excess of 20 m above sea level (Fig. 1.3).
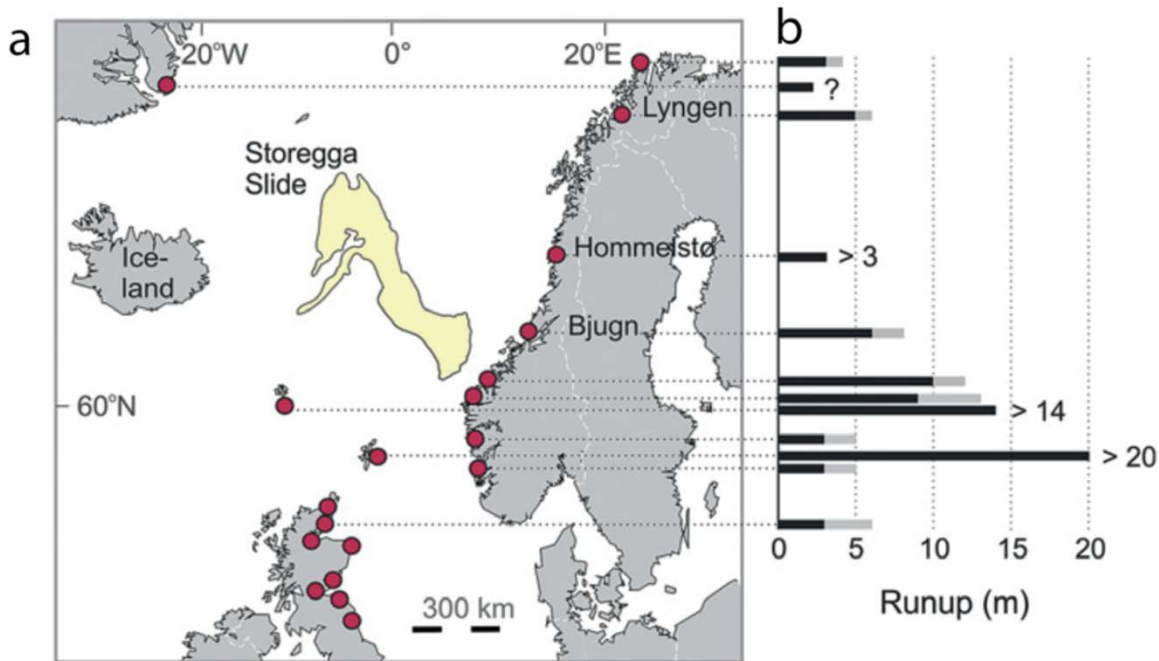
Figure 1.3 a) Location of the Storegga Slide that comprises >3,000 km^3 of material and covers an area larger than Scotland. Red dots indicate locations of tsunami deposits associated with the Storegga Slide. Tsunami runup heights above sea level are indicated in b). Black bars indicate minimum runup heights and grey bars maximum runup heights (modified from Bondevik et al., 2005 and Talling et al., 2014).

For many of the countries affected by the Storegga Slide tsunami, a tsunami generated by a similar magnitude submarine landslide is the largest magnitude hazard posed to their coastlines. Unlike societies exposed regularly to tsunami hazards, such as Japan, awareness and mitigation strategies are comparatively lacking (Bernard and Titov, 2006; Bernard et al., 2006; Bernard, 2008). It is therefore crucial to understand both the frequency and triggering mechanisms of these large events along continental margins to inform strategies for increasing resilience inspite of the fact that they may have low recurrence rates due to their potentially large impacts.

1.4.1.4   Hazard for seafloor infrastructure

The potential for submarine mass movements to damage seafloor infrastructure has been shown in a variety of locations worldwide (Milne, 1897b, a; Heezen and Ewing, 1952; Heezen, 1956;

Heezen et al., 1964; Heezen and Johnson, 1969; Heezen and Hollister, 1971; Bea et al., 1983; Dengler et al., 1984; Hsu et al., 2008; Carter et al., 2009; Cattaneo et al., 2012). They pose a particular hazard to strategically important subsea cable networks (Fig. 1.4). The global subsea fibre optic cable network currently carries in excess of 95% of global data and internet traffic (Rauscher, 2010). In 2004 this translated to more than 9 million messages and trade of upward of $7.4 trillion per day on this network (Rauscher, 2010). In the last decade, reliance on this network has greatly increased as the fibre optic telecommunications network has been integrated into the global economy (Manyika et al., 2013). Disruption to this network resulting from submarine mass movement induced cable breaks can therefore have significant economic consequences and impact on peoples day to day lives. For example, the Pingting Earthquake (26/12/2006) resulted in at least 22 submarine cable breaks south of Taiwan by sediment density flows (Gavey et al., 2017). As a consequence of this, 98% of Taiwan's communication with Malaysia, Singapore, Thailand and Hong Kong was disrupted; call capacity to the USA was down to 40% and a delay in internet traffic was still apparent >2 months after the earthquake (Rauscher, 2010). Submarine mass movements also pose a hazard to expensive oil and gas seafloor infrastructure, damage to which can have serious environmental consequences and be of great cost to the operator (Thomas et al., 2010).

Mitigation of the hazard posed by submarine mass movements to infrastructure requires an understanding of the potential recurrence times for mass movements in a given location and the possible flow dynamics. Areas where mass movements are potentially common can be avoided during planning stages for infrastructure construction (Chevron, 2014) or re-routing can occur at a later stage (SAGE, 2010). Alternatively, mass movement resistant designs can be implemented (Sonoyama et al., 2013; Nash et al., 2014). These solutions are, however, extremely costly. Increased understanding of the frequency and triggering mechanisms of submarine mass movements and their potential impacts on seafloor infrastructure is needed in order to identify the most cost effective mitigation strategies for future infrastructure projects.
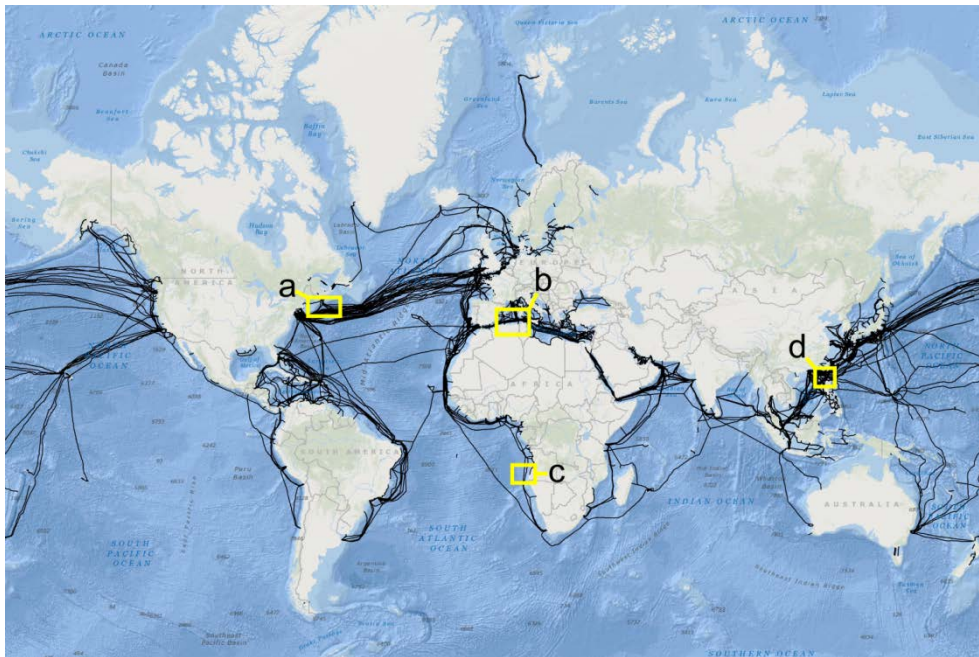
Figure 1.4 Subsea fibre-optic cable network with areas where significant numbers of cable breaks have been recorded. a) Locations of submarine cable breaks caused by the 1929 Grand Banks submarine landslide (Piper et al., 1999). b) Submarine cable breaks caused by turbidity currents triggered by the 2003 Boumerdès Earthquake (Cattaneo et al., 2012). c) Submarine cable breaks regularly occur in the Congo Canyon as a consequence of frequent turbidity current activity (Heezen et al., 1964). d) Cable breaks regularly occur offshore Taiwan as a consequence of earthquake and typhoon triggered turbidity currents (Gavey et al., 2017).

1.4.2   Preconditioning and triggering mechanisms for initiating submarine mass movements

This section serves to summarise the processes that precondition and trigger submarine mass movements. Numerous hypotheses have been proposed for how submarine mass movements can be triggered. However, in most cases evidence of a mass movement event comes primarily from its deposits. It is therefore often difficult to link a specific flow deposit to a specific triggering mechanism. It must also be recognised that many triggering mechanisms, such as rapid sedimentation, can also act as preconditioning factors; the actual failure resulting for a subsequent trigger. Examples where flows have been monitored and thus we have been able to identify a triggering mechanism are outlined in Table 1.1. Possible triggering mechanisms for submarine mass movements are summarised below.

Triggering process	Location	Year	Data Type	Reference
Earthquake	Grand Banks, USA	1929	Cable breaks	Heezen and Ewing (1952), Piper et al. (1988, 1999)
	Gaoping Canyon, Taiwan	2006	Cable breaks	Hsu et al. (2008)
	Orleansville Algeria	1954	Cable breaks	Heezen and Ewing (1952), El Robrini et al. (1985)
	Japan	2003	Moored current meters/ADCP	Mitsuzawa et al. (2004) Mikada et al. (2006)
	Japan - Sagami Bay	1997	Moored current meters/ADCP	Ikehara et al. (2012)
	Japan - Sagami Bay	1998	Moored current meters/ADCP	Ikehara et al. (2012)
	Japan - Sagami Bay	2006	Moored current meters/ADCP	Ikehara et al. (2012)
	Cariaco Basin	1997	Moored current meters/ADCP	Thunnell et al. (1999)
	Kandavu Passage, Fiji	1953	Cable breaks	Hotz and Wellman (1962)
	Western New Britain Trench, Papua New Guinea	1966	Cable breaks	Krause et al. (1970) Heezen and Johnson (1969)
Rapid deposition of sediment	Gaoping Canyon, Taiwan	2009	Cable breaks	Carter et al. (2012)
	Fraser River Delta, Canada		Current meters	Hill (2012)
	Squamish River Delta, Canada	2012	Repeat bathymetric Surveys	Clare et al. (2016)
Hyperpycnal River Water	Gaoping Canyon, Taiwan	2008	Moored current meters/ADCP	Liu et al. (2012)
	Var Canyon, France	2005 - 2008	Moored current meters/ADCP	Khripounoff et al. (2009)
	Gaoping Canyon, Taiwan	2009	Cable breaks	Carter et al. (2012)
	Squamish River Delta, Canada	2012	Repeat bathymetric Surveys	Clare et al. (2016)
Waves	Monterey Canyon, USA	sub-annual events	Beacons	Paull et al. (2003, 2005, 2010)
	Monterey Canyon, USA	sub-annual events	ADCPs	Xu et al. (2004; 2011)
	Scripps and La Jolla Canyon, USA		ADCPs	Shepard et al. (1977), Shepard and Dill (1966) Marshall (1978)
	Hueneme and Mugu Canyons		ADCPs	Xu et al. (2010)
Tropical Cyclones	Oahu, Hawaii	1982	Movement of moorings	Dengler et al. (1984)
	Gulf of Mexico	1969	Platform damage	Bea et al. (1983) Patterson et al. (1974) Prior and Coleman (1982)
	Gulf of Mexico	2005	Platform damage	Alvarado (2006) Frenkel et al. (2006)
Loading or oversteepening of slopes	Nice	1979	Observations	Dan et al. (2007) Piper and Savoye (1993)
	Squamish River Delta, Canada	2012	Repeat bathymetric Surveys	Clare et al. (2016)

Table 1.1 Monitoring data from oceanic sediment density flows adapted from Talling et al. (2013).

1.4.2.1   Earthquakes

Earthquakes have commonly been attributed as the major trigger for submarine mass movements. In recent history they have been identified as the trigger for the 1929 Grand Banks submarine landslide (Heezen and Ewing, 1952), the 1946 Aleutian Island Landslide (Fryer et al., 2004), and the 1998 Papua New Guinea slump (Tappin et al., 2001). Earthquakes mainly trigger submarine mass movements in two ways. First, acceleration-induced sliding occurs when strong seismic motions subject sediments to horizontal and vertical accelerations that exceed their yield strength (Owen et al., 2007; 2008). Second, liquefaction-induced sliding can occur as a consequence of reduced sediment strength due to accumulated deformation from cyclic shearing. Cyclic loading can also result in the generation of excess pore pressures due to the upward migration of pore fluid. The migration of this fluid can generate instability if the migrating pore fluid encounters a sediment layer or region with a lower dissipation rate thereby allowing pore pressures to build up and eventually cause a failure to occur (Biscontin et al., 2004; Özener et al., 2009). The timing of the subsequent slope failure may occur several months after the seismic event that has triggered it as the time required to reach critical conditions for different sediment profiles ranges from minutes to months according to consolidation profiles, sediment types and dissipation rates (Biscontin and Pestana, 2006; Leynaud et al., 2009)

1.4.2.2   Storm surge, wave and tsunami wave loading

Submarine mass movements can be triggered by storm surges, waves and tsunami through dynamic loading of the seafloor which eventually leads to sediment failure (Marshall, 1978; Mosher et al., 2004). The advance of a storm surge associated with an oncoming low pressure system is able to produce large hydrodynamic pressures on the seafloor. The change in hydrodynamic pressure is able to induce pore pressure changes in the subsurface (Zhang et al., 2015). These changes can lead to slope instabilities and possible slope failures. The passing of a tsunami wave front can act on the seafloor in the same way (Wright and Rathje, 2003; Arai et al., 2013).

In sufficiently shallow water surface gravity waves are able to trigger submarine mass movements through two processes (Canals et al., 2009; Palanques et al., 2009; 2011). First, they alter pore pressures through dynamic loading of the seabed. As a wave crest passes, pore pressures in the seabed increase. As the wave trough passes seepage pressures form (Seed and Rahman, 1978). In low rigidity sediments with low permeability pore water pressures are able to progressively build or flow through the sediment. Overtime this can lead to liquefaction of the sediment and subsequent failure. Second, mass movements can be triggered as a consequence of the shear stress associated with the passing of storm waves over the seabed. This is a consequence of the

orbital motion of the water particles in the wave (Jeng and Cha, 2003; Jeng and Seymour, 2007). If the strength of the sediments at the seabed are insufficient to resist the increase in shear stress then sediment failure can occur.

1.4.2.3   Hyperpycnal flows

Hyperpycnal flows occur as a consequence of the concentration of sediment in river water or different water salinities and have been observed offshore Taiwan (Carter et al., 2012), France (Mulder and Syvitski, 1995) and the Bosphorus Strait (Flood et al., 2009). Focussing on flows resulting from sediment concentration, if the sediment-laden river water is dense enough when it reaches the river mouth it will plunge. The critical concentration needed to overcome the density difference between fresh and sea water depends on the salinity and temperature of the seawater at the river mouth and the stratification of the flow itself (Parsons et al., 2001; Felix et al., 2006). Once the sediment-laden river water plunges it may then continue downslope under gravity and entrain water and additional sediments, and consequently lead to the formation of a turbidity current (Clare et al., 2016).

1.4.2.4   Rapid sedimentation

Rapid sedimentation, either on the continental shelf or slope can result in submarine mass movements in two ways. First, rapid sedimentation can lead to oversteepening of a slope resulting in the sediment eventually failing (Dugan and Flemings, 2000; Clare et al., 2016). Second, rapid sediment deposition can lead to progressively increasing pore pressures. The rapid nature of the deposition prevents effective dewatering of the deposited sediment (Flemings et al., 2008; Stigall and Dugan, 2010). This can lead to the build-up of excess pore pressure (overpressure) and eventually lead to failure (Dugan and Sheahan, 2012).

1.4.2.5   Gas hydrate dissociation

The occurrence of submarine mass movements has been suggested to be influenced by the production of free gas, through the break-down of organic matter and methane hydrate dissociation (Kennett et al., 2003). Methane hydrates form where there is sufficient supply of gas, water at moderate pressure and relatively low temperatures (Berndt, 2005; Mienert et al., 2005). Changes to either the thermal or pressure regimes in the location where the methane hydrates are stored can result in methane hydrate dissociation (Hornbach et al., 2007). Hydrate dissociation can provide overpressure through the expulsion of gas leading to the generation of a potential failure plane as a consequence of the reduction of effective yield strength. This can either cause failure to occur or increase the susceptibility of sediments to fail as a consequence of a further trigger (Prior et al., 1982; Kayen and Lee, 1991; Mienert et al., 1998; Sultan et al., 2004).

Submarine mass movements may, however, also accelerate dissociation as a consequence of exposing new horizons in the headwall and slide scar.

1.4.2.6   Slope parallel weak layers in bedded sequence

Weak layers may develop in sediment sequences as a consequence of overpressures resulting from underconsolidation (O'Leary, 1991; Bryn et al., 2003), differential shear stresses due to compositional variations, sapropels and contourites (Sultan et al., 2004; Baeten et al., 2014), and liquefaction in sand-rich horizons (Haflidason et al., 2003; Sultan et al., 2004). Once formed these layers can act as a glide plane on which overlying sediments can fail or the layer that ultimately fails.

1.4.2.7   Volcanic activity

Volcanic activity has been linked to submarine mass movement occurrence directly and indirectly. Elevated levels of seismicity occur before and during volcanic eruptions. Increased levels of seismicity can generate slope instabilities as outlined in Section 1.4.1 (Montalto et al., 1996). Volcanic activity can also directly lead to submarine mass movements through lateral flank collapses, where explosive eruptions can weaken edifice flanks and precondition failure (Martí et al., 1997; Hürlimann et al., 1999; Hunt et al., 2013). If Pyroclastic flows, lahars, and jökulhlaups associated with volcanic eruptions reach the ocean then these flows are also able to evolve into subaqueous mass movements (Mathisen and Vondra, 1983; Maizels, 1991, 1993; Mulder et al., 2003; Watt et al., 2014; Cassidy et al., 2015).

1.4.2.8   Sea level change

Sea level changes are thought to be related to submarine mass movement occurrence in a number of ways. First, sea level change affects the overburden pressure on continental slopes (Urlaub et al., 2012). Changing the overburden pressure alone is able to affect slope stability but it could also affect the stability of gas hydrates thereby generating excess pore pressures enabling failure to occur (Maslin et al., 1998; 2004; Sultan et al., 2004; Vanoudheusden et al., 2004; Leynaud et al., 2007; Owen et al., 2007). Second, changes in sea level can impact sediment delivery regimes. During sea level lowstands large portions of the continental shelf are exposed, enabling rivers to reach the shelf edge and upper slope resulting in more sand being deposited in these locations (Berné et al., 2004). The shift in the location of depocentres also alters the slope's stress state (Urlaub et al., 2012). These sedimentary regime changes can result in an increase in the frequency of submarine mass movements (Allin et al., 2016).

1.5   Key questions addressed by this thesis

This thesis addresses five major questions. Each of these questions aims to address a specific uncertainty that currently exists in terms of our present understanding of the frequency and triggering mechanisms for different submarine mass movements. These questions are listed below.

Are large submarine landslides temporally random or do uncertainties in available age constraints make it impossible to tell?

Which earthquakes trigger damaging submarine mass movements?

How do tropical cyclones trigger damaging sediment density flows?

How do glacigenic debris-flows relate to ice sheet processes?

What is the relationship between ice sheet histories and submarine mass movement occurrence?

Chapter 2:   Are large submarine landslides temporally random or do uncertainties in available age constraints make it impossible to tell?

Summary

Chapter 2 focusses on the use of statistical methodologies for evaluating the frequency and triggering mechanisms of submarine mass movements at the global scale, specifically large submarine landslides. Previous studies of global submarine landslides have found that there is no statistical correlation between sea level change and the occurrence of large submarine landslides. However, these studies left the outstanding question; what are the impacts of the large age uncertainties associated with each dated submarine landslide? This chapter addresses this question using statistical methodologies and questions the use of global records of any event type for the use of identifying globally consistent triggers. We apply specified age uncertainties to known landslide patterns to identify the impact of age uncertainties which are associated with global datasets.

Reference:

Pope, E. L., Talling, P. J., Urlaub, M., Hunt, J. E., Clare, M. A., Challenor, P. 2015. Are large submarine landslides temporally random or do uncertainties in available age constraints make it impossible to tell? *Marine Geology*, 369, 19 – 23.

Are large submarine landslides temporally random or do uncertainties in available age constraints make it impossible to tell?

Ed L. Pope[1], Peter J. Talling[1], Morelia Urlaub[2], James E. Hunt[1], Michael A. Clare[1], Peter Challenor[3].

[1]National Oceanography Centre, European Way, Southampton, Hampshire, SO14 3ZH, UK

[2]GEOMAR Helmholtz Centre for Ocean Research Kiel, Wischhofstr. 1 – 3, 24148 Kiel, Germany

[3]College of Engineering, Mathematics and Physical Sciences, Harrison Building, North Park Road, EX4 4QF, UK

Abstract: Large (>~1 km^3) submarine landslides can potentially generate very destructive tsunamis and damage expensive sea floor infrastructure. It is therefore important to understand their frequency and triggers, and whether their frequency is likely to change significantly due to future climatic and sea level change. It is expensive to both collect seafloor samples and to date landslides accurately; therefore we need to know how many landslides we need to date, and with what precision, to answer whether sea level is a statistically significant control. Previous non-statistical analyses have proposed that there is strong correlation between climate driven changes and landslide frequency. In contrast, a recent statistical analysis by Urlaub et al. (2013) of a global compilation of 41 large (>1 km^3) submarine landslide ages in the last 30 ka concluded that these ages have a temporally random distribution. This would suggest that landslide frequency is not strongly controlled by a single non-random global factor, such as eustatic sea level. However, there are considerable uncertainties surrounding the age of almost all large landslides, as noted by Urlaub et al. (2013). This contribution answers a key question that Urlaub et al. (2013) posed, but could not address – are large submarine landslides in this global record indeed temporally random, or are the uncertainties in landslide ages simply too great to tell? We use simulated age distributions in order to determine the significance of available age constraints from real submarine landslides. First, it is shown that realistic average uncertainties in landslide ages of ±3 kyr may indeed result in a near-random distribution of ages, even where there are non-random triggers such as sea level. Second, we show how combining non-random landslide ages from just 3 different settings, can easily produce an apparently random distribution if the landslides from different settings are out of phase. Third, if landslide frequency was directly proportional to sea level, we show that at least 10 to 53 landslides would need to be dated perfectly globally – to show this correlation. We conclude that it is prudent to focus on well-dated landslides from one setting with similar triggers, rather than having a poorly calibrated understanding of ages in multiple settings.

2.1   Introduction

Submarine landslides are one of the volumetrically most important mechanisms through which sediment is transported from the continental slope to the deep ocean (Hühnerbach and Masson, 2004; Masson et al., 2006; Korup, 2012; Talling et al., 2012; Urlaub et al., 2013; 2014). Landslide deposits have been mapped on many continental slopes as disparate as southeast Australia (Clarke et al., 2012) and the Grand Banks, Newfoundland (Piper et al., 1999). Submarine landslides can be far larger than any terrestrial landslide, and can involve the movement of hundreds or even several thousands of cubic kilometres of material (Hampton et al., 1996; Hühnerbach and Masson, 2004; Talling et al., 2007). Perhaps the most remarkable aspect of large submarine landslides is that they typically can occur on very low gradients of just $1 - 2°$ (Hühnerbach and Masson, 2004; Talling et al., 2007; Urlaub et al., 2012; 2014). Such low gradients are almost always stable on land. Once in motion, the submarine slide mass can entrain ambient seawater and disaggregate to form longer runout sediment flows, known as turbidity currents. These turbidity currents can themselves travel many hundreds of kilometres (Weaver and Kuijpers, 1983), and reach speeds of up to ~ 20 m/s (Piper et al., 1999; Hsu et al., 2008).

Submarine landslides, debris flows and associated turbidity currents may represent significant geohazards. Submarine landslides have the potential to generate damaging tsunamis (Ruffman, 2001; Tappin et al., 2001; Haflidason et al., 2005; Boe et al., 2007; Hornbach et al., 2007); whilst both landslides and turbidity currents can damage expensive sea floor infrastructure, such as that associated with the hydrocarbon industry or seafloor telecommunications (Bruschi et al., 2006; Parker et al., 2008; 2009; Carter et al., 2009; 2012). Some authors have argued that the occurrence of large submarine landslides can have significant climatic impacts through the release of large amounts of methane into the water column and the atmosphere (Kennett et al., 2000; Maslin et al., 2004; Pecher et al., 2005; Vanneste et al., 2006; Beget and Addison, 2007; Paull et al., 2007). Understanding the frequency and triggers of large submarine landslides is therefore important.

2.1.1   Triggering and preconditioning of submarine landslides

A large number of triggers and preconditioning factors have been hypothesised as possible causes for large submarine landslides. Potential preconditioning factors and triggers include earthquakes, rapid sedimentation that leads to high excess pore pressure and conditions close to failure, and gas hydrate dissociation that reduces sediment strength (Hampton et al., 1996; Stigall and Dugan, 2010; Goldfinger, 2011; Masson et al., 2011; Talling et al., 2014). However, not all large (>7 M_w) earthquakes appear to generate major slides (Völker et al., 2011; Sumner et al., 2013), large

submarine landslides occur in locations with slow sediment accumulation (Urlaub et al., 2012), and some landslide headwalls occur in water depths that are too deep for gas hydrate dissociation (Hühnerbach and Masson, 2004). In general, many of these hypotheses for landslide preconditioning and triggering are weakly tested, in part because we are yet to directly monitor large slides in action in sufficient detail (Talling et al., 2014).

2.1.2   Submarine landslide frequency and sea level – previous work

A series of previous studies explored the potential relationship between landslide frequency and sea level. The first set of studies used compilations of landslide ages, typically from widespread locations.

2.1.2.1   Global databases of landslide ages

The initial analyses did not include full uncertainties in landslide ages, or test the certainty of their conclusions through quantitative statistical methods. These studies suggest that increased landslide frequency occurred during specific periods in glacial cycles, corresponding to sea level low-stands, high-stands, or rapid rates of sea level change. Brothers et al. (2013) identify a causal relationship between sea level rise and landslide triggering. Paull et al. (1996) identify increased numbers of landslides during low-stands related to reduced overburden pressure of the water column on gas hydrate bearing sediments. Leynaud et al. (2009), Maslin et al. (1998; 2004), Lee (2009) and Lebreiro et al. (2009) recognised that different margins responded differently to sea level. For example, low latitude margins experienced more large submarine landslides during low-stands while high latitudes were more likely to see slope failures during rising sea levels or high-stands.

Subsequent analysis has sought to evaluate these qualitative conclusions using statistical approaches. Urlaub et al. (2013) considered a collection of 68 large (>~1 km^3) submarine landslide ages from locations worldwide, which includes the last 120 ka (Fig. 2.1). This is the largest number of landslide ages yet compiled. It included dates from landslide deposits themselves from open slope failures (but not volcanic island failures) where ages were obtained by radiocarbon AMS measurements or by applying a combination of several methods (e.g. biostratigraphy and oxygen isotopes). It also included large (>~1 km^3) turbidites inferred to be landslide-triggered. Such large volume turbidites are unlikely to be triggered by processes other than slope failure, as their volume far exceeds even the largest historical river flood (Talling, 2014). In general, such turbidites will tend to record faster moving landslides that disintegrate to produce turbidity currents. See Urlaub et al. (2013) for a fuller discussion on the consistent selection criteria.
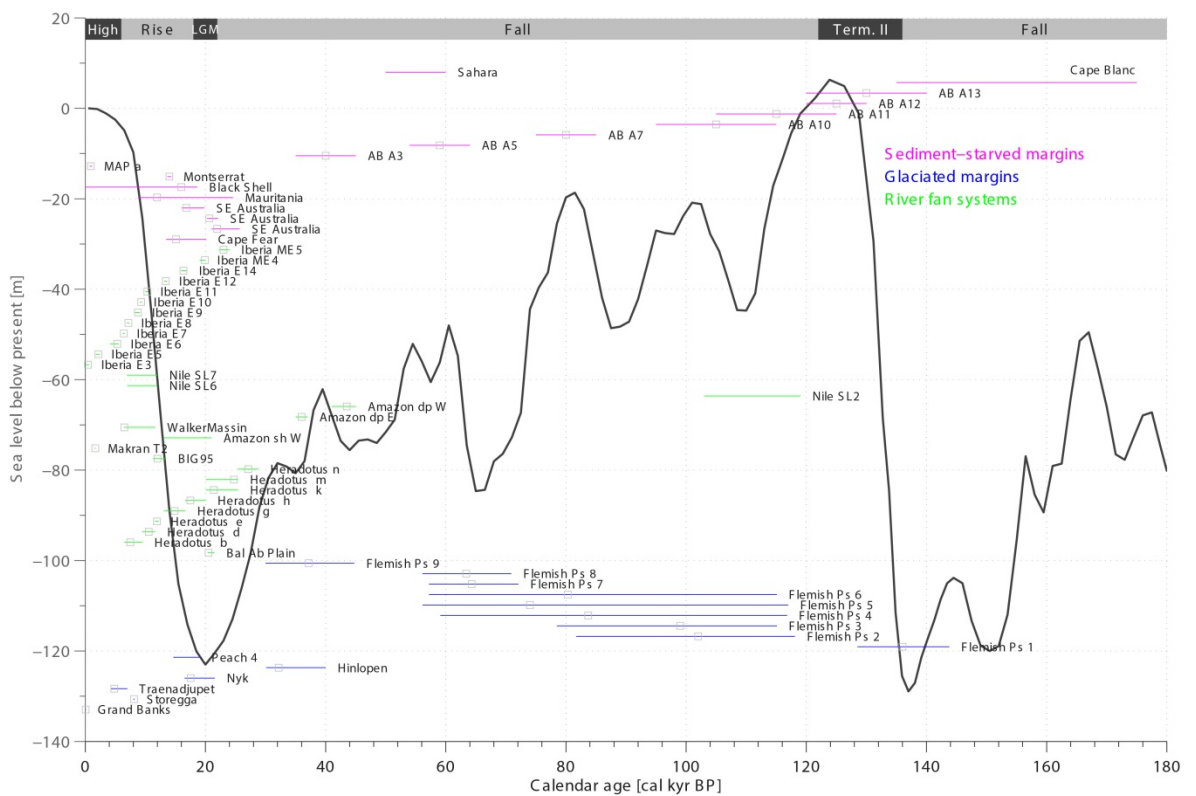
Figure 2.1 Global mean sea level (black curve, Waelbroeck et al., 2002) plotted with submarine

landslide ages which includes their uncertainty intervals (from Urlaub et al., 2013). If

available, the age with the highest probability is shown by a grey square. The colour

of the uncertainty line indicates the sediment environment. The grey time line on the

upper part of the figure indicates the sea level pattern.

The Urlaub et al. (2013) study took a subset of 41 events in the last 30 ka to analyse statistically from the compiled global database. This subset was chosen to avoid a strong bias due to undersampling of older events, caused by limits to core penetration below the seafloor; most sediment cores extend back to 30 ka, but few reached 120 ka. The analysis by Urlaub et al. (2013) included the often considerable uncertainties in landslide ages in this analysis (Fig. 2.1), unlike most previous studies that considered only the calibrated mean ages or most probably ages (Ramsey, 1998). The greatest uncertainties in landslide age typically result from where samples are taken for dating, above and below the landslide or turbidite deposits, rather than the error bars in the (typically RMS radiocarbon) dates themselves. This is discussed more fully in Urlaub et al. (2013), and illustrated by our Fig. 2.2.

Urlaub et al. (2013) analysed these 41 landslide ages. They first divided their 30 ka study period into a series of equal time intervals, termed bins (e.g. 0 – 5 kyr, 5 – 10 kyr, and 10 – 15 kyr). They then counted the number of landslide ages that fell within each bin. This allowed them to plot the number of bins with a single landslide age, two landslide ages, three landslide ages, and so forth (Urlaub et al., 2013; their Fig. 8a, b). A random number generator was then used to produce a set

23

of synthetic landslide ages, assuming landslide occurrence was temporally random. The same procedure was followed to count the number of synthetic landslide ages in each bin, and the number of bins with one, two or more landslide ages. It was found that there was no statistically significant difference between the frequency of bins with 1, 2, 3 or more landslide ages, both real and synthetic landslide ages using the χ^2 statistic (their Fig. 8c). The duration of bins was varied between 1 kyr and 5 kyr, as this affects the frequency distribution of the landslide ages. Both the 'best guess' landslide ages, and landslide ages acknowledging age uncertainties were tested in this way. In each case, landslide ages were described by the χ^2 statistic as occurring randomly, such that they approximated a Poisson distribution (Urlaub et al., 2013).
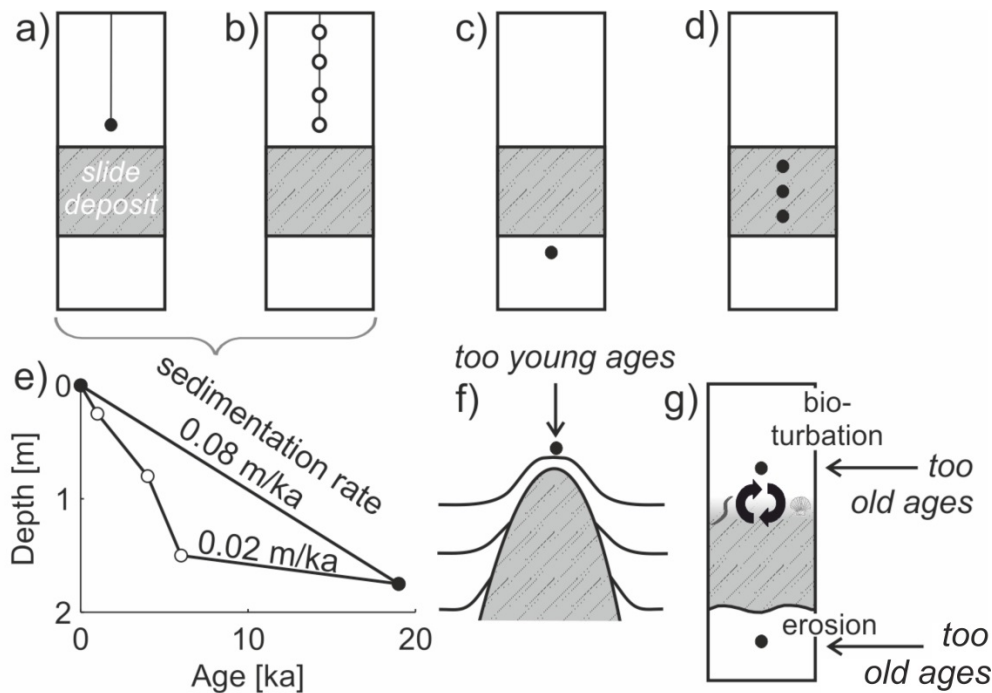
Figure 2.2 Different sampling strategies for radiocarbon dating of submarine landslides. The rectangles represent sediment cores with hemipelagic background sedimentation (white) and a landslide deposit (grey). Open and filled black circles indicate the position of the sample. A minimum age is obtained by taking one (a) or several samples (b) from the hemipelagic unit above the landslide deposit. A maximum age is obtained when samples are either taken from the hemipelagic unit below (c) or within (d) the failure deposit. A linear average sedimentation rate for the core based on one sample can be significantly different from actual temporary sedimentation rates (e), which can be calculated when several samples between the top of the core and the top of the failure deposit are available. Samples above the deposit can give an age too young if located on a local high (f) and bioturbation on the top as well as erosion at the base of the failed deposit (g) are possible sources of uncertainty to estimated ages. Fig. 1. from Urlaub et al. (2013).

2.1.2.2   Landslide recurrence intervals on margins of a single basin

A second type of study used different types of data and statistical methods to consider the recurrence intervals of landslides around the margins of a single sedimentary basin (Hunt et al., 2013; Clare et al., 2014), as opposed to a global dataset of landslide ages. These studies used large volume turbidites as a proxy for large landslides that disintegrate, which are presumably faster moving. Clare et al. (2014) considered large (>0.1 km^3 in these cases) landslide turbidite recurrence intervals in three disparate abyssal plain sequences of variable age, whilst Hunt et al. (2013) considered landslide-turbidites in the Agadir Basin offshore NW Africa. They compared the frequency distribution of landslide turbidite recurrence intervals, with a Poisson frequency distribution. It was found that the frequency distribution of the landslide-turbidite recurrence intervals did not differ significantly from the (Poisson) distribution produced by a temporally random process. Both of these studies therefore suggest that large landslides, which disintegrate to form long run-out turbidity currents, are temporally random, or near random (Hunt et al., 2013; Clare et al., 2014).

2.1.2.3   Discrete vs continuous data

The Urlaub et al. (2013), Hunt et al. (2013) and Clare et al. (2014) studies all concluded that the occurrence of submarine landslides followed a Poisson distribution. A Poisson distribution implies a lack of memory in the system which it is describing, such that the probability of a new event occurring is independent of the time since the last. The methodology used by the different studies is dependent on the type of data. The global nature of the Urlaub et al. (2013) study and the uncertainty regarding the duration of inter-event timing required the study to use 'discrete' (count) data that was binned. The number of landslides within a given time period was compared to the number that would theoretically be produced by a random process. In contrast, the availability of landslide-turbidite recurrence intervals (inter-event time) allowed Hunt et al. (2013) and Clare et al. (2014) to use 'continuous' data. This study follows the approach of Urlaub et al. (2013) and therefore uses discrete data.

2.1.3   Rationale for this study – why is it necessary, novel and valuable?

This study answers the key outstanding questions that remain from the study of Urlaub et al. (2013), which concluded that large landslide ages were temporally random. They posed, but failed to answer the important question: *is this because large submarine landslide ages are temporally random, or it is because the uncertainties in the ages are too large to tell?* Here we provide a novel answer to that question. It is important to understand what this compilation of ages is telling us about landslide frequency, as each landslide age has been costly to acquire. For

example, if landslide ages actually correlate perfectly with global sea level, is it likely that uncertainties in measuring their ages could easily produce an apparently random age distribution?

We also address two further questions that have not previously been addressed. First, *how easy is it to produce temporally random landslide ages simply from combining (non-random) landslide ages from multiple settings with different triggers and preconditioning factors?* It is important to answer this question because this is indeed the situation for most global datasets of landslide ages, which combine dates from different settings, including that presented by Urlaub et al. (2013). Second, *how many submarine landslides do we need to date, and with what precision in order to test whether landslide frequency is controlled strongly by global sea level?* This is important because it is costly to sample and date submarine landslides. We need to know what the most effective future strategy will be for determining whether landslides and sea level are linked.

2.1.3.1   Why use simulated landslide ages?

Our aim is to understand the significance of the available dates, with their uncertainties, from real large submarine landslides (such as compiled by Urlaub et al., 2013). However, to answer the three key science questions outlined above we first consider series of simulated landslide ages. We do not consider landslide ages from the original Urlaub et al. (2013) database. Our approach allows us to determine whether simulated landslide ages, which are perfectly known and lack any uncertainties, can form temporally random patterns once reasonable age uncertainties are added. Such an approach cannot be taken with real landslide ages, whose ages all have significant uncertainties. Similarly, the simulated ages allow us to investigate the ease with which perfectly known landslide ages from different settings (with variable triggers and preconditioning factors) can be combined to form apparently temporally random landslide ages. Finally, these simulated landslide ages allow us to test how many landslide ages are needed to identify a strong sea level control. It is impossible to do this using real landslide ages that all have different error bars, and for which we do not know there is a perfect association with sea level. So these synthetic landslide ages allow us to fix parameters (e.g. error bars), to answer key questions about real field datasets. An additional advantage of such simulated ages is that potential biases are avoided, such as the ages mostly coming from the northeast Atlantic as is the case for Urlaub et al. (2013).

2.2   Methods

This section first outlines the statistical method used to test for randomness in landslide ages (Section 2.2.1). It then describes how simulated (artificial) catalogues of landslide ages were

created that are non-random and have perfectly known ages (Section 2.2.2). Sections 2.2.2.1. and 2.2.2.2 outline how realistic uncertainties (error bars) were added to these simulated ages and how changes to the 1 kyr bins were investigated with regard to how event frequency is measured. Section 2.2.3 describes how simulated landslide ages from multiple settings are combined. Finally, Section 2.2.4 outlines the methodology used to test how many landslides are needed to identify a strong sea level control, whose rationale for choosing rather than other variables is detailed in Section 2.2.5.

2.2.1 χ^2 test for a temporally random (Poisson) distribution

To test for a temporally random distribution, we use the χ^2 methodology outlined by Urlaub et al. (2013). The χ^2 test assesses the goodness of fit of a dataset to a temporally random distribution by analysing whether there are statistically significant peaks, clusters or trends within the dataset (Swan and Sandilands, 1995). As the χ^2 test is testing a temporal process, the data are split into time intervals of certain lengths known as bins. The number of bins containing a certain number of landslides is counted. These are then compared to the number of bins with an expected number of events. The distribution of events is considered random if the χ^2 value is smaller than the χ^2 critical value. The χ^2 critical value is obtained from a look-up table depending on the number of classes observed (see Swan and Sandilands, 1995, for further details). The critical values at the 95% confidence level can be seen in Table 2.1.

v	95%
1	3.841
2	5.991
3	7.815
4	9.488
5	11.07
6	12.592
7	14.067
8	15.507
9	16.919
10	18.307

Table 2.1 χ^2 critical values at the 95% confidence interval. A critical value is selected according to the number of classes being compared, i.e. if three classes are being compared such that there are bins with 0, 1, and 2 landslides then the critical value for 2 degrees of freedom (v) will be selected. If there are four classes being compared such that there are bins with 0, 1, 2, and 3 landslides then the critical value for 3 v will be chosen and so on. When the calculated χ^2 value exceeds the appropriate critical value the distribution of events is deemed non-random.

In addition to the χ^2 test set out in Urlaub et al. (2013) we also use the likelihood ratio χ^2 test (Kendall et al., 1999). The likelihood ratio χ^2 test is defined as:

$$G^2 = 2 \sum \left[O_j log \frac{O_j}{E_j} \right] \qquad\qquad (2.1)$$

where O_j is the number of bins observed with a given number of events and E_j is the number of bins expected with a given number of events (Kendall et al., 1999). The likelihood ratio test provides a means to analyse the likelihood of the landslide ages being random or non-random. If the likelihood ratio exceeds a critical value then we have reason to reject the distribution prescribed by the χ^2 statistic. The critical value is obtained from the χ^2 look-up table according to the number of classes observed. Using the likelihood ratio in addition to the χ^2 statistic provides a more rigorous analysis.

2.2.2   Creating simulated non-random landslides with perfectly known ages
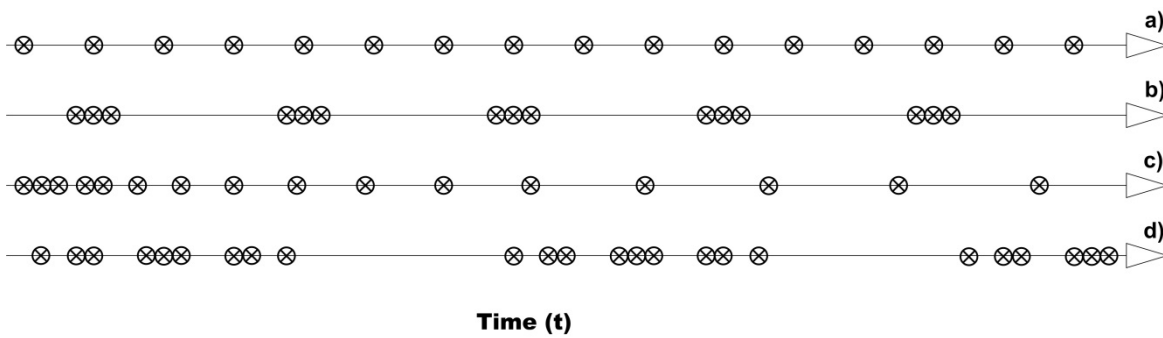
Figure 2.3 Plot showing examples of the ordered distributions used to analyse the impact of age
       uncertainties. Landslides with a) perfectly periodic patterns, b) clustered patterns, c)
       increasing inter-event time patterns, d) patterned patterns. Swan and Sandilands
       (1995).

This study initially uses a set of artificially generated landslide ages that are known perfectly, without any uncertainty, for reasons set out in Section 2.1.3.1. Four types of non-random landslide age patterns were investigated. Our aim was to understand how many of these perfectly known landslide ages we would need to measure to show if they are random or non-random. Fig. 2.3 provides a visual explanation of each type of non-random age distribution. These four types of landslide ages are perfectly periodic, clustered, with linearly increasing inter-event times, or patterned in time (Fig. 2.3; Swan and Sandilands, 1995). Examples of functions used to generate perfectly periodic (Eq. 2.2), clustered (Eq. 2.3) and linearly increasing inter-event times (Eq. 2.4) are shown below. Events are considered to occur when the value of f(x) is equal to 1.

$$f(x) = \sin(x) \tag{2.2}$$

$$f(x) = \sin(x) + \frac{1}{2} sinx + 0.1 \tag{2.3}$$

$$f(x) = \sin(x^x) \tag{2.4}$$

Patterned landslide ages were produced by using more than one of these generating functions. These patterned events were manipulated to change their average event frequency (Fig. 2.3). The number of events within an individual simulated catalogue of landslide ages ranged from 5 to 100. This range was chosen because 5 is the minimum number of events required for the χ^2 test, and 100 events is about 2.5 times more events than in the Urlaub et al. (2013) global compilation. It thus captures a reasonable minimum and maximum value for the number of available landslide ages. These patterns were used to examine if we could identify whether the occurrence of landslides in these simulated records was indeed non-random.

2.2.2.1   Addition of uncertainties in ages

Age uncertainties were subsequently applied to the patterns of landslides outlined in Section 2.2.2 in a number of different ways. First, age uncertainties of up to ±0.75 kyr were applied uniformly to all landslide ages. This was done because ±0.75 kyr represented an age uncertainty large enough for any event to be moved by at least one bin (each bin is 1 kyr). The choice of limiting uniform error results from the χ^2 test assessing the distribution through the use of bins. The use of bins combined with uniform age uncertainty means that the χ^2 test is not sensitive to the temporal order of events. Thus, with uniform age uncertainty of ±0.75 kyr, events are able to reverse their temporal order, although the χ^2 test will not recognise this.

Second, age uncertainties of a random duration between 0 kyr and 3 kyr were applied to events. Both the size of age uncertainty and the event to which it was applied were selected using random number generators. Our choice of a range between 0 and 3 kyr was informed by the uncertainties in the age of landslides from river-fan systems in the Urlaub et al. (2013) study, which have a mean error of 2.34 kyr (Rothwell et al., 1998; Reeder et al., 2000; 2002; Lastras et al., 2004; Maslin et al., 2005; Garziglia et al., 2008; Gracia et al., 2010; Bourget et al., 2011; Masson et al., 2011). This is the smallest mean uncertainty of any of the settings considered by Urlaub et al. (2013).

Third, ever increasing age uncertainties were applied to events. Age uncertainties increased progressively in accordance with the age of the event that it was being applied to, i.e. the youngest event did not have an age uncertainty whilst the age uncertainty of the oldest event was the largest (see Fig. 2.4). The largest age uncertainty applied was 20 kyr (±10 kyr) reflecting the

global record used by the Urlaub et al. (2013) study as the greatest age uncertainty present in this record was 19.98 kyr (±9.99 kyr) (Reeder et al., 2002).
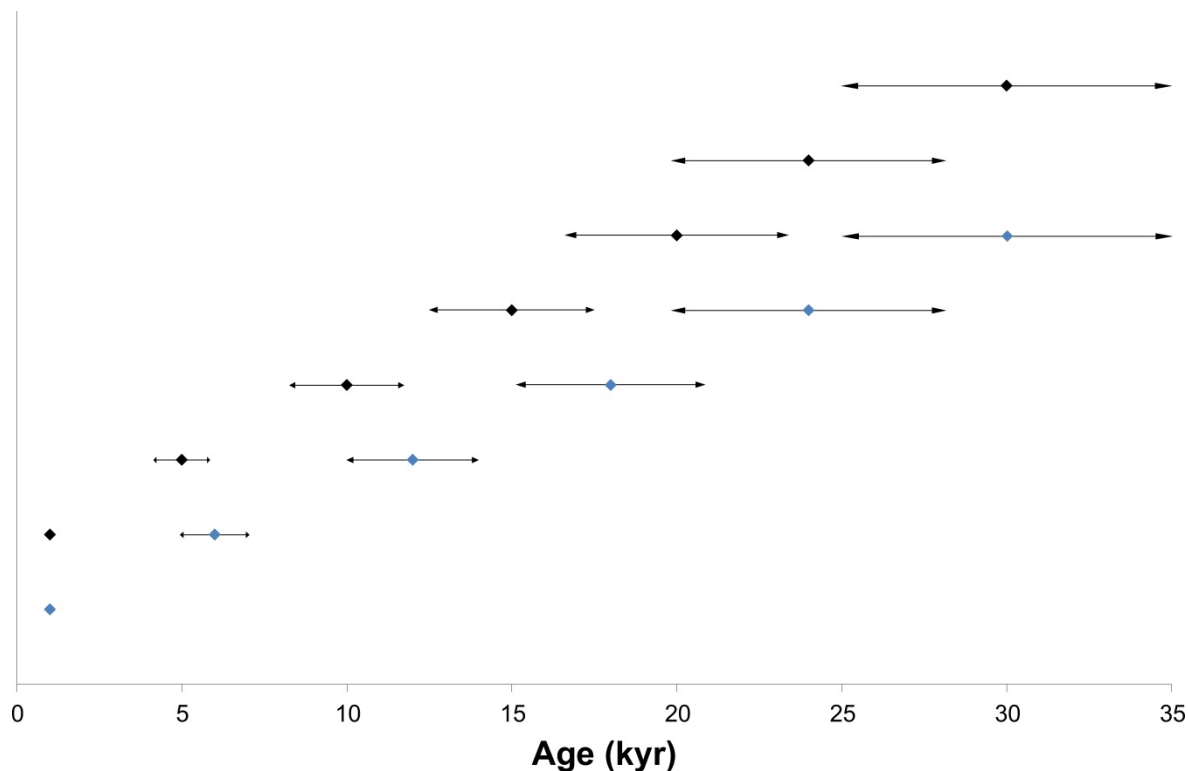
Figure 2.4 Plot showing a schematic of the application of ever increasing age uncertainties. Black and blue diamonds represent two different patterns of landslides Black arrows represent age uncertainties which increase as the landslide get older within each pattern.

2.2.2.2   Moving the positions of the 1 kyr bins

Landslide ages were assigned to 1 kyr duration bins (0 – 1 ka, 1 – 2 ka, 2 – 3 ka, etc) in order to produce a histogram of landslide frequency. Urlaub et al. (2013) noted that the position and duration of these bins could affect the analysis. We chose bin durations of 1 kyr for the following reason; that linking landslide frequency to changing environmental factors, such as sea level variations, necessitates that the bin size is sufficiently small to capture the environmental change under consideration. In the case of sea level change, 1 kyr bin size is reasonably appropriate (Waelbroeck et al., 2002). The position of the 1 kyr bins was varied during the analysis outlined in Sections 2.2.2 and 2.2.2.1 to test the extent to which bin position impacts upon our ability to recognise whether landslide are non-random.

2.2.3   Landslides from multiple settings

We also simulate different landslides coming from multiple settings. Each setting was defined to have a perfectly periodic (non-random) sequence (Fig. 2.3a), but with a different return period. For example, one setting was given a uniform recurrence interval of 1.5 kyr, another 2 kyr, and the third 3.5 kyr. Landslide ages from these multiple settings were then combined into one overall catalogue and tested for a temporally random sequence as a single dataset. This was done to simulate the generation of a global record of landslides combining different margin types, including glaciated, fluvial and sediment starved, as was seen in Urlaub et al. (2013) or different geographical margins around one basin (Clare et al., 2014) (Fig. 2.5). The datasets were then manipulated individually and as a single catalogue, by introducing different size error bars to the landslide ages and changing the position of the 1 kyr bins. This methodology was then carried out for the other pattern types seen in Fig. 2.3 It is important to test the role of multiple settings as global datasets of events will include landslides from multiple different margin types, whilst basin records will include turbidites derived from landslides which may have different environmental settings.

2.2.4   Simulated landslide ages whose frequency is dependent on sea level

A third series of landslide ages were generated to analyse the number of events needed to establish with reasonable certainty that global landslide frequency is controlled strongly by sea level. The frequency of the landslides in this catalogue was defined to be directly proportional to sea level, using a global eustatic sea level curve for the last 30 ka (Waelbroeck et al., 2002). Event frequency was simulated to be highest during the last 1 ka in accordance with the highest sea level, whilst the lowest frequency occurred around the last glacial maximum ~20 ka. A directly proportional relationship was chosen in order for there to be the strongest possible relationship between sea level and event frequency; thus it serves to enable us to identify the fewest number of events needed as part of a best case scenario to link the two processes. It also acts as a starting point for linking other processes to landslide occurrence.

This artificial catalogue of landslide ages contained 67 entries, which were numbered 0 to 66. We then explored how many events were needed to identify sea level control. Beginning with one event from the catalogue, events were added randomly to our analysis until all 67 were included. This mimics the discovery and dating of submarine landslides through continued field investigations. Bins with durations of 1 kyr are used in order to replicate the precision needed to link event frequency to sea level. The catalogue was chosen to contain 67 events as this is greater than the current global catalogue of well dated landslides for the last 30 ka (i.e. 41; Urlaub et al.,

2013), whilst being within the same order of magnitude thus acting as a useful comparison to the global landslide record.
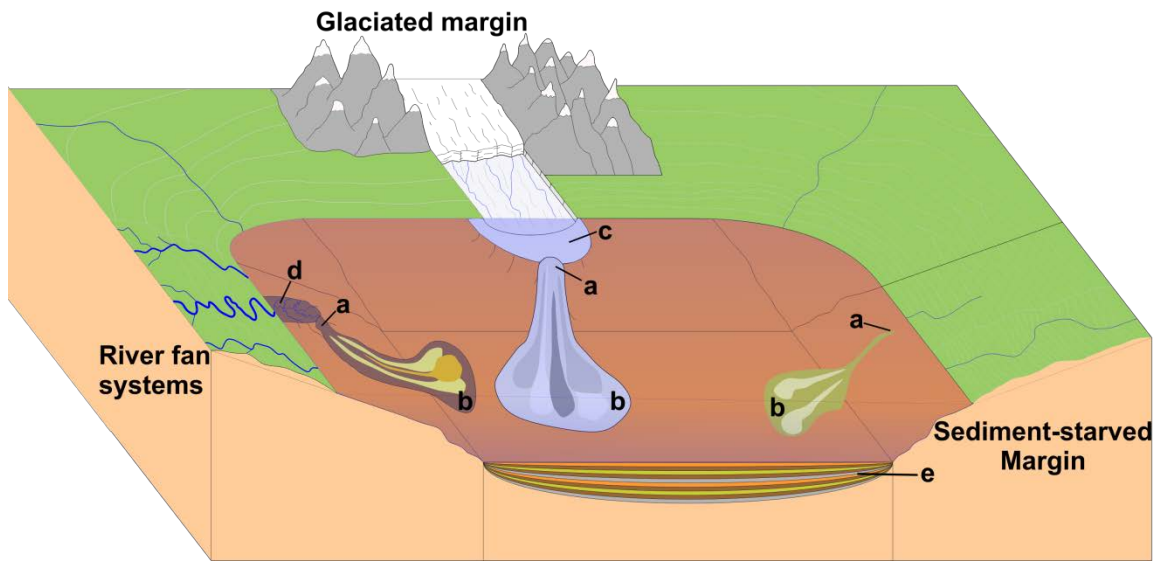
Figure 2.5 Three separate sedimentary systems feeding into one ocean basin. Each system is likely to have different characteristic landslide recurrence intervals due to different local environmental factors. River-fan systems experience the highest sediment input during deglaciation or lowstands, depending on latitude, as rivers efficiently transport terrestrial sediment (Covault and Graham, 2010; Urlaub et al., 2013). Glaciated margins are strongly influenced by climatic cycles due to the direct influence of growing and shrinking ice sheets and the position of ice streams (Lee, 2009) in terms of both local sea level and the location and timing of sediment delivery (Dowdeswell et al., 1996). Sediment starved margins are characterised by lower sediment deposition rates as they have not been affected by glaciation and are located away from major river-fan systems. Labels (a) landslide headscarp, (b) landslide deposits, (c) trough-mouth fans, (d) river-fan deltas, (e) interbedded sequence of background hemipelagic and sediment density flow deposits.

2.2.5   Why choose to investigate landslide frequency proportional to sea level?

We specifically investigate sea level due to its link to current anthropogenic climate change concerns regarding the consequence of future sea level rise on landslide frequency (Maslin et al., 2004; 2005; Owen et al., 2007; Lee, 2009). Using the global sea level curve for the last 30 ka provides us with the simplest test of how many landslides we would need to date to identify a non-random temporal distribution of events. This 30 kyr time period, used in the Urlaub et al. (2013) study, represents just over half a glacial cycle. Sea level begins the period during a low stand and rises to the end of the period. When the relationship between sea level and landslide

frequency is linearly proportional over the last 30 ka, the distribution of landslide ages is a close approximation to a trend distribution (Fig. 2.3c). If the χ^2 test is unable to identify this relationship we are unlikely to be able to identify a relationship between another variable and landslide frequency.

Importantly, whilst we analyse sea level, this analysis is also able to represent a proportionally linear response of landslide frequency to rate of sea level change over the same period. In a catalogue of 67 landslides where landslide frequency was linearly proportional to rate of sea level change, the frequency distribution using 1 kyr bins would be the same as the sea level controlled example. The only difference between the catalogues would be that they are temporally offset from each other. Crucially, the χ^2 methodology outlined using bins does not recognise the temporal order of events (see Section 2.2.2.1) merely the frequency of events in different bins. The χ^2 test used would therefore not recognise any difference between a landslide dataset linearly proportional to sea level and a landslide dataset linearly proportional to sea level change if half or a full sea level cycle is included within the period of study.

2.3   Results

We now address the three main questions that form the aims of this study.

2.3.1   Are large landslides temporally random, or are age uncertainties too large to tell?

2.3.1.1   How many perfectly known landslide ages are necessary to show they are non-random?

Simulated landslide ages were generated for the last 30 ka that were perfectly non-random and whose ages were known perfectly. It was found that when there were over 40 dated landslides in the distribution, we could always correctly determine that landslide occurrence was non-random. Where samples of >40 ages were taken from the distribution types, the χ^2 statistic allowed us to reject the hypothesis of temporal randomness for all the pattern types.

When samples of <40 ages were analysed, the results were more variable. Table 2.2 contains the results for the iteration of each landslide dataset pattern containing the largest number of event that appeared temporally random according to the χ^2 statistic. Each of these patterns is also displayed in Fig. 2.6. Here, we show how the χ^2 statistic varies as the number of landslides in each pattern changes. The apparent cyclical nature of the χ^2 statistic value is a consequence of the methodology using discrete data and the relative numbers of bins with events in them. For example, in Fig. 2.6a the χ^2 statistic is sensitive to the relative number of events in each bin, i.e.

how many bins contain 2 landslides and many contain 3. The χ^2 statistic therefore peaks when all of the bins have the same number of events in before declining until 50% of the bins contain one number of landslides while the other 50% contain a different number of landslides. The χ^2 statistic subsequently rises as the percentage of bins with the same number within them increases.

Landslide dataset Distribution	Number of events	Number of bins with 0 events (Expected number of bins with 0 events)	Number of bins with 1 events (Expected number of bins with 1 events)	Number of bins with 2 events (Expected number of bins with 2 events)	Number of bins with 3 events (Expected number of bins with 3 events)	Critical Value	χ2 test value	Likelihood-Ratio
Perfectly Periodic	14	16 (17.60)	14 (9.39)	0 (2.50)	0 (0.444)	3.841	2.9063	0.663
Clustered	37	10 (8.74)	8 (10.78)	7 (6.65)	5 (12.73)	3.841	2.7982	3.423
Linearly increasing inter-event times	17	15 (17.02)	14 (9.65)	0 (2.73)	1 (0.516)	3.841	3.212	3.744
Patterned	39	6 (8.16)	15 (10.63)	5 (6.91)	4 (2.99)	5.991	4.94	2.829

Table 2.2 χ^2 and likelihood ratio results for landslide age patterns containing the greatest number of events with no age uncertainties which appear to be random according to the χ^2 test.

Perfectly periodic distributions were only considered random when the event dataset contained 14 events or fewer (Fig. 2.6a). At 14 ages the event dataset returned a critical value of 3.814 which was below the critical χ^2 value of 3.841 at the 95% confidence interval. The likelihood ratio statistic supports identification of this distribution as random; 0.663 is well below the critical value of 3.841. Non-random landslide datasets with linearly increasing inter-event times were considered random when they contained 17 ages or fewer (Fig. 2.6c). Considering 17 ages the dataset returned a critical value of 3.212 which was below the critical χ^2 value of 3.841 at the 95% confidence interval. The likelihood ratio (0.553 does not exceed the critical value of 3.841) supports this evaluation.

The relationship between the number of events and the ability of the χ^2 statistic to recognise non-random recurrence of events was found to be more complicated for clustered and patterned datasets and showed an important influence of bin position. For clustered landslide patterns, the χ^2 statistic considered datasets with 14 events or fewer to be temporally random. For a dataset containing 14 ages, the χ^2 critical value was 3.525 which was below the critical value of 3.841 required to show non-randomness. The maximum number of ages as part of a clustered dataset of landslide ages which was considered random was 37 (Fig. 2.6b). The χ^2 statistic returned for the clustered dataset containing 37 ages was 2.798 compared to the critical value (3.423) is almost at parity with the critical value (3.841). This suggests that small changes could alter the interpretation of the distribution which supports the range of distributions interpreted for patterns containing between 14 and 37 ages. Datasets containing between 14 and 37 ages were

also often considered random. However, movement of the 1 kyr bins resulted in many of these datasets being shown to be temporally non-random.
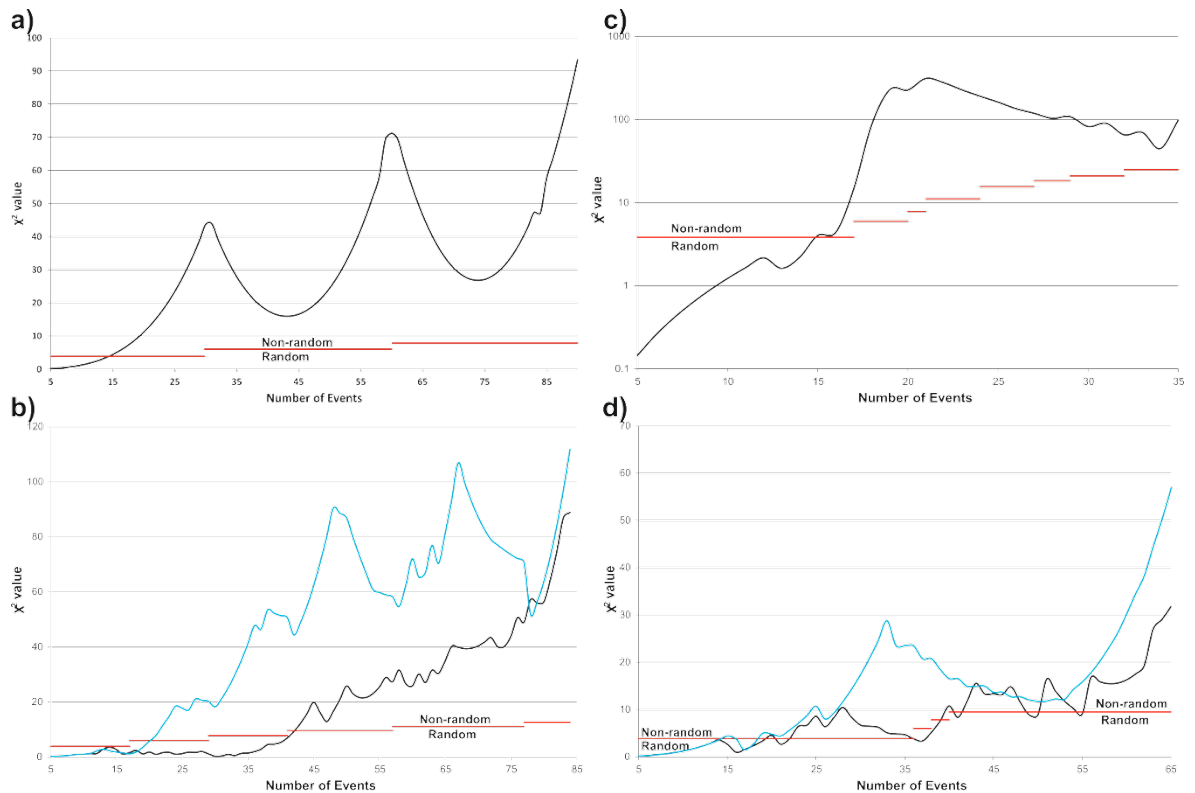
Figure 2.6 Plot showing how the χ^2 statistic value changes with increasing numbers of events in each pattern type when ages are perfectly known. a) The impact of increasing numbers of landslides on the χ^2 statistic where the pattern is perfectly periodic. b) The impact of increasing numbers of landslides on the χ^2 statistic where the pattern is clustered. The black line represents the pattern which contained the largest number of landslides before the χ^2 statistic recognised it as non-random. The blue line represents the pattern which contained the smallest number of landslides before the χ^2 recognised it as non-random. c) The impact of increasing numbers of landslides on the χ^2 statistic where the pattern has increasing inter-event times. d) The impact of increasing numbers of landslides on the χ^2 statistic where the pattern is patterned. The black line represents the pattern which contained the largest number of landslides before the χ^2 statistic recognised it as non-random. The blue line represents the pattern which contained the smallest number of landslides before the χ^2 statistic recognised it as non-random. In a-d the red line represents the χ^2 critical value; once the χ^2 statistic is above the critical value the pattern of landslides is no longer considered random.

35

The range of patterned (Fig. 2.3d) landslide age datasets considered temporally random exceeded that demonstrated by the clustered datasets. No patterned dataset with 14 ages or fewer could be discerned from a random distribution. However, a dataset with 39 patterned ages could not be accepted as different to a random distribution according to the χ^2 statistic (Fig. 2.6d). It had a χ^2 critical value of 4.94 which was less than the 5.991 critical value required to be considered non-random at the 95% confidence interval (the likelihood ratio value was 2.829 compared to a critical value of 5.991). The χ^2 statistic considered different patterned landslide age datasets containing between 14 and 39 events, to be both temporally random and non-random. For many datasets the position of the bins was crucial. It was found that movement of the bins often altered whether the dataset was considered temporally random at the 95% confidence interval.

2.3.1.2   Introduction of more realistic uncertainties (error bars) in landslide ages

We first introduced age uncertainties of up to ±0.5 kyr to the four different non-random landslide age patterns. In each case we considered more than 40 landslide events. This did not produce any submarine landslide age distributions that appeared temporally random according to the χ^2 statistic. Similarly, the introduction of error bars in landslide ages between ±0.25 kyr and ±0.75 kyr produced, with the exception of a number of patterned landslide age datasets, no distributions which appeared temporally random with >40 landslides.

In some cases it was found that movement of the bins resulted in the patterned landslide age datasets appearing to be non-random, which had previously been determined as random. For example, movement of the 1 kyr bins resulted in the same dataset, with 55 ages, having χ^2 values of between 12.121 and 7.533 with the χ^2 critical value being 9.488 (the likelihood-ratio test for these examples being 4.535 and 3.427 respectively). This implies that as age uncertainties increase the χ^2 test becomes increasingly sensitive to bin position due to its inability to recognise temporal order.

The impact of age uncertainties of ±0.75 kyr on landslide patterns is shown in Fig. 2.7. Here, we show the impact of ±0.75 kyr on the χ^2 value to the landslide patterns shown in Fig. 2.6. Fig. 2.7a-d all show that age uncertainty can reduce the χ^2 statistic value of non-random patterns. However, Fig. 2.7a, b and d all show that where patterns of landslides contain relatively few events, the response to the age uncertainty can be for the pattern to increase the χ^2 statistic value and thus appear much less random than when the pattern had no age uncertainty associated with it. Fig. 2.7c implies that where patterns of landslide have linearly increasing inter-event times the impact of introducing age uncertainties is primarily to reduce the χ^2 statistic value.
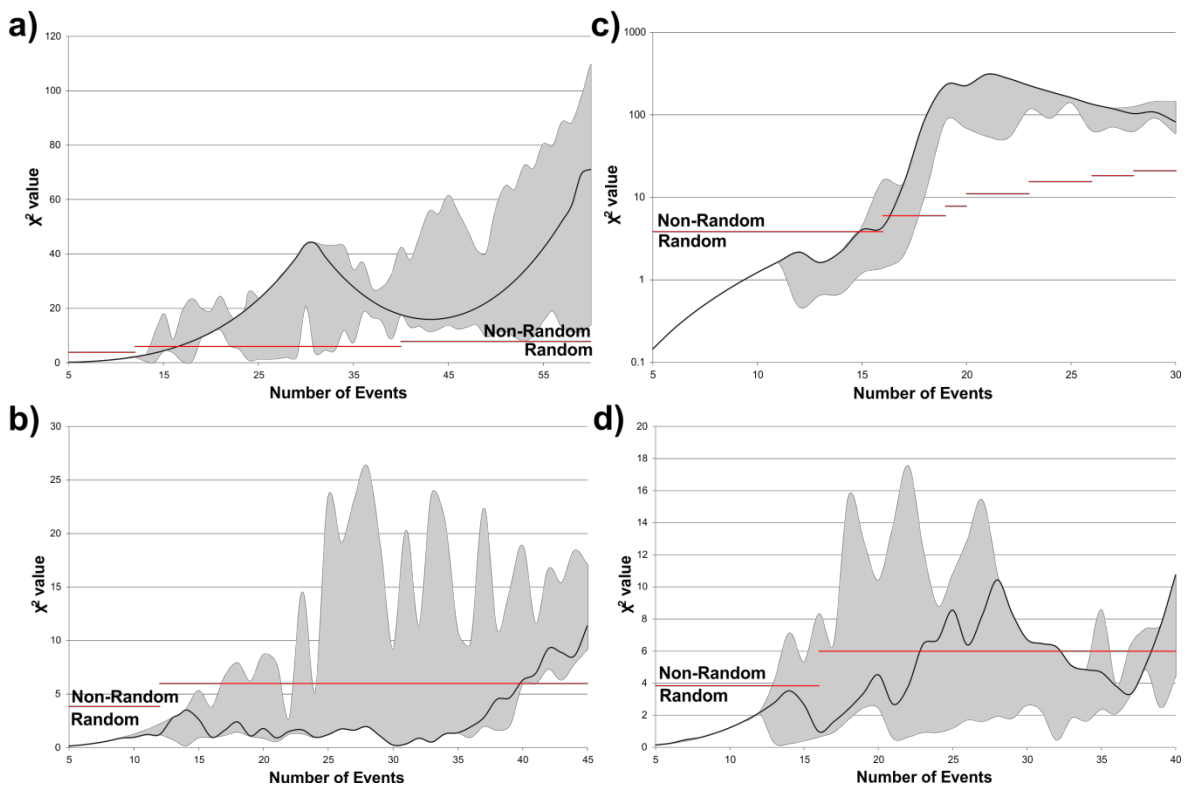
Figure 2.7 Plot showing the effect of uncertainties up to ±0.75 kyr on the different patterns of landslides shown in Figure 2.6. The black line represents the χ^2 statistic value when the ages are known perfectly. The grey areas represent the possible range of χ^2 statistic values when an uncertainty of ±0.75 kyr has been applied. a) χ^2 statistic values for increasing numbers of landslides in a perfectly periodic pattern. b) χ^2 statistic values for increasing numbers of landslides in a clustered pattern. c) χ^2 statistic values for increasing numbers of landslides in a pattern with increasing inter-event times. d) χ^2 statistic values for increasing numbers of landslides in a patterned pattern. In a-d the red line represents the χ^2 critical value; once the χ^2 statistic is above the critical value the pattern of landslides is no longer considered random.

Further analysis of larger error bars in landslide ages involved two approaches. First, randomly generated age uncertainties of between 0 and 3 kyr were assigned to events randomly using a random number generator. This allows us to define the threshold number of landslide events, which have a certain age uncertainty, that are needed to make non-random landslides appear temporally random. This threshold number of landslides with age uncertainties varied depending on the original pattern (periodic, clustered, etc.) and the number of events within the pattern. Second, it was assumed that age uncertainties increased linearly for progressively older landslides up to 20 kyr. This approach resulted in almost all of the datasets we considered, appearing temporally random. The apparent randomness was caused predominantly by the large age uncertainties (up to 20 kyr) on the older landslides in each distribution.

Urlaub et al. (2013) considered 41 landslide ages in the last 30 kyr from a series of different settings. The 24 examples from river-fed systems have the smallest average error bars (2.34 kyr). Their landslide ages from other settings have even larger error bars. Our analysis therefore shows that the inclusion of realistic error bars, even those from the better dated river-fed systems, can cause non-random landslide ages to appear random.

2.3.1.3 Can combination of multiple non-random sets of landslide ages lead to temporal randomness?

We now address our second aim; how easy is it to produce random landslide ages by combining non-random ages from multiple settings? Three different, artificially generated, perfectly periodic non-randomly distributed (Fig. 2.3a) landslide datasets were combined and analysed by the χ^2 statistic. The combined dataset often appeared to be temporally randomly. The occurrence of an apparently temporally random distribution is the result of the three sources being out of phase with one another. Phase is defined here as the timing of events within a time series. For two perfectly periodic distributions (see Fig. 2.3a) with recurrence intervals of 1 kyr for both distributions, the distributions would be considered in phase if events in both distributions occurred at the same time (i.e., 1st event at 0.5 ka, 2nd events at 1.5 ka, etc.). They would be considered out of phase if they occurred at different times (i.e., for the first distribution events occurred at 0.5 ka, 1.5 ka, 2.5 ka, etc.; for the second distribution events occurred at 0.3 ka, 1.3 ka, 2.3 ka, etc.). The overlaying of ordered patterns appears to generate randomness. Conversely, when perfectly periodic landslide ages were in phase, the distribution of the combined dataset was not perceived to be random.

Age uncertainties were applied, both uniformly across three perfectly periodic landslide age datasets and to individual datasets. The latter was intended to replicate the different sized age uncertainties associated with the various margin types seen in Urlaub et al. (2013). Addition of age uncertainty to any or all of the records acted to make the distribution of events appear more temporally random.

This methodology was applied to the other patterns of landslide ages seen in Fig. 2.3, in addition to combining datasets with different patterns of landslide ages. The same results were found when three landslide age patterns of the same type were combined. The same was also true when multiple landslide age pattern types were combined. However, assessment of whether one age pattern was in phase with another was problematic.

2.3.2   How many landslide ages are needed to test for a strong dependency on sea level?

To determine the power of the test we performed a series of model iterations. Random introduction of landslides resulted in the distribution of landslide ages appearing temporally random and non-random depending on the order that events were introduced. An example run is present in Table 2.3. After 23 events are introduced in the example run, the distribution appears to be non-random. However, addition of another (24th) event then causes the distribution to appear to be random. Only after 28 events does the distribution remain non-random with the addition of further events. We thus recorded the number of events required before the distribution did not revert to being random following the addition of further events.

Our results showed that the number of landslides needed to indicate a non-random distribution at the 95% confidence interval was highly variable. The mean number required was 38. However, the range of landslides needed was from 10 to 53, with the variability between different iterations being shown by a standard deviation of 8.34; a large figure when compared to the size of the dataset.

These results show that 10 to 53 landslide ages are needed with a mean of 38 ages, when the landslide age is known perfectly to show a strong dependency on sea level. 95% of landslide age distributions were correctly identified as non-random when they had 48 ages. However, the ages from real submarine landslides are not perfectly dated and have associated error bars (Urlaub et al., 2013). When these uncertainties are added the number of landslides required to identify a strong sea level dependency will be greater than the number shown here.

2.4   Discussion

We first discuss the implications of the answers to our three aims (Sections 2.4.1, 2.4.2, 2.4.3), and then outline the main sources of uncertainty in linking landslide ages and sea level (Section 2.4.4). Section 2.4.5 outlines the most effective strategy for dating landslides, and thus the best way forward.

2.4.1   Do available dates show that large landslides are random, or are error bars too large?

As might be expected, our results indicate that it was extremely difficult to make non-random patterns of perfectly dated landslides appear temporally random. However, the smallest error bars in the Urlaub et al. (2013) dataset were for 24 river-fed systems, with other settings tending to have much larger error bars in landslide ages. We show that such realistic (± 3kyr) error bars

Number of Events	How the Chi-Square test views the landlside ages at the 95% confidence interval	Chi-Squared Value	Critical Value	$O_j = 0$	$O_j = 1$	$O_j = 2$	$O_j = 3$	$O_j = 4$	Likelihood-ratio
5	Random	0.136	3.841	26	5				0.036
6	Random	0.237	3.841	25	6				0.452
7	Random	0.38	3.841	24	7				0.497
8	Non-random	13.449	7.815	24	6		1		0.183
9	Non-random	9.658	7.815	23	7		1		5.112
10	Random	7.343	7.815	22	8		1		16.409
11	Random	4.508	7.815	22	7	1	1		2.301
12	Random	3.332	7.815	21	8	1	1		1.961
13	Random	2.565	7.815	21	7	2	1		1.711
14	Random	1.701	7.815	20	8	2	1		1.179
15	Random	1.165	7.815	19	9	2	1		0.867
16	Random	0.905	7.815	18	10	2	1		0.760
17	Random	0.628	7.815	19	9	3	1		2.575
18	Random	1.18	7.815	18	8	4	1		1.184
19	Random	2.416	7.815	18	7	5	1		2.444
20	Random	3.683	7.815	18	7	4	2		2.892
21	Random	4.616	7.815	18	6	5	2		4.229
22	Random	6.156	7.815	18	5	6	2		6.212
23	Non-random	8.123	7.815	18	5	5	3		6.964
24	Random	6.199	7.815	17	6	5	3		5.058
25	Non-random	9.599	7.815	17	6	4	4		6.677
26	Random	7.762	9.488	17	6	4	3	1	6.572
27	Random	7.582	9.488	17	5	5	3	1	6.359
28	Non-random	10.925	9.488	17	5	5	2	2	4.011
29	Non-random	11.697	9.488	17	4	6	2	2	6.447
30	Non-random	12.081	9.488	17	4	5	3	2	6.932
31	Non-random	17.166	9.488	17	4	5	2	3	5.378
32	Non-random	17.325	9.488	17	4	4	3	3	6.254

Table 2.3 Example of the output from a single iteration using an artificial set of landslide ages whose frequency is linearly proportional to sea level. The number of events column refers to the number of randomly selected landslide ages from the overall distribution which are being analysed by the χ^2 test. Each row represents the addition of an extra randomly selected age and the output from the χ^2 test. In this example we can see that when 8 ages are analysed through the χ^2 test the distribution appears to be non-random. However, addition of further ages causes the distribution to revert to appearing temporally random. Only after 28 ages are added does the distribution appear to be non-random and remain non-random. From this iteration we take 28 ages to be the number of ages required for the χ^2 test to recognise the distribution is in fact of non-random. $O_j = 0....4$ is the number of bins observed with n ages.

resulted in the appearance of random ages, even when landslides were non-random. Thus, the error bars in Urlaub et al. (2013) are too great to tell if these 41 events represent truly random landslides.

2.4.1.1   The additional impact of bins in making landslides appear temporally random

Additional important errors were introduced into the assessment of whether the events were temporally random by the position of the bins. Bin choice in terms of both width and position is subjective. Therefore it is necessary to vary the position of the bins, up to the bin width in order to assess links between landslides and sea level. Bin width should be chosen depending on the rate of variation in the environmental record (e.g. sea level) with which event frequency is being compared. Bin use, however, remains unavoidable when assessing the statistical distribution of events in a global record (discrete data). Unlike outcrop or single core records, there is no control on the temporal order of events in the global record as deposits do not lie on top of one another. This is compounded by large age uncertainties making the exact temporal order of events unknown. We are therefore unable to use recurrence intervals (continuous data) as the exact relationship between events cannot be specified meaning we are forced to use statistical tests on the frequency of events within certain specified periods of time, i.e. bins.

2.4.2   Effects of combing landslide ages from different settings

We demonstrate that three non-random collections of landslide ages could, once combined, appear to be temporally random (Figs. 2.5 and 2.8). More formally, a time-independent, memoryless (Poisson) distribution can result from non-uniform additive influences, as documented by van Rooji et al. (2013). This is likely to be the case for global landslide databases (Urlaub et al., 2013), and it may be the case for studies based on large-volume turbidites in a single basin centre (Clare et al., 2014). This conclusion is important as it suggests that a combination of landslide ages from a small number (≥ 3) of settings can easily produce a single set of apparently random ages.

2.4.2.1   Implications for global databases of landslide ages

The global record arguably includes landslides from at least three fundamentally different settings; river-fed systems, ice stream-fed trough mouth-fans and sediment starved margins (Fig. 2.5). It is very likely that the relationship between sediment supply and sea level, and hence landslide preconditioning, will vary significantly in these three settings (Fig. 2.5; Laberg et al., 2000; 2003; Covault and Graham, 2010; Llopart et al., 2014). Therefore when combined into one record, if the events are out of phase, a temporally random distribution of events is likely. Large

age uncertainties will only act to increase the likelihood of such a random distribution in global datasets that consider multiple settings. This suggests that global compilations, or even regional compilations with multiple settings, may not be very useful in determining links between sea level and landslide frequency.
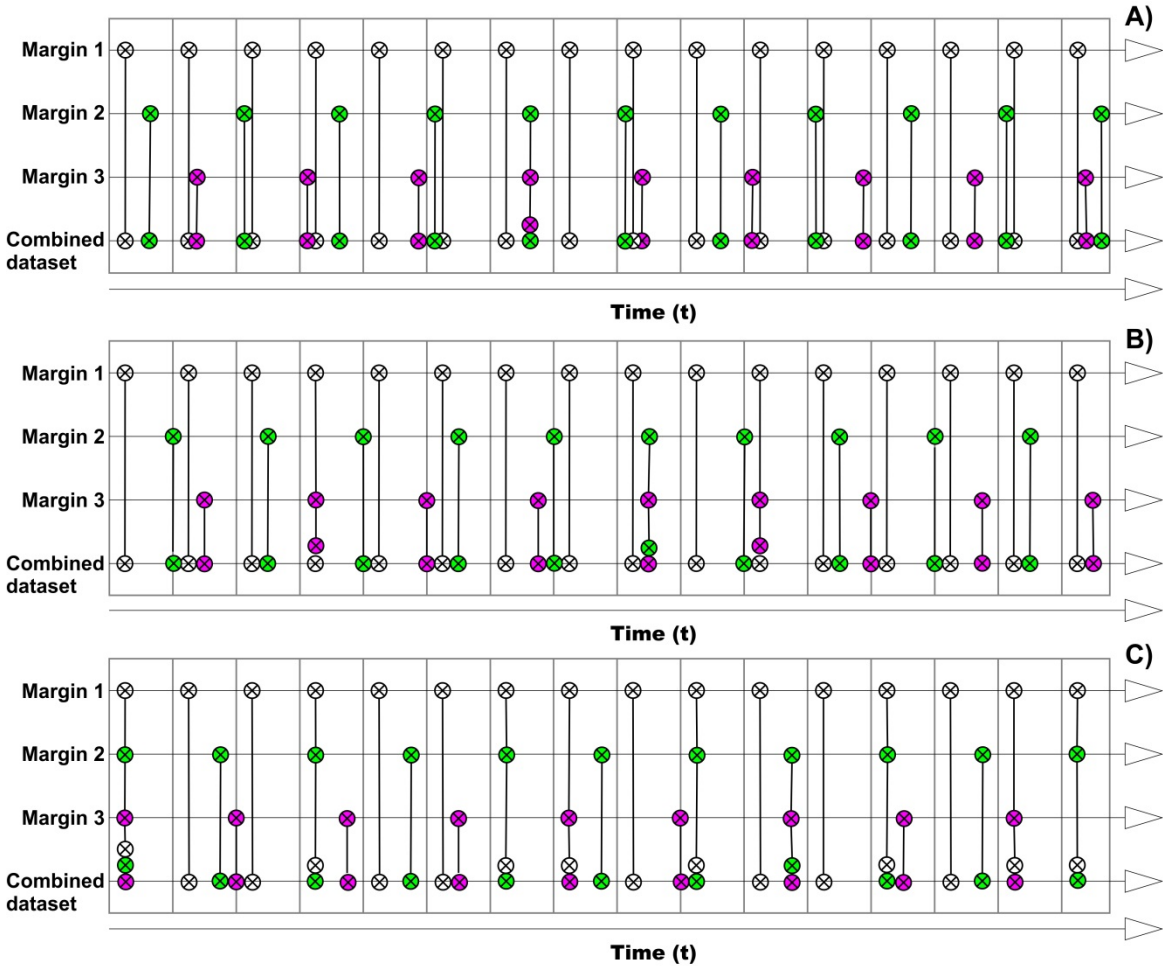
Figure 2.8 Illustration of how non-random landslides in three settings can be combined to produce
random series of landslide ages. Abacus plots showing the combination of landslide
ages from three different settings (white, green and pink circles). The lower time
series in each panel show the combined landslide age record. Each setting shows
landslide ages that are perfectly periodic, but with different recurrence intervals. The
setting with the most frequent landslides is shown by the white circles; the setting
with the most infrequent events is shown by the pink dots. The grey vertical lines are
the edges of 1 kyr bins, which would be used to calculate the histogram of landslide
frequencies through time. Parts a, b and c are used to illustrate the importance of
differences in phase, as defined by the initial slide event in each series. For example,
all three records start in phase in part c, such that they all start with a landslide at the
same instant. Part a shows the least in phase landslides and generates the most
strongly temporally random sequence.

2.4.2.2   Implications for landslide-turbidite records from a single basin

An alternative approach is to use large turbidites in a single basin, as a proxy for large submarine landslides around the basin margin (Hunt et al., 2013; Clare et al., 2014). However, our study emphasises the importance of understanding the different sources of landslide triggered turbidity currents, if they are out of phase (Rothwell et al., 1998; Rothwell et al., 2006; Talling et al., 2007; Hunt et al., 2013). Additional effort will also have to be made to clearly identify the difference between landslide and flood triggered turbidites but also to identify where large turbidity currents have been generated by the coalescence of multiple small failures. Inclusion of turbidites in the database that have not been generated by large (> 1 km^3) events will likely weaken any statistical relationship within a database.

2.4.3   How many landslides are needed to identify a strong sea level control?

If landslide frequency is linearly proportional to sea level, our study shows that 10 to 53 perfectly dated landslides are needed to statistically identify that direct correlation. It follows that considerably more than 10 to 53 landslides (mean 38) will be needed once age uncertainties are included. However, two other issues are relevant to this discussion.

2.4.3.1   Controlling factors with more distinctive patterns than sea level

First, further work is needed to determine how many landslides should be dated, if landslide frequency is proportional to rate of sea level change, and not absolute sea level. More generally, a smaller number of landslides may need to be dated if the controlling factor has a more distinctive pattern through time. Some types of controlling factors may have a more distinctive pattern of variation than near sinusoidal sea level, or occur infrequently. In such cases, a smaller number of landslide ages may be needed to test for statistically significant relationships with landslide frequency. For instance, the Storegga Slide is near synchronous with the last major very abrupt climate change, the 8.2 ka climate event (Haflidason et al., 2005; Dawson et al., 2011). Landslide frequency has also been linked to infrequent periods of very rapid sea level rise (Brothers et al., 2013; Smith et al., 2013). Events of this type are relatively rare and short-lived. A different approach may be needed to determine how many landslides should be dated to see if there is a link to such events.

2.4.3.2   Stronger proportionality between landslide frequency and sea level

A second issue is that we assume that landslide frequency is directly proportional to sea level, such that the constant proportionality is unity. It is possible that a much stronger association

exists, such that the constant proportionality is far greater than unity. In such a situation, a smaller number of landslides may be needed to test for a significant association with sea level.

2.4.3.3   Local sea level variations and delays in response to sea level

Sea level itself presents challenges for finding a statistical relationship with landslide frequency at a global scale. Local sea level change can be very different from global eustatic sea level change due to glacio-isostasy and local tectonic influences (Lambeck et al., 1998; Murray-Wallace, 2002). Additional uncertainty arises because of our limited ability to reconstruct accurate local sea level curves. Combined with delayed responses, either to changes in sea level or other identified triggering factors, this reduces the likelihood of linking event to cause. Modelling studies have indicated that continental slopes may have site-specific delayed responses to earthquake triggers (L'Heureux et al., 2013). Delayed and variable response to slow forcing mechanisms such as sea level rise is therefore likely to be even more inconsistent geographically. Submarine landslides from the global catalogue of Urlaub et al. (2013) with relatively well constrained dates are confined to one glacial sea level cycle. Dating of additional events which occurred during other glacial cycles may improve our ability to link events to changes in sea level.

2.4.4   Implications for studying landslides older than 30 ka

Several reasons may make it problematic to study landslides older than ~30 ka. First, as noted by Urlaub et al. (2013), cores from the modern seafloor may not penetrate deeply enough to reach older events. Second, the error bars in landslide ages tend to increase significantly with time (Fig. 2.1), especially once landslides become too old to date via radiocarbon (>~43 ka). However, a third reason may also be important.

2.4.4.1   Non-stationary random triggers whose average recurrence rate varies over time

We have presented a statistical analysis of perfectly non-random landslides and tested the number of landslides that would be required in order to identify non-randomness. However, the testing of these landslide patterns represents an idealised non-random case for two reasons. First, the triggering mechanisms for these events will likely add a random component to these regular patterns. The addition of a degree of randomness, combined with age uncertainties will likely lead to the non-random nature of these events being harder to discern.

Second, landslides may be occurring according to a non-stationary Poisson process. The time period considered within this study is relatively short at geological timescales. The shortness of the time period in question means that the distribution of some random events appears stationary, such that the mean recurrence rate of landslides does not change over time. However,

over longer periods, although remaining inherently random, the mean recurrence rate may change. Such processes are considered to be occurring according to a non-stationary Poisson process, i.e. occurring in clusters (Fig. 2.3b). Earthquakes represent an example of a non-stationary Poisson process. Over short time periods they have a near-random distribution. Over longer time periods the mean recurrence rate may change as fault systems move or tectonic settings evolve. For submarine landslides, triggering processes are likely to be affected by large-scale environmental change associated with climate change leading to fluctuations in triggering (Geist and Parsons, 2009).

Inherent randomness caused by specific triggers and non-stationarity of Poisson processes mean that the results of this study are somewhat idealised. These results thus represent a best case scenario for recognising non-randomness using the statistical methodology that has been outlined. Detection of a non-stationary Poisson process is not attempted here, and it would be more challenging, and could require many more events than are in Urlaub et al.'s (2013) database. Evaluation of a non-stationary Poisson process for large submarine landslides is difficult, but should be the subject of future work.

2.4.5 Future strategies for dating submarine landslides – what is the best way forward?

We have shown that realistic error bars in landslide dating, and combination of ages from as few as three different settings, make it difficult to test for links between sea level and landslide frequency. The most complete global compilation of 41 large landslide ages in the last 30 ka appears temporally random (Urlaub et al., 2013), but could plausibly result from non-random processes such as sea level. We currently have too few well-dated landslides to test for a linear dependence between landslide frequency and sea level, even using better constrained sub-sets of those landslide ages from river-fed systems (Urlaub et al., 2013). Although we would be able to test for a stronger (i.e. non-linear) dependence on sea level, or indeed links to events with more distinctive times series, such as abrupt climate warming or sea level rise events. However, these negative conclusions raise the issue; what is the most constructive way forward?

2.4.5.1 Testing scientific hypotheses – are negative results useful?

We first note that it is useful to know the answer to scientific questions, even when they are negative answers. This helps us to narrow down avenues of future research, and avoid misleading conclusions, such as that currently available landslide ages show a significant correlation with sea

level. Indeed, a broad comparison might be made to medical trials, in which there is a detrimental bias towards publication of positive tests (Goldacre, 2010).
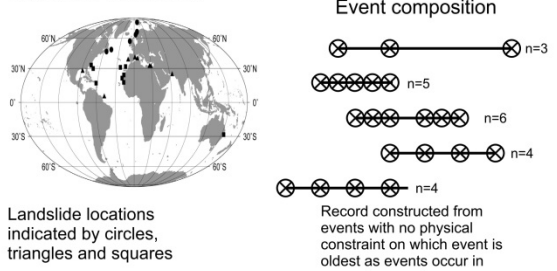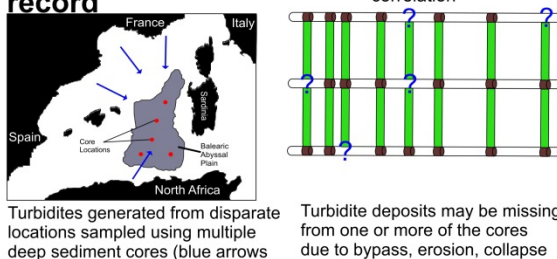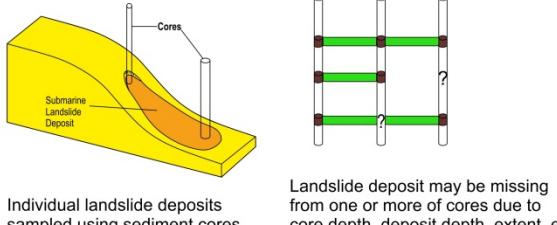
Global Record	Global record	Issues with record
Record length: 30 ka Number of events: 41 Return period: ?	Event composition Landslide locations indicated by circles, triangles and squares n=3, n=5, n=6, n=4, n=4 Record constructed from events with no physical constraint on which event is oldest as events occur in separate records	Geographical bias Temporally limited Limited by sample size
Regional Record Record length: ≥ 250 ka Number of events: >100 Return period: ≥1000 a	**Sampling regional record** France, Italy, Sardinia, Spain, Core Locations, Balearic Abyssal Plain, North Africa Turbidites generated from disparate locations sampled using multiple deep sediment cores (blue arrows indicate source direction Regional core correlation Turbidite deposits may be missing from one or more of the cores due to bypass, erosion, collapse or extent	**Issues with record** Limited to size >0.1 km³ i.e. flows of sufficient size to reach the basin Overprinting of signal i.e. multiple sources with possibly varying signals
Local Record Record length: Core dependent Number of events: <10 Return period: location dependent	**Sampling method of local data** Cores, Submarine Landslide Deposit Individual landslide deposits sampled using sediment cores Core correlations Landslide deposit may be missing from one or more of cores due to core depth, deposit depth, extent, etc	**Issues with record** Typically limited to 1-2 slides Age constraints/dating errors Limited by core depth

Figure 2.9 A simplified schematic of the existing issues associated at different spatial scales linking submarine landslide frequency to changing environmental factors. Problems associated with each of the different records have emerged as introducing significant error during different parts of this study.

2.4.5.2   Importance of using quantitative and robust statistical methods

Previous workers have proposed a number of different relationships between sea level and landslide frequency, based on qualitative analyses. They include a relationship between landslides and low sea level (Paull et al., 1996), rising or low sea level (Lee, 2009), or indeed no relationship with sea level (Urlaub et al., 2013). This study illustrates the importance of quantitative statistical techniques to understand what is significant in such datasets.

More sophisticated statistical methodologies can be used. For example treating submarine landslide hazard in a similar evidence-based manner to large magnitude volcanic and earthquake hazards (Aspinall et al., 2003; Baxter et al., 2008; Daub et al., 2012). Evidence-based refers to a

methodology where the examination of evidence from specific studies and the systematic collection of this evidence are highly weighted in decision making; intuition and unsystematic experience are de-emphasised (Sackett et al., 1996). Evidence-based hazard analysis, first used in medicine (Aspinall et al., 2003) and subsequently used on Montserrat from 1997 (Baxter et al., 2008), incorporates all available theoretical and observational information and applies probabilistic procedures using Bayesian statistics. This allows decision making that is open to revision with partial or imperfect information as the degree of evidence uncertainty is weighted accordingly (Baxter et al., 2008). Hazard assessment should therefore attempt to incorporate well dated landslides, including those whose ages are near abrupt climate events whilst also including extreme value theory statistics (Sornette, 2009; Dawson et al., 2011; Bondevik et al., 2012).

2.4.5.3   Should there be a wider spread of dated landslides to avoid spatially biased compilations?

The current global compilation of landslide ages is spatially biased (Urlaub et al., 2013). Large submarine landslides have predominantly been catalogued in certain areas, such as the North Atlantic, Iberian Margin, and Mediterranean (Fig. 2.9) (Urlaub et al., 2013). International efforts could therefore attempt to broaden the area where events are dated, and avoid such strong geographical biases. However, this might not be the most productive strategy as it will result in the combination of landslide ages from an even wider range of settings. As we show here, a greater number of settings may be very likely to generate apparently random age sequences from non-random triggers (Figs. 2.5 and 2.9).

2.4.5.4   Concentration of dating efforts at a small number of similar setting with long records

Our study suggests that efforts may need to be concentrated, such that statistically significant numbers of well-dated landslides are obtained from individual types of setting. To achieve this, controlling variables need to be isolated; something the use of disparate records may prevent (McAdoo and Watts, 2004; Brothers et al., 2013). Perhaps the simplest means of advancing knowledge is to focus specifically on river-fed systems (Covault and Graham, 2010). River-fed systems have both the greatest number of catalogued events, as well as the smallest age uncertainties (Urlaub et al., 2013). They are also the margin type where glacial cycles have been suggested to play a particularly important role, via sediment supply (Covault and Graham, 2010). Identification of additional events at these margins therefore provides the greatest likelihood of asserting, with some degree of confidence, the effects of sea level on landslide frequency (Geist et al., 2013). This could be achieved through either IODP sites or long basin core records where the input sources to the basin are well constrained. Focussing on one of these record types and

isolating local environmental factors such as local sea level change would allow for a more useful comparison of landslide frequency and sea level change. However, care will still be needed to be taken to distinguish the effects of glacio-eustatic sea level on slope stability, and factors that co-vary with glacial cycles, such as the rate of sediment supply from rivers (Covault and Graham, 2010).

2.4.5.5   Should we date fewer landslides, but with greater precision?

This question is important because finite resources can be directed towards obtaining a greater number of (lower precision) landslide ages, or a small number of very well-dated examples. This study does not provide a full statistical analysis of such a logistical trade-off. However, it is important that marginally increasing the number of poorly dated landslides in global compilations, with uncertainties that are well in excess of ~±3 kyr, may not be a constructive way forward. For instance, our work suggests that around 40 well-dated (±0.75 kyr) landslides from a single setting would be necessary to allow robust statistical analysis of links between sea level and landslide frequency. Long records from specific locations with multiple events are therefore the most appropriate for isolating triggering mechanisms.

2.5   Conclusions

Previous work found that the most complete compilation of 41 (>~1 km^3) submarine landslide ages in the last 30 ka suggests that these hazardous events are temporally random (Urlaub et al., 2013). However, it was unclear whether the landslides were temporally random, or whether the considerable uncertainties on most landslide ages made it impossible to tell. The primary conclusion of this study is that there are currently too few, sufficiently well-dated large landslides, to know whether these large submarine landslides are temporally random. The addition of realistic error bars to the ages of landslides that are non-random can produce ages that appear temporally random.

Second, we show that it is unlikely that the combination of landslide ages from different settings, each with different preconditioning and triggering factors that are offset in time, can easily produce a combined dataset that appears random in time. We show that just three distinct settings may be combined to produce apparently temporally random dates. This is important because most global databases of landslide ages probably include at least three distinct types of setting.

Third, we constrain the number of landslides, needed to test whether there is significant correlation between landslide frequency and global sea level. This was done simulating landslide

ages that are correlated perfectly with sea level. The number of landslide ages needed to test for a significant correlation with sea level ranged from 10 to 53, with a mean of 38, even when landslide ages were known perfectly.

Finally, we provide some suggestions for the best future strategy for assessing the submarine landslide hazard. We suggest focussing on specific environmental settings, and on a smaller number of well-dated landslides (~40) to test for links with sea level.

The results of this study indicate the issues inherent with using the global record of submarine landslide occurrence in its current form. Our results indicate that both realistic age uncertainties and combination of data from multiple settings may make it hard to test for links between sea level and landslide frequency. However, it may be easier to test links between landslide frequency and more episodic and shorter duration events, such as the 8.2 kyr climate event or meltwater pulse 1, which have more distinctive time-series than sea level. Finally, the best means to understand links between sea level and landslide frequency may come from local studies with more numerous recurrence intervals (e.g. Clare et al., 2014; 2015), perhaps in conjunction with detailed records of localised environmental change.

Chapter 3: Which earthquakes trigger damaging submarine mass movements: insights from a global record of submarine cable breaks?

Summary

Chapter 3 analyses earthquake triggering of submarine mass movements. Here, the first ever global analysis of the occurrence of submarine mass movements caused by earthquakes is achieved using subsea cable break data. Using a global database of subsea fibre-optic cable breaks we identify earthquakes that triggered (and did not trigger) submarine mass movements from 1989 to 2015. Having identified which earthquakes triggered cable breaking flows in different regions around the world we explore why in some regions only very strong earthquakes, i.e. >M_w 7, trigger damaging submarine mass movements whilst in others very weak earthquakes, i.e. ~M_w 3, are able to trigger submarine mass movements.

Reference:

Pope, E. L., Talling, P. J., Carter, L. 2017. Which earthquakes trigger damaging submarine mass movements: insights from a global record of submarine cable breaks? Marine Geology, 384, 131 - 146.

Which earthquakes trigger damaging submarine mass movements: Insights from a global record of cable breaks?

Ed L. Pope[1], Peter J. Talling[1], Lionel Carter[2]

[1]National Oceanography Centre, Southampton, European Way, Southampton, SO14 3ZH, UK

[2]Antarctic Research Centre, Victoria University of Wellington, Wellington, New Zealand

Abstract: Submarine landslides, debris flows and turbidity currents are significant geohazards for seafloor infrastructure in many locations around the world. Their deposits potentially provide a valuable record of major earthquakes, which extends further back in time than most terrestrial earthquake records. It is therefore important to determine their frequency and triggering mechanisms, and what types of earthquake trigger submarine slides and flows in different settings. Submarine cable breaks provided the first evidence of submarine mass movements, as shown by the 1929 Grand Banks earthquake. Even now the global network of subsea telecommunication cables provides our only means to monitor flows globally. Here, we present the first global analysis of the occurrence of submarine mass movements caused by earthquakes using cable break data. Using a global database of subsea fibre-optic cable breaks we identify earthquakes that triggered (and did not trigger) submarine mass movements from 1989 to 2015. We note that cable breaks are not a perfect record of submarine mass movements, and may only record more powerful ($>\sim 2$ ms^{-1}) flows. However, our results show, in contrast to previous assertions, that there is no specific earthquake magnitude that systematically trigger mass flows capable of breaking a cable. Some earthquakes with magnitudes >7.0 M$_w$ triggered cable breaking flows, but many >7.0 M$_w$ earthquakes have failed to break nearby cables. We also show that some very small (3.0 – 4.0) magnitude earthquakes are capable of triggering cable breaking flows. The susceptibility of slopes to fail as a consequence of large and small earthquakes is dependent on the average seismicity of the region and the volume of sediment supplied annually in addition to other preconditioning factors such as slope architecture and mechanical sediment properties.

3.1   Introduction

Since the laying of the first submarine cables in 1842, this technology has acted as a detector of natural hazards in the ocean (Carter et al., 2012). Indeed, even now there have been relatively few studies where submarine mass movements have been directly monitored, and those that have are limited to only a few locations globally (Khripounoff et al., 2003; Andrieux et al., 2013; Cooper et al., 2013; Xu et al., 2014). The use of submarine cable breaks therefore still plays a crucial role in understanding submarine mass movements in different areas around the world (Heezen and Ewing, 1955; Heezen et al., 1964; El-Robrini et al., 1985; Hsu et al., 2008; Carter et al., 2012; Talling et al., 2014).

Turbidity currents, and other types of submarine sediment density flow (Talling et al., 2012) can travel at speeds of 3 up to 19 ms^{-1} for hundreds of kilometres. These flows represent a significant geohazard for submarine telecommunication cables and other seafloor infrastructure including that for the recovery of hydrocarbons (Carter et al., 2009; Parker et al., 2009). These submarine cables now carry >95% of global data and communication traffic, giving them considerable strategic importance. Large submarine landslides also have the potential to generate damaging tsunami (Tappin et al., 2001; Haflidason et al., 2005; Boe et al., 2007; Tappin et al., 2014). Determining the frequency and triggers of these mass movements is key to submarine geohazard assessment.

A number of possible triggering mechanisms have been identified for submarine mass movements. Earthquakes, storm and tsunami wave loads, rapid depositional loading, hyperpycnal flows, volcanism and gas hydrate dissociation have all been identified as possible triggers (Adams, 1990; Mulder et al., 2003; Shanmugam, 2008; Piper and Normark, 2009; Stigall and Dugan, 2010; Talling, 2014). Despite identifying multiple triggers, there have been few occasions when a precise trigger for an event has been identified. In most case studies where a triggering mechanism has been identified, the trigger was identified using cable breaks.

3.1.1   Previous studies using cable breaks

Numerous studies have used cable breaks to study individual submarine mass movements (Heezen, 1956; Heezen et al., 1964; Heezen and Johnson, 1969; Krause et al., 1970; Piper et al., 1999; Hsu et al., 2008; Carter et al., 2012; Cattaneo et al., 2012; Su et al., 2012; Ratzov et al., 2015). Earthquakes, hurricanes and hyperpycnal flows have all been identified as triggering mechanisms for submarine mass movements using cable breaks. The classic example is the 1929 Grand Banks submarine landslide. This submarine landslide was triggered by a M_w 7.2 earthquake (Heezen and Ewing, 1952; Piper et al., 1999). More recently cable breaks identified multiple

submarine landslides offshore Algeria triggered by the 2003 Boumerdès Earthquake (Cattaneo et al., 2012), whilst multiple submarine flows were caused by the 2006 Pingtung Earthquake offshore Taiwan (Carter et al., 2012). In these cases, geophysical and shallow cores have corroborated the cable break data showing cable breaks can be used as a proxy for mass flow triggering. Submarine cable breaks were also used to identify the occurrence of turbidity currents offshore Oahu, Hawaii as a result of the passing of Hurricane Iwa (Dengler et al., 1984). The passing of Typhoon Morakot over Taiwan in 2006 did not generate a submarine mass movement itself; it did, however, generate an exceptional discharge from the Gaoping River which generated a hyperpycnal flow (Kao et al., 2010). This was followed a few days later by the main flow triggered by failure of the recently deposited sediment (Carter et al., 2012). Cable break studies have also provided us with unique insights into submarine mass movement dynamics. Sequential breaks in networks of cables have enabled turbidity current flow speeds to be calculated (Heezen and Ewing, 1952; Piper et al., 1999; Carter et al., 2012).

In spite of the insights afforded by breaks to submarine cable networks, no study has previously been able to analyse the frequency and triggering mechanisms of submarine mass movements globally. Here, for the first time we have access to a global compilation of cable breaks over 25 years. The compilation allows us to analyse precisely what triggers and does not trigger submarine mass movements globally and identify whether these triggers are regionally specific or act at the global scale.

3.1.2   Turbidite palaeoseismology

Earthquakes and their related hazards (tsunami, fire, etc.) are predicted to claim >2.5 million lives during the 21st Century (Holzer and Savage, 2013). Efforts to reduce losses use estimates of earthquake size and recurrence. To achieve this, palaeoseismology attempts to extend the earthquake record beyond the instrumental record. One method of extending the earthquake record beyond the instrumental record is turbidite palaeoseismology (Adams, 1990; Gràcia et al., 2013). This approach relies on discriminating between the mechanisms, which trigger turbidity currents and the resulting deposits (Goldfinger, 2011; Gràcia et al., 2013). It is achieved by (1) establishing synchronous triggering of sediment gravity flows over large areas using correlation of core deposits (Adams, 1990; Beck et al., 2007; Goldfinger, 2011; Patton et al., 2013; Atwater et al., 2014), (2) identifying specific seismo-turbidite facies within core deposits (Nelson et al., 1995; Goldfinger et al., 2012; Talling, 2014), (3) confluence tests (Adams, 1990), and (4) linking onshore geological records with offshore core data (Nanayama et al., 2007). The methods for testing whether a turbidite is earthquake triggered are summarised in Table 3.1.

How do you know if a turbidite records earthquake triggering?	Comment
1. *Confluence test*: Same number of turbidites on upstream and downstream sides of confluence indicates synchronous widespread triggering. Origin of flow is too widespread for other triggers of synchronous turbidity currents, such as cyclones that can produce hurricane-force winds across distances of several hundred kilometres.	Number of turbidites can vary with height above channel flow as flow thickness is variable. It is difficult to precisely locate cores (e.g. at a consistent height above the channel floor) using ship-mounted coring methods.
2. *Synchronous deposition of turbidites in multiple basins* indicates widespread slope failure. Origin of flow is too widespread for other triggers of synchronous turbidity currents.	Uncertainties in dating 'synchronous' turbidites
3. *Turbidite volume* is much larger than that expected for other trigger mechanisms such as river floods.	Deposit volume is rarely precisely known. Note that flows may incorporate sediment and increase their volume, through conduit erosion. Processes other than earthquakes can have the potential to trigger large landslides.
4. *Earthquake and turbidite timing is independently well known*, as timing observed directly – or in the case of earthquakes – through reliable historical records.	Cable breaks or mooring data may be needed to date turbidity currents precisely, as other methods (e.g. Pb^{-210} or Cs^{137}) profiles of 'recent' turbidites have greater uncertainties. Ideally, repeat coring or mapping of the seafloor is needed to establish timing of turbidite emplacement. 4 is generally more reliable than 1-to-3.
5. *Multiple stacked fining upward sequences inferred to be characteristic of earthquake triggered turbidites,* as failure occurs in many locations across a wide area.	The grading pattern is not strongly diagnostic as multiple fining upward sequences can also result from multi-stage slope failure, flow reflection, or pulsing hyperpycnal flows.

Table 3.1 Methods for testing whether a turbidite is earthquake triggered. After Talling (2014).

Robust reconstruction of earthquake histories requires (1) deposits to be precisely dated; (2) the sedimentary regime of the region to be well constrained; (3) the sedimentary record to be complete; and (4) knowledge of which magnitude earthquakes do and do not trigger sediment gravity flows (Atwater and Griggs, 2012; Sumner et al., 2013; Atwater et al., 2014). Of these requirements, understanding which magnitude earthquakes do (and do not) trigger submarine mass movements is of critical importance. Onshore, landslides triggered by earthquakes can be directly observed (Keefer, 1984). From observations onshore it is possible to link different earthquake magnitudes, distances from hypocentres and changes in local geology to mass movements (Keefer, 1984, 2002; Owen et al., 2008). In contrast, it is more problematic to identify the occurrence or extent of well-dated synchronous mass movements in the marine environment. Access to a global submarine cable fault dataset provides the first opportunity to attempt such a study offshore.

3.1.3   Aims

Two main questions are posed. First, which magnitude earthquakes do (and do not trigger) submarine mass movements that break cables and does this vary on a regional basis? Second, do other parameters such as local sediment supply need to be assessed as part of turbidite palaeoseismology rather than just ground shaking (e.g. earthquake magnitude/peak ground acceleration)?

3.2   Terminology

Throughout this study the term 'cable break' or 'break' is used. Here we these terms to refer to clean breaks and other faults in the cables. Faults can result from damage to a fibre-optic cable casing that allows the ingress of seawater and shorting of the power supply and/or stretch the cable to a point where optical fibres are damaged (Burnett et al., 2013).

We use the term *submarine mass movement* to donate an overall flow event driven by the excess density of the sediment that it contains. *Submarine mass movements* can refer to *turbidity currents*, *debris flows*, *hyperpycnal flows*, *slumps* and *landslides*. Transformation may occur between these different flow types as the submarine mass movement evolves. For further information on terminology for different types of flow see Talling et al. (2012). We refer to *submarine mass movements* and later *mass flows* as the cable break database donates that a cable experienced a fault and the day of that the fault was experienced. It does not denote the type of flow that caused the cable to break or the precise timing of the break (i.e. minute accuracy). We are therefore unable to apply methods that have been used previously to estimate flow velocity (Piper et al., 1999; Carter et al., 2012) or identify the specific type of flow which has broken each cable.

3.3   Data and methods

3.3.1   Cable break database

This study is based on non-public, aggregated data supplied by Global Marine Systems Limited (UK) on a non-disclosure basis. The database contains information on the location of each subsea cable when it was laid (Fig. 3.1). It includes any other installation information such as sea bed type and the duration the cable has been in service. Cable breaks within the database are identified and generally related to specific causes, i.e., seismic, trawling, anchor, etc. Each 'break' refers to a break or failure along a section of a specific cable. Each 'break' may therefore represent multiple

breaks along a single section of cable. For example, it has previously been reported that cable SEA-ME 3 suffered 11 breaks as a result of the 21/05/2003 Boumerdès Earthquake offshore Algeria (Cattaneo et al., 2012), but these appear as a single break within the database.
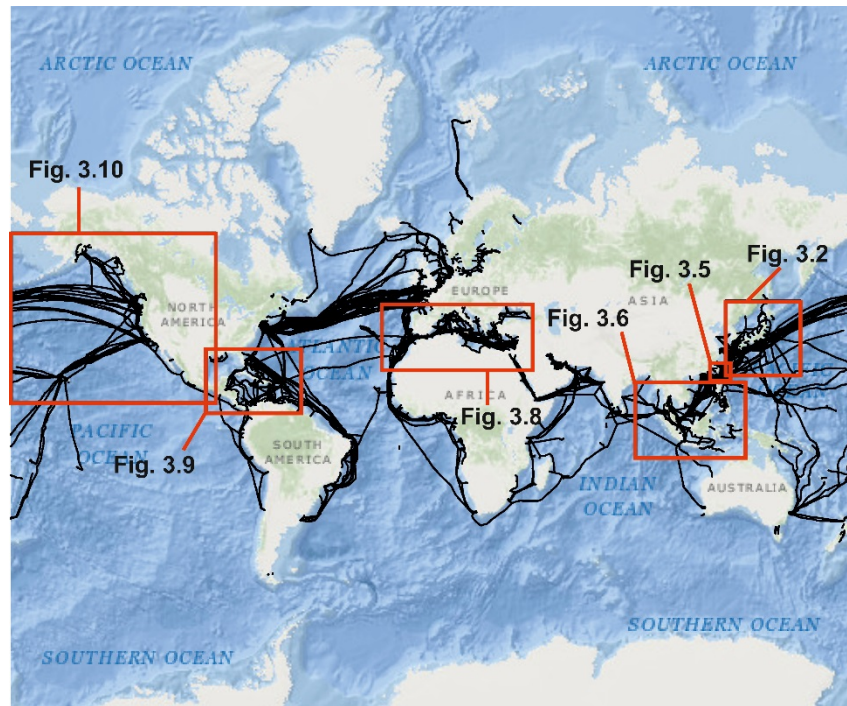
Figure 3.1 Global submarine communication network with each study area identified.

3.3.2   Earthquakes

3.3.2.1   Earthquake magnitudes

Earthquake records from 1989 to present were obtained from the USGS ANSS Comprehensive Earthquake Catalogue (ComCat; http://earthquake.usgs.gov/earthquakes/search/). The catalogue provides location, timing, type of earthquake, hypocentre depth, magnitude and magnitude type of each earthquake. Three types of magnitude are presented; surface wave magnitude (M_s), body wave magnitude (M_b) and moment magnitude (M_w). However, in order to assess the relationship between earthquake magnitude, ground shaking and submarine cable breaks, required earthquake magnitudes in the catalogue to be homogenised. To achieve this, M_s and M_b were converted to M_w using empirical relationships (Scordilis, 2006; Das et al., 2011; Di Giacomo et al., 2015).

3.3.2.2   Earthquake peak ground acceleration

In sub-aerial settings, earthquake M_w is not directly related to the number or size of co-seismic landslides that occur (Makdisi and Seed, 1977; Ambraseys et al., 1996; Meunier et al., 2007). Instead the number of landslides correlates well with the intensity and duration of seismic

acceleration (Makdisi and Seed, 1977). The intensity and duration of seismic acceleration can vary from site to site for a given earthquake. Generally ground-shaking gets weaker with increasing distance from the ruptured fault that produced the seismic energy but it is also a function of local ground conditions, fault type and focus depth. A similar relationship may exist for submarine slope failures (Strasser et al., 2006; Noda et al., 2008; Pouderoux et al., 2014). Initiation of underwater slope failure may depend on excess pore pressure generated by earthquake induced shaking and other preconditioning factors such as slope architecture and mechanical properties of the sediment (Seed and Idriss, 1971; ten Brink et al., 2014). It is therefore necessary to compare ground shaking as well as magnitude to breaks in the subsea cable network. Only then are we able to evaluate earthquake triggering of submarine mass movements that break cables.

As part of the ComCat database the USGS also produces ShakeMaps for specific earthquakes. These maps provide estimates of ground shaking at sites depending on distance from the earthquake, the rock and soil conditions at each site and variations in the propagation of seismic waves from the earthquake resulting from complexities in the structure of the Earth's crust (Wald et al., 1999; 2005; Boore and Atkinson, 2008; Allen et al., 2009). These maps have a number of inherent uncertainties (Wald et al., 2008). Uncertainty at any point is dominated by (1) the influence of any proximal ground motion observations, and (2) estimation of ground motions from ground motion prediction equations. These uncertainties on land are compounded offshore as ground motion observations are usually unavailable. ShakeMaps are also only available for a small number of earthquakes. An independent method of producing estimates of Peak Ground Acceleration (PGA) for all the earthquakes in this study was therefore needed. This was achieved using the following empirical relationship (Si and Midorikawa, 1999).

$$\log A = b - \log(X + c) - kX \tag{3.1}$$

where A is PGA and X is fault distance in km set to 50 km. The coefficient k is fixed at 0.003. The terms b and c are calculated using the following relationships.

$$b = aM_w + hD + \sum d_i S_i + e + \varepsilon \tag{3.2}$$

$$c = 0.0055 \times 10^{0.50M_w} \tag{3.3}$$

where D is the hypocentre depth (km), S_i is fault type, ε is a standard deviation. a, h, d, and e, are regression coefficients (see Si and Midorikawa, 1999 for more detail). Analysis of which earthquake PGAs did and did not trigger mass flows requires the location of mass flow initiation to be known. The cable break database, however, only provides a location for a break and not an initiation location. A fault distance of 50 km at which to calculate PGA was therefore arbitrarily chosen to enable comparison of earthquake PGAs and triggering of mass flows. These calculations

therefore represent a simplified quantification of ground shaking and not a precise calculation of local shaking at the point of mass flow initiation (for a full discussion see Section 3.5.1).

3.3.3   How cable break and earthquake databases were compared

3.3.3.1   Earthquakes which triggered submarine mass movements

The cable break database was divided into different regions. Regions were chosen on the basis of similar seismic, sedimentary and climatic regimes. By analysing specific regions we can determine whether specific earthquake M_w can trigger submarine mass movements in each environmental setting. The regions are: (1) the Japanese Archipelago and the Korean Peninsula, (2) Taiwan, (3) Indonesia, Malaysia and the Philippines, (4) the Mediterranean, (5) the Caribbean, and (6) Pacific North America. We included all cable breaks in the dataset identified as having a seismic, landslide, chafe under current action, and other natural causes. Among these categories, cable breaks with a known cause unrelated to an earthquake were removed, e.g. shark bites. An earthquake was attributed to have caused a submarine mass movement if the cable break and the earthquake date were coincident, or within 24 h of one another. The 24 h threshold was set for an individual earthquake triggering a submarine mass movement as the database contained only the date and not the specific time of the break.

For each cable break we also analysed the earthquake record up to seven days before an actual break occurred. Longer seismic records were assessed to determine whether earthquakes swarms could be linked to cable breaks instead of individual earthquakes. In this study a swarm is defined as multiple small (<M_w 5.5) earthquakes occurring across a limited area in a short period of time, i.e. less than 7 days. If an earthquake swarm was identified as the possible triggering mechanism for the cable break, the break was not considered in the main analysis. This was because we were able to identify precisely which earthquake triggered the mass movement. The actual cause of the eventual failure may also have been repeated seismic loading rather than the final seismic acceleration of the earthquake attributed as the trigger.

3.3.3.2   Earthquakes which did not trigger submarine mass movements

All earthquakes that failed to trigger a cable break were also collated. Earthquakes were collated from ComCat using the installation and decommission dates for cables presented in the cable database. Not all of these earthquakes are displayed in the subsequent analysis. For each region only earthquakes of a specific M_w are included. The M_w of earthquakes displayed reflects the seismicity of each region, i.e. earthquakes with lower magnitudes are included in the Caribbean

analysis than are included in Japanese analysis. This decision was made due to the extremely high number of low magnitude earthquakes, which affect some regions without breaking cables.

3.3.3.3   Cable breaks prior to 1989

Cable breaks caused by earthquakes and associated submarine mass movements have been reported before the period of observation of the cable break database in this study, e.g. (Heezen and Ewing, 1952). These are not considered in this paper. The benefit of the cable break database used in this study is that we can observe when subsea cables survive seismic events. We do not have information regarding when cables were not broken in historical subsea cable networks. We would therefore bias our analysis in favour of earthquake triggering of submarine mass movements if this historical data were included within our analysis.

3.4   Results

The results section is broken up into the different regions. For each region the number of cable breaks caused by earthquakes and their magnitudes (M_w) are reported. We also show how many earthquakes of a given M_w occurred whilst cables remained operational according to the seismicity of each region. This is because smaller magnitude earthquakes are only associated with cable breaks in a few locations.

3.4.1   Japan

Between January 1990 and January 2015 there were 18 cable breaks attributed to earthquakes off Japan (see Fig. 3.2a). These breaks occurred in water depths of between 2596 m and 6945 m. During this period there was a total of 230 earthquakes $\geq M_w$ 6.0. The 18 cable breaks were associated to only 4 earthquakes with M_w ranging from M_w 7.2 to M_w 9.0. No cable breaks occurred in either the Sea of Japan or offshore Kyushu between 1990 and 2015. Earthquake swarms failed to cause cable-damaging mass flows.

The largest earthquake is the March 2011, M_w 9.0 Tohoku-oki Earthquake, which caused 15 of the cable breaks. The earthquake had a PGA >25 ms^{-1} (Fig. 3.3a). The submarine slope failure(s) triggered by the Tohoku-oki earthquake therefore were more extensive than the failures caused by the lower M_w events (Fig. 3.4). The cable breaks all occurred at the southern end of a major fault rupture in the Japan Trench, in a zone south of the submarine slumps proposed by Strasser et al. (2013) and Tappin et al. (2014). Strasser et al. (2013) contend that the observed slump did not contribute significantly to the Tohoku-oki tsunami whilst Tappin et al. (2014) suggest that the high run-up of the tsunami can only be explained by a submarine mass failure east of the central

Snariku Coast. No evidence of the mass flows are present in the cable break dataset as they occurred westward of the submarine cables running parallel to the Japanese coastline (see Figs 3.2 and 3.4). We have no evidence of major mass flows, large enough to rupture cables, triggered along the central or northern areas of the fault rupture.
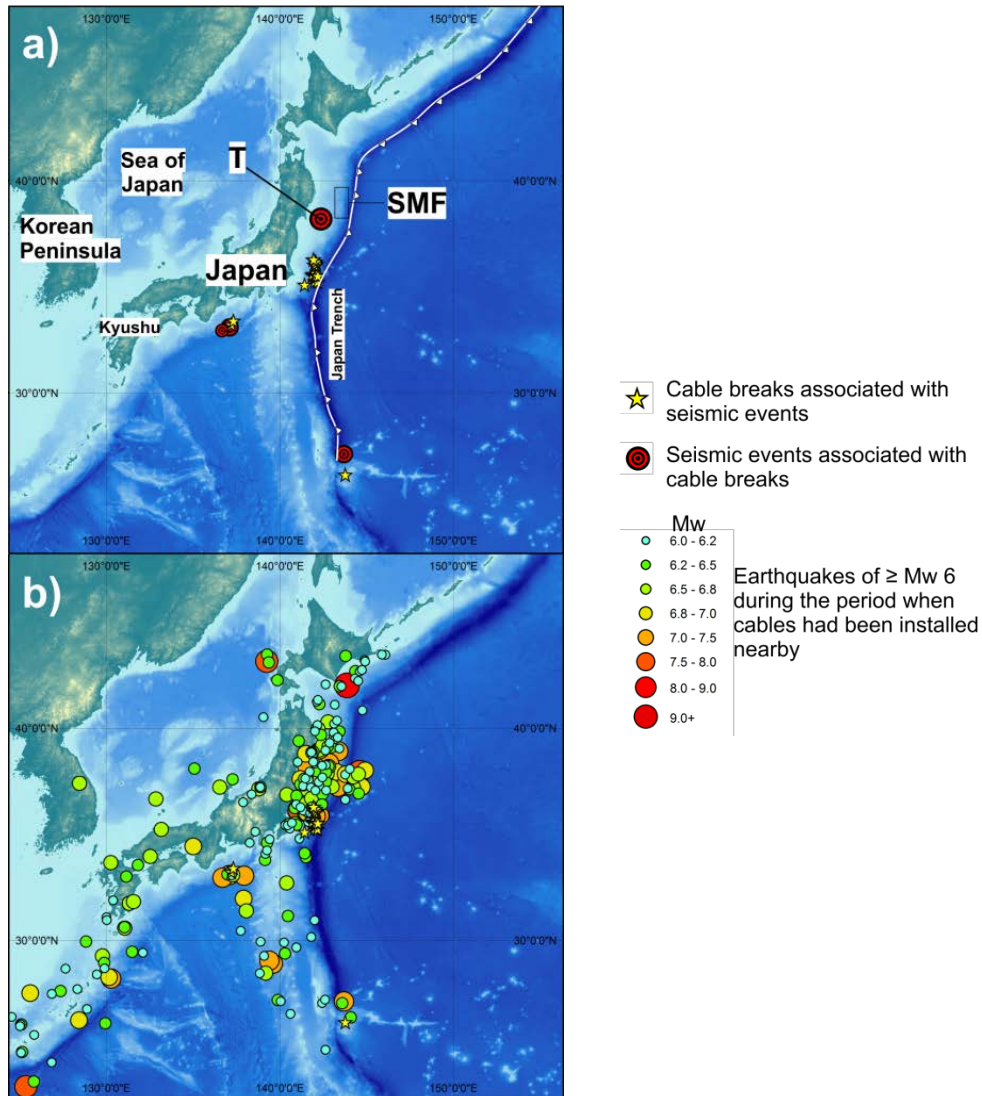
Figure 3.2 Locations of submarine cable breaks and earthquakes around Japan and the Korean Peninsula. a) Locations of submarine cable breaks (yellow stars) and the epicentres of seismic events regarded to have triggered mass flows resulting in cable breaks. Diameter of earthquake epicentres reflects the M_w of the earthquake. b) Cable breaks (yellow stars) and the epicentres of all earthquakes $\geq M_w$ 6 which occurred during the operational period of nearby cables. T = epicentre of the Tohoku-oki Earthquake. SMF = region where sediment mass failures caused by the Tohoku-oki earthquake have been thought to occur (Strasser et al., 2013; Tappin et al., 2014).
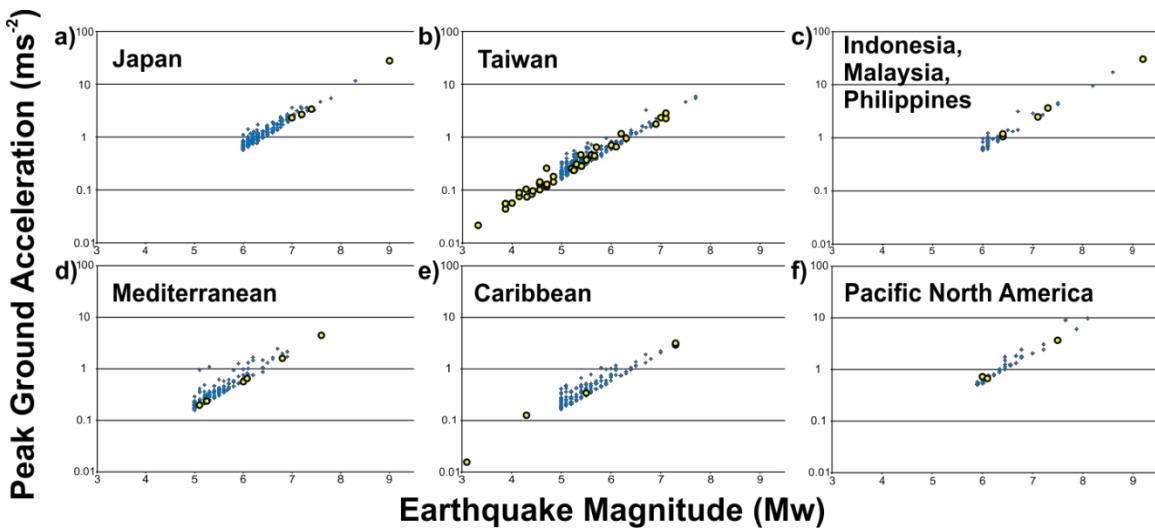
Figure 3.3 Relationship between peak ground acceleration (PGA) felt 50 km away from the epicentre and magnitude (M_w). Blue diamonds indicate earthquakes, which are not associated with cable breaks. Yellow circles with black borders indicate earthquakes, which are associated with cable breaks. a) Earthquakes in Fig. 3.2b. b) Earthquakes in Fig. 3.5b. c) Earthquakes in Fig. 3.6b. d) Earthquakes in Fig. 3.8b. e) Earthquakes in Fig. 3.9b. f) Earthquakes in Fig. 3.10b.
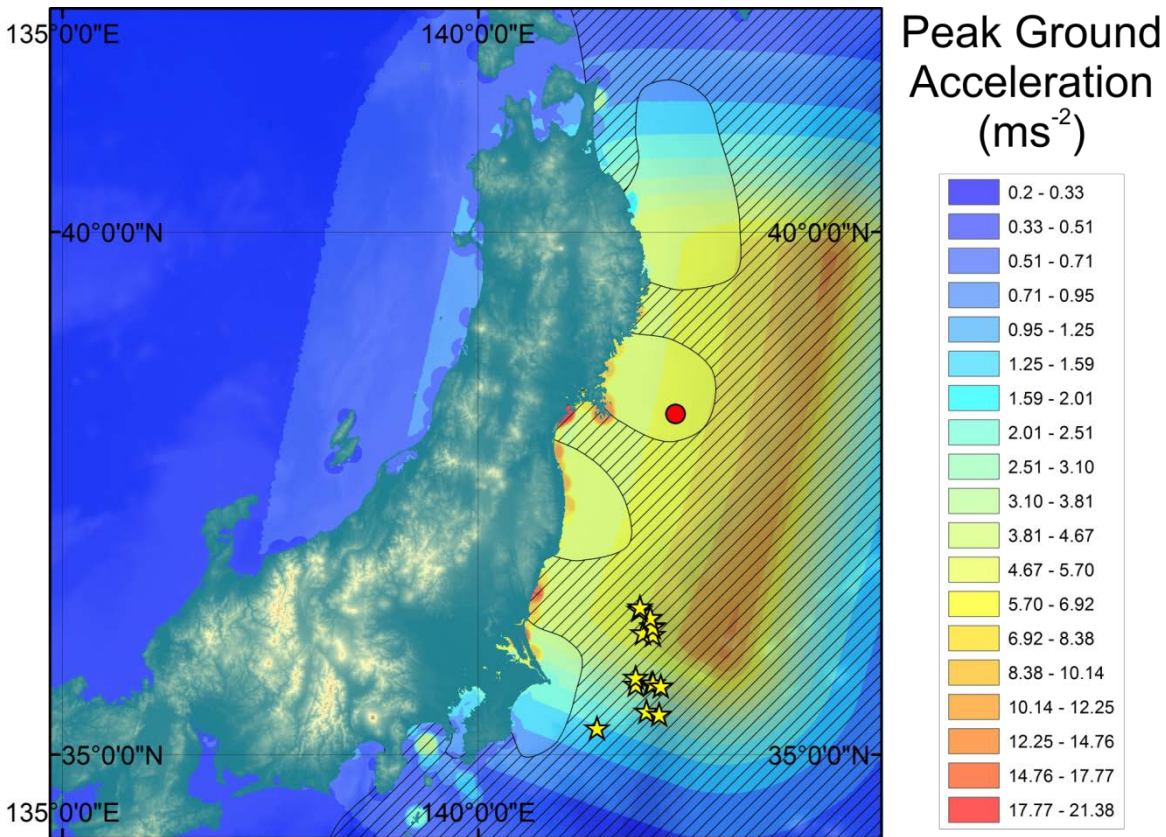
Figure 3.4 ShakeMap generated by the USGS for the Tohoku-oki 2011 Earthquake. Shows Japan with known submarine cable breaks denoted by yellow stars. Red dot represents earthquake epicentre. Areas covered with cables represented by hatch shading.

3.4.2   **Taiwan**

Between January 1993 and January 2015 there were 71 cable breaks associated with earthquakes around Taiwan (Fig. 3.5). These occurred in water depths of between 50 m and 6320 m. During this period there were 445 earthquakes $\geq M_w$ 5.0. The 71 cable breaks are related to 37 earthquakes. Earthquake M_w which triggered mass flows ranged from M_w 3.0 to M_w 7.1. There is no apparent threshold of PGA for triggering mass flows around Taiwan (Fig. 3.3b). There were no cable breaks off western Taiwan directly related to earthquakes. This is likely a consequence of the sparseness of the cable network in this area, burial of cables beneath the seabed to protect them from fishing activities and the near-flat topography of the continental shelf and seabed. In addition to the 71 cable breaks attributable to individual earthquakes there are also 10 cable breaks that may be attributed to earthquake swarms.
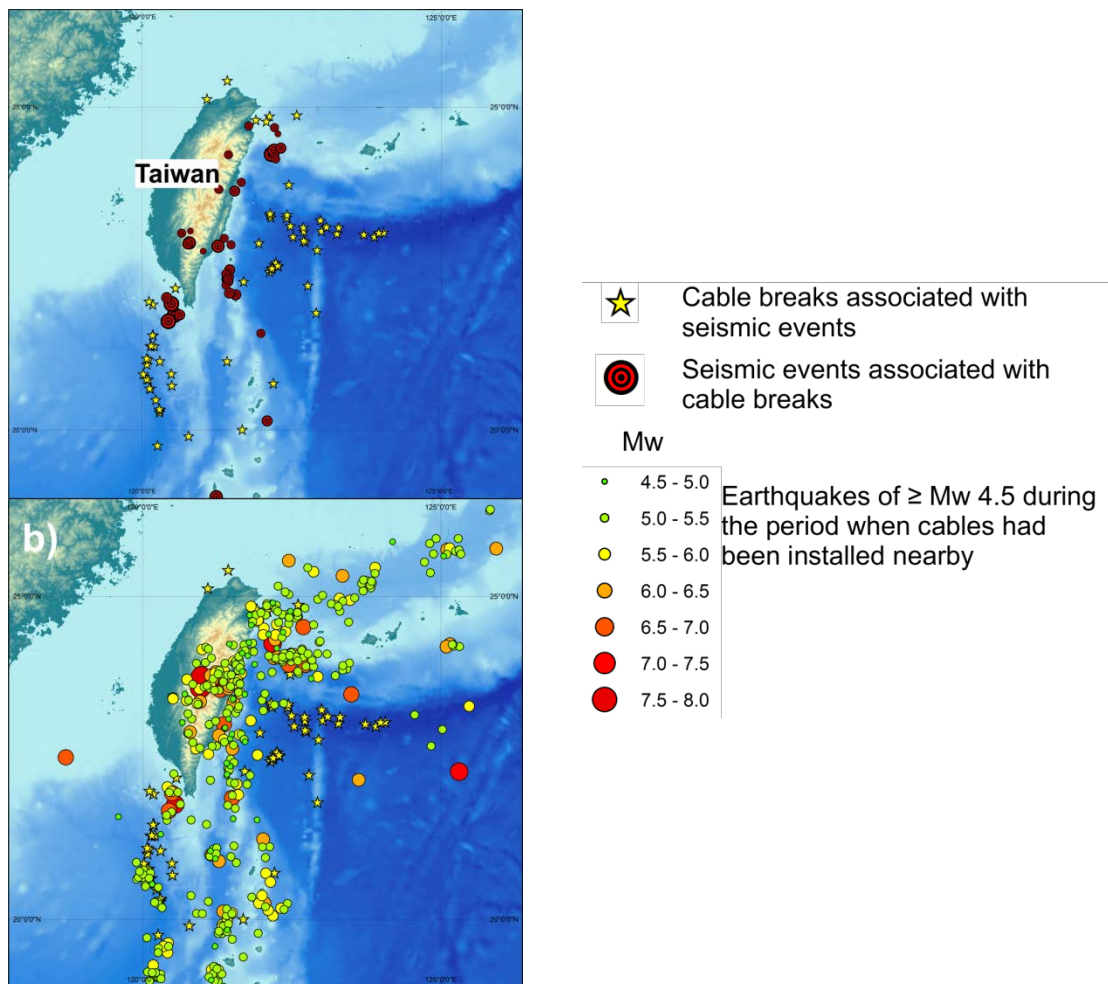
Figure 3.5 Locations of cable breaks and earthquakes around Taiwan. a) Locations of submarine cable breaks (yellow stars) and the epicentres of seismic events regarded to have triggered mass flows resulting in cable breaks. Diameter of earthquake epicentres reflects the M_w. b) cable breaks (yellow stars) and the epicentres of all earthquakes $\geq M_w$ 4.5, which occurred during the operational period of nearby cables.

3.4.3   Indonesia, Malaysia and the Philippines

Between January 1997 and January 2015 there were 7 cable breaks potentially caused by earthquakes in the region (Fig. 3.6). These cable breaks occurred in water depths of between 1000 m and 2340 m. During the period of observation there were 72 earthquakes ≥M_w 6.0, 5 of which (M_w 6.0 to M_w 9.2) caused the cable breaks. One cable break was attributed to an earthquake swarm. The greatest magnitude earthquake recorded in this region, and the largest in the database was the M_w 9.2 26/12/2004 Boxing Day Earthquake. The earthquake caused three cable breaks near the Andaman and Nicobar Islands (Figs. 3.6a and 3.7) but did not break all the cables in these areas. Three cables run between the Andaman and Nicobar Islands and perpendicular to the subduction trench. Here, only one of the cables was broken. Three subsea cables run between Sumatra and the Nicobar Islands perpendicular to the trench. Here, two of the cables were broken. The earthquake therefore resulted in flows which broke only 50% of the cables in the area.
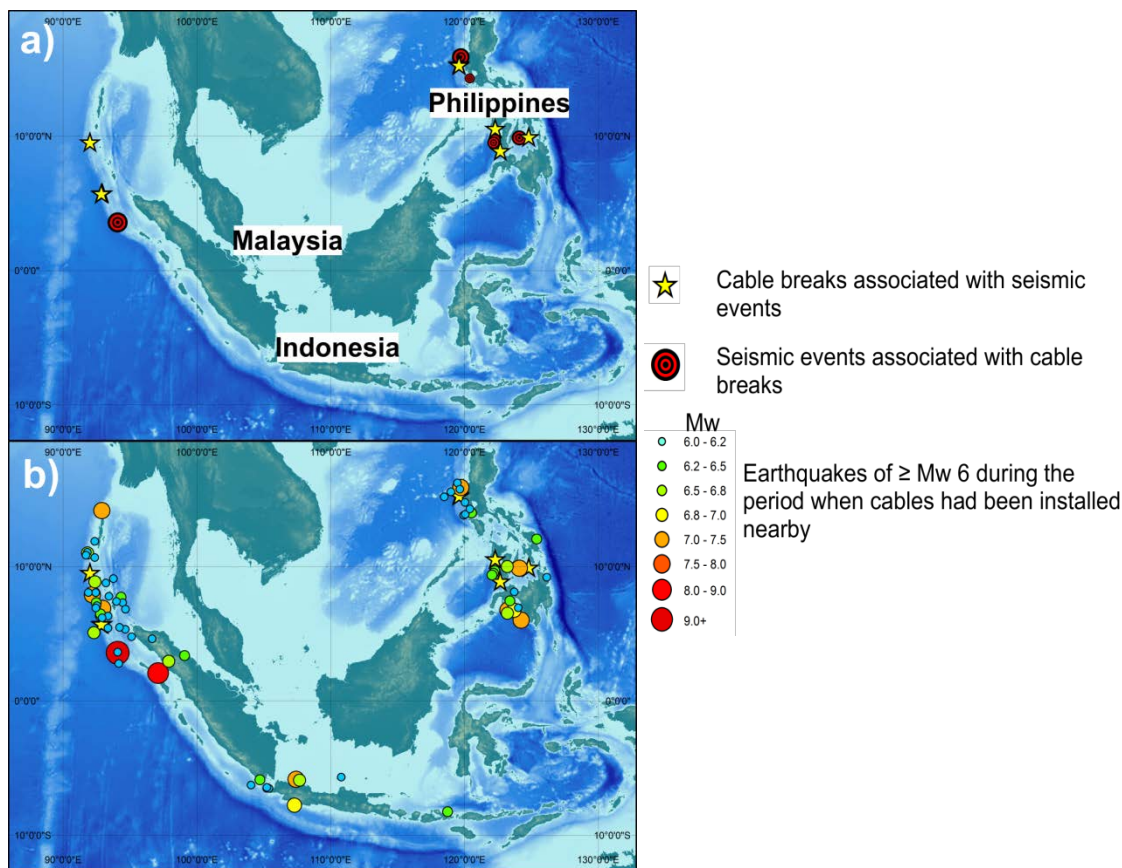
Figure 3.6 Locations of cable breaks and earthquakes around Indonesia, Malaysia and the Philippines. a) Locations of submarine cable breaks (yellow stars) and the epicentres of seismic events regarded to have triggered mass flows resulting in cable breaks. Diameters of earthquake epicentres reflect the M_w of the earthquake. b) Cable breaks (yellow stars) and the epicentres of all earthquakes ≥M_w 6, which occurred during the operational period of nearby cables.
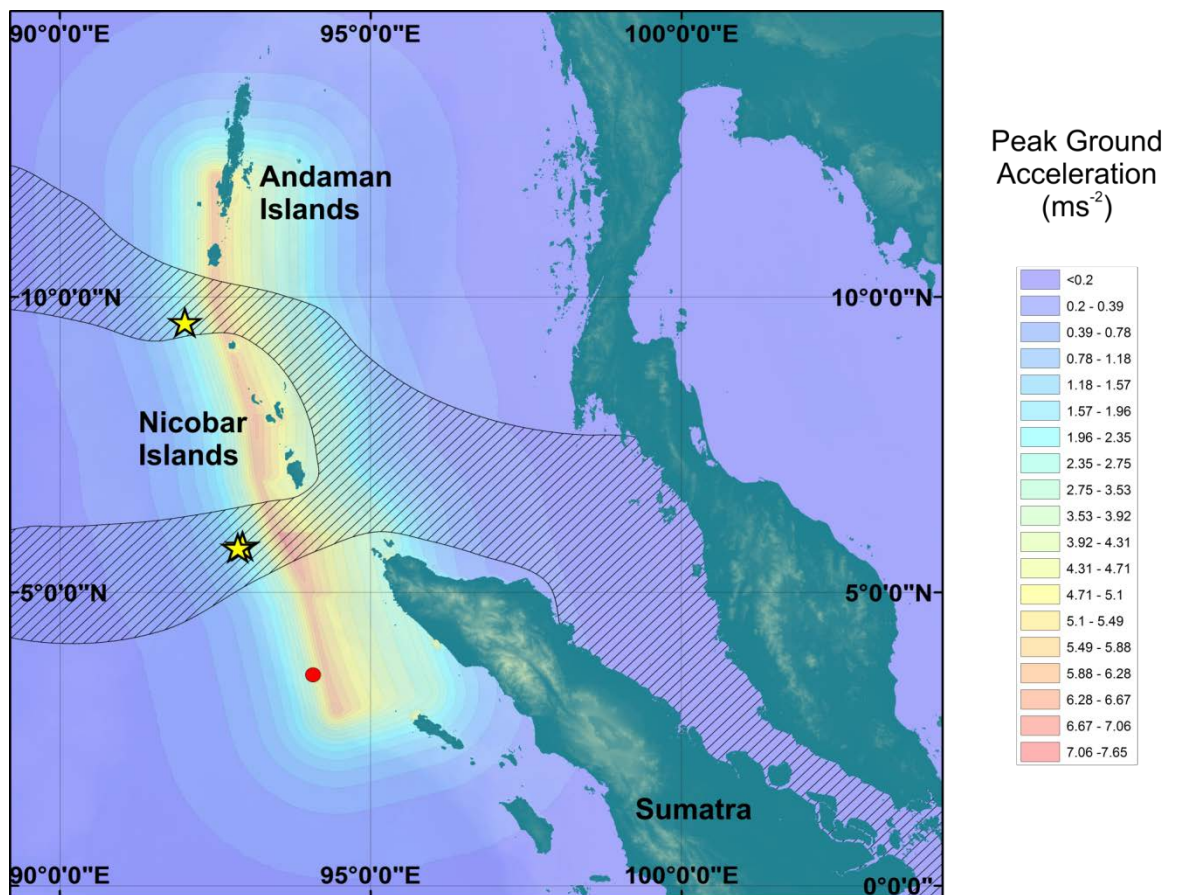
Figure 3.7 ShakeMap generated by the USGS for the Boxing Day 2004 Earthquake. Sumatra, the Nicobar and Andaman Islands, and Thailand are shown with submarine cable breaks denoted by yellow stars. Red dot represents earthquake epicentre. Hatch shading denotes the areas covered by submarine cables.

3.4.4   Mediterranean

Between January 1989 and January 2015 there were 8 cable breaks, which could be attributed to earthquakes in the Mediterranean Sea and Atlantic Ocean off Morocco and Spain (Fig. 3.8). These cable breaks occurred in water depths of between 398 m and 2739 m. During the period of observation there were 208 earthquakes ≥M_w 5.0. The 8 cable breaks are attributed to 4 earthquakes from M_w 5.1 to M_w 7.6. The strongest of these was the Izmit Earthquake in Turkey on 17/08/1999, which caused mass flows in the Marmara Sea (Tinti et al., 2006). This was the only >M_w 7.0 event during the study period. No cable breaks were reported for the same period in the eastern Mediterranean despite its relatively higher seismicity compared with the rest of the Mediterranean. The largest number of cable breaks occurred in the central Mediterranean as a consequence of the 2003 Boumerdès Earthquake. It was responsible for 28 cable breaks (Cattaneo et al., 2012). In our database this earthquake caused 5 cable breaks. The discrepancy between studies is a consequence of multiple breaks to the same cable being presented as one

cable break in our database. This large number is a consequence of the cable orientation which is parallel with the continental margin — the site of multiple landslides in the area. Two additional cable breaks occurred offshore Algeria in a similar location to the Boumerdès Earthquake breaks (Dan et al., 2009; Cattaneo et al., 2012; Ratzov et al., 2015). These are probably the result of subsequent earthquake swarms.
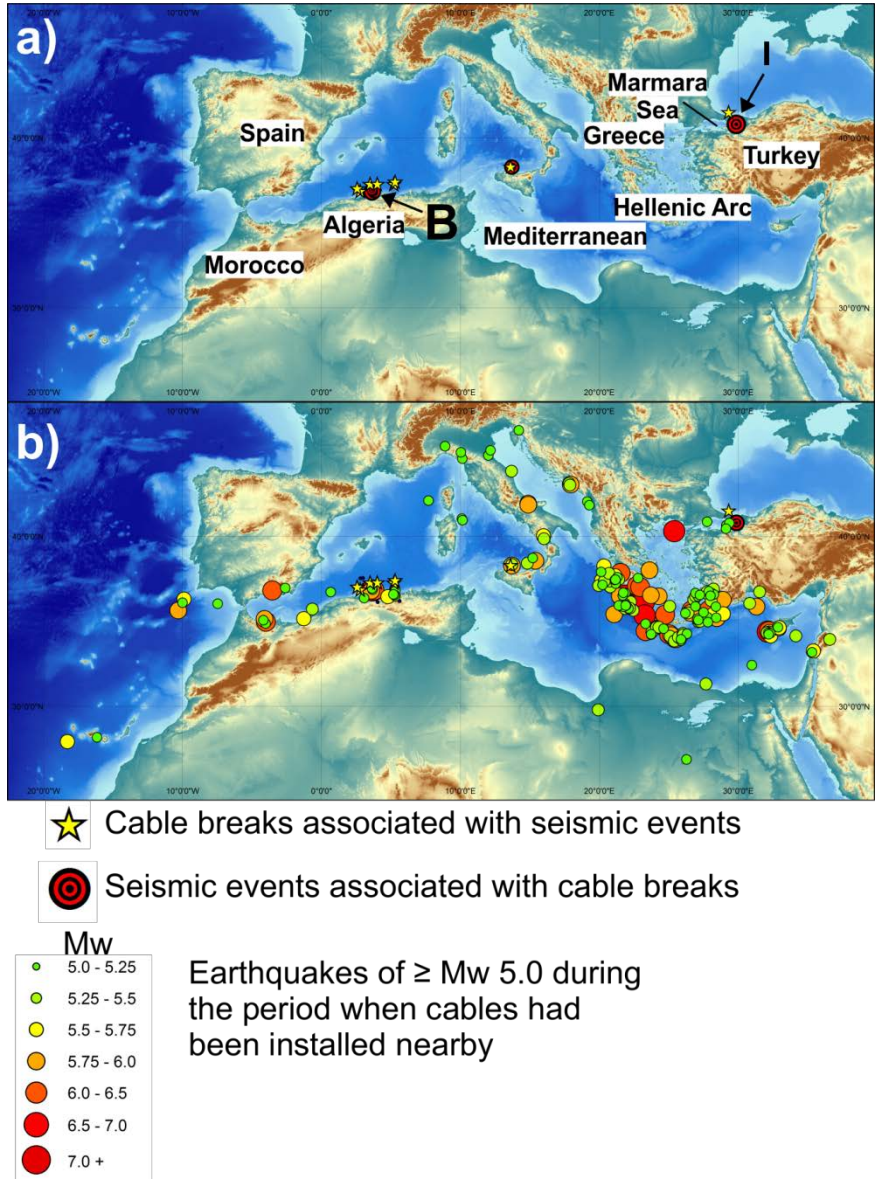
Figure 3.8 Locations of cable breaks and earthquake around the Mediterranean. a) Locations of submarine cable breaks (yellow stars) and the epicentres of seismic events regarded to have triggered mass flow resulting in cable breaks. Diameter of earthquake epicentres reflects the M_w of the earthquake. b) Cable breaks (yellow stars) and the epicentres of all earthquakes ≥M_w 5, which occurred during the operational period of nearby cables. Note B = 2003 Boumerdès epicentre; I = 1999 Izmit epicentre.

3.4.5   Caribbean

From January 1995 to January 2015 there were 5 cable breaks probably caused by earthquakes (Fig. 3.9). These breaks occurred in water depths between 558 m and 2150 m. During the period there were 170 earthquakes ≥M_w 5.0. The 5 cable breaks are attributed to 4 seismic events with magnitudes of M_w 3.1 to M_w 7.3. Every earthquake with a PGA >2.5 ms^{-2} triggered a mass flow. There were no cable breaks caused by earthquake swarms.
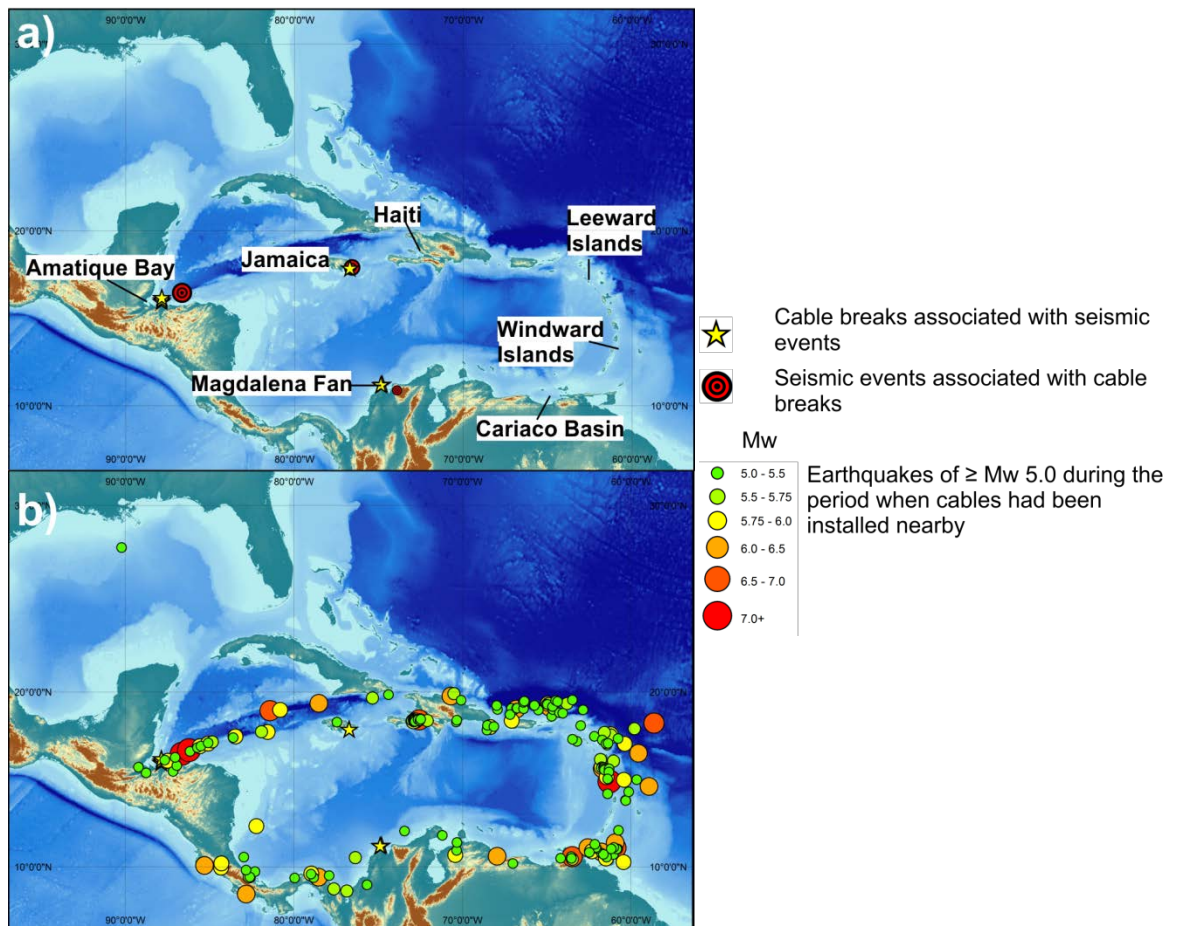
Figure 3.9 Locations of cable breaks and earthquake around the Caribbean. a) Locations of submarine cable breaks (yellow stars) and the epicentres of seismic events regarded to have triggered mass flows resulting in cable breaks. Diameter of earthquake epicentres reflects the M_w of the earthquake. b) Cable breaks (yellow stars) and the epicentres of all earthquakes ≥M_w 5.0, which occurred during the operational period of nearby cables.

3.4.6   Pacific North America

From January 1995 to January 2015 there were 5 cable breaks, which could be attributed to earthquakes in Pacific North America (Fig. 3.10). Breaks occurred in water depths of 171 m to

3220 m. During the period of observation there were 46 earthquakes of ≥M_w 6.0. All breaks are attributed to 3 earthquakes with magnitudes ranging from M_w 3.2 to M_w 7.5. The greatest M_w earthquake, M_w 8.0 (09/10/1995), was not associated with a cable break. No breaks resulted from earthquake swarms.
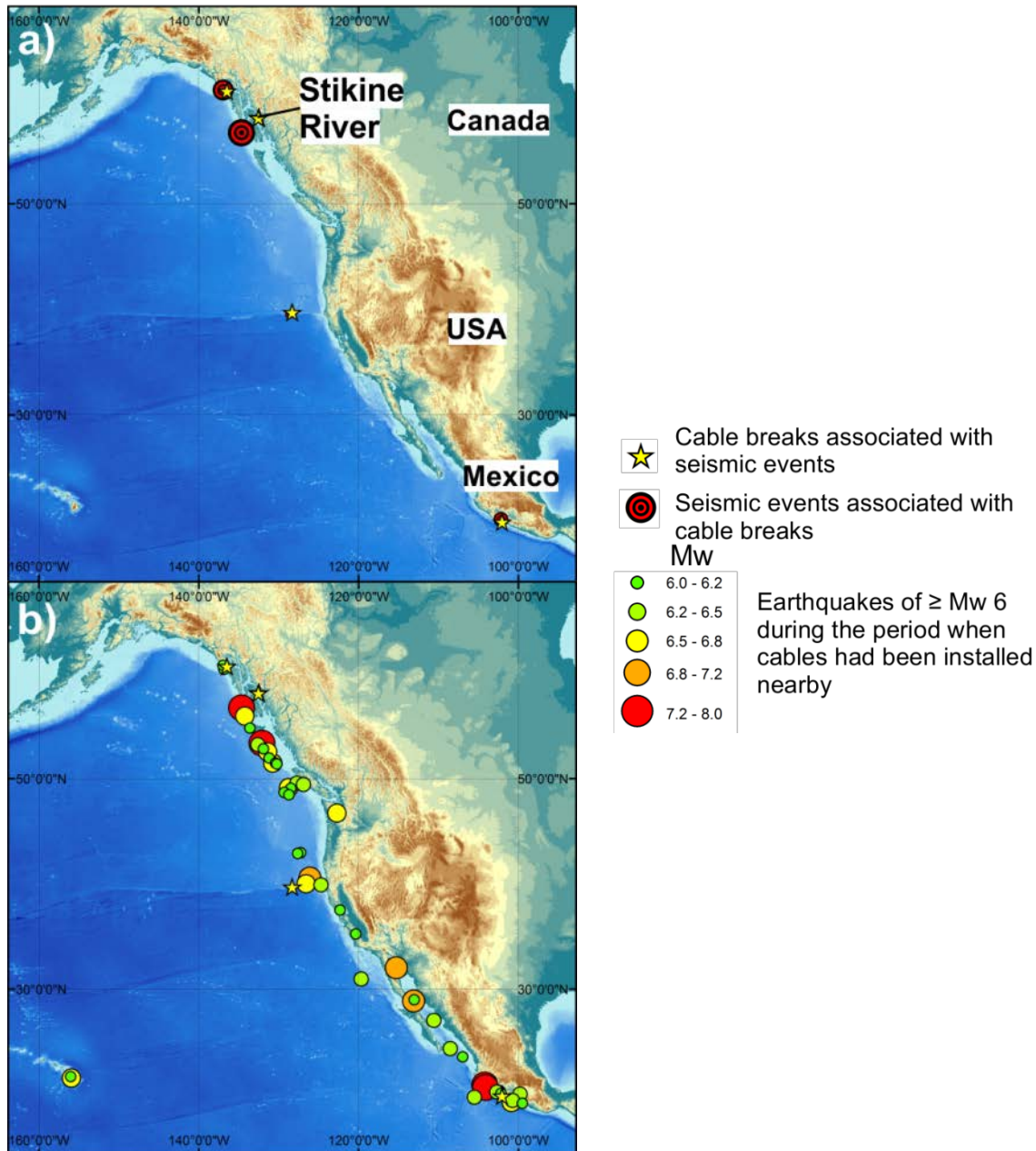
Figure 3.10 Locations of cable breaks and earthquakes around Pacific North America. a) Locations of submarine cable breaks (yellow stars) and the epicentres of seismic events thought to have triggered mass flows resulting in cable breaks. Diameter of earthquake epicentres reflects the M_w of the earthquake. b) Cable breaks (yellow stars) and the epicentres of all earthquakes ≥M_w 6 which occurred during the operational period of nearby cables.

3.4.7   Global analysis

In the cable break database there were 113 separate cable breaks caused by individual earthquakes and 13 caused by earthquake swarms. Most breaks were found around Taiwan (see Table 3.2) which reflects the high density of submarine cables, an exceptional fluvial discharge and the island's high seismicity (Milliman and Meade, 1983; Dadson et al., 2004; Kao et al., 2010; Su et al., 2012; Liu et al., 2013). Globally there was no apparent threshold of earthquake M_w for causing mass flows. Fig. 3.11 shows the 2 recorded $\geq M_w$ 9.0 earthquakes triggered mass flows, but that non all of the M_w 8.0 – 8.9 events caused mass flows. The sample size of M_w 9.0 earthquakes (N = 2) prevents any robust conclusions regarding their triggering potential. Fig. 3.11 also indicates that the number of earthquakes, which triggered mass flows increases with the frequency of earthquakes of that given M_w. However, the number of earthquakes of a given M_w does not directly relate to the number of flows triggered. With the exception of the two $\geq M_w$ 9.0 events, the cable break database does not indicate a globally consistent threshold magnitude and PGA that systematically produce mass flows.
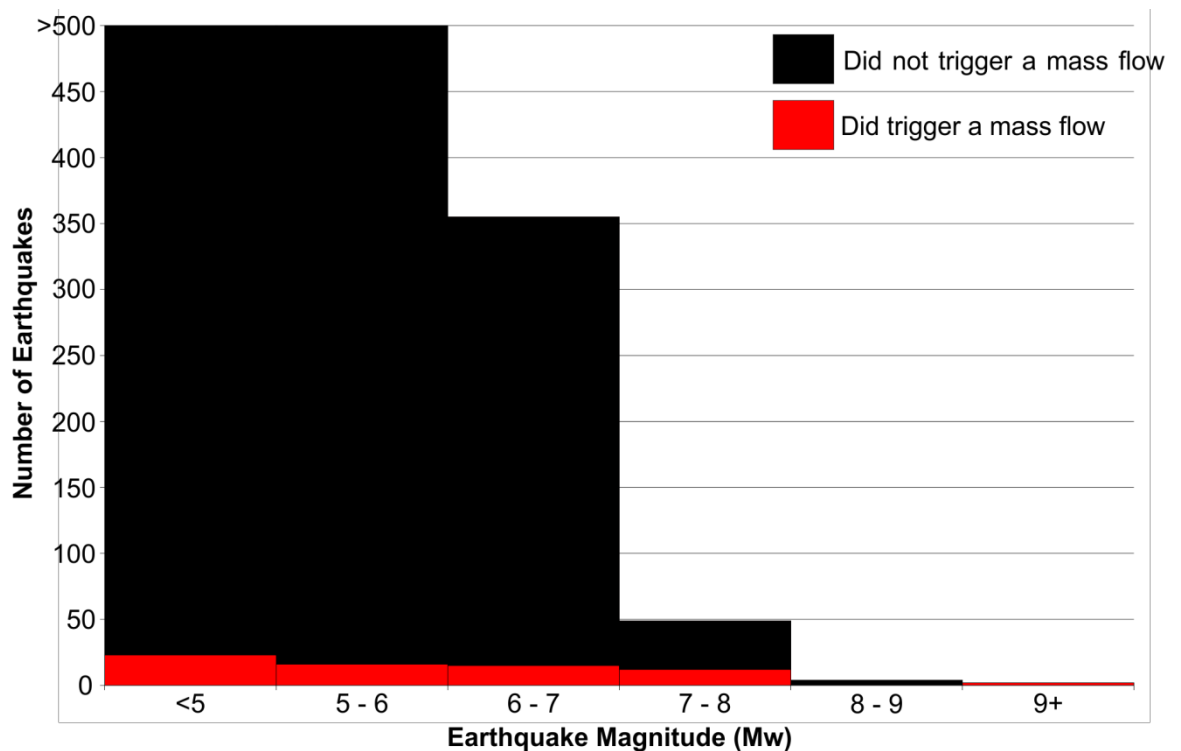
Figure 3.11 Comparison of the number of earthquakes which triggered mass flow which broke cables to those which did not trigger cable breaking mass flow events.

Region	M_w range	Triggered mass flow that broke cable	Did not triggered mass flow that broke cable	Percentage of earthquakes which triggered a mass flow
Global	6 - 7	13	350	4
	7 - 8	13	37	26
	8 - 9	0	4	0
	9+	2	0	100
Japan	6 - 7	0	176	0
	7 - 8	4	19	17
	8 - 9	0	1	0
	9+	1	0	100
Taiwan	5 - 6	12	330	4
	6 - 7	5	41	11
	7 - 8	3	3	50
	8 - 9	0	0	-
	9+	0	0	-
Indonesia Malaysia and the Philippines	6 - 7	2	49	4
	7 - 8	2	5	28
	8 - 9	0	2	0
	9+	1	0	100
Mediterranean	5 - 6	1	167	100
	6 - 7	3	28	10
	7 - 8	1	0	100
	8 - 9	0	0	-
	9+	0	0	-
Caribbean	5 - 6	1	144	0.7
	6 - 7	0	22	0
	7 - 8	2	2	50
	8 - 9	0	0	-
	9+	0	0	-
Pacific North America	6 - 7	3	37	5
	7 - 8	1	6	14
	8 - 9	0	1	0
	9+	0	0	-

Table 3.2 Counts of earthquakes which trigger mass flows which broke cables and earthquakes which did not trigger mass flows that broke cables. Counts for each region are stated as well as the total counts for all regions.

3.5   Discussion

3.5.1   Uncertainty within the cable break analysis

Access to the cable break database is extremely valuable for identifying which earthquakes trigger, and do not trigger, submarine mass movements. However, a number of the following

points should be noted. First, in most cases the coincidence of cable breaks with earthquakes is compelling. However, we cannot say with absolute confidence that each submarine mass movement was triggered by the earthquake itself, or if other triggering mechanisms also occurred on the same day as the earthquake. Such a coincidence is, however, relatively unlikely. It is also possible that the submarine mass movement occurred independently of the earthquake which we have identified as being the triggering mechanism.

Second, the cable break database is a record of where a submarine mass movement has broken a cable. It does not indicate the location of the initial failure of the seafloor. We have therefore been unable to calculate a PGA for the mass failure initiation location. Nor is it appropriate to calculate the PGA at the cable break location as flows are capable of running out 100s of kilometres. The decision was therefore made to choose an arbitrary distance from the epicentre of each earthquake, namely 50 km, in order to calculate comparable PGAs for each earthquake (Campbell, 1997, 2003). It must, however, be recognised that this represents a simplification of a complex processes. A large magnitude (>8 M_w) will result in a large rupture zone compared to a small magnitude earthquake. The area that will therefore be affected by the highest PGA values for a given earthquake will be highly variable (Wells and Coppersmith, 1994). Our analysis simplifies these differences meaning that there remains a large uncertainty with regards to the relationship of the area of the seafloor impacted by high intensity seismic shaking and the initiation of mass flows.

Third, the cable break database may not represent every submarine mass movement. To break a cable, the flow has to impart sufficient force to physically stretch and break the cable, or abrade the casing. The required force to achieve this varies according to flow type (see Section 3.2), cable type (armoured, not armoured, etc.), the age of the cable, orientation to the mass flow and the amount of slack or whether the flow buries the cable rather than breaks it. Even where flows have been sufficiently powerful to break a cable, it has been shown that it may not break all adjacent cables (Hsu et al., 2008; Carter et al., 2012). If a flow fails to break a cable it will not be registered. A limitation of cable break techniques used to detect flows is that they are partly controlled by the distribution of cables. Globally, the ocean coverage by cables is uneven (see Fig. 3.1). Areas such as Taiwan have a high density of cables compared to other regions such as the Eastern Pacific. The combination of these factors means that it is more likely that submarine mass movements will be identified in areas with high cable densities. Thus flows may not be captured where cables are sparse, such as off South America (Fig. 3.1).

A number of examples of where mass flows are known to have occurred but have not been detected by the cable break database exist. First, the Haiti Earthquake on 12/01/2010 did not

produce a mass flow according to the cable break database, as no cables were broken. However, McHugh et al. (2011) report core evidence of a turbidite derived from the earthquake. The location of the cores and the local bathymetry suggest that the cable in the area was not affected by the flow. They suggest that from its initial triggering location, the bathymetry would have interacted with the flow resulting in it being diverted away from the cable. Second, turbidity currents appear to have been triggered by earthquakes in the Cariaco Basin, Venezuela (Lorenzoni et al., 2012). An active cable is present across the basin but was not broken. Possible explanations for this are (1) a turbidity current was triggered but it was of insufficient strength to break the cable; (2) the cable was protected by local bathymetry or was buried by the turbidity current; or (3) the increased backscatter which was recorded by optical instruments in the basin was actually measuring an increase in river suspended sediment as a result of the earthquake but not a turbidity current. Unfortunately, the correct scenario remains as yet unclear.

Fourth, not all cable breaks worldwide during the study period are recorded in the database. The database is a compilation of breaks repaired by Global Marine Systems Ltd. together with other breaks reported by clients and collaborators. There may, however, be cable breaks that are unreported.

3.5.2 Which magnitude earthquakes do and do not trigger submarine mass movements?

3.5.2.1 Is there an earthquake magnitude that will systematically trigger a mass flow?

It is well known that earthquakes trigger sub-aerial landslides (Keefer, 1984). The minimum earthquake magnitude often cited to trigger a sub-aerial landslide is ~M_w 5.0 (Keefer, 1984, 2002). In submarine environments earthquakes of >M_w 5.0 have been suggested to cause small volume failures (Niemi and Ben-Avraham, 1994; Piper et al., 1999; Lorenzoni et al., 2012; Patton et al., 2013). Magnitudes >M_w 7.0 have been cited as the minimum required for the generation of a turbidity current through the triggering of a submarine landslide (Nakajima and Kanai, 2000; Goldfinger et al., 2003; Pouderoux et al., 2012; Moernaut et al., 2014). The cable break database does not, however, demonstrate that earthquakes >M_w 7.0 will necessarily generate submarine mass movements, or at least mass flows sufficiently powerful to cause cable breaks. In every region, except the Mediterranean (see Figs 3.3d and 3.8b), there are >M_w 7.0 earthquakes that failed to generate mass flows with sufficient force to break a cable (Fig. 3.3).

In the regions considered in this study there were 365 earthquakes between M_w 6.0 and M_w 7.0; 43 earthquakes between M_w 7.0 and M_w 8.0; 4 between M_w 8.0 and M_w 9.0 and 2 ≥M_w 9. The proportions of these earthquakes which did and did not trigger flows are outlined in Table 3.2.

If we consider PGA rather than M_w as the factor affecting mass flow formation, a similar relationship can be seen (Fig. 3.3) Both M_w ≥9 earthquakes generated mass flows which broke cables. These earthquakes had PGAs >25 ms^{-2}. The PGAs of the 4 M_w 8.0 earthquakes varied between 8.5 and 17 ms^{-2}, yet no mass flows were generated. These PGA values all exceed the threshold for slope failure and turbidity current generation as proposed for the Hikurangi Margin, New Zealand (Pouderoux et al., 2014), the Eel Margin, California (Lee et al., 1999), the Aegean Trough, Mediterranean Sea (Lykousis et al., 2002) and the Southern Kuril Trench, North Pacific Ocean (Noda et al., 2008). Considering the PGA values of earthquakes <M_w 8.0, there is no simple relationship between earthquakes which do, and do not, trigger mass flows according to the cable break database. Worldwide, increasing PGA, increases the probability that a submarine mass failure will occur, but it does not necessitate one.

3.5.2.2   What is the minimum earthquake magnitude which can trigger a mass flow?

The minimum earthquake magnitude previously suggested to be capable of triggering a submarine mass movement is ~M_w 5.0. However, the cable break database contains information contrary to this assumption. Individual earthquakes with M_w as low as 3.1 are shown to have triggered mass flows in two locations (see Fig. 3.3). Whilst these may be rare (there are only 2 in the database) there are a large number of earthquakes with M_w between 4.0 and 5.0 which have caused cable breaking mass flows (15 events). In both cases, however, these represent only a very small proportion of the number of M_w 3.0 − 5.0 earthquakes which occur globally every year. These records indicate that certain conditions can arise on the seafloor where the release of small amounts of energy from low magnitude earthquakes can cause slope failures. From our analysis these conditions appear to be most prevalent around Taiwan (see Fig 3.3).

3.5.2.3   Earthquake swarms

The cable break database contains 11 cable breaks which have been caused by mass flows triggered by earthquake swarms. The spatial characteristics of these events closely match those for mass flows triggered by individual earthquakes. The majority of earthquake swarm triggered flows (8) occurred offshore of Taiwan. The continental slopes in these locations may therefore be more susceptible to failure resulting from seismic shaking as a consequence of local site characteristics (see subsequent discussion).

The two earthquake swarms which triggered mass flows in the Mediterranean occurred shortly after the 2003 Boumerdès Earthquake, which itself triggered 5 cable breaks. These events add a further degree of complexity to understanding which earthquakes do (and do not) trigger flows. The flows triggered as a result of the earthquake swarms occurred within 2 months of the main

earthquake and consequently there are two possible explanations for their triggering. First, the main earthquake preconditioned the slope to further failures. This could have been the result of either unloading as a consequence of the landslides triggered by the main earthquake or weakening of the substrate due to the shaking itself. Both scenarios facilitate slope failures to be triggered by further low intensity seismic shaking. Second, the large number of landslides caused by the main earthquake indicates that the continental slope in the region was susceptible to failures caused by seismic shaking. Therefore, the low intensity high frequency shaking associated with the earthquake swarms may have been sufficient to trigger mass flows. In either case, identification the different timing of the swarm related flows to the main earthquake triggered flows would be extremely difficult using only their deposits.

3.5.3   Is there a regional relationship between seismicity, sediment supply and mass flow occurrence?

Here, we discuss the relationships observed between earthquake magnitude and cable breaks for the regions outlined in Section 3.4.

3.5.3.1   Japan

The Japan results support previous suggestions that submarine slope stability is greater in high magnitude seismic areas (Noda et al., 2008; Sumner et al., 2013). No earthquake <M_w 7.0 triggered a submarine mass movement in the Japanese region. This could either mean that there was no sediment suitable for mass flow formation or repeated ground shaking has resulted in consolidation and strengthening of seafloor sediments (Lee et al., 1993; 1996; Sultan et al., 2004; Vanoudheusden et al., 2004; Völker et al., 2011; Sumner et al., 2013). Enhanced consolidation resulting from seismic shaking is made more likely by low sediment supply to the continental shelf in this region (Fig. 3.12). The low sediment supply prevents large accumulations of unstable sediment from developing. Thus the likelihood of weak seismic shaking causing a slope failure is greatly reduced resulting in the small number of triggered mass flows that we observe. Enhanced consolidation of seafloor sediment would also reduce the probability that large magnitude earthquakes will trigger mass flows; the cable break database suggests that out of the 25 earthquakes with ≥M_w 7.0 only 5 of these actually triggered mass flows.

3.5.3.2   Taiwan

In contrast to Japan, earthquakes ranging from M_w 3.7 to M_w 7.1 triggered mass flows causing cable breaks off Taiwan. The magnitude range and the number of cable breaks, suggests that the continental slopes offshore Taiwan are inherently more unstable than other areas within this

study as events are commonly triggered by very low M_w earthquakes. The preponderance of mass flows off Taiwan is likely due to local site characteristics.
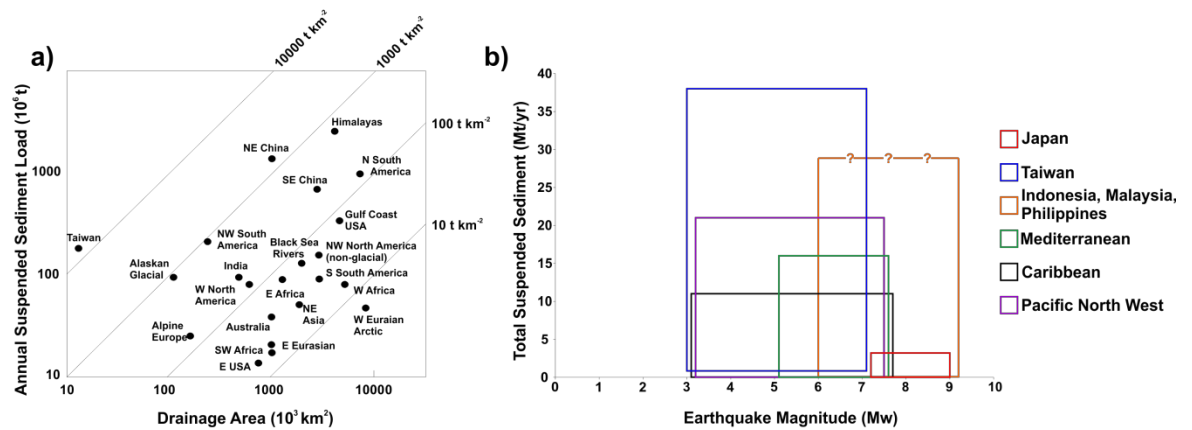
Figure 3.12 a) Variations of annual suspended sediment load with drainage area (Milliman and Meade, 1983; Milliman and Farnsworth, 2011). Compared to the rest of the world, Taiwan is shown to be exceptional in terms of the volume of sediment generated when the drainage area of its rivers is taken into consideration. b) Range of estimated total suspended sediment discharged by major rivers within each study area where earthquakes have occurred against earthquake magnitudes known to trigger cable breaking flows. The volume of discharged sediment from Taiwan is shown to be exceptional. There is a large amount of uncertainty regarding the maximum amount of total suspended sediment discharged from rivers in Indonesia, Malaysia and the Philippines. This is a consequence of the lack of data for the majority of large rivers in the regions where earthquake occur. Note that the total suspended sediment discharge data from the Magdalena River (140 Mt yr^{-1}; Milliman and Farnsworth, 2011) has been omitted from the figure due to its exceptional nature compared to other rivers in the Caribbean region. There is also a lack of sediment discharge data from rivers on small Caribbean islands.

A combination of active tectonism, steep topography, heavy rainfall and intense human activity results in sediment discharge from Taiwan of 180 – 380 Mt a^{-1} (Dadson et al., 2004; Kao et al., 2010; Liu et al., 2013). This reflects an erosion rate 50 times more than the global average (see Fig. 3.12). A narrow eastern continental shelf, steep continental slope (Ramsey et al., 2006) and large volumes of poorly consolidated sediment that are replenished annually, collectively favour formation of seismically induced mass flows compared to almost any other location worldwide (Milliman and Meade, 1983; Milliman and Syvitski, 1992). Large numbers of cables also cross submarine canyons offshore Taiwan and lie perpendicular to the flow direction. The likelihood

that they will be hit by a channelized flow sufficiently strong enough to break them is therefore increased.

Despite the favourable conditions for seismically triggered mass flow events, the three largest earthquakes (M_w 7.0 – 8.0) did not trigger mass flow events. It is remarkable that earthquakes which do not trigger mass flows can have PGAs two orders of magnitude greater than those that have triggered mass flows. It is also noteworthy that the 2006 M_w 6.9 Pingtung Earthquake (M_L 7.0) caused a turbidity current which broke 14 subsea cables and ran out >300 km, but larger earthquakes did not trigger similar flows. Understanding why very small earthquakes triggered mass flows whilst large earthquakes do not produce mass flow events is a crucial question with regards to understanding the triggering mechanisms of submarine flows.

3.5.3.3   Indonesia, Malaysia and the Philippines

Contrasts between the sedimentary regimes across the region are shown by their response to earthquake shaking. Only the M_w 9.2 Boxing Day Earthquake was able to trigger a mass flow event capable of breaking cables offshore of Sumatra, Java and the Andaman and Nicobar Islands. Neither M_w 8 earthquakes nor lower M_w earthquakes generated mass flows. Whilst the full impact of the Boxing Day event cannot be realised because of an absence of cables it appears that this area has a similar sediment consolidation regime to Japan. It is, however, difficult to directly compare the flow responses to the Boxing Day Earthquake and the Tohoku-oki Earthquake as a consequence of the contrasting cable coverages. Japan has at least 25 cables whilst Sumatra has about 5. This means that realistic comparisons can only be made through extensive sedimentary and geophysical surveys of both margins to identify mass flow deposits. It also means that the likelihood of detecting events from smaller earthquakes is much higher around Japan than Sumatra.

In contrast to Sumatra, around the Philippines, earthquakes between M_w 7.3 and M_w 6.4 triggered flow events. Lower magnitude earthquake swarms have also triggered mass flows. Like Taiwan, a large amount of sediment is discharged annually from the Philippines as a result of high annual precipitation, typhoons and readily eroded rock (Milliman and Meade, 1983; Milliman and Farnsworth, 2011). It is therefore unsurprising that all of the cable breaks are within 50 km of the shore and are associated with river mouths as large amounts of sediment is deposited annually in these locations. Compared to Taiwan, there are comparatively few breaks in this area which is likely a result of (1) the low density of the cable network; (2) the younger age of much of the cable network; (3) a lower seismicity regime than Taiwan and, (4) the limited number of cables which cross submarine canyons. It is likely therefore that more flows occurred in this region than have been documented.

3.5.3.4   Mediterranean

The seismic and sedimentary regimes of the Mediterranean are highly variable. The majority of earthquakes in the region occurred around Greece and the Hellenic Arc (Fig. 3.8). Previous studies have identified that despite the irregular, steep relief, active faults and high seismicity seen around Greece and the Hellenic Arc there are comparative few slope failures (Chronis et al., 2000; Camerlenghi et al., 2010; Strozyk et al., 2010). Few slope failures occur as a consequence of tectonically exhumed sediments being over-consolidated and bear high shear resistance and thus need a large earthquake to induce failure (McAdoo et al., 2000; McAdoo and Watts, 2004). Our results support these assertions suggesting similar processes to Japan and Sumatra.

3.5.3.5   Caribbean

The Caribbean shows large contrasts between different areas in terms of triggering regimes. Half of the M_w 7.0 earthquakes triggered mass flows. These cable breaks occurred just east of Amatique Bay, Guatemala. In the rest of the Caribbean there was no evidence of a mass flow triggered by an earthquake with a M_w >5.5. The other flows triggered by low magnitude events occurred on river fans along channels where turbidity currents have previously been identified. Cable breaks offshore Colombia occurred on the Magdalena Fan. Previous studies of the fan have shown that it regularly produces turbidity currents (Ercilla et al., 2002aa; 2002bb). Numerous historical cable breaks associated with this system have also been documented (Heezen, 1956). The cable break south of Jamaica also occurred in a region with an active turbidity current system (Burke, 1967). In these locations, it appears that earthquakes are one of multiple triggering mechanisms causing mass flows but that high sediment supply is a vital component to their occurrence (Fig. 3.12b). In contrast, no earthquake triggered a mass flow around the high seismicity regions of the Windward and Leeward Islands (Fig. 3.9). This is likely due to a lack of available sediment resulting from limited river catchments and transportation of sediment.

3.5.3.6   Pacific North America

The three strongest earthquakes in this region did not trigger mass flows (see Fig. 3.3). The strongest earthquake (M_w 7.5) which triggered a mass flow, resulted in the failure of the Stikine River delta (Wilt, 2015). This delta failure and the proglacial delta failure which was caused by a low M_w earthquake swarm clearly demonstrate the importance of sediment supply. Large numbers of cable breaks have also previously been identified in similar high sediment supply areas (see Fig. 3.12) in Western Canada and Alaska (Heezen and Johnson, 1969). However, the number of cables in this region has significantly decreased and thus the number of earthquake triggered flows which have not interacted with cables is likely much higher.

In terms of the regional picture of mass flow triggering a number of addition features must also be recognised. First, a number of earthquakes produced very different sedimentary responses offshore Mexico. Here, a M_w 6.0 earthquake triggered a cable breaking flow. However, neither a M_w 8.0 earthquake nor the M_w 7.6 in the same area triggered a mass flow. Assuming that the properties of the sediment did not drastically change, this observation is problematic for estimating which earthquakes should and should not trigger mass flows. Second, during the period of observation there was only 1 M_w 8.0 earthquake and none larger. Therefore the dataset of large magnitude events are too small to determine their capability to trigger mass flows.

3.5.4   Implications of the cable break database for turbidite palaeoseismology linking deposits to earthquake magnitudes

Turbidite palaeoseismology relies on specific large earthquake magnitudes generating recognisable turbidites (Atwater and Griggs, 2012; Goldfinger et al., 2012; Gràcia et al., 2013; Atwater et al., 2014). For this to be robust, similar earthquakes of a given magnitude should generate similar deposits. The relationship between earthquake magnitudes and deposits does not have to be globally consistent. However, it does require regional consistency.

Our analysis of the cable break database shows there to be large regional variations in terms of the earthquake magnitudes which will trigger mass flows. These variations appear to be driven by a combination of the local seismicity and the supply of sediment. In order for turbidite palaeoseismology to be robust for a specific region, local sediment supply and slope response to earthquake shaking needs to be quantified. It is also important to recognise that the cable break database has implied that local responses to earthquakes of the same magnitude are not always similar. Around Japan the cable break database suggests that only ≥M_w 7.0 earthquakes will generate slope failures. Other studies using historical records around Japan support this conclusion as they find turbidites associated with known ≥M_w 7.0 earthquakes (Noda et al., 2008; Shirai et al., 2010). However, the cable break database suggests that not all ≥M_w 7.0 earthquakes produce mass flows. Therefore if it is assumed that all ≥M_w 7.0 earthquakes produce mass flows and that such flows produce turbidites, then the palaeoseismology studies using cores will underestimate turbidite frequency and hence the frequency of ≥M_w 7.0 earthquakes. These studies will also have to reconcile the problem of turbidites resulting from low magnitude earthquakes and earthquake swarms.

Quantifying uncertainties in turbidite palaeoseismology studies is extremely challenging. These uncertainties also directly affect our cable break analysis. Fig. 3.13 represents a possible Bayesian network for assessing the probability of an earthquake triggering a mass flow and it being

detected by the cable network. We have not tried to assign probabilities to each node, nor define relationships between nodes. Currently we feel that any measurement of likelihood in a given scenario would be artificial. This is a result of the degree of uncertainty that still exists in terms of flow triggering and flow interaction with cable networks that we have outlined above. A more reliable application of Bayesian networks to the different areas could be made once local geotechnical data regarding local geological conditions has been obtained. Once this is achieved, the results can be directly applied to future studies using cable breaks; information which can be subsequently applied to turbidite palaeoseismology studies.
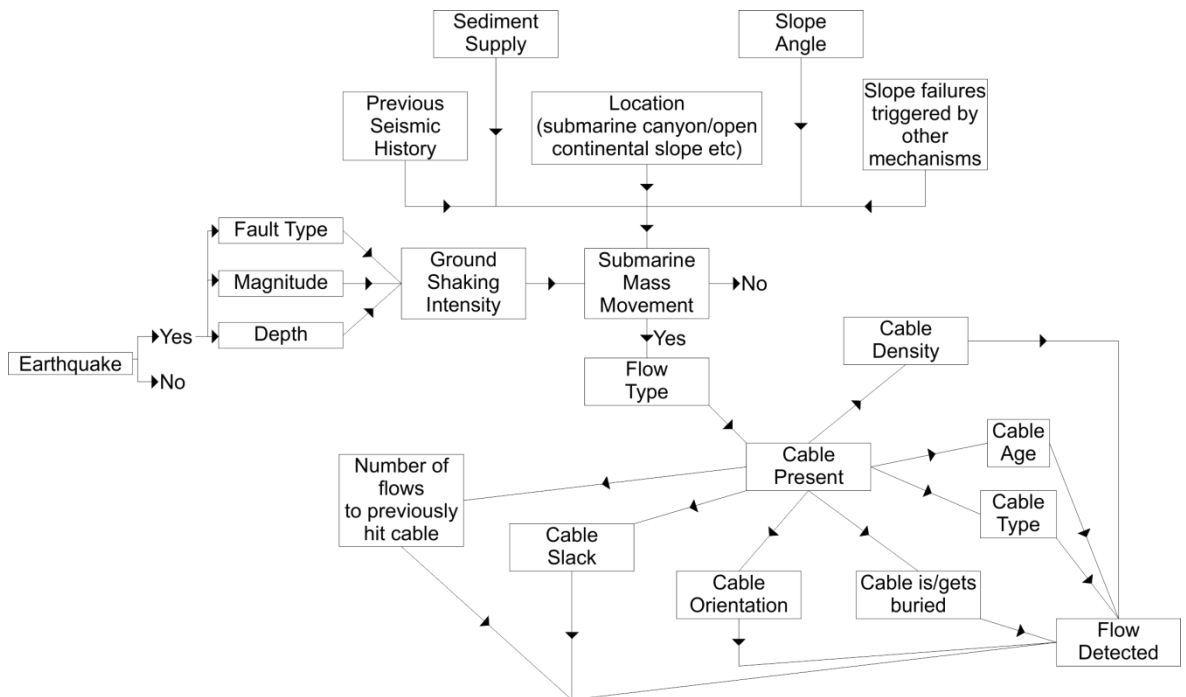
Figure 3.13 A possible Bayesian network for assessing the probability that a cable would be broken by an earthquake triggered mass flow.

3.6   Conclusions

Submarine mass movements are known to have several triggers. This study is the first to identify earthquake triggered submarine mass movements worldwide. The primary conclusion is that there is no obvious earthquake magnitude, which will consistently trigger a submarine mass flow. The only possible exception is that all M_w 9.0 earthquakes trigger submarine mass flows. However, the small number of M_w 9 earthquakes (2) is too small to make any robust conclusions.

Second, it appears that the relationship between earthquake magnitude, peak ground acceleration and the triggering of mass flow events varies on a regional basis. In some regions small magnitude (M_w 3.0 – 5.0) earthquakes can trigger mass flows whilst in others mass flows

can only be triggered by large earthquakes ($\geq M_w$ 7.0). This is a response to variations in regional sediment supply, submarine topography, seismic regime and their temporal variability.

Third, not all earthquakes above a certain magnitude generate powerful (cable breaking) submarine mass movements. Indeed, globally only 15 of 56 (27%) earthquakes above M_w 7.0 produced mass flows that broke cables. This suggests that not all major earthquakes may produce powerful flows that cover large areas.

Subsea cables have been clearly shown to be an important means of detecting submarine mass flows. However, the use of cables has limitations that include (i) uneven distribution through the world ocean, (ii) only detect mass flows sufficiently powerful to break cables, (iii) several cables can respond differently to the same mass flow, i.e. some break whilst others remain intact, the causes of which are unclear and (iv) the absence of a fully comprehensive universal cable break database.

Chapter 4:   How do tropical cyclones trigger damaging sediment density flows?

Summary

Chapter 4 analyses the triggering of submarine mass movements as a result of tropical cyclones. Using a global database of subsea fibre-optic cable breaks we identify submarine mass movements triggered by tropical cyclones from 1989 to 2015. During the 25 year period tropical cyclones triggered sediment density flows in nearly all areas exposed to tropical cyclones. They were found to trigger sediment density flows by three sets of mechanisms. Flows were triggered synchronous to the passage of a tropical cyclone, as a consequence of dynamic loading. Flows were also triggered indirectly as a consequence of river flood discharges. Last, flows were triggered following a delay, hypothesised to be a consequence of the large volumes of deposited sediment.

Reference:

Pope, E. L., Talling, P. J., Carter, L., Clare, M. A., Hunt, J. E. 2017. Damaging sediment density flows triggered after the passage of tropical cyclones. Earth and Planetary Science Letters, 458, 161 – 169.

Damaging sediment density flows triggered by tropical cyclones

Ed L. Pope[1,2*], Peter J. Talling[1,3], Lionel Carter[4], Michael A. Clare[1], James E. Hunt[1]

[1]*National Oceanography Centre, University of Southampton Waterfront Campus, European Way, Southampton, SO14 3ZH, UK.*

[2]*Department of Geography, Durham University, Science Laboratories, South Road, Durham, DH1 3LE, UK.*

[3]*Departments of Earth Science and Geography, Durham University, Science Laboratories, South Road, Durham, DH1 3LE, UK.*

[4]*Antarctic Research Centre, Victoria University of Wellington, Wellington, New Zealand.*

Abstract

The global network of subsea fibre-optic cables plays a critical role in the world economy and is considered as strategic infrastructure for many nations. Sediment density flows have caused significant disruption to this network in the recent past. These cable breaks represent the only means to actively monitor such flows over large oceanic regions. Here, we use a global cable break database to analyse tropical cyclone triggering of sediment density flows worldwide over 25 years. Cable breaking sediment density flows are triggered in nearly all areas exposed to tropical cyclones but most occur in the NW Pacific. They are triggered by one of three sets of mechanisms. Tropical cyclones directly trigger flows, synchronous to their passage, as a consequence of storm waves, currents and surges. Cyclones also trigger flows indirectly, with near-synchronous timing to their passage, as a consequence of peak flood discharges. Last, cyclones trigger flows after a delay of days as a consequence of the failure of large volumes of rapidly deposited sediment. No clear relationship emerges between tropical cyclone activity (i.e. track, frequency and intensity) and the number of sediment density flows triggered. This is a consequence of the short period of observation. However, expansion of the cable network and predicted changes to cyclone activity in specific regions increases the likelihood of increasing numbers of damaging flows.

4.1   Introduction

Tropical cyclones are common in many regions of the world and affect nearly all tropical areas (Emanuel, 2005). Associated with these meteorological phenomena are extreme winds, torrential rains and subsequent river floods, increased surface run-off and/or landslides, large waves and damaging storm surges leading to coastal flooding (Peduzzi et al., 2012). An often unrecognised hazard is that posed to subsea infrastructure by cyclone-triggered sediment density flows.

Sediment density flows (a generic term used here to encompass turbidity currents, debris flows, hyperpycnal plumes and submarine landslides, etc.) can travel at speeds of up to 19 ms^{-1} and runout for several hundreds of kilometres. These flows can damage critical seafloor infrastructure, such as that associated with the offshore hydrocarbon industry or subsea telecommunication cable networks (Carter et al., 2009; Pope et al., 2017). The seafloor telecommunication network currently carries >95% of global intercontinental data and internet traffic making it integral to the global economy and strategic infrastructure for many countries (Carter et al., 2009; Burnett et al., 2013). Determining the timing and triggering of these flows is important for submarine geohazard assessment, especially whether their frequency may change as the oceans warm due to predicted climate change (Stocker, 2014).

Multiple triggering mechanisms have been identified for sediment density flows. These include earthquakes, tsunami and storm wave loading, rapid sediment deposition and oversteepening, direct plunging of dense river water (hyperpycnal flows) and volcanic activity (Piper and Normark, 2009). However, we have limited understanding of the frequency of flows worldwide or how often they are triggered by specific mechanisms because their exact timing and character are often problematic to measure. In most cases where a specific triggering mechanism has been identified, it has been based on cable breaks or damage to other seafloor infrastructure (e.g. Hsu et al., 2008; Cattaneo et al., 2012; see Talling et al., 2013 for more detail). This is particularly true

of triggering of sediment density flows by tropical cyclones (Bea et al., 1983; Dengler et al., 1984; Alvarado, 2006; Carter et al., 2012; Gavey et al., 2017).

Using a global database of cable breaks, here we specifically focus on the role tropical cyclones play in triggering damaging sediment density flows. Furthering previous spatially and temporally restricted studies; the use of a global compilation of cable breaks allows the identification of areas where damaging sediment density flows, triggered by cyclones occur and how frequent these events have been globally over a 25 year time period.

4.1.1   Aims

Three main questions are addressed. First, how important are tropical cyclones for causing cable breaks on a global basis, and in which settings (submarine canyons, etc.) and water depths do cyclone induced breaks occur? Second, can the mechanisms by which cyclones trigger sediment density flows be identified from cable breaks? For example, are flows triggered by storm waves and currents during the tropical cyclone and/or are flows typically delayed and triggered a few days after the passing of the tropical cyclone (Carter et al., 2012)? Third, is the frequency of cyclone-triggered sediment density flows and cable breaks likely to change due to projected climate change?

4.2   Data and methods

4.2.1   Cable break database

This study is based on non-public, aggregated data supplied by Global Marine Systems Limited (UK) on a non-disclosure basis. The database contains information on the location of each subsea cable when it was laid (Fig. 4.1). It includes other installation information such as seabed type and duration the cable has been in service. Cable breaks within the database are identified and generally related to likely causes, i.e. seismic, trawling, anchor, etc. Each 'break' refers to a break or failure along a section of a specific cable. A 'break' can range from internal damage of the

power conductor or optical fibres to the complete physical separation of the entire cable assembly. Each recorded 'break' may therefore also represent multiple breaks along a single section of cable. The timing of a break in the database is recorded to the nearest day.
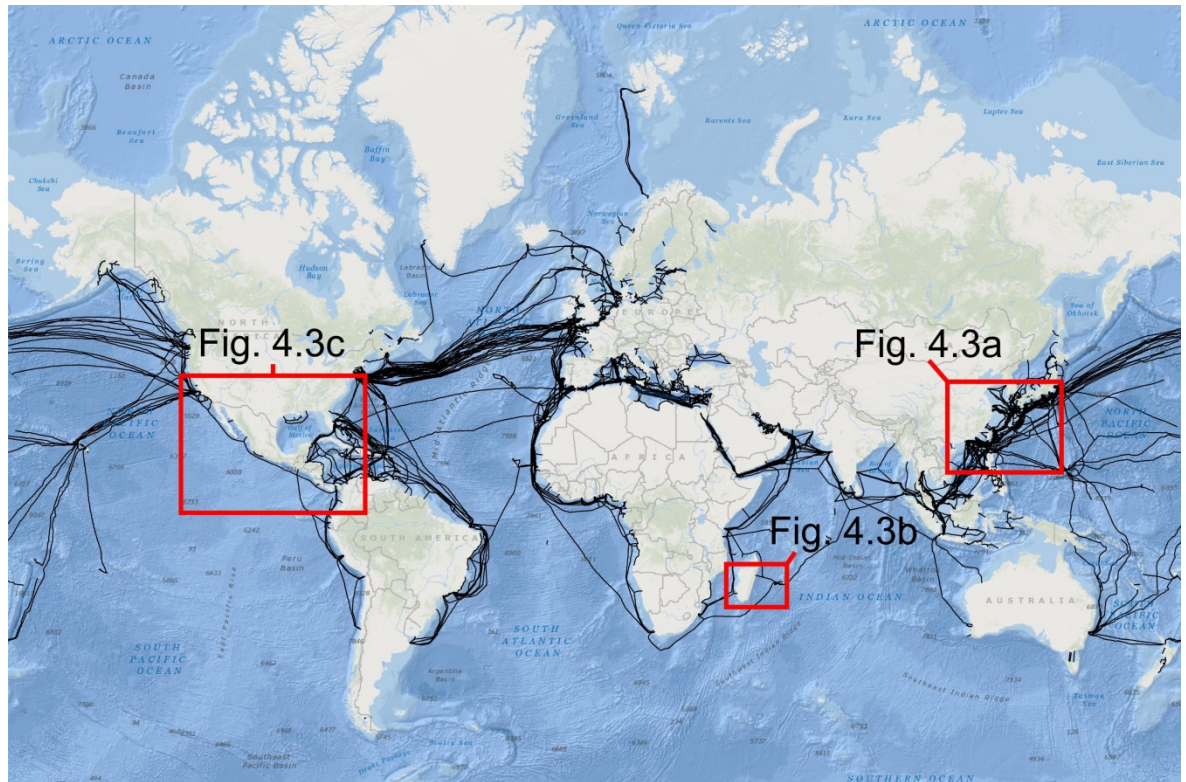
Figure 4.1 Map of the submarine cable network used in this study.

4.2.2   Tropical cyclone data

4.2.2.1   Tropical cyclone track data

Historical tropical cyclone track data were obtained from the National Hurricane Center (NHC) Hurdat-2 "best track" dataset (Landsea et al., 2013). This dataset is an archive compiled every 6 hours (at 0000, 0600, 1200, 1800 UTC) and includes reports of storm position and maximum wind speeds.

4.2.2.2   Tropical cyclone characteristics: ECMWF ERA-interim reanalysis data

The global coverage of ocean buoys recording variables such as surface pressure and wave height is spatially variable, and such data are not always freely available. The same is true of terrestrial weather stations. Thus to analyse specific tropical cyclone characteristics we used global model

data in order to homogenise data quality. Records of tropical cyclone characteristics came from ERA-Interim global atmospheric reanalysis produced by the European Centre for Medium-Range Weather Forecasts (Dee et al., 2011). ERA-Interim covers the period from 1 January 1979 onwards, and continues to be extended forward in near-real time. 3-hourly estimates of surface pressure (Pa), significant wave height (m), total precipitation (m) and surface runoff (m) data were obtained from the ERA-interim model. These data were gridded at a spatial resolution of 0.125° x 0.125°.

4.2.3   Comparison of cable break and tropical cyclone databases

All cable breaks within the database attributed to the following causes were included in our analysis: earthquakes, landslides, chafe under current action, other natural causes, and unknown causes. Among these categories, cable breaks with a known cause unrelated to tropical cyclones were removed, such as those due to earthquakes (Pope et al., 2017). A tropical cyclone was attributed to be the cause of a sediment density flow if the cable break coincided with the passing of a tropical cyclone according to the best-track data and the ERA-interim data, or occurred within 14 days of the end of a related river discharge peak if no other apparent triggers could be found.

Where a tropical cyclone appears to have triggered a sediment density flow, local environmental variables were extracted from the ERA-Interim data. Where a cable break occurred beyond the continental shelf edge, surface pressure and significant wave height measurements were measured at the nearest point on the shelf edge. Where a cable break occurred on the shelf itself, surface pressure and significant wave height were measured at the location of the cable break. Total precipitation was measured at the nearest terrestrial location to each cable break; the maximum distance was 260 km on the Mississippi Fan (mean distance of all the breaks; 95 km).

Breaks were attributed to specific triggers depending on the timing of the break itself. A cable break was specified as Type 1 if it occurred during the initial passing of the tropical cyclone and coincided with rising or peaking significant wave heights, or a drop in surface pressure (Fig. 4.2). A

Type 2 cable break occurred after the peak in significant wave height, but coincident with the peak in river flood discharges (Fig. 4.2). A Type 3 cable break followed the peak in cyclone-related river flood discharge (Fig. 4.2). The time limit set for this was 14 days as a consequence of the variable flood hydrographs, which can occur (Williams, 1969). Flood hydrographs can vary between different basins as a consequence of the different shape and size of individual basins but also as a consequence of differing relief and land-use patterns (Woods and Sivapalan, 1999). They can also vary in shape in the same basin at different times according to different antecedent conditions. It must also be acknowledged that as time between the hydrograph peak and the cable break occurring increases, it becomes increasingly difficult to directly link the occurrence of a cable break to the passage of the tropical cyclone rather than a separate mechanism. However, no obvious trigger, such as an earthquake was observed in these cases.
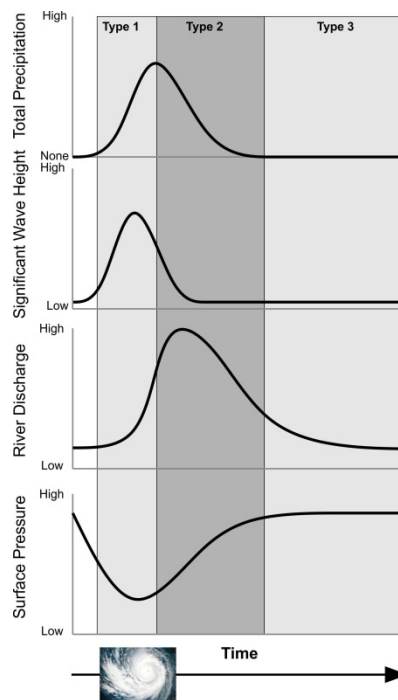
Figure 4.2 Idealised schematic of the relationship between environmental variables during the passage of a tropical cyclone and the timing of a cable break. Type 1 breaks are defined as occurring with rising and peaking significant wave heights and storm driven flows or the drop in surface pressure associated with the passage of a tropical cyclone. Type 2 occur after the peak in significant wave height but associated with the peak in river flood discharges. Type 3 occur if the break was within 14 days of the peak in cyclone related river flood discharge.

4.3   Results

Globally, between January 1989 and January 2015, there were 35 cable breaks that could potentially be attributed to tropical cyclone activity (Table 4.1). Cables broke in water depths of between 20 m and 6120 m, of which 19 cables broke at water depths >2000 m. The largest number of breaks was found offshore Taiwan; here 20 cable breaks were associated with tropical cyclones (Fig. 4.3a). There were also 3 cable breaks off Japan and 1 off the Philippines (Fig. 4.3a). In the Indian Ocean, tropical cyclone-related breaks were found offshore Madagascar (1 break) and La Reunion (6 breaks; Fig. 4.3b). Elsewhere 3 breaks were found to have occurred in the Caribbean Sea and 1 break in the Eastern Pacific (Fig. 4.3c).

The 35 cable breaks in the dataset were caused by 22 separate tropical cyclones. Multiple breaks were caused by three tropical cyclones. Typhoon Sinlaku was the potential cause of 2 cable breaks off East Taiwan in 2002. Cyclone Gamede was associated with 2 cable breaks offshore La Reunion in 2007. Typhoon Morakot resulted in 10 cable breaks. This number differs from previous studies of Typhoon Morakot, which recorded "at least nine" cable breaks (Carter et al., 2012; Gavey et al., 2017) as a consequence of additional data.

The 35 cable breaks potentially associated with tropical cyclones are found in several distinct environmental settings (Table 4.1). The largest number of cable breaks (22) are found in or closely associated with submarine canyons. Most of these are offshore Taiwan (19); others occurred offshore the Philippines and Madagascar. The second most common location (9) for cable breaks is close to river mouths or on associated deep-sea fans where turbidity currents are known to occur (i.e. the Mississippi Fan, the Yellahs Fan). Of these, 6 are located within the sediment wave fields of the Mafate and Saint-Denis Fans offshore La Reunion. The remainder of cable breaks (4) occurred on open continental shelves and deep-sea fans.

Location	Water Depth (m)	Date	Setting	Distance from likely source (km)	Relative Timing	Related Tropical Cyclone	Interpreted Type
Izu-Bonin Ridge	1560	15/06/2005	Continental slope (Possible sediment wave field)	36	Significant wave height peak	Typhoon Nesat	Type 1
La Reunion	1214	19/02/2006	Mafate and Saint-Denis Fans	13	Significant wave height peak Surface pressure trough	Severe Tropical Storm 9	Type 1
Taiwan	1518	03/07/2001	Chilung Canyon	78	Significant wave height rising limb	Severe Tropical Storm Utori	Type 1
Pacific North America	4100	13/09/2000	Deep sea fan	185	Surface Pressure Trough	Hurricane Lane	Type 1
Belize	20	01/11/2011	Open continental shelf	16	Peak runoff	Hurricane Rina	Type 2
Japan	2000	25/09/1996	Boso Canyon	98	Peak discharge	Typhoon Violet	Type 2
La Reunion	903	02/03/2007	Mafate and Saint-Denis Fans	9	Peak discharge	Cyclone Gamede	Type 2
La Reunion		03/03/2007	Mafate and Saint-Denis Fans	10	Peak discharge	Cyclone Gamede	Type 2
La Reunion		04/10/2008	Mafate and Saint-Denis Fans	1	Peak discharge	Zone of disturbed weather	Type 2
Philippines	4646	07/10/1993	Cagayan Canyon	210	Falling limb of peak discharge	Typhoon Kadiang	Type 2
Philippines	1683	07/12/2004	Cagayan Canyon	140	Falling limb of peak discharge	Typhoon Nanmadol	Type 2
Taiwan	5700	12/09/2002	Taitung Canyon	213	Rising limb of peak discharge	Typhoon Sinlaku	Type 2
Taiwan	5500	21/08/2007	Haulien Canyon	126	Peak discharge	Typhoon Sepat	Type 2
Taiwan	5200	28/07/2014	Taitung Canyon	187	Rising limb of peak discharge	Typhoon Matmo	Type 3
Taiwan	2876	09/08/2009	Gaoping Canyon	157	Falling limb of peak discharge	Typhoon Morakot	Type 2
Taiwan	1992	09/08/2009	Gaoping Canyon	117	Falling limb of peak discharge	Typhoon Morakot	Type 2
Taiwan	4440	09/08/2009	Taitung Canyon	145	Falling limb of peak discharge	Typhoon Morakot	Type 2
Jamaica	996	21/09/2004	Yellahs Fan	7	1 after peak discharge	Hurricane Ivan	Type 3
Japan	6120	07/10/2007	Mogi Fan	129	10 days after peak discharge	Typhoon Krosa	Type 3
La Reunion	550	16/02/2009	Mafate and Saint-Denis Fans	9	7 days after peak discharge	Typhoon Gael	Type 3
La Reunion	820	28/10/2006	Mafate and Saint-Denis Fans	4	10 days after peak discharge	Tropical Disturbance 1	Type 3
Madagascar	2897	12/03/2011	Onilahy Canyon	64	14 days after peak discharge	Cyclone Bingiza	Type 3
Mississippi	1541	15/10/2008	Mississippi Fan	104	17 days after peak discharge	Hurricanes Fay, Gustav, Ike	Type 3
Philippines	77	30/12/1994	Continental Shelf	40	7 days after peak discharge	Typhoon Axel	Type 3
Taiwan	6024	21/09/2002	Haulien Canyon	135	11 days after peak discharge	Typhoon Sinlaku	Type 3
Taiwan	6000	18/11/2003	Haulien Canyon	170	8 days after peak discharge	Typhoon Melor	Type 3
Taiwan	1516	24/07/2004	Chilung Canyon	73	20 days after peak discharge	Typhoon Mindulle	Type 3
Taiwan	3990	12/08/2009	Gaoping Canyon	384	4 days after peak discharge	Typhoon Morakot	Type 3
Taiwan	4025	12/08/2009	Gaoping Canyon	364	4 days after peak discharge	Typhoon Morakot	Type 3
Taiwan	2646	12/08/2009	Gaoping Canyon	260	4 days after peak discharge	Typhoon Morakot	Type 3
Taiwan	1304	12/08/2009	Gaoping Canyon	110	4 days after peak discharge	Typhoon Morakot	Type 3
Taiwan	3816	13/08/2009	Gaoping Canyon	320	4 days after peak discharge	Typhoon Morakot	Type 3
Taiwan	3800	12/08/2009	Gaoping Canyon	355	4 days after peak discharge	Typhoon Morakot	Type 3
Taiwan	2800	12/08/2009	Gaoping Canyon	218	4 days after peak discharge	Typhoon Morakot	Type 3
Taiwan	5200	17/08/2009	Taitung canyon	170	9 days after peak discharge	Typhoon Morakot	Type 3

Table 4.1 Tropical cyclone triggered cable breaks. Depending on setting, the distance from likely source is defined as the approximate distance between the cable break and the canyon head, the river mouth or the shelf edge in the case of those occurring on the continental slope.
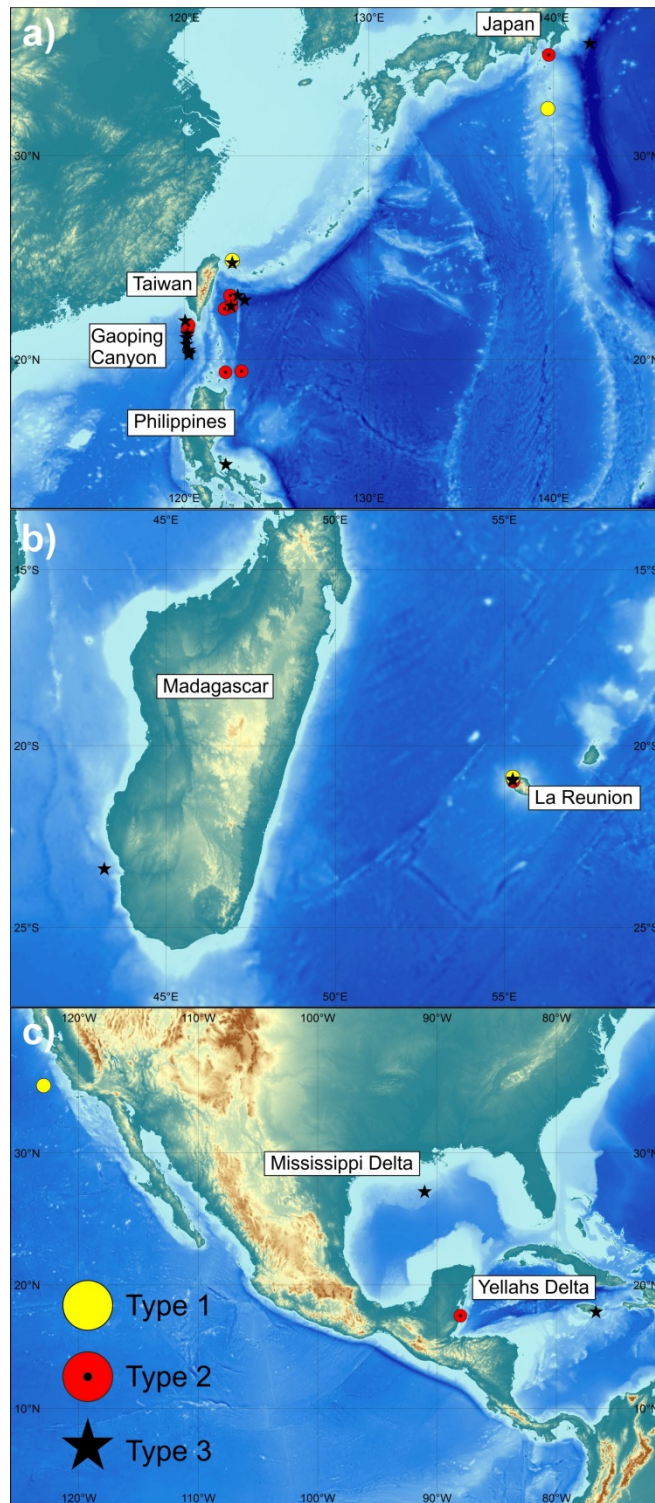
Figure 4.3 Locations of submarine cable breaks inferred to be associated with tropical cyclones. a)
Cable breaks offshore Japan, Taiwan and the Philippines. b) Cable breaks offshore
Madagascar and La Reunion. c) Cable breaks offshore the USA, Central America and
the Caribbean Islands. Bathymetry and topographic data were obtained from the
GEBCO database (Becker et al., 2009).

Assuming that each cable-breaking flow originated at the head of their associated submarine canyon or at the mouth of close-by rivers, cables were broken at distances of between 1 and 384 km from their source. The environmental settings of the cable breaks suggests that the majority of cable-breaking sediment flows triggered by tropical cyclones began in areas where large volumes of sediment had previously accumulated, such as in the heads of submarine canyons. They also suggest that most damaging flows were channelized. Channelization likely increased the probability that the flow would have sufficient power to break a cable, thus increasing the likelihood of detection in the cable break database.
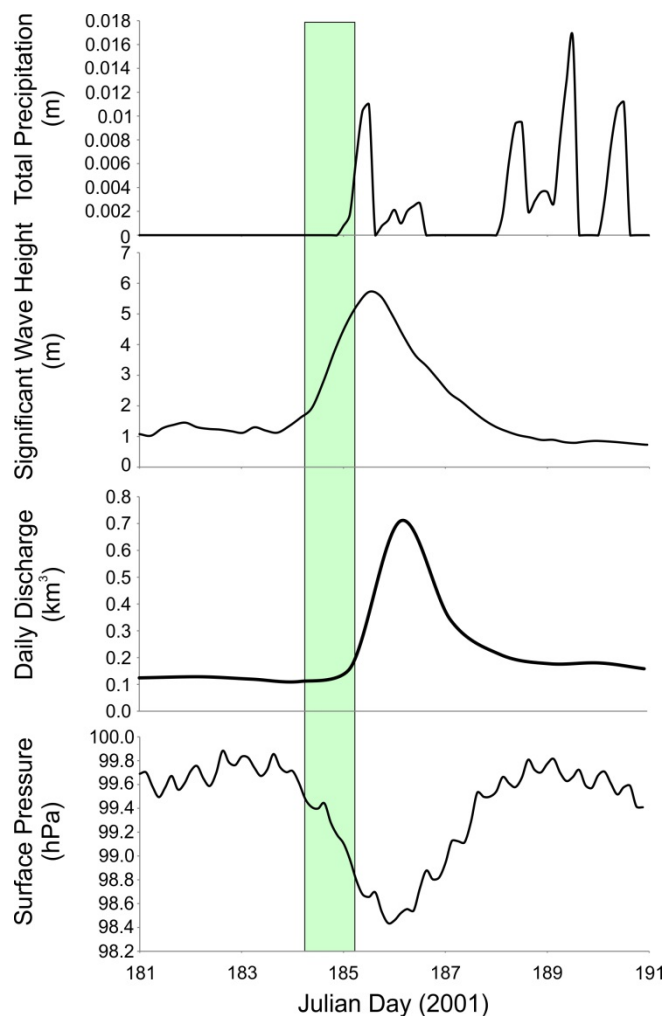
Figure 4.4 An example of a Type 1 cable break that is synchronous with typhoon induced wave height increases. Changes in rainfall, wave height and surface air pressure during a tropical cyclone and the relative timing of cable breaks offshore Taiwan in 2001. ERA-Interim data for the cable break occurring offshore Taiwan during the passage of Severe Storm Utor, 2001. Green bar represents the time when the cable broke.

The timing of the 35 cable breaks relative to the passing of a tropical cyclone is highly variable (Table 4.1). Peaks in significant wave height and drops in surface pressure as the tropical cyclone passed correspond to 4 cable breaks; each break was associated with an individual storm. Fig. 4.4 shows the timing of a cable break coincident with the initial passing of Severe Tropical Storm Utor offshore Taiwan in 2001. Tropical cyclone precipitation-related peaks in river discharge were associated with 13 cable breaks (Fig. 4.5). Both breaks associated with Cyclone Gamede were related to river discharge. Most cable breaks (18) occurred following a delay from peak flood discharge of at least 2 days (Figs. 4.6 and 4.7). The longest delay was 12 days after river discharge had returned to pre-cyclone levels (20 days after the peak discharge). Cable breaks associated with delays were associated with 9 tropical cyclones.
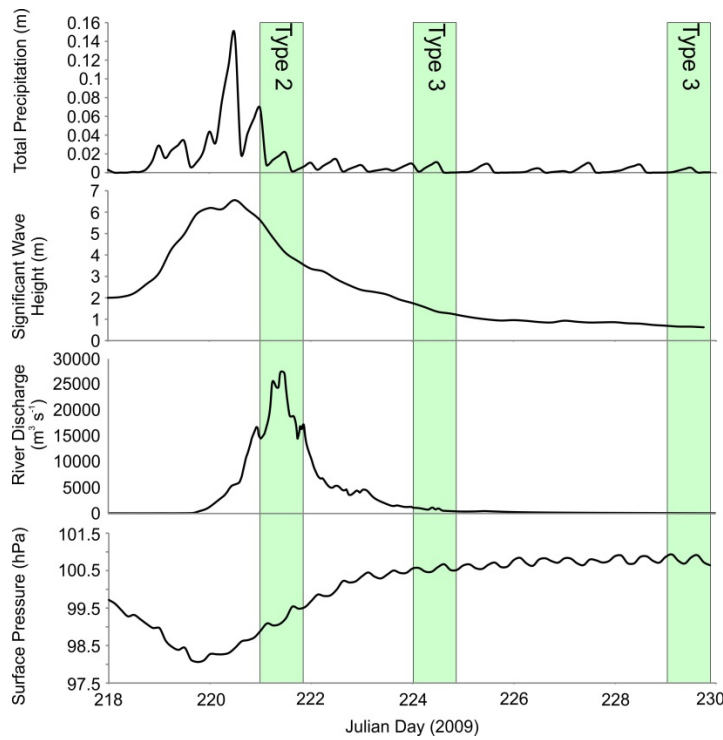
Figure 4.5 An example of Type 2 and 3 cable breaks. Environmental conditions for cable breaks occurring at the peak flood discharge resulting from the passing of a tropical cyclone. ERA-Interim data for total precipitation, significant wave height and surface pressure displayed are for offshore Taiwan at the head of the Gaoping Canyon for Typhoon Morakot in 2009. River discharge for the Gaoping River during Typhoon Morakot is also displayed (Carter et al., 2012). Green bars represent the time when cables were broken. The first set of cable breaks represents a Type 2 break. The second and third sets of cable breaks represent Type 3 breaks.

4.4   Discussion

4.4.1   Tropical cyclone triggering of sediment density flows

4.4.1.1   Type 1 breaks: Direct and synchronous triggering of sediment density flows

The cable break database shows that sediment density flows can be triggered (Type 1) during the initial passing of a tropical cyclone (Figs. 4.4 and 4.7b). We attribute a Type 1 break to slope failure and run-out triggered most likely by dynamic loading of the seafloor. Dynamic loading is the result of storm waves, storm surges or internal waves occurring during a tropical cyclone (Prior et al., 1989; Wright and Rathje, 2003). These breaks are attributed to dynamic loading-triggered sediment density flows and not wave action alone because the breaks occur well below the wave base; at depths greater than 1200 m (see Table 4.1). However, the lack of sequential breaks as seen in other studies (Carter et al., 2012; Cattaneo et al., 2012; Gavey et al., 2017) means we cannot rule out other causes.

Storm surges are generated by a combination of wind stresses and reduced atmospheric pressure (Karim and Mimura, 2008). At the continental shelf edge, the advance of a storm surge can exert large hydrodynamic pressures on the seafloor and elevate subsurface pore pressures (Zhang et al., 2015). Such transient changes can promote slope instability and its run-out (Bea et al., 1983; Wright and Rathje, 2003).

Storm waves can trigger sediment density flows through two processes. First, they can alter pore pressures through dynamic loading. Passing wave crests increase pore pressures, while wave troughs generate seepage pressures (Seed and Rahman, 1978). Where sediment lacks rigidity or has low permeability, pore water pressures are able to progressively build or migrate laterally through the sediment. Over time this can cause liquefaction or the rupture of inter-particle cohesive bonds (Puig et al., 2008) leading to sediment failure (Lamb and Parsons, 2005). Second, the orbital motion of the water particles can impart horizontal shear on the seabed (Jeng and Seymour, 2007). Where the sediment shear strength is insufficient to resist the shear stress,

failure and sediment transport can occur in the form of plane shear, liquefied flow sliding or slope

failure (Lambrechts et al., 2010). Horizontal shear stresses induced by cyclone-forced currents can

induce failure of weak sediments in the same way (Alford, 2003).
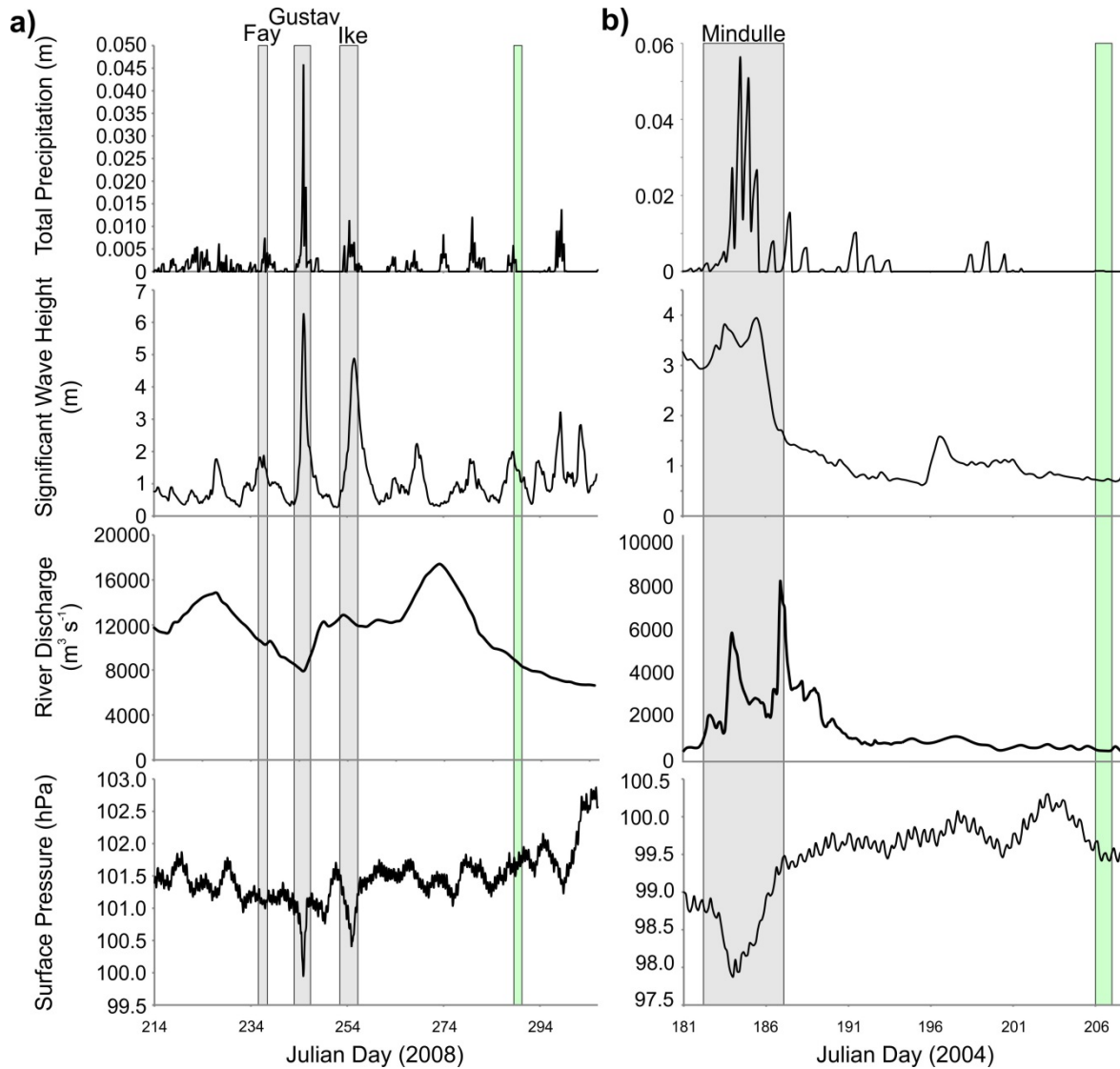
Figure 4.6 Examples of Type 3 breaks. Environmental conditions for cable breaks occurring after
the reduction in peak flood discharge following the passing of a tropical cyclone. a)
ERA-Interim data for total precipitation, significant wave height and surface pressure
displayed are for the Mississippi Delta following the passing of Tropical Storm Fay,
Hurricane Gustav and Hurricane Ike in 2008. River discharge data is from a river
station at Baton Rouge on the Mississippi. b) ERA-interim data for total precipitation,
significant wave height and surface pressure displayed are for Taiwan following the
passing of Typhoon Mindulle in 2004. River discharge data is from the Choshui River
(Lu et al., 2008). Green bar represents the time when the cable break occurred.

The limited number (4 breaks) of Type 1 events compared to other break types suggests that dynamic loading itself does not trigger large numbers of long run-out and damaging sediment density flows. These processes are therefore likely to be more important for the entrainment and deposition of shelf sediments (Sullivan et al., 2003). Failures of the deposited sediment may then result from other triggers.
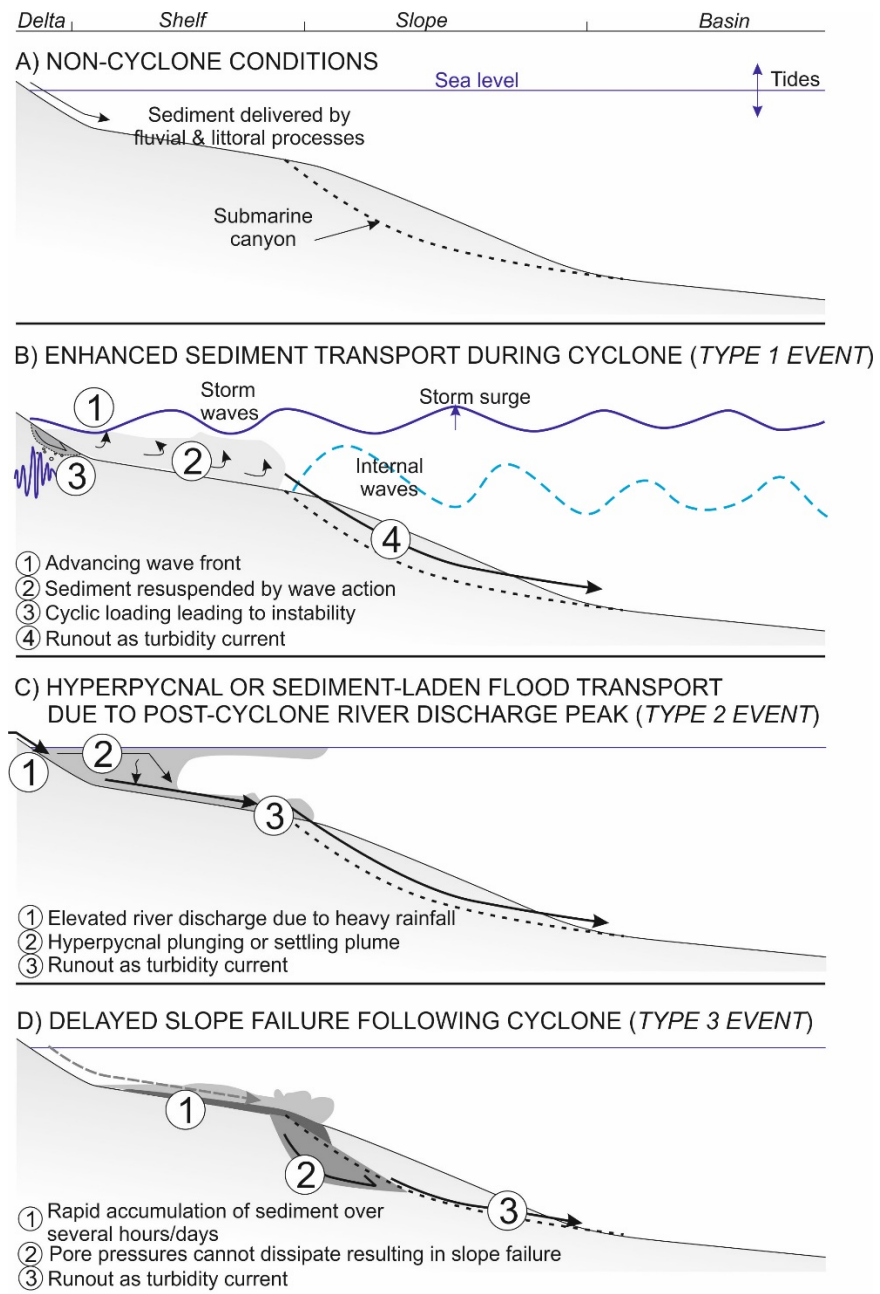
Figure 4.7 Illustration of the various hypothesis for the triggering of sediment density flows during and after cyclones. a) Sediment delivery and transport during non-tropical cyclone conditions. b) Type 1 event triggering mechanisms. c) Type 2 event triggering mechanisms. d) Type 3 event triggering mechanisms.

4.4.1.2   Type 2 breaks: Indirect and near-synchronous triggering

Type 2 cable breaks were three times more common (13 breaks) during the passage, or after the peak of, a tropical cyclone, but after coincident peaks in wave height, surface pressure and rainfall (Fig. 4.7c). Type 2 breaks are related to sediment density flows triggered by either cumulative effects (rather than the peak event as in Type 1) of storm wave/current activity, or indirectly as a consequence of peak river flood discharges resulting from tropical cyclone precipitation. Peak flood discharges often coincide with continued storm wave activity; hence isolation of a specific mechanism for Type 2 breaks is difficult from the cable break database alone. Typhoon Morakot (Fig. 4.5; Carter et al., 2012) is the best known example of a peak flood discharge trigger for a sediment density flow that lagged behind the peak intensity of the cyclone itself. Sufficiently large flood discharges can trigger sediment density flows either through the generation of hyperpycnal plumes (Parsons et al., 2001; Mulder et al., 2003; Piper and Normark, 2009) or through rapid deposition and subsequent remobilisation of river plume sediments (Parsons et al., 2001; Clare et al., 2016; Gavey et al., 2017). In both cases the initial flow entrains water and sediment; thus giving the flow sufficient energy to break a subsea cable (Fig. 4.7c).

4.4.1.3   Type 3 breaks: Indirect and delayed triggering

The largest number of cable breaks (18), occurred shortly after the passage of a tropical cyclone. Here, we suggest that these Type 3 breaks relate to processes that lag behind the passage of a tropical cyclone, but are still related to its residual effects (Figs 4.6 and 4.7d). Such lagged-triggering may be related to the deposition of large volumes of sediment during and immediately after a storm. Alternatively sediment at the shelf break or in canyon heads may have been destabilised by the cumulative effects of surface gravity waves and internal tide/wave effects (Lee et al., 2009).

Storm wave/current action and flood discharges can transport and deposit large volumes of sediment at the shelf edge or in canyon heads (Puig et al., 2004; Liu et al., 2009). The rate of deposition may depend on; (1) the extent to which the water column on the continental shelf has

been stirred up by the passage of the cyclone (Sullivan et al., 2003) and; (2) the response and size of the nearby river basin (Chen et al., 2012). These aspects can lead to delayed failures due to oversteepening and loading by rapidly deposited sediment, and inhibited dissipation of excess pore pressures (Clare et al., 2016; Figs 4.6 and 4.7d).

Liquefaction related to storm waves may also cause delayed failures. Laboratory and field tests focussing on earthquake shaking have shown that soil liquefaction beneath silt laminae, beds or lenses present in sand layers can lead to the generation of water film layers (Scott and Zuckerman, 1972; Kokusho and Kojima, 2002). These water films can persist for several days after an earthquake, acting as sliding surfaces for delayed sediment failures (Özener et al., 2009). If storm waves cause liquefaction of seafloor sediments by the processes outlined in Section 4.4.1.1, then it is possible for water film layers to be generated. Delayed failures can subsequently occur following these water film layers.

4.4.1.4   Do delayed cable breaks result from other factors?

We now consider whether delayed cable breaks result from either the time taken for a sediment density flow to reach a cable or whether the flow is in fact triggered by a process unrelated to the tropical cyclone.

The time taken for a flow to reach a cable and be recorded as a cable break has inflated the delay times given. A significant number of cable breaks (12) were located more than 100 km from the likely initiation point for sediment density flows. Given reasonable flow speeds (Carter et al., 2012; Cattaneo et al., 2012; Gavey et al., 2017) and the distances between the likely point of initiation and the cable break, a delay of up to 2 days (48 hours) is likely. The format of the cable break database may contribute to this delay, as it only records the timing of each break to the nearest day.

Quantifying whether a cyclone triggered a sediment density flow following a long delay, i.e. more than 7 days, is more difficult. Prior to this study, delayed triggering of sediment density flows was

observed in several locations (Hsu et al., 2008; Carter et al., 2012; Clare et al., 2016). These studies identified delays between peak discharge and the occurrence of a flow of between a few hours to a week. There are, however, no measurements of changing subsurface properties up until eventual failure in these previous studies or in this study. It is therefore difficult to precisely define the point at which deposited sediment will no longer fail as a consequence of cyclone forcing, and thus require an additional trigger. This should be the subject of future studies.

4.4.2   Will climate change make tropical cyclone triggered sediment density flows more likely?

Understanding whether the frequency of cyclone-triggered sediment density flows will increase as a consequence of climate change faces a number of challenges. First, possible trends in tropical cyclone activity remain uncertain as a consequence of the short period of accurate observation and the large amount of natural inter-annual variability (Knutson et al., 2010). This variability contributes to uncertainty in predictive modelling of different warming scenarios (Sugi et al., 2009; Knutson et al., 2010). Second, the number of fibre-optic cables and the diversity of cable locations have increased due to growing reliance on this communications network (Carter et al., 2014; Pope et al., 2017). These factors complicate the interpretation of whether changes to the number of observed tropical cyclone triggered flows are a consequence of changes to tropical cyclone activity or to hazard exposure of the cable network. It is therefore difficult to make projections of trends in the number of cable breaks. One exception is the northwestern Pacific (Mei and Xie, 2016). Here, increasing cyclone intensity (Emanuel, 2005), poleward migration of storm tracks (Kossin et al., 2014) and slower tropical cyclone passage (Lee et al., 2015) have been linked to increased sediment discharge to the continental shelf (Lee et al., 2015; Mei and Xie, 2016). The likelihood that cyclones will trigger sediment density flows or at least precondition slopes to fail, triggered by other processes (e.g. earthquakes; Gavey et al., 2017; Pope et al., 2017) is thereby enhanced. Increased tropical cyclone activity does therefore appear to increase the likelihood of flow triggering.

4.5   Conclusions

Tropical cyclones trigger cable-breaking sediment density flows in almost all areas where cyclones occur globally. Cyclone-forced flows are particularly common around South East Asia, especially off Taiwan and the Philippines. Flows can be triggered by dynamic loading of the seabed through storm surge and storm-wave action, but are more commonly the result of fluvial flood discharge. Importantly, they are also triggered indirectly after a tropical cyclone has passed when large volumes of rapidly deposited fluvial and shelf sediment are prone to failure. Such deposits may be subject to delayed failure to form cable-damaging flows. It is unclear whether climate change will affect the global frequency of tropical cyclone triggered flows, but it is likely to increase the number of cable breaks in major cable corridors such as off Taiwan.

Chapter 5:   How do glacigenic debris-flows relate to ice sheet processes?

Summary

Chapter 5 analyses the timing and triggering of submarine mass movements on the Bear Island Trough-Mouth Fan. It specifically focusses on the timing and frequency of glacigenic debris-flows. Previous studies have suggested that glacigenic debris-flow occurrence is indicative of ice being present at (or near to) the shelf edge. However, owing to the thickness of glacigenic debris-flow deposits no study has been able to date more than a single deposit. Using methodologies identified in **Chapter 2**, the frequency of glacigenic debris-flows is analysed using distal deposits on the Bear Island Trough-Mouth Fan. From the timing of these deposits over the last 140,000 years we are able to construct an ice sheet history for the Bear Island Trough and the Barents Sea Ice Sheet. The timing of advance and retreat cycles are identified as well as changes to ice sheet dynamics and configurations.

This chapter was submitted to *Quaternary Science Reviews* in April 2016 and has been modified following review and was accepted in August 2016. Neil Glasser and an anonymous reviewer are thanked for their comments which added the manuscript. All analyses and interpretation were completed by myself, with editorial help provided by my co-authors during the paper writing process.

Reference:

Pope, E. L., Talling, P. J., Hunt, J. E., Dowdeswell, J. A., Allin, J. R., Cartigny, M. J. B., Long, D., Mozzato, A., Stanford, J. D., Tappin, D. R., Watts, M. 2016. Long-term record of Barents Sea Ice Sheet advance to the shelf edge from a 140,000 year record. Quaternary Science Reviews, 150, 55 – 66.

Long-term record of Barents Sea Ice Sheet advance to the shelf edge from a 140,000 year record

Ed L. Pope[1], Peter J. Talling[1,2], James E. Hunt[1], Julian A. Dowdeswell[3], Joshua R. Allin[1], Matthieu J. B. Cartigny[1], David Long[4], Alessandro Mozzato[1], Jennifer D. Stanford[5], David R. Tappin[4], Millie J. Watts[1]

[1]National Oceanography Centre, Southampton, European Way, Southampton, SO14 3ZH, UK

[2]Department of Geography, University of Durham, Durham, DH1 3LE, UK

[3]Scott Polar Research Institute, University of Cambridge, Lensfield Road, Cambridge, CB1 1ER, UK

[4]British Geological Survey, Keyworth, NG12 5GG, UK

[5]Department of Geography, University of Swansea, SA2 8PP, UK

Abstract: The full-glacial extent and deglacial behaviour of marine-based ice sheets, such as the Barents Sea Ice Sheet, is well documented since the Last Glacial Maximum about 20,000 years ago. However, reworking of older sea-floor sediments and landforms during repeated Quaternary advances across the shelf typically obscures their longer-term behaviour, which hampers our understanding. Here, we provide the first detailed long-term record of Barents Sea Ice Sheet advances, using the timing of debris-flows on the Bear Island Trough-Mouth Fan. Ice advanced to the shelf edge during four distinct periods over the last 140,000 years. By far the largest sediment volumes were delivered during the oldest advance more than 128,000 years ago. Later advances occurred from 68,000 to 60,000, 39,400 to 36,000 and 26,000 to 20,900 years before present. The debris-flows indicate that the dynamics of the Saalian and the Weichselian Barents Sea Ice Sheet were very different. The repeated ice advance and retreat cycles during the Weichselian were shorter lived than those seen in the Saalian. Sediment composition shows the configuration of the ice sheet was also different between the two glacial periods implying that the ice feeding the Bear Island Ice stream came predominantly from Scandinavia during the Saalian, whilst it drained more ice from east of Svalbard during the Weichselian.

5.1   Introduction

High-latitude continental shelves have experienced multiple glacial advance and retreat cycles during the Quaternary (Dowdeswell et al., 1998; Ó Cofaigh et al., 2003; Svendsen et al., 2004a; Winsborrow et al., 2012; Patton et al., 2015). The ice dynamics and retreat of the Late Weichselian (29,000 – 14,000 years Before Present) ice sheets are quite well constrained because relatively well-preserved and dated sediments (Sættem et al., 1994; Vorren and Laberg, 1997; Landvik et al., 1998; Solheim et al., 1998) and submarine geomorphology (Andreassen et al., 2008; Winsborrow et al., 2010; 2012) allow reconstruction of ice sheet history. However, the most recent glacial advance and retreat reworked earlier sediments and overprinted older geomorphology, thereby obscuring the record of past ice behaviour. It is therefore difficult to reconstruct the timing of advance and retreat cycles and ice stream dynamics of ice sheets beyond the Late Weichselian (Ingólfsson and Landvik, 2013; Patton et al., 2015). An exception to this is the archive of former continental-slope sediments which make up trough-mouth fans.

Trough-mouth fans are found at the outer margins of bathymetric cross-shelf troughs which extend across the continental shelf to the shelf edge (Batchelor and Dowdeswell, 2014). During full-glacial periods, these cross-shelf troughs are frequently filled by ice streams, which are curvilinear areas of fast-flowing ice that are critical to the dynamics and stability of ice sheets (Ó Cofaigh et al., 2003; Schoof, 2007). Where ice streams overlie deformable sedimentary beds, exceptionally large volumes of debris can be transferred across the continental shelf (Dowdeswell and Siegert, 1999; Ó Cofaigh et al., 2003; Dowdeswell et al., 2010). Once deposited at the shelf edge, the glacial sediment is re-mobilised on the upper continental slope and redeposited by gravity-flow processes to form a trough-mouth fan (Vorren et al., 1998; Nygård et al., 2005; 2007). Sedimentary deposits that make up trough-mouth fans are therefore a potentially valuable long-term record of ice streams and their dynamics. This study focusses on the sedimentary record contained in the Bear Island Trough-Mouth Fan.

5.1.1   Regional setting

The Bear Island Trough-Mouth Fan is situated beyond the Bear Island cross-shelf trough (Fig. 5.1). The trough is about 150 km wide and 500 m deep at its mouth and served as a major drainage pathway for the Barents Sea Ice Sheet. The Bear Island Trough-Mouth Fan covers an area of 215,000 km^2 and has a volume of approximately 395,000 km^3 (Vorren and Laberg, 1997; Taylor et al., 2002a; 2002b). It is one of the largest sediment accumulations on Earth, with a volume comparable to submarine fans developed offshore of the World's largest rivers. Sediment

accumulation here is episodic and its rate can be an order of magnitude greater than is seen on river-fed systems (Dowdeswell et al., 2010).
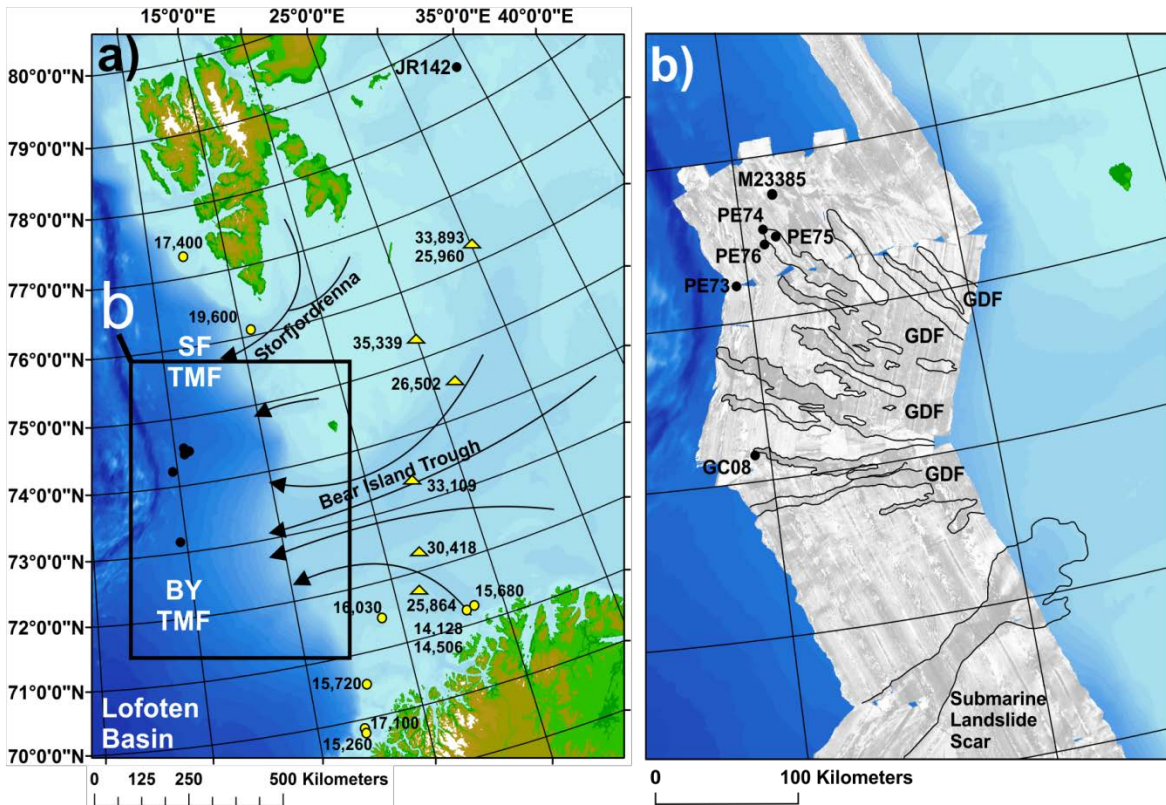
Figure 5.1 Regional setting of the Bear Island Trough-Mouth Fan. a) Core locations (black dots) shown with respect to Last Glacial Maximum ice flow direction inferred from the orientation of streamlined seafloor bedforms (Winsborrow et al., 2010). SF TMF = Storfjorden Trough-Mouth Fan. BY TMF = Bear Island Trough-Mouth Fan. Yellow triangles show dates from till units giving maximum age estimates for the onset of the last glacial advance; yellow circles show dates from glaciomarine sediments giving minimum estimates for the onset of deglaciation (Winsborrow et al., 2010). b) Bear Island Trough-Mouth Fan with GLORIA long range side-scan sonar imagery – superimposed. Core positions are labelled. Glacigenic debris-flows (GDF) and the Bjørnøya submarine landslide are identified using the GLORIA imagery.

The Bear Island Trough-Mouth Fan extends from the continental shelf edge at water depths of ~500 m to over 3000 m in the Lofoten Basin (Fig. 5.1). The most recently active (Late Weichselian) part of the Bear Island Trough-Mouth Fan is at the northern end of the fan and covers ~125,000 km^2 (Taylor et al., 2002a; 2002b). Here, side-scan sonar mapping revealed a series of low backscatter, debris-flow lobes that radiate out from the top of the fan with runout distances of up to 490 km (Fig. 5.1; Laberg and Dowdeswell, 2016). Each of these numerous debris-flows is estimated to have remobilised ~15-20 km^3 of sediment. They are also thought to indicate the

presence of ice at (or close to) the shelf edge (Vorren and Laberg, 1997; Taylor et al., 2002a). However, no previous study has dated a long record of stacked debris-flows on the Bear Island Trough-Mouth Fan due to the thickness of these debris-flow deposits (Laberg and Vorren, 1995).

In this study we demonstrate a novel methodology for understanding the growth and decay of ice streams by dating the times at which the Bear Island Ice stream was at the shelf edge. This is achieved using muddy distal deposits on the lower part of the Bear Island Trough-Mouth Fan beyond glacigenic debris-flows higher up the continental slope (Figs. 5.1 and 5.2).
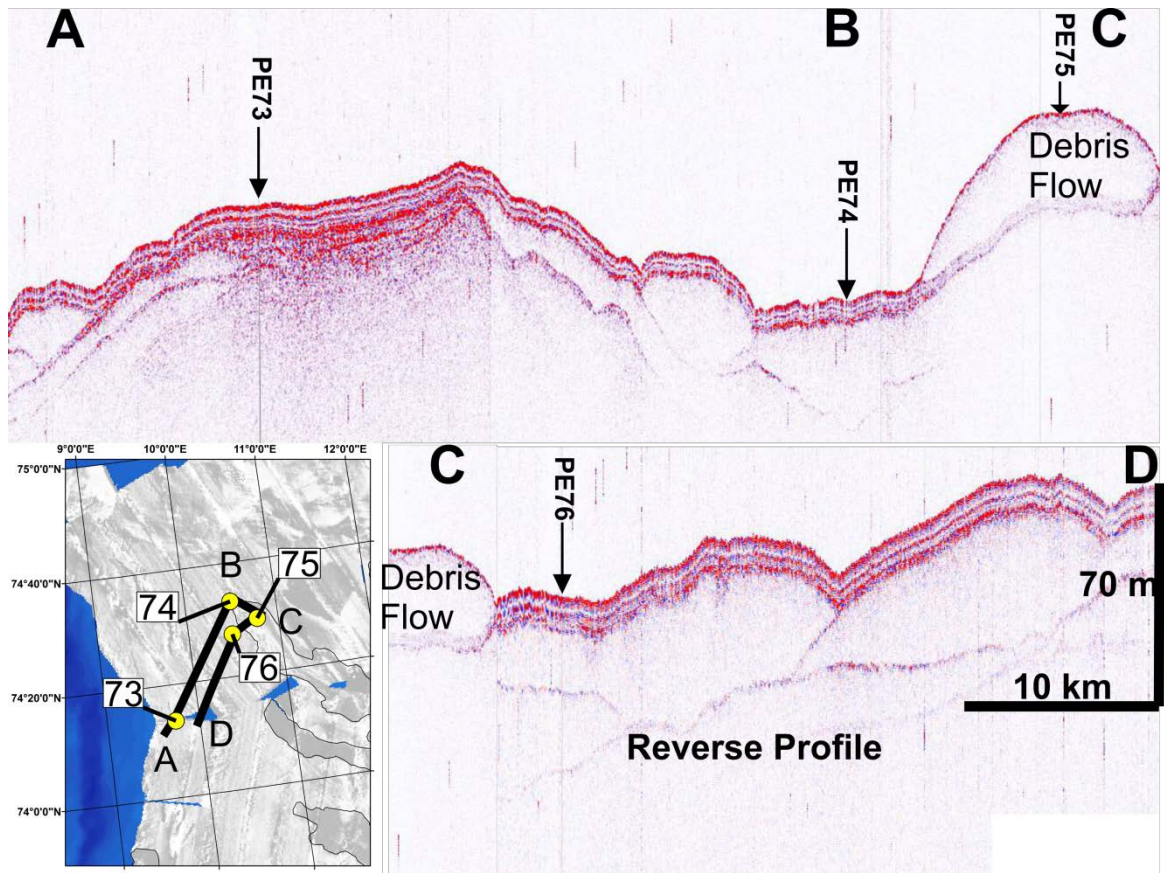
Figure 5.2 3.5 kHz seismic profile across the distal Bear Island Trough-Mouth Fan between core locations. The most recent glacigenic debris-flow, where PE75 is situated, is shown to have very little drape. Other glacigenic debris-flows are found beneath multiple reflectors. From this we suggest that the glacigenic debris-flows identified in the GLORIA imagery represent the glacigenic debris-flows which occurred during the Late Weichselian glacial advance to the shelf edge of the Bear Island Trough. The glacigenic debris-flows found deeper, beneath multiple reflectors are from older glacial advances, probably originating during or before the Saalian glacial advance to the shelf edge.

5.1.2   Aims

Our aim is to address the following questions. First, can multiple glacigenic debris-flows on the Bear Island Trough-Mouth Fan be dated and can they be used to reconstruct a history of the advance and retreat of the Barents Sea Ice Sheet? Secondly, did the dynamics of the Barents Sea Ice Sheet vary between different advance and retreat cycles and can this information be elicited from glacigenic debris-flow deposits? As an example, does the lithofacies or geochemical composition of glacigenic debris-flows vary? Last, can we use glacigenic debris-flows to help understand the controls on marine-based ice sheet retreat?

5.2   Material and methods

The principal data source for this paper is a suite of gravity cores collected during cruise 64PE391 of the RV *Pelagia* to the Norwegian Sea in 2014. These cores are supplemented by gravity cores collected during cruises JR51 and JR142 of the RRS *James Clark Ross* in 2000 and 2006 respectively (Table 1). In addition, the paper uses geophysical data collected during cruises of the RV *Pelagia* in 2014 and RRS *James Clarke Ross* in 2000. These data comprise 3.5 kHz sub-bottom profiler records and 6.5 kHz GLORIA side-scan sonar imagery with a swath width of about 20 km.

Core Name	Latitude	Longitude	Water Depth (m)	Length (cm)
PE73	74°12.30'N	09°40.49'E	2440	916
PE74	74°33.12'N	10°34.55'E	2465	821
PE75	74°29.01'N	10°49.38'E	2416	377
PE76	74°27.52'N	10°32.07'E	2403	798
GC08	73°10.00'N	09°40.00'E	2289	320
JR142	78°34.07'N	34°03.40'E	212	100

Table 5.1 Site information for sediment cores. Core locations are shown in Fig. 5.1.

5.2.1   Core logging

Cores were logged visually, identifying colour, facies and grain size. Cores were also analysed using a Geotek MSCL core logger for p-Wave velocity, gamma-ray density and magnetic susceptibility. Measurements were taken at a 0.5 cm resolution. X-radiographs of cores PE73 and PE75 were taken using an ITRAX µXRF core scanner. X-radiograph conditions were 60 kV and 45 mA, with a dwell time of 400 ms, at a resolution of 200 µm (Croudace et al., 2006).

5.2.2   Dating

5.2.2.1   Radiocarbon dating

Monospecific samples of the planktonic foraminifera *Neogloboquadrina pachyderma* sinistral from PE73 and PE75 were dated by Accelerator Mass Spectrometry (AMS). The radiocarbon ages were converted to calibrated ages (Cal years BP) using the Marine 13 database (Reimer et al., 2013).

5.2.2.2   Coccolithophore biostratigraphy

To provide accurate and robust datum horizons beyond radiocarbon dating, coccolithophore biostratigraphy was used. Toothpick hemipelagite samples were taken, from which species abundance counts were made. Species present were counted using a *Hitachi TM1000 SEM* which enabled high resolution (1,000 – 10,000x) images to be taken. The species present in each sample were counted for abundance across 10 fields of view on the *SEM* at a magnification of 2000.

Age (ka)	OIS stage	Abundance	Description
0 – 8	Recent – mid/lower 1	High	Assemblage is dominated by *C. pelagicus* and *E. huxleyi*. *Calcidiscus leptoporus* and *Gephyrocapsa* spp. are present in low numbers. Rare specimens of *Helicosphaera carteri*. Lower boundary usually coincides with the end of the last barren interval.
8 – 66	Mid/lower 1 – mid 4	Mainly barren	Interval is mainly barren of nanno-fossils but thin horizons with some *E. huxleyi* and *Gephyrocapsa* spp. are occasionally present.
66 – 79	Mid 4 – 5a	High	*Gephyrocapsa mullerae* and *E. huxleyi* show abundance peaks. Both *G. caribbeanica* and *C. pelagicus* are present.
79 – 97	5b – 5d	Low	Assemblage is almost exclusively composed by *Gephyrocapsa spp.* with some *E. Huxleyi.* In some cases in northerly areas this is partly or completely barren.
97 – 119	Upper 5e	High	Total amount of nanofossils forms an abundance peak in this subzone. Dominated by *Gephyrocapsa mullerae* and *E. Huxleyi* with abundance peak of *C. leptoporus.*
119 - 280	Lowermost 5 – lowermost 8	Mainly barren	Low amounts of nannofossils occur. Assemblage dominated by *Gephyrocapsa aperta*. Minor numbers of *C. pelagicus, E. Huxleyi* and *C. leptoporus* may also be present

Table 5.2 Coccolithophore biostratigraphy zonation scheme for the Lofoten Basin; from Gard (1988).

These abundance counts were then compared to coccolith abundances that had previously been made by Gard (1988) and Backman et al. (2009). These two studies demonstrated that abundances of *Emiliania huxleyi, Gephyrocapsa mullerae, Gephyrocapsa caribbeanica, Gephyrocapsa apperta, Calcidiscus leptoporus* and *Coccolithus pelagicus* could be calibrated to oxygen isotope stages in the polar North Atlantic. Each datum horizon is outlined in Table 5.2 and Fig. 5.3.
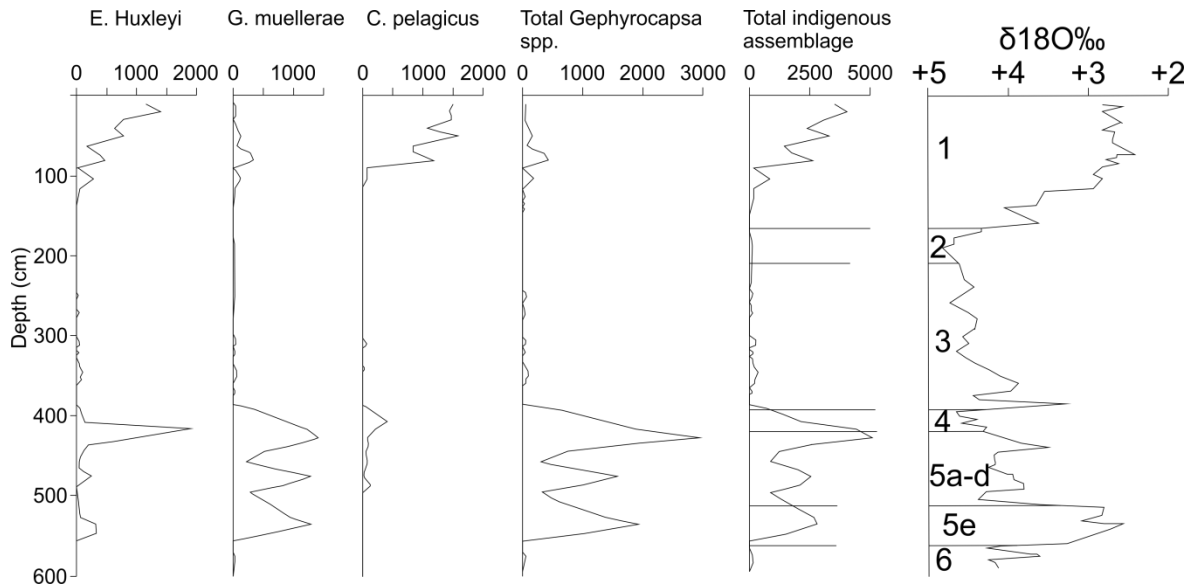
Figure 5.3 Abundances of calcareous nannofossils from Norwegian Sea Core V27-60 (78°11N, 8°35E). Oxygen isotope stratigraphy is taken from Labeyrie and Duplessy (1985). Figure is adapted from Backman et al. (2009).

5.2.2.3   ITRAX µXRF Geochemistry

ITRAX µXRF was used to collect high resolution (1 mm) major element geochemical records from four cores. Cores PE73, PE75, GC08 and JR142 were analysed using this method. Proxy dating was achieved by removing glacigenic-debris flow deposits from the cores to leave the hemipelagite µXRF records. The hemipelagite calcium (Ca) record was used as a proxy for $\delta^{18}O$ as changes should be primarily driven by changes to biogenic $CaCO_3$ production which is affected by changing surface water conditions, changing circulation patterns and sea level (Richter et al., 2001; Cheshire et al., 2005; Croudace et al., 2006; Rothwell et al., 2006; Lebreiro et al., 2009; Hibbert et al., 2010; Solignac et al., 2011; Hunt et al., 2013). Located on the distal areas of the Bear Island Trough-Mouth Fan, hemipelagite composition should therefore reflect open water conditions. The µXRF calcium record, combined with AMS dating and the Coccolith biostratigraphy enables a robust chronology of glacigenic debris-flows on the fan to be constructed.

5.2.3   Dating glacigenic debris-flows

Dating of glacigenic debris-flows on the Bear Island Trough-Mouth Fan was achieved in the upper part of the core using ^{14}C AMS dates. Average hemipelagic accumulation rates between radiocarbon dates were calculated and then the hemipelagic depth between the deposits was used to calculate the timing of the emplacement of the deposits (Wetzel, 1984; Hunt et al., 2013; Clare et al., 2014). To do this, we assumed that flows were not erosional and that the rate of sedimentation between radiocarbon dates was constant. Beyond the depth which we could use radiocarbon ages we used tie points in the coccolith biostratigraphy (Weaver and Kuijpers, 1983; Weaver et al., 1992; Hunt et al., 2013) and the calcium proxy curve (Hibbert et al., 2010) to estimate the rate of hemipelagite accumulation and thus the timing of the events.

5.2.3.1   Statistical analysis of glacigenic debris-flow recurrence

In order to try to identify the possible triggering mechanism for glacigenic debris-flows on the Bear Island Trough-Mouth Fan the distribution of recurrence intervals was analysed. Here, we define the recurrence interval of a glacigenic debris-flow as the length of time since the glacigenic debris-flow that preceded it. Previous work has identified sediment gravity flows to be temporally random, i.e. their recurrence intervals followed a Poisson distribution, meaning no precise triggering mechanism could be identified (Clare et al., 2014; Pope et al., 2015). However, these studies suggest that the use of statistical tests on recurrence intervals at local, rather than on regional or global datasets as they used, may provide insight into the triggering mechanisms of submarine sediment gravity-flows (Pope et al., 2015).

To assess whether the recurrence intervals between glacigenic debris-flows come from a Poisson distribution or a different statistical distribution we used the Anderson-Darling test. The Anderson-Darling test is defined as:

$$A^2 = -N - S \qquad\qquad (5.1)$$

where

$$S = \sum_{i=1}^{N} \frac{(2i-1)}{N} [lnF(Y_i) + \ln(1 - F(Y_{N+1-i}))] \qquad\qquad (5.2)$$

In addition to the Anderson-Darling test, we also analysed the degree of clustering of the recurrence intervals. The degree of clustering of low and high values of recurrence within the sequence was analysed using a rescaled range exponent which was developed by Hurst (1951). Hurst (1951) presented the following relationship, using *K* as an estimator for a modified Hurst Exponent, h:

$$K = \frac{\log_{10}(R/S)}{\log_{10}(N/2)} \tag{5.3}$$

where R is the maximum range in cumulative departure from the mean, N is the number of observations, and S is the standard deviation (Chen and Hiscott, 1999). Values that are closer to K = 1 show persistent or trend reinforcement (i.e. a large value is most likely followed by a large value; Mandelbrot and Van Ness, 1968) and those that are closer to K = 0 are mean reverting or anti-persistent (i.e. a large value is most likely followed by a small value; Barkoulas et al., 2000). Values that approximate K = 0.5 are deemed to be randomly distributed.

5.2.4   Geochemical composition of the glacigenic debris-flows

To analyse the geochemical composition of the glacigenic debris-flows the mud fraction was first grain-sized. Sediment samples of 1 cm³ were added to 30 mL RO water with a 0.05% sodium hexametaphosphate dispersant and shaken for a minimum of 12 hours. The dispersed sediment mixtures were then analysed using a *Malvern Mastersizer 2000* particle size analyser. Standard reference (SRM) of mean average 32 µm and 125 µm was used to monitor accuracy.

Once comparable sample deposits from the glacigenic debris-flows were identified in terms of similar grain sizes their major element records produced by the ITRAX µXRF scanner were compared. Both single element records and major element ratios were compared.

5.3   Results

5.3.1   Glacigenic debris-flow sedimentary characteristics

Cores PE73, PE74, PE75 and PE76 were located several hundred kilometres from the palaeo-ice front on the Bear Island Trough-Mouth Fan at water depths in excess of 1750 m (Fig. 5.1). In such distal locations, the downslope evolution of glacigenic debris-flows (Ó Cofaigh et al., 2003) results in the deposition of fine muds. We henceforth refer to these fine-mud deposits as distal debris-flow muds.

Cores PE73, PE74 and PE76 contained 59, 42 and 38 thin fine-mud layers, respectively, which originated from glacigenic debris-flows further upslope. Located furthest from the shelf edge, the largest number of distal debris-flow mud layers are found in core PE73 (Fig. 5.4). These deposits are mainly dark grey muds; their grain size distribution is 55% mud (<1 – 10 microns), 24% silt (10 – 62.5 microns) and 21 % sand (62.5 – >2000 microns) (Fig. 5.5). These deposits have sharp basal contacts and higher average grainsizes than the background sediments (67% mud, 19% silt, 12% sand). Deposits in cores PE74 and PE76 have similar characteristics. However, the bottom-most

sediments in these two cores are massive glacigenic debris-flow deposits (diamictons; see Fig. 5.5c) described elsewhere in the literature (Vorren et al., 1991; Vorren and Laberg, 1997; Taylor et al., 2002a; 2002b; Ó Cofaigh et al., 2003). The diamictons consist of lithic clasts supported by an unsorted dark sand-mud matrix (39% mud, 32% silt, 27% sand).
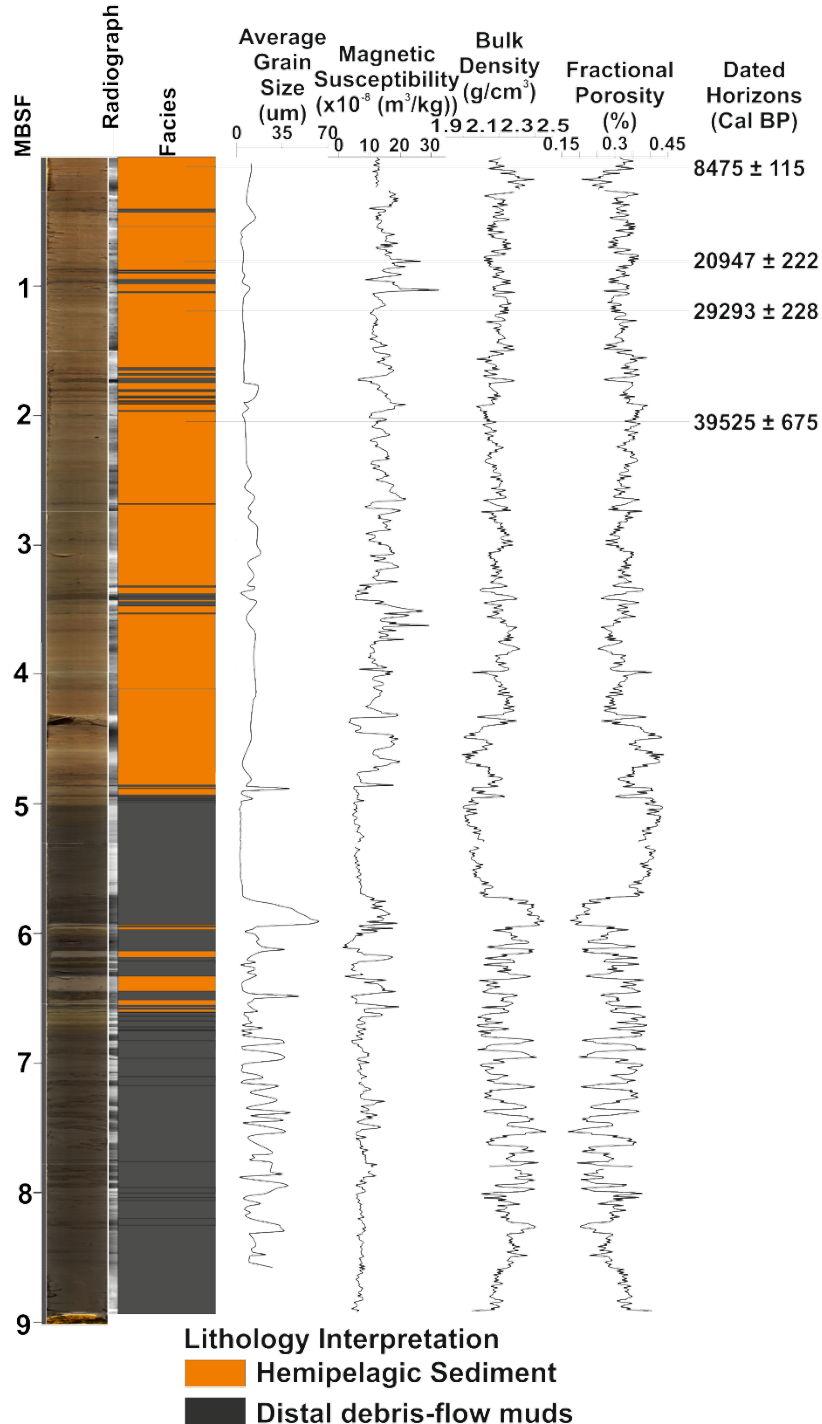
Figure 5.4 Core panel for PE73. Panel includes core photos, x-radiographs of each core section, facies interpretation, average grain size, geophysical data and radiocarbon dates.
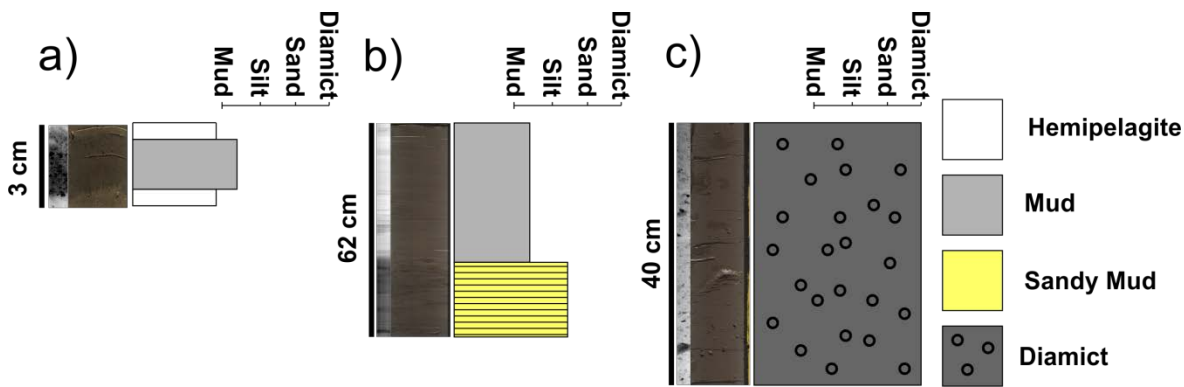
Figure 5.5 Sedimentary logs and their radiographs that summarise the deposits seen in cores PE73, PE74, PE75 and PE76 related to glacigenic debris-flows. a) A typical distal debris-flow mud. b) Laminated sand underlying a distal debris-flow mud. c) A glacigenic debris-flow massive diamicton.

Core PE75 was located on what is the youngest glacigenic debris-flow in the study area stratigraphically and contained three sediment-flow deposits. Two were distal debris-flow muds seen in cores PE73, PE74 and PE76. The largest deposit was composed of a massive diamicton (Figs 5.5c and 5.6). The cross-core correlation illustrated in Figure 5.7 shows how the thick glacigenic debris-flow in the base of PE75 is laterally equivalent to the thin mud layers seen in PE73, PE74 and PE76 more distally on the trough-mouth fan. We use this to justify our use of the thinner distal debris-flow muds as representative of glacigenic debris-flow occurrence further upslope.

5.3.2   Timing and frequency of glacigenic debris-flows

The most recent distal debris-flow mud layer in PE75 dates to <11,000 Calibrated years Before Present (Cal BP), and its timing is consistent with dated glacigenic debris-flows from other studies (Laberg and Vorren, 1996). The large glacigenic debris-flow deposit at the base of core PE75 dates to ~23,000 Cal BP. These deposits are consistent with the Late Weichselian glacial advance (Winsborrow et al., 2010; 2012; Patton et al., 2015). In core PE73, Late Weichselian distal debris-flow muds occur between 26,000 and 20,900 Cal BP. The radiocarbon dates and the cross-correlations (Figs. 5.7 and 5.8) show a consistent phase of deposition of these distal debris-flow mud layers across the Bear Island Trough-Mouth Fan during this period. The next group of distal debris-flow mud deposits in core PE73 date to between 39,400 and 36,000 Cal BP. The last set of distal debris-flow mud-layers during the Weichselian were emplaced between 68,000 and 60,000 BP (Fig. 5.8). The largest number and greatest thickness of distal debris-flow mud deposits in core PE73 occurred earlier, during the Saalian glaciation with the youngest of these dated at ~128,000

BP (Fig. 5.8). The number and thickness of deposits from the Saalian also correlate well between cores PE74 and PE76 (Fig. 5.7).
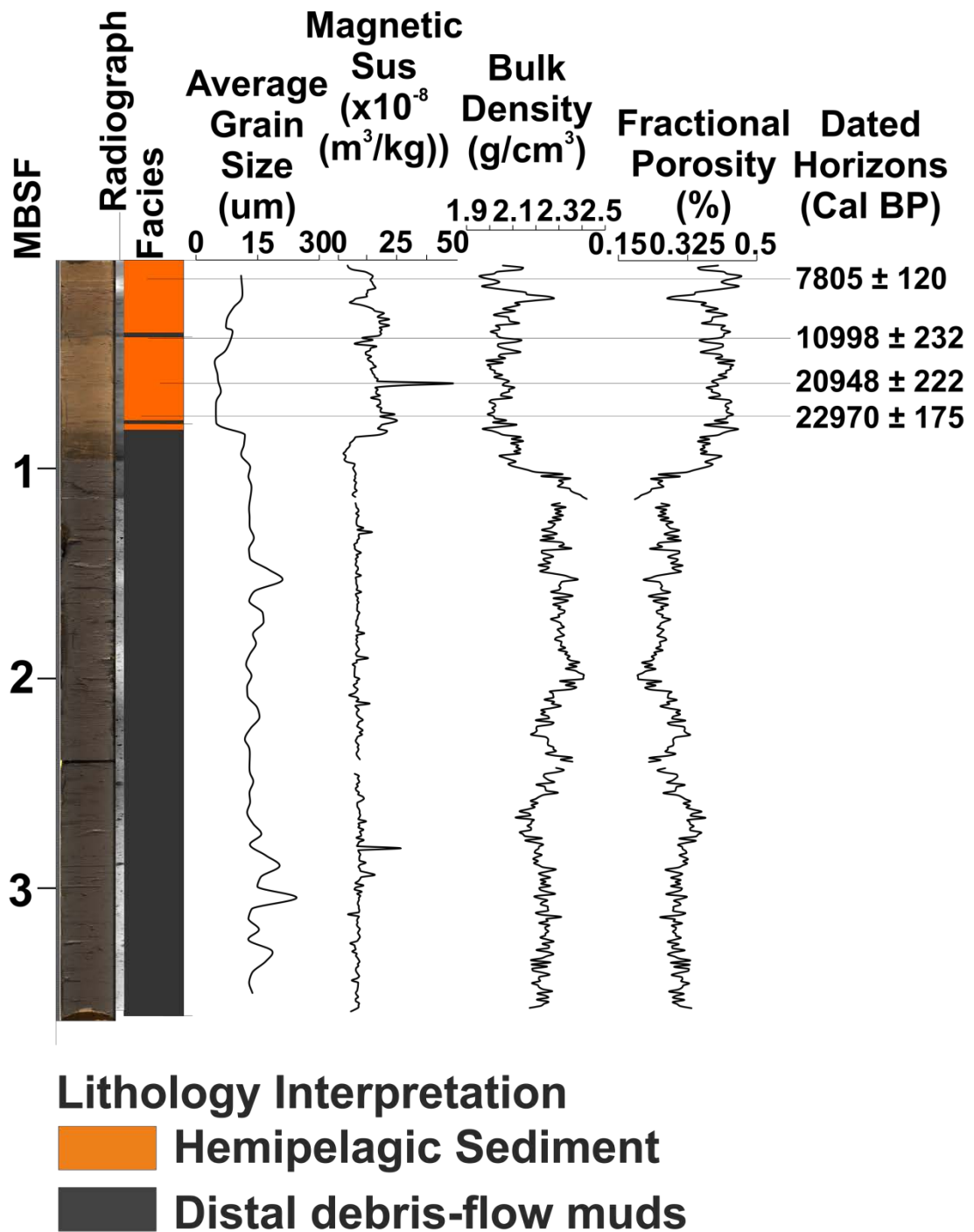
Figure 5.6 Core panel for PE75. Panel includes core photos, x-radiographs of each core section, facies interpretation, average grain size, geophysical data and radiocarbon dates.
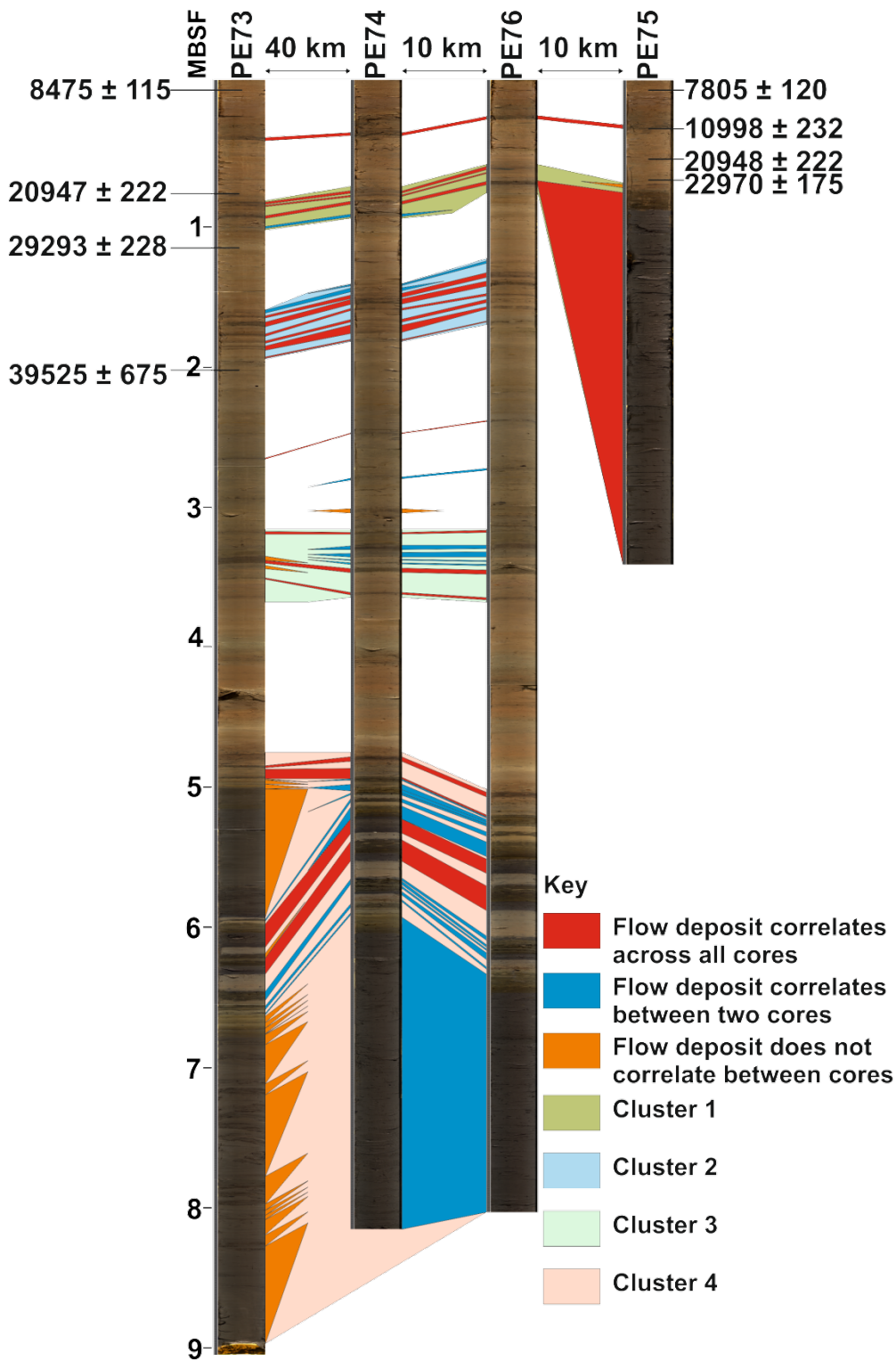
Figure 5.7 Core correlations between cores PE73, PE74, PE75 and PE76. Distances between the cores and radiocarbon dates from cores PE73 and PE75 are shown. MBSF = Meters Below Sea Floor. Four clusters of distal debris-flow muds correlate well across the three long cores. Few deposits from glacigenic debris-flows occur outside of these main clusters.

5.3.2.1   How do the core deposits relate to the seismic stratigraphy?

Dating of the glacigenic debris-flow at the base of PE75 (Fig. 5.6) and the cross-core correlations suggest that there is only a thin amount of hemipelagic drape over the most recent glacigenic debris-flows. The glacigenic debris-flow deposit at the base of PE75 can be seen in the seismic profile (Fig. 5.2) to only have a single overlying reflector and is also visible in GLORIA side-scan sonar (Figs 5.1b and 5.2). We therefore suggest that the glacigenic debris-flows mapped using the GLORIA side-scan sonar imager and illustrated in Figure 5.1b represent only those that occurred during the Late Weichselian glaciation. The other debris-flows visible in the seismic profiles as many reflectors beneath thicker sediment drapes (Fig. 5.2) thus date to earlier glacial advances.

5.3.2.2   Is the clustering of glacigenic-debris flows supported statistically?

Visual inspection and cross-core correlations suggest that there are four apparent clusters of distal debris-flow muds on the northern end of the Bear Island Trough-Mouth Fan (Fig. 5.7). The significance of this clustering was tested by analysing the statistical distribution of recurrence intervals, the time between one event and the next, on deposits in core PE73. The Anderson-Darling Test and Hurst Exponent were applied to 47 recurrence intervals from PE73. The discrepancy between the 59 distal debris-flow muds in the core and the 47 recurrence intervals used is a result of the large number of deposits at the base of the core. These distal debris-flow muds have no hemipelagite between the events. We are therefore unable to calculate the time between events. Whilst this may be the result of large numbers of glacigenic debris-flows occurring over very short time intervals, we are unable to rule out the possibility that the hemipelagic sediment has been eroded. Consequently we treat the multiple distal debris-flow muds at the bottom of the core as a single mass-transport complex.

Using the Anderson-Darling Test, the distribution of recurrence intervals most closely followed a 3-parameter Weibull distribution ($p > 0.5$; for the Anderson Darling Test to be significant at the 95% confidence interval the p value must be >0.05). The recurrence intervals also had a Hurst's Exponent of 0.808. The statistical tests suggest that the distribution of distal debris-flow muds is therefore highly clustered rather than random; i.e. a short recurrence interval is likely to be followed by another short recurrence interval. These statistical tests suggest that the triggering of glacigenic debris-flows on the Bear Island Trough-Mouth Fan are probably related to a specific non-random process such as the presence of ice at the shelf edge.

Figure 5.8 Core panel for PE73 showing hemipelagic ITRAX Ca profile. Radiocarbon dates are initially used to correlate the core record with a local benthic δ¹⁸O curve from core V27-60 offshore of the Bear Island Trough-Mouth Fan (Labeyrie and Duplessy, 1985). Beyond the range of radiocarbon dating, the ITRAX Ca profile is correlated with the δ¹⁸O curve. Coccolithophore counts from toothpick hemipelagic samples are shown to corroborate the proxy dating using the ITRAX Ca profile based on the coccolith abundance curve from Backman et al. (2009) which was obtained from core V27-60.

5.3.3   Geochemical composition of distal debris-flow muds

The geochemical composition of the mud fraction of the flow deposits in cores PE73, PE75, GC08 and JR142 (Fig. 5.1) were analysed using ITRAX µXRF data. Ratios of major elements of the flow deposits were shown to have distinct differences (Fig. 5.9a). In core PE73 the ratios of the Weichselian distal debris-flow mud compositions were shown to be distinct from the Saalian deposits. Ratio data from the debris-flow deposits in PE75 matched the Weichselian deposits in PE73. This shows temporally similar deposits have the same composition at the northern end of the Bear Island Trough-Mouth Fan.
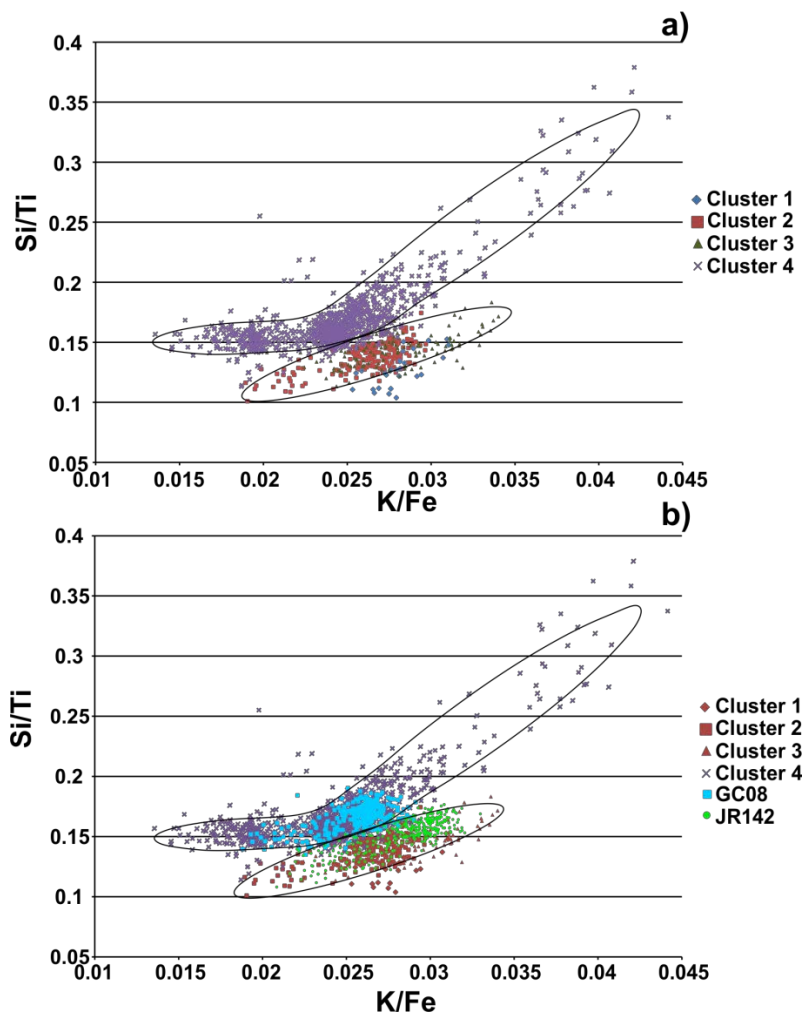
Figure 5.9 a) Geochemical ratios of the mud fraction of the distal debris-flow deposits in core PE73. Cluster 1 includes distal debris-flow muds from the Late Weichselian. Cluster 2 includes distal debris-flow muds from between 39,400 Cal BP and 36,000 Cal BP. Cluster 3 includes distal debris-flow muds from between 68,000 BP and 60,000 BP. Cluster 4 includes distal debris-flow muds from before ~128,000 BP. b) Geochemical ratios of the distal debris-flow muds in core PE73 overlain with the same ratio data

from mud fractions in GC08 and JR142. GC08 ratio data is similar to Cluster 4. JR142
ratio data is similar to Clusters 1 – 3.

To identify whether the differences in deposit composition were a consequence of changes in provenance of the sediment, major element ratios from cores located in different areas of the Barents Sea and the Bear Island Trough-Mouth Fan (Fig. 5.1) were compared to the ratio data from cores PE73 and PE75. When ratio data from a distal debris-flow mud deposit in GC08 was compared to the ratios of deposits in PE73, it was shown to be similar to those of the Saalian distal debris-flow muds in PE73 (Fig. 5.9b). The geochemical ratio data from JR142, located east of Svalbard about 750 km north-east of the Bear Island Trough-Mouth Fan was, by contrast, shown to be similar to the Weichselian deposits in core PE73.

5.4   Discussion

5.4.1   How do reconstructions of past Barents Sea Ice Sheet advances compare to the timing of glacigenic debris-flow clusters?

Dating of the large glacigenic debris-flow deposit in core PE75 at ~23,000 Cal BP and the cluster of distal debris-flow muds in cores PE73, PE74 and PE76 (Fig. 5.7) between 26,000 and 20,900 Cal BP, is consistent with proposed dates for the initial advance to the shelf edge of the Late Weichselian Barents Sea Ice Sheet (Elverhøi et al., 1995; Laberg and Vorren, 1995; Vogt et al., 2001; Vorren et al., 2011). The timing is also contemporaneous with dated mass-transport deposits from trough-mouth fans offshore Western Svalbard (Dowdeswell and Elverhøi, 2002). In both areas, the ice retreated from the shelf edge as early as 20,000 Cal BP, inferred from a lack of younger glacigenic debris-flow deposits. Deposition of laminated mud and sand layers from meltwater plumes occurred at a later date as deglaciation accelerated and thus we see no evidence of this in our distally located cores (Jessen et al., 2010; Lucchi et al., 2013). The timing of this cluster of events, when ice was known to be at the shelf edge through independent radiocarbon dating of deposits (Fig. 5.1), and the statistical analysis (see Section 5.3.2.1.), validates the use of distal debris-flow mud deposits as an indicator of an ice advance to the shelf edge of the Bear Island Trough.

Assuming that each cluster of distal debris-flow muds represents an ice advance in the Bear Island Trough, earlier in the Weichselian ice reached the shelf edge between 39,400 and 36,000 Cal BP. An ice advance during this period is contrary to reconstructions made using terrestrial deposits on Svalbard (Mangerud et al., 1998; Svendsen et al., 2004b; Hughes et al., 2016). However, its timing is consistent with ice-rafted debris records from other dated cores on or near the Bear Island

Trough-Mouth Fan (Dowdeswell et al., 1999; Dreger, 1999; Knies et al., 2001) and records of a glacial advance associated with the Jæren-Skjonghelleren advance in Scandinavia (Lambeck et al., 2010). The discrepancy between the Bear Island Trough-Mouth Fan records and those on Svalbard, 300 km to the north, can be explained through either: (1) a re-advance occurred on Svalbard; however, there are few terrestrial records of this advance on Svalbard; or (2) the response to climatic forcing of an ice dome east of Svalbard, and its outlet glaciers, which differs from that of glaciers on the archipelago itself.

The oldest Weichselian distal debris-flow muds occur between 68,000 and 60,000 BP. These are consistent with proposed glacial advances during Marine Isotope Stage 4 from terrestrial outcrops on Svalbard and ice-rafted debris records (Mangerud et al., 1998; Svendsen et al., 2004a; Ingólfsson and Landvik, 2013). During Marine Oxygen Isotope Stage 5 (124 to 80,000 BP) the cores contain increased amounts of ice-rafted debris. There is, however, no evidence of distal debris-flow muds in the cores during Marine Oxygen Isotope Stage 5 (Figs. 5.7 and 5.8). We therefore propose that, whilst ice volumes increased in the Barents Sea, resulting in deposition of greater volumes of ice-rafted debris, the ice sheet did not reach the shelf edge of the Bear Island Trough at this time. This supports modelling studies of ice sheet growth for the Barents Sea during Marine Oxygen Isotope Stage 5 (Svendsen et al., 1999; 2004a; 2004b) and suggestions that the location of the largest ice dome migrated from east to west across the Barents-Kara Sea during each subsequent major glacial advance during the Weichselian (Siegert et al., 2001; Patton et al., 2015).

The presence of distal debris-flow muds occurring at >128,000 BP is consistent with reconstructions of the Late Saalian glacial maximum that occurred during Marine Isotope Stage 6 (Mangerud et al., 1998; Mangerud et al., 2001).

5.4.2   Contrasts between the Weichselian and Saalian Barents Sea Ice Sheets

5.4.2.1   Ice-margin stability

The thickest and most numerous distal debris-flow mud deposits in cores PE73, PE74 and PE76 occur at the base of the cores. These deposits are dated biostratigraphically to >~128,000 BP (Fig. 5.8). If the number and thickness of distal debris-flow muds is representative of the volume of sediment advected to the shelf edge by the Bear Island Ice stream, then the duration or rate of sediment delivery was far greater during the Saalian than the Weichselian glacial interval. This could be explained by greater ice thicknesses associated with the Late Saalian ice-sheet leading to higher velocities, and an ice-front position stable at the shelf edge for a longer time period. This view is supported by model reconstructions of the Late Saalian ice sheet (Svendsen et al., 2004b;

Colleoni et al., 2009), Arctic Ocean ice-rafted debris records (Spielhagen et al., 2004) and terrestrial records (Mangerud et al., 1998; Ehlers and Gibbard, 2004) indicating that the extent and duration of the Late Saalian ice sheet was greater than those which occurred during the Weichselian.

By comparison with the Saalian Barents Sea Ice Sheet, the Weichselian ice sheets produced comparatively few glacigenic debris-flows. Only four distal debris-flow muds were found in cores associated with the Late Weichselian advance. The two Middle Weichselian advances to the shelf edge were characterised by only 7 and 8 distal debris-flow mud deposits. The contrasts suggest that the time taken for ice sheet advance and retreat was shorter during the three ($\sim$26,000, 40,000 and 68,000 Cal BP) Weichselian glaciations, leading to smaller volumes of sediment reaching the shelf edge than during the (>128,000 BP) Saalian glaciation (Siegert et al., 2001).

5.4.2.1.1   Ice-margin stability and rates of sediment delivery

The following section briefly explores the implications of the newly dated ice stream advances and retreats for volumetric rates of sediment delivery to the Bear Island Trough-Mouth Fan, and thus for processes affecting the base of the ice stream.

Previous work suggests that around 4,200 km^3 of sediment was supplied to the Bear Island Trough-Mouth Fan during the last glacial advance between 24,000 and 12,000 BP (Laberg and Vorren, 1996), although the exact volume is uncertain due to limitations in seismic coverage of the fan and dating uncertainties. However, even given the uncertainties, this is still a remarkably large volume of sediment. Subsequent modelling reconstructions have suggested that this sediment may have accumulated primarily during a period of about 13,000 years between 27,000 and 14,000 years BP (Dowdeswell and Siegert, 1999). This implied a sediment delivery rate of $\sim$0.32 km^3 a^{-1} which is comparable to the annual sediment supply rate from the Amazon River (Milliman and Syvitski, 1992).

The chronology in this study, however, shows that the Barents Sea Ice Sheet was most likely present at the shelf edge in the Bear Island Trough for a much shorter period during the last 30 ka than was previously implied by the numerical modelling of Dowdeswell and Siegert (1999). The period may have only been 5.1 ka, from 26,000 to 20,900 Cal BP (Fig. 8). This is based on the assumption that the duration over which distal debris-flow muds occur is comparable to the period which ice was at the shelf edge and that there was minimal delay between glacigenic debris-flow run-out to our core sites and appearance and disappearance of the ice at the shelf edge. If these assumptions hold, then the rates of sediment supply to the shelf edge by the ice

stream may have been about twice those inferred from numerical modelling. This would make the sediment supply rate twice that of the modern Amazon River.

Such high sediment-supply rates have implications for the processes of sediment deformation and advection along the submerged base of the ice stream, which themselves play a key role in ice sheet dynamics (Benn et al., 2007a; 2007b; Schoof, 2007) and are thus important to better constrain. In particular, the thickness of deforming sediment affects basal drag on the ice stream and, hence, its velocity. The Dowdeswell and Siegert (1999) model implies that the high sediment-delivery rate needed to delivery 4200 km^3 of sediment in 5.1 ka would require an actively deforming layer in excess of 6 m thick or an ice stream velocity greatly exceeding the 1 km a^{-1} predicted in the numerical model. Modern observations of ice stream beds in Antarctica suggest, however, that deforming basal layers a number of metres in thickness are unlikely (Engelhardt and Kamb, 1998; Tulaczyk et al., 2000; Whillans et al., 2001; Dowdeswell et al., 2004b).

Assuming, instead, that ~4,200 km^3 of sediment was delivered to the Bear Island Trough-Mouth Fan over the period which distal debris-flow muds suggest ice was present at the shelf edge during the whole Weichselian suggests that the sediment accumulated over 16.5 ka (5.1 ka during MIS 2, 3.4 ka during MIS 3 and 8 ka during MIS 4). This would advocate a rate of sediment delivery of 0.25 km^3 a^{-1} by the Bear Island Ice stream. A rate of sediment delivery of 0.25 km^3 a^{-1} is more comparable to the modelled rates of sediment transport by Dowdeswell and Siegert (1999) and to estimates of sediment delivery made for the palaeo-ice stream draining Marguarite Bay (Dowdeswell et al., 2004b). The disparity between these two scenarios makes it clear that better constraint of Bear Island Ice stream velocities and rates of bed deformation need to be made in order to improve our understanding of the Barents Sea Ice Sheet. This can only be achieved through more precise dating and correlation of sedimentary units across the entire Bear Island Trough-Mouth Fan.

5.4.2.2   Ice-sheet configuration

The geochemical composition of the mud fraction of the distal debris-flow muds in cores PE73, PE75, GC08 and JR142 were analysed using ITRAX µXRF data (Fig. 5.9). In core PE73 there were shown to be distinct differences between the major element ratios of the distal debris-flow muds from the Weichselian glaciations and the muds from the Saalian glaciation. When these ratios were compared to ratios from other regions, the composition of the Weichselian distal debris-flow muds was found to be similar to ratio data from east of Svalbard (Figs. 5.1 and 5.8b). The composition of the Saalian distal debris-flow muds was found to be similar to ratio data from a distal debris-flow mud from the central Bear Island Trough-Mouth Fan (Fig. 5.8b). These findings

suggest that the configuration of the Barents Sea Ice Sheet may have changed between the Saalian and the Weichselian.
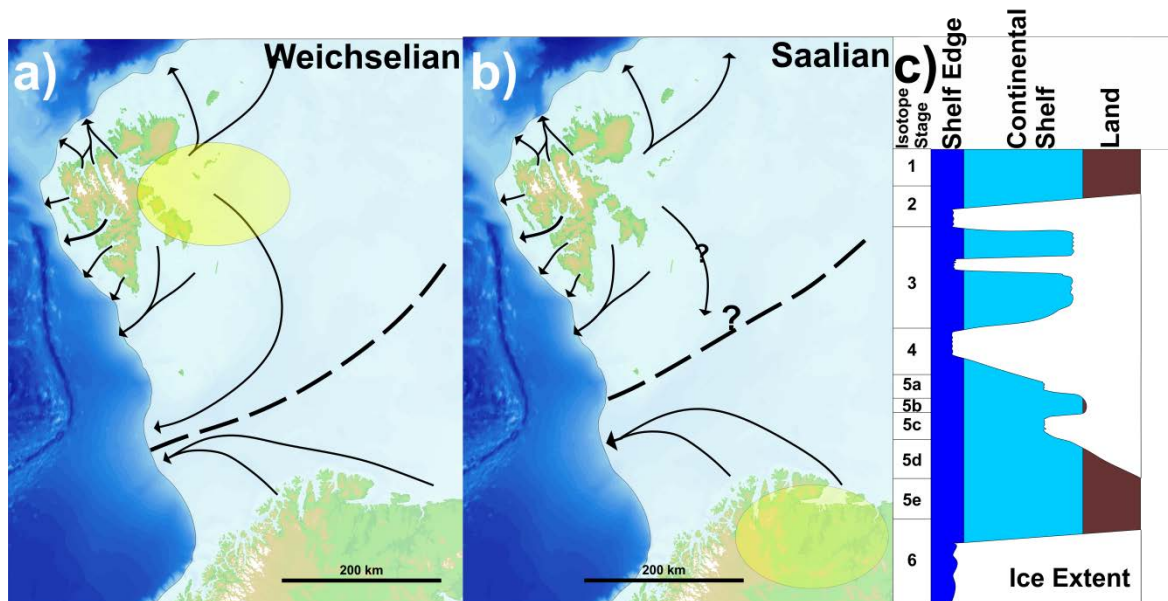
Figure 5.10 Ice sheet chronology for the Bear Island Trough during the last 140 ka. a) Palaeo ice-flow directions during the Weichselian with respect to the Bear Island Trough-Mouth Fan. During the Weichselian the northern end of the fan is dominated by an ice dome (in yellow) east of Svalbard. b) Palaeo ice-flow directions during the Saalian glaciation. During the Saalian the northern end of the fan is dominated by an ice dome (in yellow) associated with northern Scandinavia. c) A schematic plot of glacial advance and retreat in the Bear Island Trough. Ice advances are in white, areas currently below sea level are in blue and areas currently above sea level are in brown.

The similarities in the mud geochemical compositions between distal debris-flow muds in the cores indicate a change in sediment provenance between glaciations for the northern end of the Bear Island Trough-Mouth Fan. During the Weichselian, sediment was predominantly derived from the east of Svalbard in the Barents Sea (Fig. 5.10a). The location of an ice dome east of Svalbard delivering ice and sediment to the Bear Island Trough is consistent with regional seafloor geomorphology and flow-direction indicators for the Last Glacial Maximum (Andreassen et al., 2008; 2014; ; Hogan et al., 2010; Winsborrow et al., 2010). The geochemical composition of sediment in GC08 on the central Bear Island Trough-Mouth Fan during the Last Glacial Maximum suggests a more southerly source for this sediment (Fig. 5.10b). Ice input to the Bear Island Trough during the Saalian may therefore have originated from an ice dome that was centred on either Scandinavia or in the central Barents Sea (Fig. 5.10b). The ice-sheet configuration during the Saalian could have therefore resulted in little or no ice from an ice dome east of Svalbard being drained through Bear Island Trough.

5.4.3   Controls on ice sheet dynamics

The importance of ocean-atmosphere-ice interactions over long timescales are indicated by contrasts between the distal debris-flow muds. The Saalian Bear Island Ice stream was possibly fed predominantly by ice from Scandinavia, or at least from a dome further south in the Barents Sea (Fig. 5.10b). The Weichselian Bear Island Ice stream was dominated by ice derived from east of Svalbard (Fig. 5.10a; Winsborrow et al., 2010; 2012; Andreassen et al., 2014). The contrasts between the two regimes are probably a result of different patterns of snow accumulation (Mangerud et al., 1998; Siegert et al., 2001). The dominance of a more southerly ice dome during the Saalian is likely due to greater accumulation occurring further south during this time period; the difference in accumulation patterns leading to a different flow-partition pattern (Siegert and Marsiat, 2001; Bennett, 2003; Svendsen et al., 2004b; Ottesen et al., 2007).

The importance of ocean-atmosphere-ice interactions over short timescales is indicated by the timing of emplacement of the last glacigenic debris-flow deposits on the Bear Island Trough-Mouth Fan suggesting retreat prior to the global Last Glacial Maximum. Similarly early retreats from the shelf edge (~20,000 Cal BP) have also been reconstructed for ice streams offshore Svalbard (Rasmussen et al., 2007; Jessen et al., 2010; Hormes et al., 2013). On Svalbard, the cause of early thinning and retreat has been cited as possible changes to regional precipitation patterns. Biomarker proxies have been used to show an increased extent and duration of sea-ice prior to and at the Last Glacial Maximum (Müller et al., 2009; Müller and Stein, 2014). Greater sea-ice coverage would have acted to increase the distance between a possible moisture source and the ice-sheet interior. In addition, atmospheric modelling has suggested a southerly shift of the Oceanic Polar Front as a consequence of topographical forcing by the Barents Sea Ice Sheet (Pausata et al., 2011). A southerly shift of the Oceanic Polar Front would reduce the number of low-pressure systems reaching Svalbard (Siegert et al., 2001). This climatic adjustment would have led to a reduction in the amount of precipitation reaching the accumulation areas of Svalbard's ice streams. Reduced precipitation would lead to glacier thinning and possible retreat from the shelf edge (Helsen et al., 2008).

Coincident retreat of the Bear Island Ice stream from the shelf edge, and ice streams from the shelf edge around Svalbard to the north, implies a consistent forcing mechanism. The climatic reorganisation suggested regionally for Svalbard, may therefore not have been limited to Svalbard but affected the interior of the Barents Sea Ice Sheet. Given the position of the ice dome feeding the Bear Island Ice stream to the east of Svalbard (Fig. 5.10; Hogan et al., 2010; Winsborrow et al., 2010) it is perhaps unsurprising that atmospheric forcing is similar here to that on Svalbard itself. The reduction in surface accumulation across the interior of the Barents Sea Ice Sheet is likely to

be a factor in the retreat of the Bear Island Ice stream from the shelf edge and into the deeper water of the cross-shelf trough (Hebbeln et al., 1994). The early retreat into deeper water and thinning of the ice-sheet interior may have made the ice-sheet more sensitive to future climate and oceanic forcing as a consequence of increased calving associated with the higher buoyancy of deeper water (Benn et al., 2007a; 2007b; Amundson et al., 2010). Both factors would have enhanced the likelihood of further rapid retreat.

5.5　　Conclusions

Previous work on the Barents Sea Ice Sheet has inferred four advances to the shelf edge during the past 140,000 years (Fig. 5.10c). The number and timing of these advances was estimated using terrestrial records and proxies for ice advance such as ice-rafted debris. This study is the first to use distal debris-flow mud layers, and thus constrain the dynamics of the Barents Sea Ice Sheet in the Bear Island Trough over the last 140,000 years. The primary conclusion of our work is that distal debris-flow muds have been emplaced during four distinct time periods and are inferred to be representative of the times when ice was at the shelf edge. The timing of these ice advances differs from reconstructions of glacial history made previously but is consistent with ice-rafted debris deposits offshore of the Bear Island Trough-Mouth Fan. The four ice advances to the shelf edge occurred between 26,000 to 20,900, 39,400 to 36,000, 68,000 to 60,000 and >128,000 years BP.

Secondly, we show that the number and thickness of distal debris-flow mud deposits associated with each ice advance differs. We suggest that that this is a consequence of the stability of the ice-margin position and that it differed between the Weichselian and Saalian advances. Following the advance to the shelf edge during the Saalian, the Barents Sea Ice Sheet ice-margin was more stable and longer-lasting than any of the Weichselian advances as indicated by the thinner and less numerous distal debris-flow muds emplaced during the Weichselian.

Thirdly, we show that the geochemical composition of the distal debris-flow muds differs between the Saalian and the Weichselian. Using geochemical data from cores elsewhere around the Barents Sea, we suggest that this is a result of changing Barents Sea Ice Sheet configurations. We suggest that the Bear Island Trough drained ice predominantly from Scandinavia during the Saalian and drained ice predominantly from east of Svalbard during the Weichselian.

The results of this study indicate that deposits on trough-mouth fans can be used to reconstruct ice-sheet chronologies. Specifically, it is possible to use the presence or absence of glacigenic debris-flow deposits to identify when ice is present at the shelf edge and where the ice has drained from over multiple advance and retreat cycles. Where multiple glacial advances and

retreats can be identified using glacigenic debris-flow deposits, future efforts should be directed at reconstructing regional environmental variables such as sea-surface temperature and sea-ice coverage to identify whether there is any commonality of forcing associated with retreats. This may help to better understand forcing of contemporary marine-based ice masses.

Chapter 6:   What is the relationship between ice sheets and submarine mass movement occurrence?

Summary

Chapter 6 reviews the relationship between ice sheets and submarine mass movements. It specifically focusses on the growth and decay of the Greenland, Barents Sea and Scandinavian Ice Sheets around the Nordic Seas during the Quaternary. By tracking the growth and decay of these ice sheets and the related record of submarine mass movements, Chapter 6 analyses how the record of sediment delivery, submarine mass movement frequency and type is affected by changing climate. By combining these observations with those from other glaciated margins around the world, Chapter 6 attempts to derive first order controls on sediment delivery at ice sheet scales, propose new conceptual models for trough-mouth fan and glacial margin development. The relationship between large submarine landslides and ice sheets on different margins is also analysed in the context of previously proposed models. Using this information an additional model to explain some large submarine landslides is also proposed.

This chapter was submitted to *Earth Science Reviews* in June 2017. All analyses and interpretation were completed by myself, with editorial help provided by my co-authors during the paper writing process.

Reference:

Pope, E. L., Talling, P. J., Ó Cofaigh, C. *in review*. The relationship between ice sheets and submarine mass movements in the Nordic Seas during the Quaternary. Earth Science Reviews.

The relationship between ice sheets and submarine mass movements in the Nordic Seas during the Quaternary

Ed L. Pope[1], Peter J. Talling[2], Colm Ó Cofaigh[1]

[1]Department of Geography, Durham University, Science Laboratories, South Road, Durham, DH1 3LE, UK.

[2]Departments of Earth Science and Geography, Durham University, Science Laboratories, South Road, Durham, DH1 3LE, UK.

Abstract: Quaternary evolution of high-latitude margins has, to a large degree been shaped by the advance and retreat of ice sheets. Our understanding of these margins and the role of ice sheets is predominantly derived from the polar North Atlantic during the Late Weichselian. This region has formed the basis for conceptual models of how glaciated margins work and evolve through time with particular focus on trough-mouth fans, submarine landslides and channel systems. Here, by reviewing the current state of knowledge of the margins of the Nordic Seas during the Quaternary we provide a new set of models for different types of glaciated margin and their deposits. This is achieved by tracking the growth and decay of the Greenland, Barents Sea and Scandinavian Ice Sheets over the last 2.58 Ma and how these ice sheets have influenced sedimentation along their margins. The reconstructed histories show 1) the completeness of records along each ice sheet margin is highly variable. 2) Climatic deterioration and the adoption of 100 kyr cyclicity has had progressive impacts on each ice sheet and the resulting sedimentation and evolution of its related margin. These reconstructions and records on other margins worldwide enable us to identify first order controls on sediment delivery at ice sheet scales, propose new conceptual models for trough-mouth fans and glaciated margin development. We are also able to show how the relationship between large submarine landslide occurrence and ice sheet histories changes on different types of margin.

6.1   Introduction

Sediment is transported across our planet most efficiently by ice sheets and submarine mass movements (Boulton, 1978; Hallet et al., 1996; Dowdeswell et al., 2010; Talling et al., 2014). Rates of erosion by ice sheets and the subsequent transport and deposition of the eroded material in marine settings can be an order of magnitude greater than river catchments with larger areas (Milliman and Meade, 1983; Elverhøi et al., 1998). Once deposited this material is then often reworked by submarine gravity-flow processes. For example large submarine landslides, such as the Storegga Slide that occurred 8.2 ka offshore Norway, can contain several thousand cubic kilometres of predominantly glacigenic sediments (Haflidason et al., 2005). A clear relationship therefore exists between ice sheet processes, submarine mass movements and the sedimentary architecture of glaciated continental margins (Heezen and Ewing, 1952; Kuvaas and Kristoffersen, 1996; Vorren et al., 1998; Ó Cofaigh et al., 2003). Understanding the links between the two phenomena is therefore crucial to reconstructing ice sheet histories from the sedimentary record, and understanding the evolution of glaciated margins.

Delivery of sediment to the marine environment by ice sheets is characterised by its sporadic nature and the exceptional volumes involved. The rate of sediment delivery by ice sheets is a function of climatic variability, internal dynamics and the substrate over which the ice is moving. Over long timescales, the growth and decay of ice sheets is controlled by orbital forcing (Jansen and Sjøholm, 1991; Raymo and Ruddiman, 1992; Thiede et al., 1998; Jansen et al., 2000; Ehlers and Gibbard, 2004). At shorter timescales ice sheets can also be affected by sub-orbital forcing, such as reduced thermohaline circulation (Broecker and Denton, 1990; Bond et al., 1999), or the switch on/off of ice streams draining the ice sheet interior (Bennett, 2003; Catania et al., 2006; Dowdeswell et al., 2006b; Christoffersen et al., 2010). Spatially, ice sheet sedimentation also varies according to the position of fast and slow flowing ice (Ottesen et al., 2005), the drift tracks of icebergs (Mugford and Dowdeswell, 2010), the location of meltwater discharge from the ice front (Dowdeswell et al., 2015) and the type of substrate. This temporal and spatial variability

should be reflected in the sedimentary history of glaciated margins and therefore provide insights for ice sheet reconstructions. However, to assess this, accurate ice sheet and sedimentation histories need to be reconstructed and diagnostic facies need to be identified.

6.1.1   Why is it important to understand the links between ice sheet and sedimentation histories?

The geological record of high-latitude continental margins contains key information on former ice sheets (Dowdeswell et al., 2016b). Specific landforms and sedimentary sequences have been used to provide information on the extent of palaeo-ice sheets as well as the direction and nature of past ice flow and dynamics (Clark, 1993; Ottesen et al., 2005; Ottesen and Dowdeswell, 2006; Jakobsson et al., 2014; Hogan et al., 2016). Multiple sequences of alternating till and pro-/deltaic muds have been used to infer short-term advance and retreat cycles (Funder and Hansen, 1996). Eskers and tunnel valleys have been used as indicators of the geometry of past subglacial hydrological systems (Stewart et al., 2013; Greenwood et al., 2016). Trough-mouth fans, covering areas of $10^3 - 10^5$ km^2 with volumes of $10^4 - 10^5$ km^3, are thought to be indicative of the delivery of large volumes of sediment by fast-flowing ice streams present at the shelf edge (Dowdeswell et al., 1997; Vorren and Laberg, 1997; Canals et al., 2003; Ó Cofaigh et al., 2003). These landform interpretations can subsequently by used to constrain/validate ice sheet models, which in turn can be used to model possible future ice sheet changes (Kleman et al., 1997; Greenwood and Clark, 2009).

6.1.1.1   Ice sheets, climate and sedimentation histories

Interpretations of landforms and sedimentary sequences are based on a combination of observations from contemporary glacial environments and interpretations of the environmental conditions that existed under full-glacial conditions. At the most fundamental level these interpretations reflect our understanding of the relationship between glacier dynamics and climate (Hallam, 1989). To first order, glacial sediment delivery and thus landform genesis is often linked to temperature. It is hypothesised that colder climates result in lower basal temperatures

in glaciers and ice sheets (Cuffey and Paterson, 2010). These temperatures reduce meltwater production which in turn impacts upon glacial sliding, erosion and therefore sediment transfer (Herman et al., 2011; Egholm et al., 2012; Koppes et al., 2015). At a process scale, processes dominating glacier-influenced delivery of sediment to marine environments are also linked to temperature. Modern/Quaternary interglacial glacier delivery of sediment to marine environments is conceptualised as a continuum between meltwater dominated (e.g. Southern Alaska) to iceberg dominated (e.g. West/East Antarctica) environments (Fig. 6.1a; Dowdeswell et al., 1998). Under full-glacial conditions, the position of each system and thus the dominance of a given mechanism for sediment delivery, shifts its position on the continuum (Fig. 6.1b; Dowdeswell et al., 2016b).
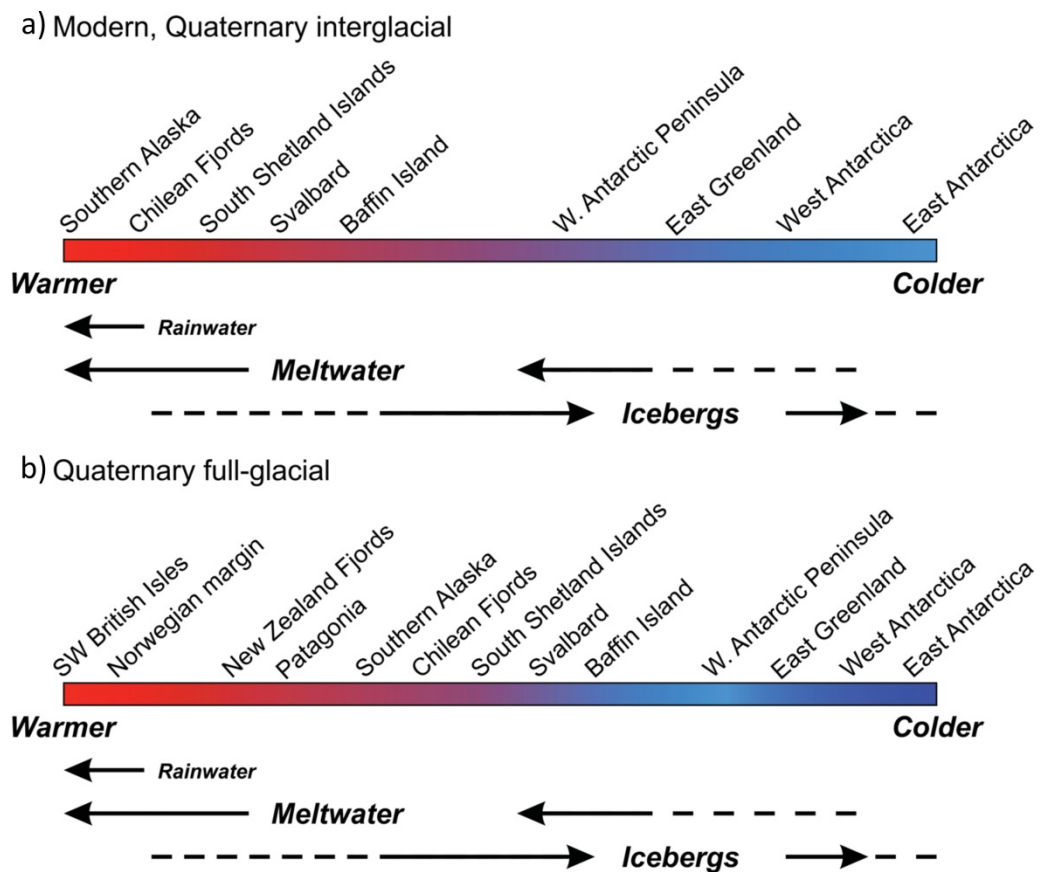
Figure 6.1 The climatic continuum of glacier-influenced marine settings for, a) the modern or Quaternary interglacial Earth, and b) Quaternary full-glacial conditions (modified from Dowdeswell et al., 2016b).

The evolution and history of sedimentation on continental margins should not, however, be conceptualised simply as glacial vs. interglacial conditions. The length and severity of glacial periods has varied throughout the Quaternary (Thiede et al., 1989; Raymo and Nisancioglu, 2003; Ehlers and Gibbard, 2004). At the simplest level, glacial periods can be divided into those which occurred when climate was dominated by 41 kyr cyclicity and those that occurred under 100 kyr cyclicity (Raymo and Nisancioglu, 2003; Tziperman and Gildor, 2003). In terms of erosion and sediment delivery to the continental margin, it has been proposed that the adoption of the 100 kyr climate cycle led to an intensification of glacial erosion and sediment transport (Faleide et al., 2002; Gulick et al., 2015). However, this assertion, linked to the severity and intensity of the 100 kyr world is at odds with the understanding of temperature/climate controlling the rate of glacier driven sedimentation. Long-term marine sedimentary records provide one of the few means through which these relationships can be tested over multiple glacial cycles and thus allow us to reconstruct ice sheets and ice sheet processes and their response to variable climatic forcing.

6.1.1.2   Geohazard assessment

Understanding the links between ice sheets and sedimentary processes on continental margins is also critical for hazard assessment. Since the 1929 Grand Banks submarine landslide, increasing numbers of slide scars and deposits have been mapped on previously glaciated margins (Heezen and Ewing, 1952; Bugge, 1983; 1987; Piper and Aksu, 1987; Dowdeswell et al., 1996; Vorren et al., 1998; Hogan et al., 2013). Considered to be one of the main morphological features of glaciated margins, these events have the potential to generate damaging tsunami and damage local subsea infrastructure (Heezen and Ewing, 1952; Bondevik et al., 1997; 2003; Grauert et al., 2001; Pope et al., 2017). The Storegga Slide is known to have generated a tsunami with wave run-up heights >20 m (Bondevik et al., 2003) while the Grand Banks Slide caused 23 telegraph cable breaks (Piper et al., 1999). The locations of the slides, specifically their often close association with trough-mouth fans, has led to the hypothesis that rapid rates of ice sheet driven sedimentation is a critical factor in the triggering of these slides (Bryn et al., 2003; 2005; Haflidason et al., 2004; Owen et al., 2007).

Understanding the timing and emplacement mechanisms of these slides over multiple glacial cycles relative to changing ice sheet dynamics is therefore crucial to quantifying the potential risk associated with these hazards.

6.1.2   Previous models linking ice sheet with sedimentation processes and continental margin morphology

Conceived in the mid-1990s, an original model (Fig. 6.2; Dowdeswell et al., 1996) for large-scale sedimentation on glaciated margins was based on a combination of GLORIA imagery, seismic data and models of former ice sheet behaviour. This model linked the sedimentary architecture seen on the margins of the Nordic Seas (i.e. submarine channels, glacigenic debris-flows, etc.) to the presence/velocity of ice delivering sediment to the shelf break (Dowdeswell et al., 1996; Dowdeswell and Siegert, 1999). Low velocity ice associated with low sediment delivery or ice terminating inshore of the shelf edge was hypothesised to be associated with submarine channel systems. Fast flowing ice streams delivering large amounts of sediment were associated with glacigenic debris-flows, submarine landslides and the build-up of trough-mouth fans (Dowdeswell et al., 1996).

With the available data this model effectively identified where specific sedimentary features and processes were likely to occur and how they related to palaeo-ice sheets. However, since the inception of this model a number of key advances have been made. First, studies have been able to identify how sedimentation has changed over time on specific sections of a margin (e.g. Solheim et al., 1998; Nygård et al., 2005). This implies that a static model of ice sheet driven sedimentary processes is perhaps not appropriate. Second, there has been growing recognition of the importance of specific processes, such as meltwater delivery of sediment, on glaciated margins (Lekens et al., 2005; Lucchi et al., 2013). These processes therefore may have to be incorporated within a model of glacial margin sedimentation. Third, our understanding of other glaciated margins around the world has improved (Escutia et al., 2000; Ó Cofaigh et al., 2008; 2013; Montelli et al., 2017). This enables us to analyse whether models of glaciated margins based

on observations around the Nordic Seas are applicable to other margins. For these reasons, it is

timely to re-evaluate our current models of glaciated margin sedimentation and evolution.
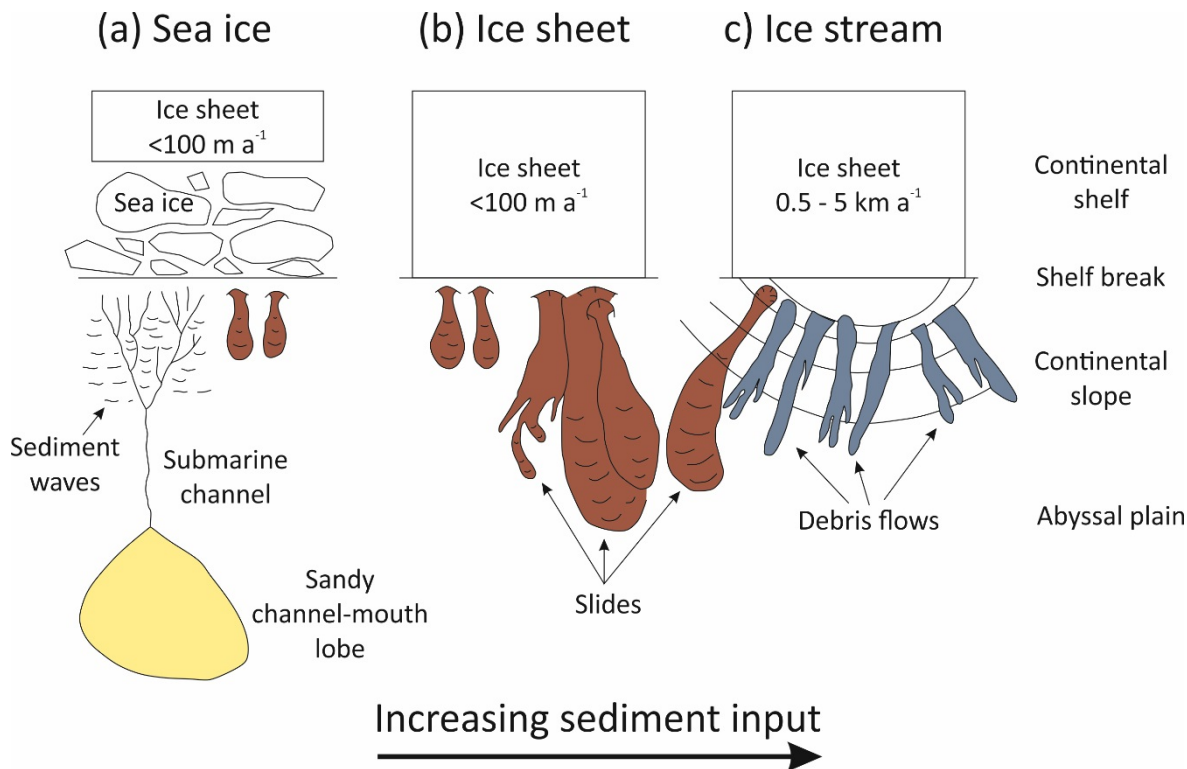
Figure 6.2 Conceptual model of sedimentation on glacier-influenced continental margins. a) Sediment starved margin with an ice sheet terminating inshore of the shelf edge. b) Inter-ice stream areas with ice at the shelf edge. c) Continental margin dominated by ice stream delivery of sediment and the resulting formation of a trough-mouth fan (from Dowdeswell et al., 1996).

6.1.3   Why focus on the Nordic Seas?

This study of ice sheet and submarine mass movement histories is focussed initially on their

relationship in the Nordic Seas (Fig. 6.3). We chose to focus at first on this region for a number of

reasons. First, the Nordic Seas and their surrounding margins have been subject to multiple

glaciations during the Quaternary. During the Quaternary four major ice sheets, the Greenland,

the Barents Sea, the Scandinavian and the British-Irish Ice Sheet have grown and decayed on the

continents surrounding the Nordic Seas (Ehlers and Gibbard, 2004; Hibbert et al., 2010; Funder et

al., 2011; Patton et al., 2015). Each of these ice sheets has different climatic, topographic and

geological settings which can affect the processes of ice movement, advance and retreat, and the

delivery of sediment (Patton et al., 2016). These contrasts allow us to assess how variable

histories of sedimentation are across and between glaciated margins through different glacial

cycles.
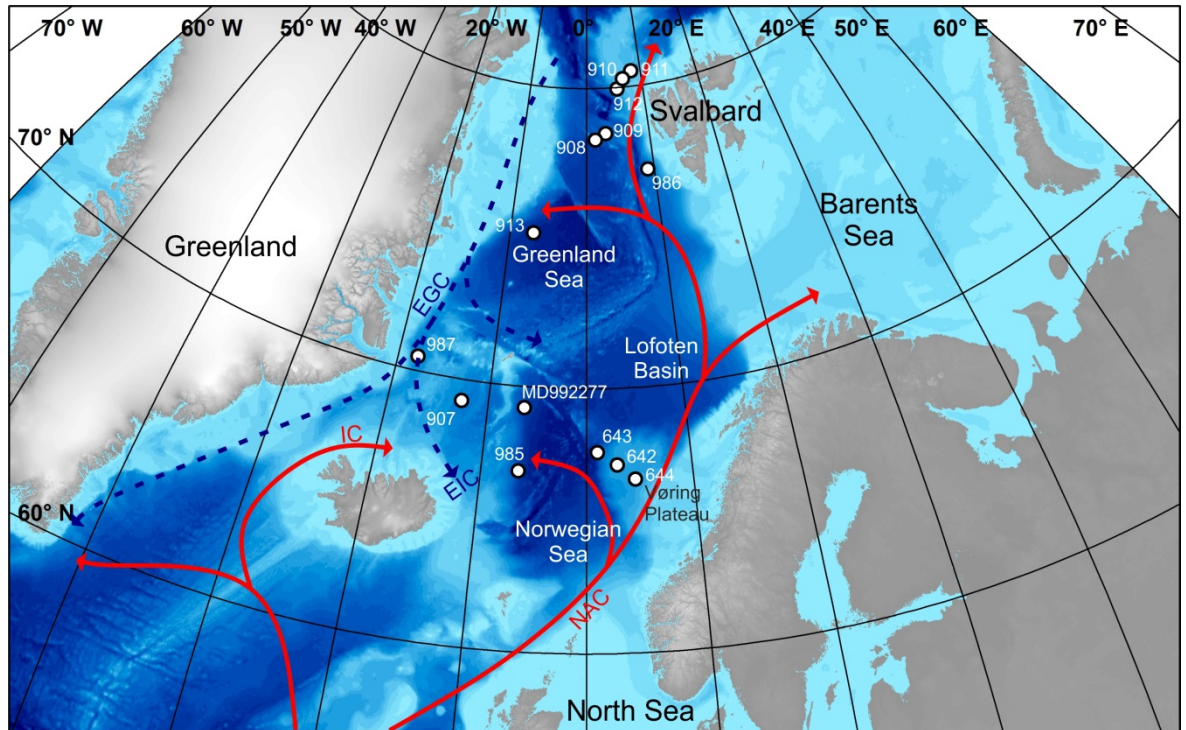
Figure 6.3 Map of the Nordic Seas and the ODP sites used in this study. General ocean circulation
during the present interglacial is also shown (red – warm; blue – cold). NAC –
Norwegian Atlantic Current; EGC – East Greenland Current; EIC – East Iceland Current;
IC – Irminger Current.

Second, the Nordic Seas and their surrounding land masses are one of the best studied glaciated

margins. The economic resources found here, combined with multiple long-running scientific

consortia projects (e.g. PONAM and QUEEN) have resulted in regional scale mapping of the

surface and sub-surface of the continental shelf and slope (Faleide et al., 1996; Solheim et al.,

1998; Svendsen et al., 2004a). Combined with sedimentological studies, this has resulted in one of

the most complete records of ice sheet change and the associated history of sedimentation

during the Quaternary (Mangerud et al., 1998; Eidvin et al., 2000; Jansen et al., 2000; Svendsen et

al., 2004a; and references therein). It is therefore appropriate that any attempt to understand the

evolution of glaciated margins should include a detailed study of the margins of the Nordic Seas.

The transferability of models based on the Nordic Sea margins to other glaciated margins can subsequently be assessed.

6.1.4   Aims

The purpose of this study is to draw together various records from around the Nordic Seas to achieve the following aims.

1) We aim to reconstruct the growth and decay histories of the Greenland, Barents Sea and Scandinavian Ice Sheets on the margins of the Nordic Seas and outline the history of sedimentation associated with these ice sheets.

2) We compare sedimentary records on different margins to those from the Nordic Seas in order to understand the appropriateness of models derived from the Nordic Seas for understanding other glaciated margins.

3) From these records, we aim to derive a set of general models for ice sheet driven sedimentary processes and landform formation on the continental shelf and slope. These general models for different types of system aim to provide a basis for understanding the evolution of glaciated margins.

6.2   Ice sheet and submarine mass movement histories

The following section will first outline the Late Pliocene history for the Greenland Ice Sheet, Barents Sea Ice Sheet and Scandinavian Ice Sheet. It will then analyse the evolution of each ice sheet during the Quaternary and the associated sedimentation record. First, we focus on the Greenland Ice Sheet; second, the Barents Sea Ice Sheet and last the Scandinavian Ice Sheet.

6.2.1   Ice sheet histories in the Late Pliocene

The Pliocene spans a period from 5.3 – 2.58 Ma. This period was characterised by significant cooling of high latitude regions (Fronval and Jansen, 1996; Kleiven et al., 2002). The climatic

deterioration that occurred during this period led to the expansion of ice sheets around the Nordic Seas (Solheim et al., 1998; Forsberg et al., 1999) and the adoption of orbitally forced climatic cyclicity (Kleiven et al., 2002). The progression of ice sheet development can be seen in the Ice-Rafted Debris (IRD) histories of ODP sites from around the Nordic Seas (Fig. 6.3).

Sedimentary records show that the Greenland Ice Sheet was the earliest to expand and was the most expansive ice sheet in the region during this period. The earliest and largest IRD peaks (before 3 Ma) are recorded at ODP Sites 987 and 907. Located on the Scoresby Sund Trough-Mouth Fan and on the Iceland Plateau (Fig. 6.3), the IRD records from these cores and the lack of comparable records from sites elsewhere around the Nordic Seas suggest that the Greenland Ice Sheet was producing the largest volumes of IRD during this period (Jansen et al., 1988; 2000; Channell et al., 1999).

With the exception of an ice advance ~2.7 Ma, there is little evidence of ice sheet activity on the Northern European Margin during the Pliocene comparable to the expansion proposed for the Greenland Ice Sheet. IRD records on the Yermak Plateau (Sites 910 and 911; Fig. 6.3) indicate glacial ice growth on the northern, sub-aerially exposed Barents Sea between 3.5 and 2.6 Ma (Rasmussen and Fjeldskaar, 1996; Butt et al., 2002). However, IRD records from the Fram Strait indicate that this growth was fairly limited (Knies et al., 2009). Further south, along the Norwegian continental margin, ODP Sites (644 and 642) on the Vøring Plateau indicate growth of Scandinavian glaciers at this time (Spiegler and Jansen, 1989; Jansen and Sjøholm, 1991). However, the IRD is two to three orders of magnitude smaller than Quaternary IRD fluxes indicating far less extensive glaciations before 2.58 Ma (Jansen and Sjøholm, 1991).

6.2.1.1   Sedimentary records of ice sheet and submarine mass movement histories: Late Pliocene

The impact of ice sheets on the continental shelves of the Nordic Seas varies according to local ice sheet history. The continental shelf of Greenland underwent significant changes during the Late Pliocene. Evidence for repeated glaciation of the shelf comes primarily from IRD records around

Greenland (Larsen, 1990; Jansen and Sjøholm, 1991; Larsen et al., 1994). However, this period is also marked by an erosional unconformity across the East Greenland continental shelf, marking the most pronounced depositional change within the geological record of this region (Vanneste et al., 1995; Fig. 6.4). Correlation of seismic and core records from the Scoresby Sund Trough-Mouth Fan also indicate the presence of glacigenic debris-flow deposits from this period (Larsen, 1990; Vanneste et al., 1995; Solheim et al., 1998). The presence of debris-flow deposits is inferred to be indicative of fast flowing ice reaching the shelf edge and depositing large volumes of sediment. The increased delivery of sediment to the fan during the Late Pliocene is hypothesised to mark the start of the main construction phase of the fan in conjuncture with widespread progradation of the continental shelf (Larsen, 1990; Jansen and Raymo, 1996; Solheim et al., 1998).

With the exception of a correlatable regional till layer produced by the glacier advance ~2.7 Ma, there is little evidence of significant Late Pliocene ice sheet related influence on the sedimentary evolution of the Scandinavian or Svalbard/Barents Sea continental margin (Sejrup et al., 1996; 2005; Lee et al., 2012). There is also no evidence of any link between ice sheet activity and submarine mass movement occurrence at this time.

6.2.2   Greenland Ice Sheet

The following section focuses on the evolution of the Greenland Ice Sheet. Specifically it will focus on the sectors of the ice sheet that border the Nordic Seas.

6.2.2.1   2.58 – 1.3 Ma

The Greenland Ice Sheet was the largest ice sheet around the Nordic Seas and advanced the furthest onto the shelf during the Early Quaternary. This is suggested by both IRD records close to the Greenland continental shelf and records further out into the Nordic Seas (Jansen et al., 2000; Helmke et al., 2003b) as well as erosional unconformities on the continental shelf (Fig. 6.4). These records show the 41 kyr periodicity of Greenland Ice Sheet expansion and contraction and a

dominant contribution of IRD into the Nordic Seas compared to other surrounding ice masses
(Jansen and Sjøholm, 1991; Jansen et al., 2000; Helmke et al., 2003b).
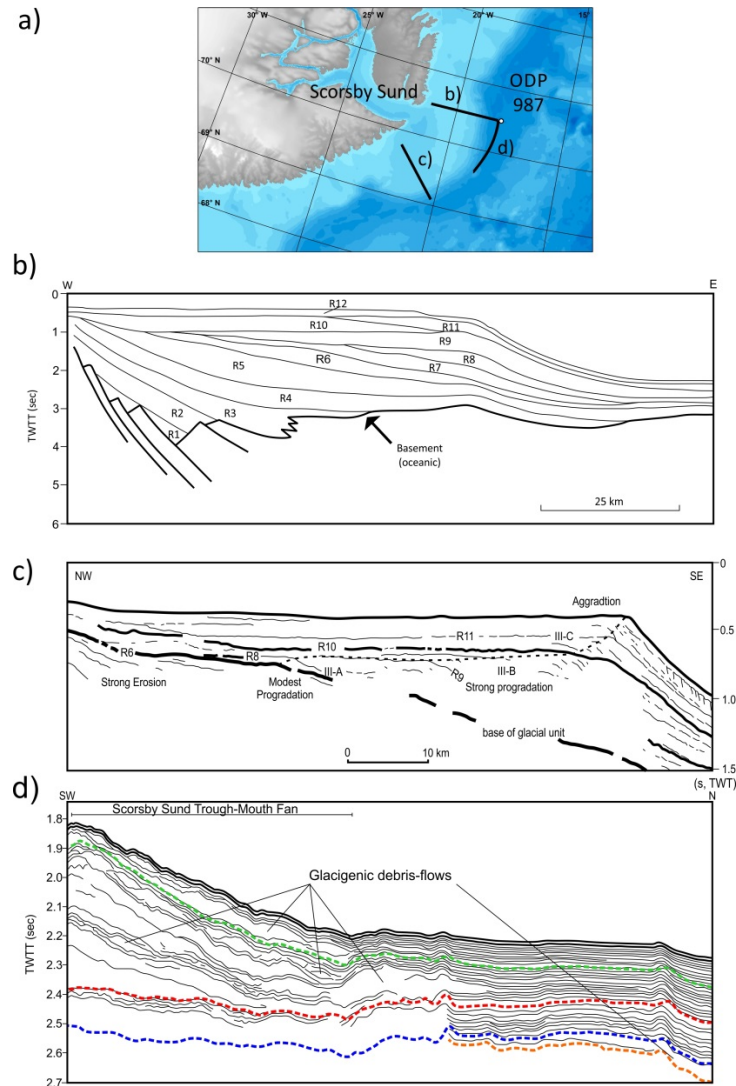
Figure 6.4 Multichannel seismic lines on the Scoresby Sund Trough-Mouth Fan (modified from
Vanneste et al., 1995; Solheim et al., 1998; Laberg et al., 2013). a) Location map
showing seismic lines GGU 82-12 and 90600 and the line of Laberg et al. (2013),
relative to the position of ODP Site 987. b) Seismic line GGU 82-12. According to
Larson's (1990) original interpretation, sequences 9 – 11 represent Late Miocene to
Pliocene and 12 represents the Pleistocene. c) Interpretation of the stratal geometry
in the continental shelf part of line 90600. Based on variations in the aggradation and
progradation components, the glacial unit, Unit III, has been divided into subunits A,
B, and C. d) Single channel seismic profile extending from ODP Site 987 southward.
Lithological units, age model and seismic reflections according to Shipboard Scientific
Party (1996) are reflected by dashed lines. Green – 0.78 Ma; Red – R1 reflector at 1.77
Ma; Blue – R2 reflector; Orange – 2.58 Ma.

IRD records imply the two largest advances occurred at the start of the Early Quaternary from 2.5 – 2.4 Ma and ~2.1 Ma. Subsequent IRD peaks are smaller, suggesting later advances were not as spatially or temporally as great or did not produce similar numbers of icebergs (Jansen and Sjøholm, 1991). It does not appear that the ice sheet underwent widespread collapses that characterised the Laurentide and northern European ice sheets in the Late Quaternary. This is inferred from the amplitude of $\delta^{18}O$ variations (Lisiecki and Raymo, 2007) and the continuous presence of IRD beyond the shelf edge (Jansen et al., 2000).

6.2.2.1.1   Sedimentary records of ice sheet and submarine mass movement histories

The initial 2.5 – 2.4 Ma advance left the largest sedimentary signature during the Early Quaternary. This advance is marked by reflector R6 in Fig. 6.4c which identifies the base of the glacial units in the Scoresby Sund area (Vanneste et al., 1995). This advance was characterised by the emplacement of glacigenic debris-flow deposits on the Scoresby Sund Trough-Mouth Fan implying a high rate of sediment delivery during this period (Solheim et al., 1998; Channell et al., 1999). Subsequent sedimentation was characterised by silty clays containing variable amounts of IRD, turbidites ranging in thickness from 5 to 60 cm and lower volume glacigenic debris-flows emplaced on the upper parts of Scorsby Sund Trough-Mouth Fan (Solheim et al., 1998; Wilken and Mienert, 2006). The change in depositional character may be a consequence of lower rates of sediment transport to the shelf edge by continental ice and storage on the shelf. This hypothesis is supported by limited progradation of the shelf edge of only 5 km during the Early Quaternary (Vanneste et al., 1995); a rate of progradation 16 times lower than would occur from 1.3 – 0.7 Ma. Alternatively, deposition of sediment by meltwater processes may have led to enhanced turbidity current activity and the transportation of sediment to the deep ocean.

6.2.2.2   1.3 – 0.7 Ma

Compared with the northern European ice sheets, the Greenland Ice Sheet underwent comparatively little change between 1.3 and 0.7 Ma. The ice sheet underwent advance and

retreat cycles consistent with climatic forcing. However, the extent of these advances is contentious.

Early analysis of the Greenland Ice Sheet during this time period concluded that the ice sheet was relatively stable. Neither its advances, nor its retreats were particularly extensive; the ice sheet remaining on or near to the continental shelf (Solheim et al., 1998; Butt et al., 2001). This scenario was supported by the continuous supply of IRD provided by the Greenland Ice Sheet to sites both in and outside of the Nordic Seas (Larsen, 1990; Larsen et al., 1994; St. John and Krissek, 2002; Helmke et al., 2003a). Large peaks of accumulated IRD indicating widespread collapse/retreat of an extensive ice sheet were also less common (Jansen et al., 2000).

Subsequent analysis of offshore records has challenged the view of a 'stable' confined ice sheet. Glacigenic debris-flows on the Scoresby Sund Trough-Mouth Fan (Fig. 6.4d) suggest the ice sheet may in fact have advanced sufficiently during this period to reach the shelf edge. The exact timing of advances to the shelf edge are uncertain (Laberg et al., 2013), but is suggestive of a more dynamic glacial regime, more akin to reconstructions of for the Late Quaternary Greenland Ice Sheet (Håkansson et al., 2009; Winkelmann et al., 2010).

6.2.2.2.1   Sedimentary records of ice sheet and submarine mass movment histories

Contrasting sedimentary processes are invoked to be associated with the Greenland Ice Sheet between 1.3 and 0.7 Ma. First, glacigenic debris-flow deposits on the central and southern sides of the Scoresby Sund Trough-Mouth Fan suggest direct input of sediment by an ice stream active at the shelf edge (Laberg et al., 2013; Laberg and Dowdeswell, 2016). Second, the dominant ice sheet driven process responsible for the majority of margin evolution is meltwater delivery of sediment. From 1.3 – 0.6 Ma the eastern Greenland shelf margin moved seawards by 38 km (Vanneste et al., 1995). This progradation has been attributed to glacimarine deposition through meltwater plumes and the occurrence of turbidity currents (Solheim et al., 1998; Wilken and Mienert, 2006). The delivery of sediment through these processes is also thought to be responsible for vertical aggradation of the shelf by 130 m (Vanneste et al., 1995). The

predominance of sediment delivery through meltwater processes and the triggering of turbidity currents is also thought to have led to submarine channel formation along the East Greenland Margin during this period (Ó Cofaigh et al., 2004; Wilken and Mienert, 2006; Laberg et al., 2013).

6.2.2.3   0.7 – 0.13 Ma

Repeated glaciations of the Greenland continental shelf are inferred from 0.7 – 0.13 Ma from IRD records but the advance extent remains unclear (Solheim et al., 1998; Jansen et al., 2000). Between 0.7 – 0.13 Ma background levels of IRD are greater than they were during earlier periods, although IRD pulses are less common (St. John and Krissek, 2002). This could be a consequence of either a larger and more stable ice sheet or a function of greater sea ice coverage preventing IRD reaching the continental shelf (Funder et al., 2011). One exception to this is the Saalian glaciation. Terminating at ~130 ka, terrestrial and continental shelf records suggest that the Saalian Greenland Ice Sheet represents the maximum ice cover achieved during the Late Quaternary (Funder et al., 1998; Nam and Stein, 1999; Adrielsson and Alexanderson, 2005; Håkansson et al., 2009).

6.2.2.3.1   Sedimentary records of ice sheet and submarine mass movement histories

The Late Quaternary is primarily associated with aggradation of sediment on the continental shelf (Fig. 6.4b; sequence 10 and 11). From 0.7 – 0.13 Ma the continental shelf aggradated over 260 m, whereas progradation is reduced to less than 5 km (Vanneste et al., 1995). This is attributed to the reduced erosional capabilities of successive advancing ice sheets and the increased distance to the shelf edge (Vanneste et al., 1995; Solheim et al., 1998). As a consequence there is limited evidence for submarine mass movement occurrence on or beyond the continental shelf, although this may be a consequence of subsequent erosion by the Saalian and Weichselian ice sheets.

The shelf edge Saalian advance led to a phase of intense sediment remobilisation. Glacigenic debris-flows occurred on the southern part of the Scoresby Sund Trough-Mouth Fan (Fig. 6.4; Dowdeswell et al., 1997; Laberg et al., 2013). The shift in location of glacigenic debris-flows on the fan is a consequence of a cross-shelf trough migration. The change of drainage path direction is

reflected by a lack of mass movement deposits and the lower sedimentation rate after about 0.78 Ma at ODP Site 987 (Nam et al., 1995; Funder et al., 2011; Laberg et al., 2013).

Ice also reached the shelf edge along the section of the Greenland Basin where submarine channels had previously formed between 1.3 and 0.7 Ma (Wilken and Mienert, 2006). The continental margin in this sector was also characterised by limited glacigenic debris-flow emplacement during the Saalian advance. However, unlike earlier advances or indeed the Weichselian advances, evidence suggests that the submarine channel system that was previously present along this margin was not active and was in fact overridden by glacigenic debris-flows (Wilken and Mienert, 2006). From this we infer that turbidity currents played a far less pivotal role in sediment transport during the Saalian compared to previous and later glacial advances in this area (Wilken and Mienert, 2006).

6.2.2.4   0.13 – 0 Ma (Weichselian – Present)

Greenland Ice Sheet history during the Weichselian is the best constrained of any period during the Quaternary. Our understanding of the ice sheet is, however, based primarily on a number of key sites and thus reconstructions involve a large amount of interpolation. Along the East Greenland Margin reconstructions are based primarily on sites around Scoresby Sund and Jameson Land (Funder et al., 2011). The consequence of this is that we are unable to build precise advance and retreat chronologies with the same level of detail that we are able to for the Barents Sea and Scandinavian Ice Sheets.

Five glacial advances are envisaged in East Greenland. The earliest advances are attributed to Marine Isotope Stage (MIS) 5d and 5b (Funder et al., 1994; Landvik, 1994; Tveranger et al., 1994). During the former, glaciers are believed to have advanced at least onto the inner shelf (Tveranger et al., 1994). IRD records also suggest an advance during MIS 4 followed by a limited retreat between MIS 4 and 3 (Funder et al., 1998; 2011). In Scoresby Sund the extent of the MIS 4 ice sheet around 60 ka Before Present (BP) has been suggested to be close to the limit of the MIS 2 ice sheet (Hansen et al., 1999). Small IRD peaks during MIS 3 which coincide with heavy and light

$\delta^{18}O$ values are inferred to represent small advance and retreat cycles (Nam et al., 1995; Stein et al., 1996). However, they may also represent fluctuations in sea ice cover along the East Greenland Coast (Nam et al., 1995; Stein et al., 1996).

The last glacial advance occurred in MIS 2. IRD records indicate that glaciers in East Greenland reached their maximum extent from 21 – 16 ka BP (Stein et al., 1996). Changes to glacier margin positions may also be indicated by pulses of IRD at ~32720, ~30850 – ~29670, ~27000 – ~25900, ~24840 ± 67 – ~23600 ± 81, ~21280 – ~20000, ~17800 – ~16350 cal BP (Funder et al., 1998). However, the extent and style of glaciation of the MIS 2 advance is uncertain. Observations from the south east and south west sectors of the Greenland Ice Sheet show that glaciers expanded to the shelf edge (Funder et al., 2011). In contrast, seismic records of the central East Greenland continental shelf show no seismically resolvable layers associated with this advance (Solheim et al., 1998). Two scenarios have been suggested to explain this; (1) glaciers reached the coast and fjord mouths but did not expand greatly onto the continental shelf (Solheim et al., 1998); or (2) glaciers were cold-based with restricted flow and sediment transfer (Funder et al., 1998). However, more recent cosmogenic dating in the Scoresby Sund region has suggested that ice may have reached the outer shelf (Håkansson et al., 2009). In the northeast sector of the Greenland Ice Sheet, submarine landforms (mega-scale glacial lineations and elongate bedforms) indicate that the MIS 2 ice sheet expanded to at least the middle-outer continental shelf (Evans et al., 2009). Contrary to the suggested restricted flow pattern in the central eastern sector, bathymetric cross-shelf troughs in this sector were filled by warm-based, fast flowing ice. There is also evidence to suggest active ice flow across shallow intra-trough regions (Evans et al., 2009).

The exact timing of retreat from the MIS 2 maximum is equally contentious. Funder and Hansen (1996) suggested that the ice margin began retreating from the outer part of fjord basins at ca. 17.8 cal ka BP in the central East Greenland sector. The timing is coincident with a marked decrease in IRD in continental slope records (Nam et al., 1995). An alternative scenario proposes that deglaciation occurred shortly before 10 ka BP (Björck et al., 1994a; 1994b). In the northeast

sector, glacier retreat is envisaged to occur after 19530 ± 67 cal BP, marked by an increase in IRD

on the continental slope (Nothold, 1998; Evans et al., 2009).
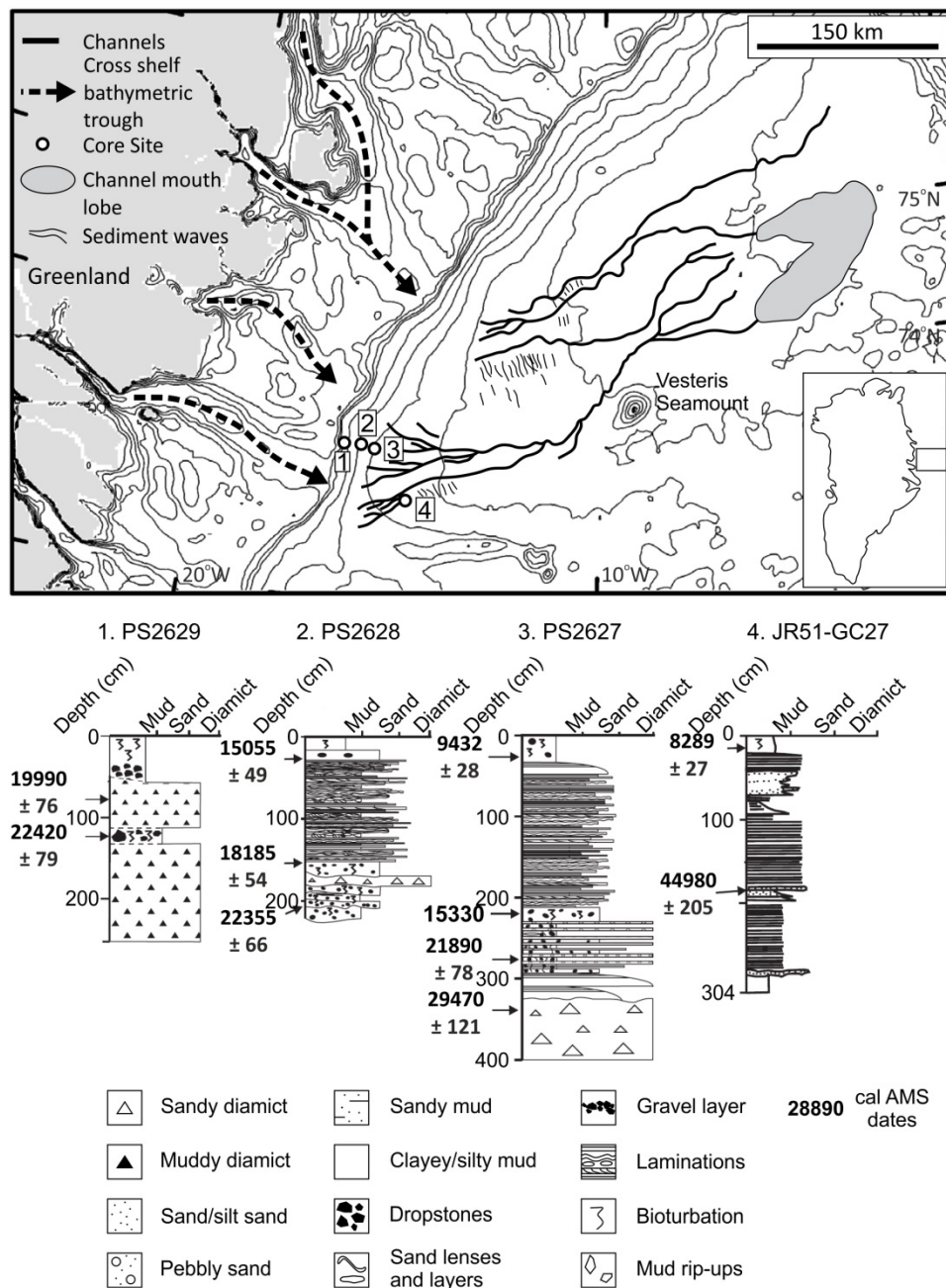
Figure 6.5 Bathymetry of the Greenland Basin and the adjoining continental shelf, Northeast Greenland and major submarine geological features (channel systems, sediment waves and channel-mouth lobes). Major cross-shelf troughs on the continental shelf are highlighted by arrows. Core sites are numbered 1 to 4. Sediment logs of gravity cores identified on the bathymetric map are included with calibrated AMS radiocarbon dates. Bathymetric data on continental shelf are derived from the IBCAO Arctic bathymetry database (Jakobsson et al., 2000). Figure is adapted from Ó Cofaigh et al. (2004).

6.2.2.4.1   Submarine records of ice sheet and submarine mass movement histories

The sedimentary signature of the Weichselian glaciation along the East Greenland Margin is extremely varied but beyond the shelf break is associated with widespread submarine mass movement occurrence. In more proximal settings, the multiple cycles of expansion and contraction can be identified within fjord settings by sedimentary successions. Advances are characterised by tills and overridden/thrusted sediments (Tveranger et al., 1994; Funder et al., 1998). Retreats are indicated by pro- and deltaic mud and sand sequences (Funder et al., 1994; 1996). Additional sequences include thick laminated fine-grained sediments likely resulting from glacier proximal sediment plumes (Stein et al., 1993; Funder et al., 2011).

Beyond the continental shelf, submarine mass movement processes vary by sector. In the Scoresby Sund sector, glacigenic debris-flows occurred on the southern side of the Scoresby Sund Trough-Mouth Fan (Nam et al., 1995; Dowdeswell et al., 1997). The previously active northern side does not appear to have experienced any mass wasting processes during the Weichselian (Laberg et al., 2013).

North of the Scoresby Sund Trough-Mouth Fan, glacigenic debris-flow, turbidity current deposits and extensive channel systems have been identified beyond the shelf break (Fig. 6.5; Ó Cofaigh et al., 2004; Wilken and Mienert, 2006). Associated with cross-shelf troughs, glacigenic debris-flow lobes are found on the upper and mid- continental slope. Below 2000 m water depth turbidites are the dominant sedimentological facies (Ó Cofaigh et al., 2004). The glacigenic debris-flows are dated >22,820 yrs BP (Wilken and Mienert, 2006). Turbidity current activity ceased by 13,000 yrs BP (Fig. 6.5; Ó Cofaigh et al., 2004). Prior to the cessation of turbidity current activity, deposition on this part of the margin was characterised by laminated silt and mud layers associated with deglaciation. Sedimentation rates peaked between 51 – 79 cm kyr^{-1} between 15,000 and 13,000 BP before falling to <4 cm kyr^{-1} after 13,000 BP (Ó Cofaigh et al., 2004; Wilken and Mienert, 2006). An extensive submarine channel network is also found along this part of the margin. The channels cross-cut the glacigenic debris-flow deposits on the upper and mid-slope implying their formation

post-dates the emplacement of these deposits (Ó Cofaigh et al., 2004). The direct link between ice

sheet delivery of meltwater and sediment, the occurrence of turbidity currents and the cessation

of activity within any of the channels following the withdrawal of the ice sheet illustrates the role

of the Greenland Ice Sheet in the sedimentary evolution of the margin.
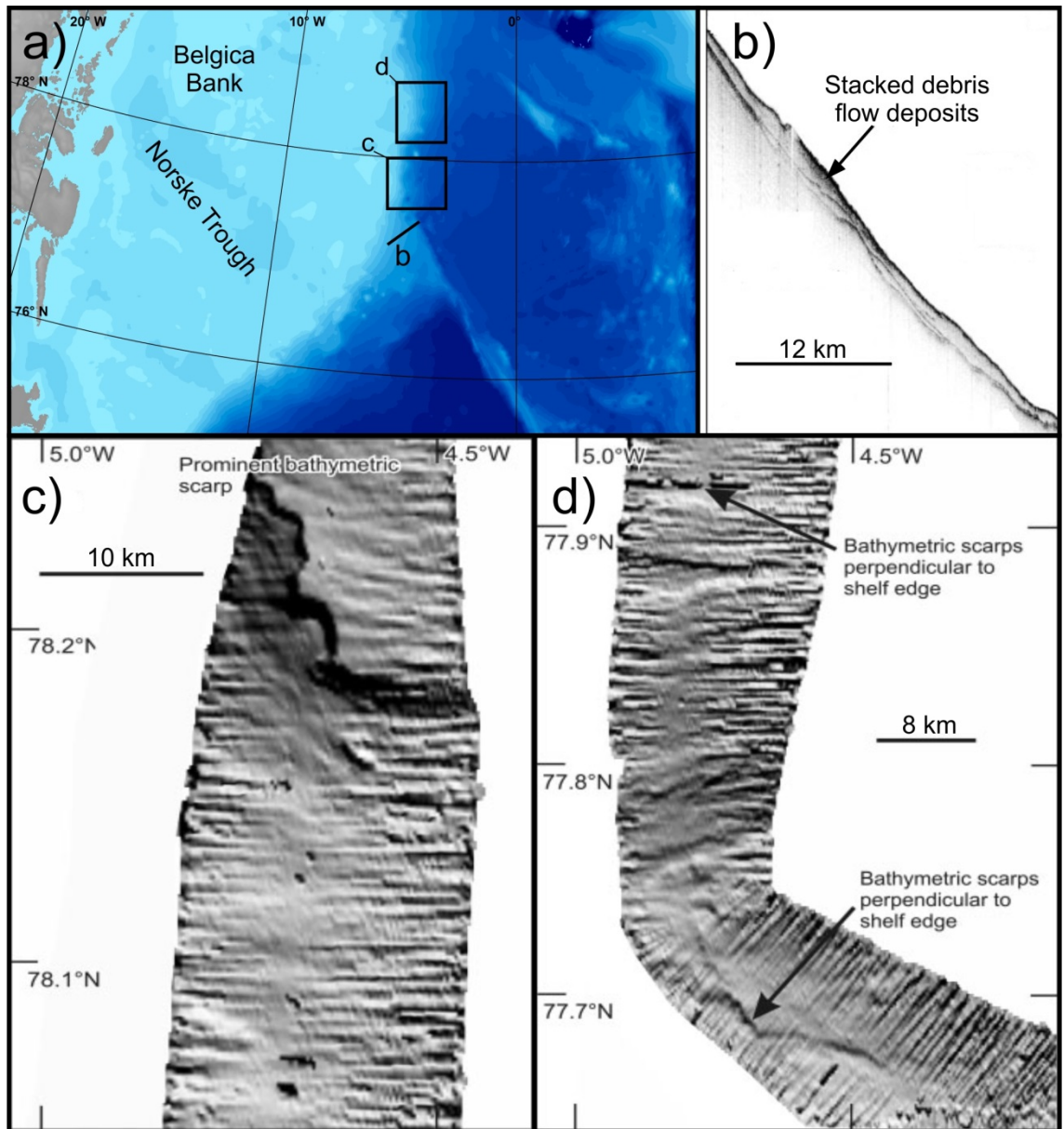
Figure 6.6 a) Location map of the Northeast Greenland continental margin. b) TOPAS sub-bottom
acoustic profile. Along slope profile from the upper-middle slope showing acoustically
transparent sediment lenses interpreted as stacked debris-flow deposits. c) and d)
EM120 shaded swath bathymetry from the Northeast Greenland continental slope
showing prominent and sinuous bathymetric scarps consistent with slide scars

produced during the process of sediment failure and sliding (adapted from Evans et al., 2009).

The Weichselian northeast sector of the Greenland continental shelf is characterised by multiple mass wasting processes. Here, as in the previous sector, the upper and mid- continental slopes are characterised by glacigenic debris-flows (Fig. 6.6; Evans et al., 2009). The lower continental slope is characterised by turbidite deposition. These turbidites are inferred to be the result either of downslope evolution of debris-flows higher up the slope or the triggering of turbidity currents by other mass-wasting events (Dowdeswell et al., 1997; Evans et al., 2009). Swath bathymetry showing prominent scarps also indicates that submarine landslides have occurred along this part of the East Greenland Margin (Fig. 6.6c and 6.6d; Evans et al., 2009). There is little evidence of submarine landslide occurrence along any other part of the East Greenland Margin.

The history of the Greenland Ice Sheet and the related sedimentation processes are summarised in Fig. 6.7a and Table 6.1.
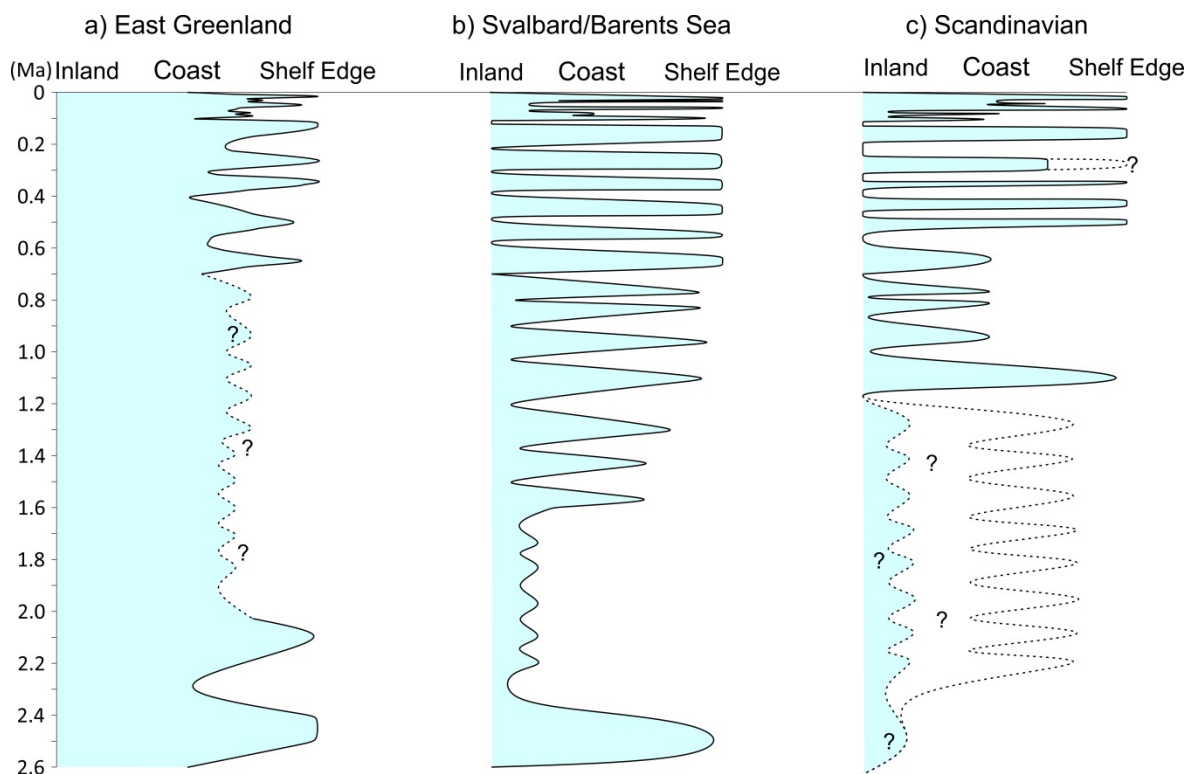
Figure 6.7 Schematic glaciation diagram for the Greenland, Barents Sea and Scandinavian Ice Sheets. Dashed lines and question marks represent time periods where there is a lack of data from various margins or conflicting interpretations of the ice sheet extent.

Period (Ma)	Ice sheet history	Sedimentation record
2.58 - 1.3	Most extensive ice sheet surrounding the Nordic Seas Largest advances from 2.5 - 2.4 Ma and about 2.1 Ma Little evidence of widespread collapses during deglaciation	Dominates IRD signal in the Nordic Seas 2.5 - 2.4 Ma advance marked by regional reflector and glacigenic debris-flows on Scoresby Sund Trough-Mouth Fan Subsequent advances on Scoresby Sund sector characterised by silty clays with variable IRD content, turbidites and glacigenic debris-flows limited to the upper slope 5 km progradation of shelf edge
1.3 - 0.7	Hypothesis 1: relatively stable ice sheet remaining on/near to the continental shelf Hypothesis 2: repeated advances to and retreat from the shelf edge	Glacigenic debris-flows on the central and southern sides of Scoresby Sund Trough-Mouth Fan Enhanced glacimarine sedimentation through meltwater plumes and turbidity currents Submarine channel formation on east Greenland Margin 38 km progradation of the shelf edge 130 m vertical aggradation of the continental shelf
0.7 - 0.13	Expanded and more stable ice sheet Extent of advances relatively uncertain Saalian Greenland Ice Sheet represents the maximum ice extent reached during the Quaternary	Limited evidence of submarine mass movement occurrence beyond the continental shelf before the Saalian Saalian aged glacigenic debris-flows on the Scoresby Sund Trough-Mouth Fan and the east Greenland margin Submarina channel system was inactive during the Saalian <5 km progradation of the shelf edge >260 m vertical aggradation of the shelf
0.13 - 0	Advances during MIS 5d and 5b at least to the inner shelf Advance during MIS 4 (close to MIS 2 limit in Scoresby Sund sector) followed by a limited retreat MIS 3 limited advance and retreat cycles Maximum extent of Late Weichselian ice sheet between 21 - 16 ka BP Expansion to the shelf edge in Northeast and Scoresby Sund sectors; central east Greenland extent is uncertain	*Scoresby Sund:* Glacigenic debris-flow emplacement *East Greenland margin:* Glacigenic debris-flow emplacement on the upper and mid- continental slope Below 2000 m sedimentological facies dominated by turbidites Laminated silt and mud layers on the upper continental slope and shelf Sedimentation rates peaked during deglaciation between 51 and 79 cm/kyr Channel system cross-cuts glacigenic debris-flow deposits *Northeast sector:* Glacigenic debris-flow emplacement on the upper and mid- continental slope Turbidite deposition on the lower continental slope Submarine landslide headscarps visible in bathymetry

Table 6.1 Summary of the important steps in glacial evolution of the East Greenland Margin and the resulting record of sedimentation.

6.2.3   Barents Sea Ice Sheet

The following section focusses on the evolution of the Barents Sea Ice Sheet and the Svalbard/south west margin of the Barents Sea. Compared to the East Greenland Margin, the Svalbard/Barents Sea Margin has been much more intensively studied and this is shown by the comparatively better understanding of this margin during the Quaternary.

6.2.3.1   2.58 – 1.6 Ma

The initial part of this period was characterised by the retreat of an extensive ice sheet based on Svalbard and the northern Barents Sea (Myhre et al., 1995; Solheim et al., 1998; Knies et al., 2009). The retreat is inferred from a substantial reduction in IRD at ODP sites on the Yermak Plateau (Wolf-Welling et al., 1996; Winkler et al., 2002), and the presence of a regional seismic reflector (R7 in Fig. 6.8) on the continental shelf and slope that marks a distinctive change in sedimentation regime (Faleide et al., 1996).

Following the initial ice sheet retreat, the period from 2.5 – 1.6 Ma was characterised by limited advance and retreat of glaciers on Svalbard and in the northern Barents Sea (Sejrup et al., 2005). The presence of ice in the northern Barents Sea is indicated by the reduction of minerals (specifically smectite) at ODP sites on the Yermak Plateau and Fram Strait. Smectite in these areas was previously sourced from Siberian rivers and transported across the northern Barents Sea. A reduction in the amount of smectite is thought to be indicative of ice blocking the transport path (Knies et al., 2009). The limited extent of ice expansion is inferred from the lack of IRD at the same ODP sites and is thought to indicate that glaciers have remained too small to calve large numbers of icebergs (Knies et al., 2009).

6.2.3.1.1   Sedimentary records of ice sheet and submarine mass movement histories

The average sedimentation rate on the continental shelf offshore Svalbard and in the southwest Barents Sea from 2.5 – 1.6 Ma was higher than during the majority of the Pliocene (Solheim et al., 1996). However, the limited nature of glacier expansion means that sediment was likely

transported by meltwater, either through fluvial action or in sediment-laden plumes and deposited in glaciofluvial/glaciomarine sequences (Laberg et al., 2010; Vorren et al., 2011). These interpretations are supported by numerical modelling suggesting that the continental shelf of the Barents Sea was still subaerial at this time (Butt et al., 2002), and incised palaeo-channels beneath present-day trough-mouth fans are filled with sand and gravel implying a strong meltwater influence (Sættem et al., 1992; 1994; Vorren and Laberg, 1997; Vorren et al., 2011). Beyond the shelf break offshore Svalbard, this period is also characterised by alternating deposition of hemipelagite and emplacement of submarine mass movement deposits (Fig. 6.8). These deposits are characterised as massive, sandy units with soft sediment deformation structures containing contorted and/or variably inclined beds (Jansen, 1996; Forsberg et al., 1999). These deposits are not, however, characteristic of glacigenic debris-flows. Glaciofluvial and submarine gravity flow deposit emplacement during this period resulted in gradual aggradation and progradation of sedimentary wedges at the continental shelf (Faleide et al., 1996; Dahlgren et al., 2005).

6.2.3.2   1.6 – 1.3 Ma

The period, 1.6 – 1.3 Ma, is characterised by greater expansion of the Barents Sea Ice Sheet. Expansion is indicated by higher rates of IRD accumulation (Knies et al., 2009). Stratigraphically, this expansion is marked regionally by the R6 seismic reflector (Fig. 6.8; Faleide et al., 1996; Forsberg et al., 1999). During this period, glaciers sourced from Svalbard expanded sufficiently to reach the shelf edge (Faleide et al., 1996; Solheim et al., 1998). Ice masses present in the northern Barents Sea also expanded. However, their expansion southwards was relatively limited. There is no evidence that the ice sheet expanded sufficiently in this sector to reach the shelf edge, and thus the south western margin of the Barents Sea, i.e. the Bear Island Trough, remained unglaciated during this period (Sættem et al., 1992; 1994; Solheim et al., 1998).

6.2.3.2.1   Sedimentary records of ice sheet and submarine mass movement histories

From 1.6 – 1.3 Ma the sedimentary processes along the Svalbard/Barents Sea margin can be divided into two sectors. The southwestern margin of the Barents Sea continued to be dominated

by glaciofluvial and glacimarine processes (Fig. 6.8; Sættem et al., 1994; Solheim et al., 1998).

Around Svalbard, reflecting greater glacial expansion, continental slope deposits are characterised

by the onset of a period of major glacigenic debris-flow emplacement and the acceleration of

sedimentary wedge progradation (Solheim et al., 1998; Dahlgren et al., 2005). These deposits are

both thicker and seismically distinct from those associated with the glaciofluvial/glaciomarine

period of deposition from 2.5 – 1.6 Ma indicating the enhanced efficiency of glacial sediment

transportation.

Figure 6.8 a) Location map of seismic profiles along the Svalbard/Barents Sea continental margin.
b) Seismic stratigraphic framework for the Svalbard/Barents Sea Margin, with
correlation of the main sequence boundaries between the Svalbard Margin
(Isfjorden), Storfjorden and Bear Island Trough-Mouth Fans. Internal reflection
pattern in b) and c) is indicated with changes between stratified (parallel lines) and
chaotic with mass movement structures (half circle pattern). Regional reflectors
based on chronology from ODP Site 986 are indicated. Modified from Faleide et al.
(1996), Jansen et al. (1996) and Solheim et al. (1998).

153

6.2.3.3   1.3 – 0.7 Ma

The largest change from 1.3 – 0.7 Ma in the Svalbard/Barents Sea sector was the greater expansion of the Barents Sea Ice Sheet (Vorren et al., 2011). On the Svalbard margin, glaciers originating on the archipelago continued to advance to and retreat from the shelf edge (Solheim et al., 1996). Further south, the Barents Sea Ice Sheet expanded sufficiently to reach the shelf edge along the southwestern margin of the Barents Sea for the first time (Andreassen et al., 2004; 2007). Moreover, fast flowing ice has been inferred to have been present in the Bear Island Trough from the presence of buried megascale glacial lineations (Andreassen et al., 2007; Vorren et al., 2011). Further evidence of intensified glacial activity in the Barents Sea during this time comes from IRD records at Site 908 and 909 which show large increases in accumulation during this period (Knies et al., 2009).

6.2.3.3.1   Sedimentary records of ice sheet and submarine mass movement histories

The record of sedimentary processes along the Svalbard/Barents Sea Margin from 1.3 – 0.7 Ma is best examined in two parts; the Svalbard and Barents Sea margins. Continued glacial sediment delivery from 1.3 – 0.7 Ma to the Svalbard continental shelf edge led to sustained progradation of glacigenic-wedges through glacigenic debris-flow emplacement (Faleide et al., 1996; Solheim et al., 1998; Dahlgren et al., 2005). Between 1.0 and 0.78 Ma seismic stratigraphy also indicates the presence of small scale slumps on a number of trough-mouth fans, e.g. Isfjorden (Andersen et al., 1994). Although the volumes of these failures appears to be relatively limited, it is important to note this is the first evidence of trough-mouth fan instability in this region beyond those associated with the occurrence of glacigenic debris-flows.

In contrast to the Svalbard margin, the expansion of the Barents Sea Ice Sheet to the shelf edge resulted in a significant change of deposition style marked by regional seismic reflector R5 (Fig. 6.8; Faleide et al., 1996; Fiedler and Faleide, 1996; Solheim et al., 1998; Vorren et al., 2011). Ice sheet expansion to the shelf edge increased the rate of sedimentation to 130 cm/kyr across the Bear Island Trough-Mouth Fan from 1.3 – 1.0 Ma resulting in glacigenic debris-flow emplacement

(Fig. 6.9; Hjelstuen et al., 2007). This rate of sedimentation is nearly double that seen from 2.5 –

1.3 Ma and is attributed to ice sheet expansion over readily erodible sediments on the continental

shelf previously deposited by glacimarine processes. Similar erosion of the outer shelf and

deposition on and beyond the shelf break was seen in the Storfjorden Trough (Solheim et al.,

1998).
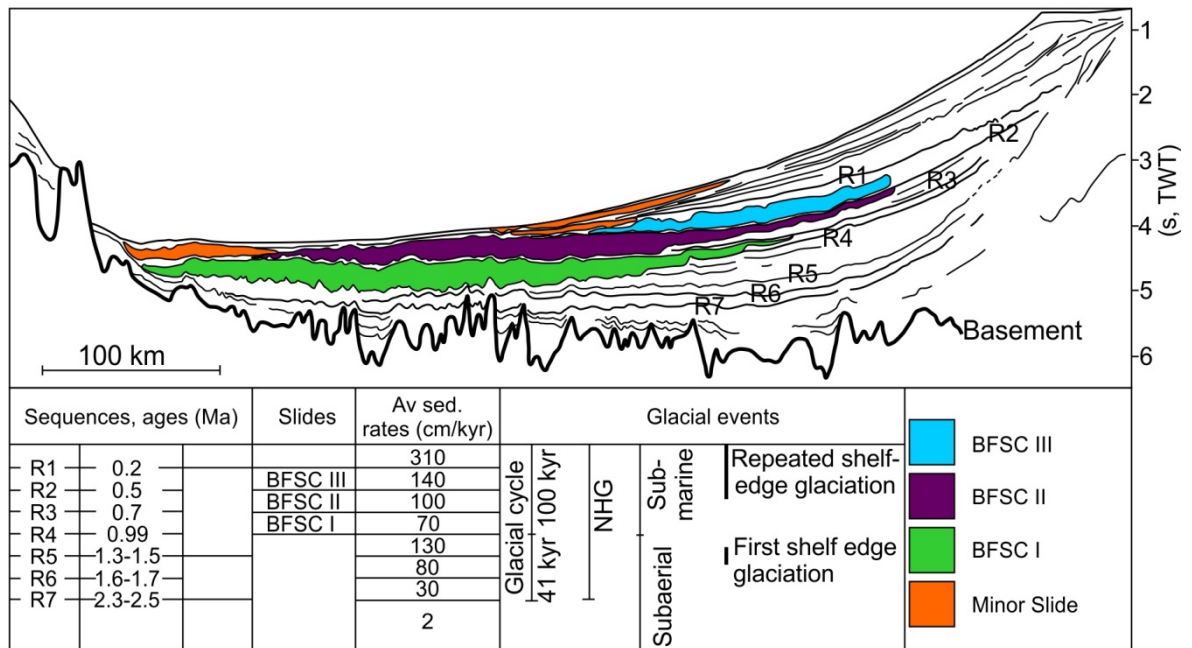
Figure 6.9 Seismic transect across the Lofoten Basin from the Bear Island Trough-Mouth Fan to the
Vøring Plateau (see Fig. 6.10a). Sequence boundaries (R1 – R7) and submarine
landslide deposits (BFSC I – III) are indicated. GDF = Glacigenic Debris-Flows deposits.
Summary of chronology, average depositional rates and main glacial events are
shown in the lower panel. Modified from Hjelstuen et al. (2007).

From 1.0 – 0.78 Ma the rate of sedimentation at the shelf edge of the Bear Island Trough dropped

to ~70 cm/kyr (Hjelstuen et al., 2007). The reduced rate of sedimentation is thought to result

from the drowning of the Barents Sea and the transition from a subaerial ice sheet to a marine-

based ice sheet (Butt et al., 2002). Despite the reduced rate of sedimentation, seismic

stratigraphy suggests that a large submarine landslide occurred on the Bear Island Trough-Mouth

Fan between 1.0 – 0.78 Ma (Fig. 6.9; Hjelstuen et al., 2007). The slide is estimated to have

mobilised in excess of 25,000 km^3 of material and is the largest yet found on the planet, nearly 10

times larger than Storegga (Table 2; Kuvaas and Kristoffersen, 1996; Hjelstuen et al., 2007). The

occurrence of this slide after 1.0 Ma suggests that its occurrence is related to the increased

delivery of sediment associated with glacial intensification associated with the Mid-Pleistocene

Transition (Fiedler and Faleide, 1996; Solheim et al., 1998). However, the imprecise dating (Slide

BFSC I has an age range of 0.21 Myr; Hjelstuen et al., 2007) makes identification of a specific

trigger difficult, although it does appear that the slide in fact occurred after the average rate of

sedimentation decreased.

Slide	Area (x 10^3 km²)	Volume (x 10^3 km³)	Age (Ma)	Reference
BFSC I	115	25.5	1.0 - 0.78	Hjelstuen et al. (2007)
BFSC II	120	24.5	0.78 - 0.5	Hjelstuen et al. (2007)
BFSC III	66	11.6	0.5 - 0.2	Hjelstuen et al. (2007)
Slide B			0.6 - 0.5	Laberg et al. (1996)
Slide A	12	5.1	0.6 - 0.5	Laberg et al. (1996)
Bjørnøya	12.5	1.1	0.2 - 0.3	Laberg et al. (1996) Lindberg et al. (2004)
Andøya	9.7		Holocene	Laberg et al. (2000)
Trænadjupet	4 - 5	0.4 - 0.72	0.0035 - 0.0028	Allin et al. (in review)
Nyk	4 - 6	0.4 - 0.72	0.0218 - 0.0193	Mozzato et al. (in review)
Vigrid	2.5		>0.2	Solheim et al. (2005)
Sklinnadjupet	7.7		0.3	Solheim et al. (2005)
Storegga	95	<3.2	0.0072	Haflidason et al. (2005)
R	6.8		0.3	Solheim et al. (2005)
W	63.7	24.6	2.7 - 1.7	Hjelstuen and Andreassen (2015)
S	72.3	15	0.5	Solheim et al. (2005)
Tampen			0.059	Watts et al. (2016)
Møre		1.2	0.4 - 0.38	Nygård et al. (2005)
U	86.7	24.6	1.7 - 1.1	Evans et al. (2005) Hjelstuen and Andreassen (2015)

Table 6.2 Areas, volumes and ages of known large submarine landslides in the Nordic Seas (adapted from Hjelstuen et al. 2007).

6.2.3.4   0.7 – 0.13 Ma

The adoption of the 100 kyr climate cycles was associated with regular expansion of the Barents

Sea Ice Sheet to the shelf edge along the Svalbard/Barents Sea Margin of the Barents Sea

(Solheim et al., 1996; Solheim et al., 1998). The ice sheet is interpreted to have reached the shelf edge during MIS 16 (676 – 621 ka BP), 12 (478 – 423 ka BP), 8 (303 – 245 ka BP) and 6 (186 – 128 ka BP) (Laberg and Vorren, 1996; Vorren and Laberg, 1997; Sejrup et al., 2005; Knies et al., 2009). Each isotope stage could contain multiple advances to the shelf edge that are unresolvable in seismic data or in IRD records; five advances is therefore the minimum which occurred from 0.7 – 0.13 Ma (Vorren and Laberg, 1997). An advance is also inferred to have occurred during MIS 14 (565 – 524 ka BP) but its extent is contentious. From ODP Sites around Svalbard, Knies et al. (2009) suggest ice advanced but did not reach the shelf edge. In contrast, interpretation of deposits on the Bear Island Trough-Mouth Fan suggests that the advance did indeed reach the shelf edge (Sættem et al., 1994; Laberg and Vorren, 1996; Vorren and Laberg, 1997). It is, however, possible that the ice sheet reached the shelf edge of the Bear Island Trough but did not around Svalbard. Of the identified advances, the advance associated with the Saalian Glacial (MIS 6) is interpreted to be the longest lasting (Svendsen et al., 2004b; Ingólfsson and Landvik, 2013; Pope et al., 2016).

6.2.3.4.1   Sedimentary records of ice sheet and submarine mass movement histories

Here, we record sedimentary processes along specific sections of the margin, reflecting the large number of studies undertaken which cover this time period compared to older periods along this margin.

6.2.3.4.1.1   Western Svalbard Margin

Ice regularly reached the shelf edge of western Svalbard between 0.7 and 0.13 Ma (Solheim et al., 1998). Each shelf edge advance was characterised by trough-mouth fan glacigenic debris-flow emplacement (Fig. 6.8; Andersen et al., 1994; Faleide et al., 1996; Fiedler and Faleide, 1996). During this period there was a shift from net-erosion of the continental shelf to net sediment accumulation on the outer continental shelf. As a consequence debris-flow deposit thickness declined compared with deposits before the onset of 100 kyr cyclicity (Elverhøi et al., 1998; Solheim et al., 1998).

6.2.3.4.1.2   Storfjorden Trough-Mouth Fan

Seven distinct seismic units associated with ice stream advance to the shelf edge in the Storfjorden Trough have been identified (Laberg and Vorren, 1996; Vorren and Laberg, 1997). These equate to advances to the shelf edge during MIS 14, 12, 10, 8 and 6. Glacigenic debris-flows are hypothesised to dominate each unit (Vorren and Laberg, 1997). However, despite growth of the Storfjorden Trough-Mouth Fan throughout this period by the same sedimentary process, the rate of sedimentation across the fan decreased after 0.44 Ma (Faleide et al., 1996; Hjelstuen et al., 1996). Between 1.0 and 0.44 Ma, an average of 2400 t $km^{-2}a^{-1}$ was deposited across the fan. This decreased to 420 t $km^{-2}a^{-1}$ between 0.44 and 0 Ma (Hjelstuen et al., 1996) showing that the adoption of the 'more' intense 100 kyr glacial cycle does not necessarily increase the sediment supply to the shelf edge.

6.2.3.4.1.3   Bear Island Trough-Mouth Fan

Ice sheet sedimentary processes dominated the Bear Island Trough-Mouth Fan from 0.7 – 0.13 Ma, each advance being correlated to a specific seismic package (Fig. 6.10). Each of these units I – VI (Fig. 6.10) is dominated on the upper fan by a chaotic seismic facies (Sættem et al., 1992; 1994; Laberg and Vorren, 1996). On the middle and lower fan they have a mounded geometry (Laberg and Vorren, 1996). The facies and their associated bounding seismic reflectors are interpreted to represent glacigenic debris-flow lobes, interbedded with hemipelagic sediments (Vorren et al., 1990; Laberg and Vorren, 1995; Vorren and Laberg, 1997). Distally, these sequences are characterised by fine-grained turbidites, derived from the downslope evolution of glacigenic debris-flows, and hemipelagic sediments (Laberg and Vorren, 1996; Pope et al., 2016).

Rates of sediment accumulation and debris-flow emplacement are not constant over either the fan or between the different advances. The MIS 12 advance is estimated to have the delivered the most sediment at the highest rate to the fan. Represented by seismic unit III (Fig. 6.10b), 17,650 km^3 of sediment is estimated to have accumulated at a rate of 63 cm/ka during this glacial with the depocentre on the central part of the fan (Laberg and Vorren, 1996). During the following two

glaciations (MIS 10 and 8) 7266 km^3 of sediment is estimated to have accumulated at a rate of 14

cm/ka with the depocentre situated on the southern end of the fan (Laberg and Vorren, 1996).

The MIS 6 advance depocentre was on the northern and southern parts of the fan. An estimated

4061 km^3 of sediment accumulated at a rate of 19 cm/ka (Laberg and Vorren, 1996).

Sedimentation rates and depocentres could not be calculated for the oldest two units, although

accumulation rates of ~14 cm/ka have been hypothesised (Laberg and Vorren, 1996). These

variations in depocentre and sediment accumulation rate indicate the frequent nature of flow

migration of the Bear Island Ice Stream and possible range of sediment delivery rates

(Dowdeswell and Siegert, 1999).
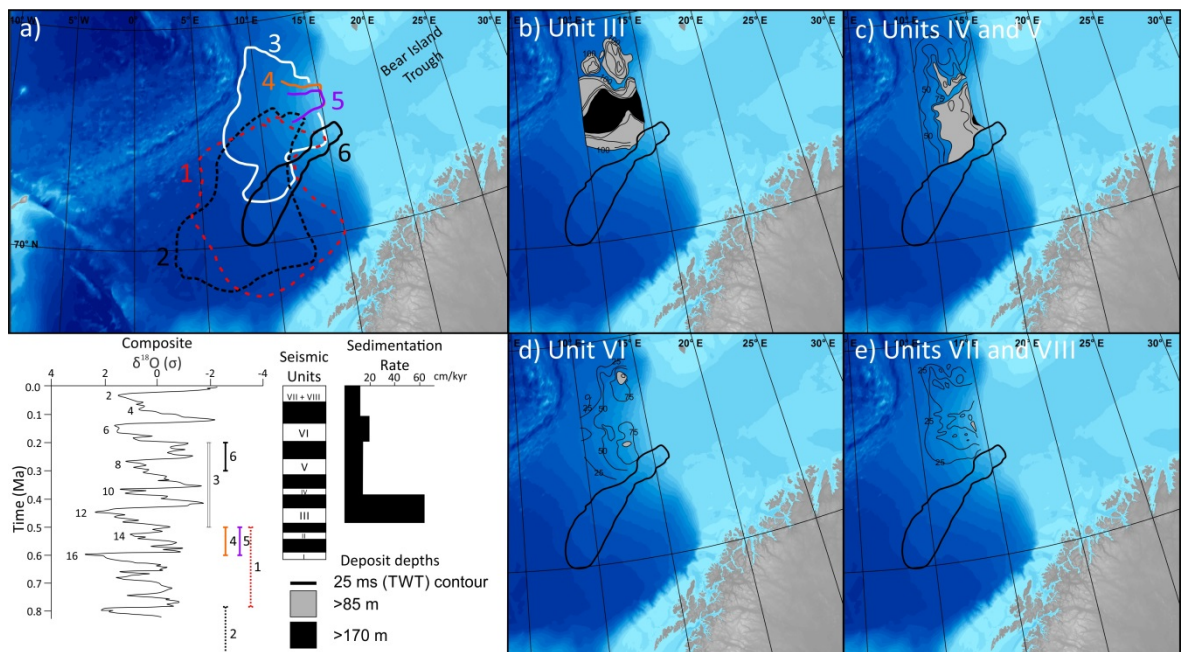
Figure 6.10 a) Location of large submarine landslides sourced from the Bear Island Trough-Mouth Fan. 1) BFSCII; 2) BFSCI; 3) BFSCIII; 4) Slide B; 5) Slide A; 6) Bjørnøya Slide. b) – e) Isopach maps of units deposited on the Bear Island Trough-Mouth Fan. Each isopach map is correlated to a given time period which can be compared to a composite δ^{18}O curve and the relative timings of the large submarine landslides outlined in a). b) = Units III; c) = Unit IV and V; d = Unit VI; e) = Units VII and VIII. Contour intervals 25 ms (TWT). For depth conversion an internal velocity of 1700 m/s was used. Modified from Laberg and Vorren (1996) and Hjelstuen et al. (2007).

Five large submarine landslides are also believed to have affected the fan between 0.7 and 0.13 Ma (see Table 2). These landslides range in size from 1.1 km^3 to 24.5 km^3 (Fig. 6.9; Hjelstuen et al., 2007). The three oldest slides occurred between 0.78 and 0.5 Ma, indicating a period of large-scale instability on the Bear Island Trough-Mouth Fan. Unfortunately, their age and the unresolvable Units I and II in seismic profiles prevent a comparison between depocentres and landslide triggering (Laberg and Vorren, 1996). The next youngest slide occurred between 0.5 and 0.2 Ma (Hjelstuen et al., 2007). The headwall of this landslide occurred on the northern margin of the depocentre associated with the MIS 10 and 8 advances (Fig. 6.10; Laberg and Vorren, 1996). The Bjørnøya Slide occurred between 0.3 – 0.2 Ma, post-dating units IV and V and is located on the southern margin of the depocentre of these units (Fig. 6.10; Laberg and Vorren, 1996).

6.2.3.5   0.13 – 0 Ma (Weichselian – Present)

Understanding of the Barents Sea Ice Sheet is most complete during the Weichselian period. Onshore and offshore records show that the ice sheet underwent multiple advance and retreat cycles over this glacial period (Mangerud et al., 1998; Svendsen et al., 1999; 2004a; 2004b; Patton et al., 2015; Hughes et al., 2016).

The prevailing view of Barents Sea Ice Sheet history during the Weichselian is for four advances. The earliest expansion occurred during MIS 5d from 115 – 105 ka (Patton et al., 2015). This advance is believed to have been limited to Svalbard (Mangerud and Svendsen, 1992) but is envisaged to have reached the shelf edge along the western margin (Knies et al., 1998).

A second expansion is reconstructed from 100 – 70 ka BP (MIS 5b; Mangerud et al., 1998). On Svalbard, this expansion is believed to be shorter (~90 – 80 ka BP) and less extensive, i.e. only reaching the coastline, than in the Barents Sea (Svendsen et al., 1999). Ice sheet expansion in the Barents Sea itself was limited to the eastern Barents and Kara Seas (Svendsen et al., 1999, 2004a, b; Siegert et al., 2001).

During the Middle Weichselian (MIS 4 – 3/70 – 50 ka BP), the Barents Sea Ice Sheet advanced to the shelf edge along the western Svalbard margin and in the southwestern Barents Sea (Mangerud and Svendsen, 1992; Andersen et al., 1996; Knies et al., 2001). In the Bear Island Trough, ice is envisaged to have been at the shelf edge between from 68 – 60,000 ka BP (Pope et al., 2016). Reconstructions of glacier extent on Svalbard from marine records suggest similar timings for maximum extension to the shelf edge (Mangerud, 1991; Dowdeswell et al., 1995; Andersen et al., 1996; Knies et al., 2001).

The last advance to the shelf edge occurred during MIS 2. During this period ice began to build up at ~32 cal ka BP (Andersen et al., 1996; Siegert et al., 2001). West of Svalbard, ice reached the shelf break ~24 cal ka BP (Elverhøi et al., 1995; Dowdeswell and Elverhøi, 2002; Andreassen et al., 2004; Jessen et al., 2010; Hughes et al., 2016). Along the southwestern Barents Sea margin ice reached the shelf edge ~26 cal ka BP (Elverhøi et al., 1995; Laberg and Vorren, 1995; Vorren et al., 2011; Pope et al., 2016). Ice retreated from the shelf edge in both areas as early as 20 cal ka BP (see Hughes et al., 2016 for more detail).

In addition to these ice advances, an ice advance has also been suggested during MIS 3. Pope et al. (2016) suggest that ice advanced in the Bear Island Trough and was present at or close to the shelf edge between 39.4 and 36 cal ka BP. An ice advance during this period is contrary to reconstructions made using terrestrial deposits on Svalbard (Mangerud et al., 1998; Svendsen et al., 2004b). It is, however, consistent with offshore IRD records (Dowdeswell et al., 1999; Dreger, 1999; Knies et al., 2001).

6.2.3.5.1   Sedimentary records of ice sheet and submarine mass movement histories

6.2.3.5.1.1   Western Svalbard Margin

The detailed offshore record of Svalbard glaciation begins at ~80 ka associated with the inferred beginning of the shelf edge advance during MIS 4 (Mangerud et al., 1998; Svendsen et al., 2004b). This period was characterised by the deposition of turbidites beyond the shelf edge (Andersen et

al., 1996) and the deposition of large amounts of IRD, especially following retreat of the ice after

60 ka (Landvik et al., 1992; Dowdeswell et al., 1999).

Different sedimentary deposits are found offshore western Svalbard in conjunction with different

phases of ice advance during later periods. Ice began to build up ~32 cal ka BP, and reached the

shelf edge by ~24 cal ka BP (Elverhøi et al., 1995; Jessen et al., 2010). On Bellsund and Isfjorden

Trough-Mouth Fans, deposition of laminated and massive muds and frequent turbidite

emplacement are thought to be reflective of periodic increases of meltwater and sediment

delivery associated with ice sheet advance (Andersen et al., 1996; Dowdeswell and Elverhøi, 2002;

Landvik et al., 2005). This was followed by the emplacement of glacigenic debris-flow deposits

reflecting the arrival and 'switch-on' of ice streams at the shelf edge (Alley et al., 1989; Andersen

et al., 1996; Dowdeswell and Siegert, 1999; Dowdeswell and Elverhøi, 2002).

Initial retreat ~20 cal ka BP was characterised by a return to hemipelagic sedimentation and

higher IRD concentrations (Knies et al., 2001; Rasmussen et al., 2007; Jessen et al., 2010). Unlike

other regions (e.g. along the Norwegian slope or Storfjorden) there was no period of rapid

sedimentation associated with meltwater deposition. Between 15.7 and 14.65 cal ka BP, a second

phase of retreat associated with enhanced iceberg calving resulted in increased concentrations of

IRD and sedimentation rates offshore western Svalbard (Elverhøi et al., 1995; Andersen et al.,

1996; Vogt et al., 2001). Further accelerated retreat after 14.65 cal ka BP is linked to thick, fine-

grained laminated mud deposits on the continental slope indicative of meltwater processes

(Elverhøi et al., 1995; Rasmussen et al., 1997; Jessen et al., 2010). Sediment accumulation rates

during this period were between one and two orders of magnitude higher during this later period

of glacier retreat than they had been when the ice margin was at the shelf edge (Dowdeswell and

Siegert, 1999; Dowdeswell and Elverhøi, 2002; Jessen et al., 2010).

6.2.3.5.1.2   Storfjorden Trough-Mouth Fan

Estimates of accumulated sediment volumes on Storfjorden Trough-Mouth Fan during the

Weichselian glacial come from seismic stratigraphy. According to these calculations 422 t km^{-2} yr^{-1}

were accumulated during the Weichselian (Hjelstuen et al., 1996). This figure is part of an average calculated for the last 440 ka (Hjelstuen et al., 1996). Dating of deposits on the Storfjorden Trough-Mouth Fan associated with each of the Weichselian advances has not yet been achieved. This section will therefore focus on the deposits associated with the Late Weichselian (MIS 2) advance.

During the Late Weichselian varying thicknesses of diamict were deposited across the trough-mouth fan. >45 m and ~20 m of diamict were deposited on the northern and southern ends of the fan respectively. Assuming an average rate of duration of ice being at the shelf edge of 3 ka, the 45 m thick diamict was emplaced at an average rate of 1.5 cm a^{-1} (Lucchi et al., 2013).

Three depositional lobes can be seen on the Storfjorden Trough-Mouth Fan associated with the Late Weichselian advance. Each of these lobes in inferred to be associated with a sub-ice stream within the larger Storfjorden palaeo-ice stream and has different depositional characteristics (Pedrosa et al., 2011). The two northernmost lobes are characterised by diamicts and over 50 m of glacigenic debris-flow deposits (Lucchi et al., 2013). Radiocarbon dating suggests that these deposits were emplaced around 23820 ± 260 cal BP (Lucchi et al., 2013). On the upper part of the fan these deposits have subsequently been incised by gullies and a thin (2 − 3 m) drape of deglacial and Holocene sediments (Pedrosa et al., 2011; Lucchi et al., 2013). These gullies disappear on the mid-slope.

The southern sector of the fan has markedly different sedimentary characteristics. The southernmost lobe is characterised by multiple submarine landslides with headwalls on the middle and upper slopes (Lucchi et al., 2012; Rebesco et al., 2012). Stacked mass transport deposits are found in the middle and lower slope subsurface (Rebesco et al., 2011; 2012). The nearby Kveithola Trough-Mouth Fan exhibits similar characteristics (Lucchi et al., 2012).

The southern sector is also characterised by interlaminated sequences interbedded with discontinuous diamicts which can reach 45 − 50 m thick. Related to the Middle and Late Weichselian advances, these facies are believed to be the result of subglacial meltwater plume

deposition (Lucchi et al., 2013). The thickness of the interlaminated sediments decreases with distance from the shelf break. 42 km away the sediments are only 15 cm thick, compared to meter thicknesses up slope. This is consistent with meltwater plume deposition in modern environments (Mackiewicz et al., 1984; Powell, 1990; Powell and Domack, 1995). As on the northern sections of the fan, gullies are also found on the upper slopes (Pedrosa et al., 2011).

To the south of the Storfjorden and Kveithola Trough-Mouth Fans the continental slope is characterised by a dendritic sediment drainage system comprising a number of canyons which converge to form the INBIS Channel (Fig. 6.11; Taylor et al., 2002b; Laberg et al., 2010).
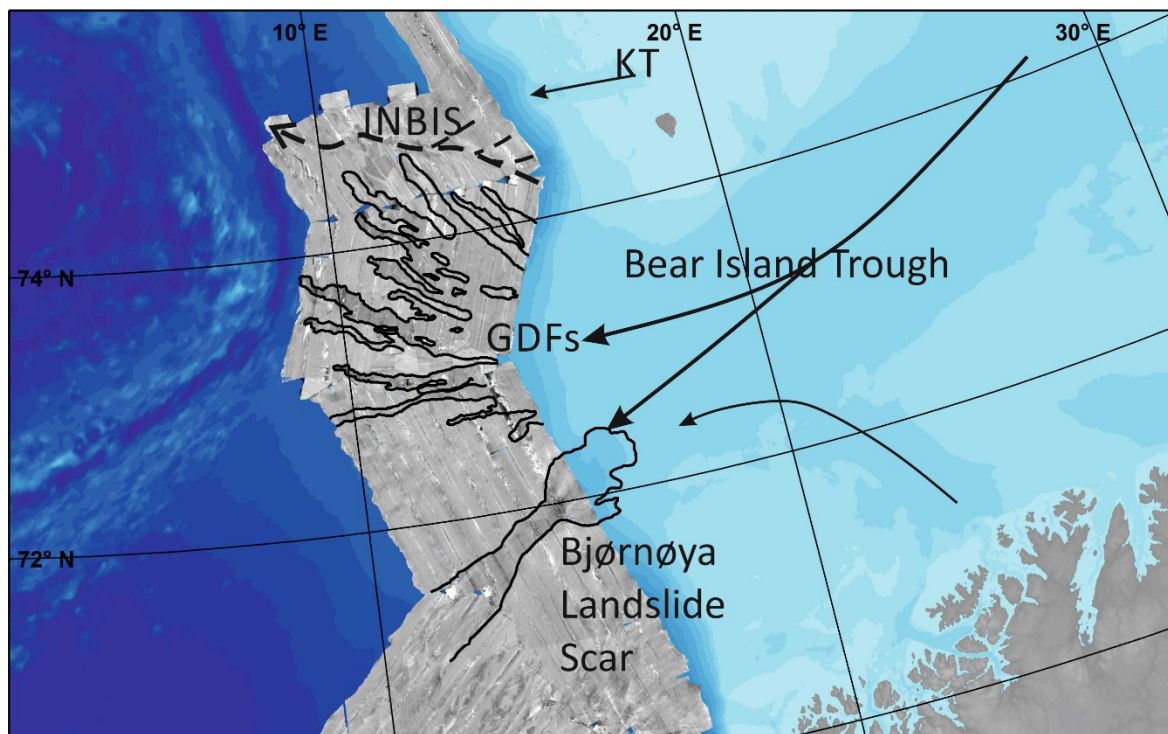
Figure 6.11 GLORIA long range side-scan sonar imagery superimposed on the Bear Island Trough-Mouth Fan. Glacigenic Debris-Flows (GDF), the INBIS Submarine Channel system and the Bjørnøya submarine landslide are identified using the GLORIA imagery. Palaeo-ice flow directions are indicated by arrows. KT = Kviethola. Glacigenic debris-flows visible in the GLORIA imagery are thought to relate to the Late Weichselian (MIS 2) glacial advance.

6.2.3.5.1.3   Bear Island Trough-Mouth Fan

Based on seismic stratigraphies, the estimated ~2400 km^3 of accumulated sediment (13 cm/ka) on the Bear Island Trough-Mouth Fan during the Weichselian is the lowest of any of the 100 kyr glacial cycles (Laberg and Vorren, 1996). This is perceived to be a consequence of ice being stable at the shelf edge for less time during the Weichselian compared to preceding glacials (Laberg and Vorren, 1995, 1996; Vorren et al., 2011; Pope et al., 2016).

The Weichselian sedimentary history of the Bear Island Trough-Mouth Fan is dominated by the emplacement of glacigenic debris-flow deposits (Fig. 6.11; Taylor et al., 2002a; 2002b; Laberg and Dowdeswell, 2016; Pope et al., 2016). Initial studies using side-scan sonar mapping showed the most recently active (MIS 2) part of the fan was at its northern end and covered 125,000 km^2 where debris-flow lobes radiated out from the top of the fan (Sættem et al., 1992; 1994; Taylor et al., 2002a; 2002b; Laberg and Dowdeswell, 2016). These flows were shown to have run-out distances of up to 490 km and contain between 10 and 35 km^3 of sediment (Laberg and Vorren, 1995; Laberg and Dowdeswell, 2016).

Dating of more distal deposits on the northern end of the Bear Island Trough-Mouth Fan has subsequently shown that glacigenic debris-flows have been emplaced in four distinct clusters during the Weichselian. Each cluster is proposed to be associated with an ice advance to the shelf edge of the Bear Island Trough (Pope et al., 2016). The number and thickness of deposits also suggests that the largest number of glacigenic debris-flows was in fact associated with advances during MIS 4 and MIS 3 rather than the MIS 2 advance (Pope et al., 2016).

In addition to the glacigenic debris-flows, the northern end fan is characterised by the presence of gullies (Vorren et al., 1989; Laberg and Vorren, 1995). Gullies are also present on the southern margin of the fan (Bellec et al., 2016). Two hypotheses for gully formation exist. First, cold and turbid dense water related to brine rejection during sea ice formation during the Holocene was able to erode and transport sediment from the shelf and/or generate turbidity currents (Laberg and Vorren, 1995). Second, hyperpycnal flows resulting from meltwater and sediment delivery

when ice was at or near to the shelf edge resulted in channel incision (Laberg and Vorren, 1995; Mulder et al., 2003; Dowdeswell et al., 2006a; Bellec et al., 2016). This was, however, concentrated to the margins of the trough-mouth fan.

Following retreat of the Bear Island Ice stream from the shelf edge, a relatively thin sequence (<10 m) of glacimarine sediments was left in the trough (Vorren et al., 1990). On the upper fan, less than 1 m of glacimarine sediments have been recovered above debris-flow deposits (Laberg and Vorren, 1995). On the lower part of the fan, no glacimarine sediments have been found (Laberg and Vorren, 1995; Pope et al., 2016). This supports the rapid rate of retreat of the Bear Island Ice stream which has been inferred from seafloor geomorphology in the Barents Sea (Winsborrow et al., 2010; 2012).

The history of the Barents Sea Ice Sheet and the related sedimentation processes are summarised in Table 6.3 and Fig. 6.7b.

Period (Ma)	Ice sheet history	Sedimentation record
2.58 - 1.6	Retreat of initially extensive ice sheet on Svalbard and the northern Barents Sea Subsequent limited advance and retreat of glaciers on Svalbard and in the Northern Barents Sea	Meltwater related increase in sedimentation on Svalbard continental slope Submarine mass movement deposits (not glacigenic debris-flows) on the Svalbard continental slope Meltwater sediment driven incision of channels into the continental slope Gradual aggradation and progradation of sedimentary wedges
1.6 - 1.3	Expansion to the shelf edge of glaciers sourced from Svalbard Limited southward expansion of Barents Sea Ice Sheet	**Svalbard margin:** Period of major glacigenic debris-flow emplacement Acceleration of sedimentwary wedge progradation Deposits are thicker and seismically distinct from previous period **Barents Sea margin:** Glaciofluvial and glacimarine deposition
1.3 - 0.7	Advance to and retreat from the shelf edge of Svalbard glaciers First expansion to the shelf edge in the Bear Island Trough of the Barents Sea Ice Sheet	**Svalbard margin:** Emplacement of glacigenic debris-flows on the continental shelf **Barents Sea margin:** 1.3 - 1.0 Ma ? emplacement of glacigenic debris-flow deposits; rate of sedimentation increased to 130 cm/kyr 1.0 - 0.78 Ma ? emplacement of glacigenic debris-flow deposits; rate of sedimentation drop to 70 cm/kyr; submarine landslide on Bear Island Trough-Mouth Fan (>25,000 km3) Change in sedimentation rate hypothesised to be a consequence of Barents Sea shelf submergence
0.7 - 0.13	Ice sheet expands to the shelf edge during MIS 16, 12, 8 and 6 MIS 14 advance believed to have reached shelf edge of Bear Island Trough but not around Svalbard	**Svalbard margin:** Glacigenic debris-flow emplacement (decline in deposit thick with the adoption of 100 kyr climate cyclicity) Shift from net-erosion to net-accumulation of sediment on the continental shelf **Storfjorden Trough-Mouth Fan:** Each advance is associated with a package of glacigenic debris-flows **Bear Island Trough-Mouth Fan:** Upper and mid- slopes of the trough-mouth fan characterised by glacigenic debris-flow emplacement; lower slope is characterised by fine-grained turbidites and hemipelagic sediments MIS 12 advance ? 17,650 km3 of sediment deposited at a rate of 63 cm/ka across the fan MIS 10 and 8 advance ? 7266 km3 of sediment deposited at a rate of 14 cm/ka across the fan MIS 6 advance ? 4061 km3 of sediment deposited at a rate of 19 cm/ka Five large submarine landslides on the trough-mouth fan with volumes between 1.1 and 24.5 km3
0.13 - 0	MIS 5d (115 - 105 ka) advance to shelf edge limited to Svalbard MIS 5b (90 - 80 ka BP) advance on Svalbard is less extensive MIS 5b (90 - 80 ka BP) advance in Barents Sea limited to eastern Barents and Kara Seas MIS 4 (70 - 50 ka BP) advance to the shelf edge MIS 2 (32 - 20 cal ka BP) advance to the shelf edge Proposed advance to shelf edge of the Bear Island Trough during MIS 3 (40 - 35 cal ka BP)	**Svalbard margin:** Deposition of turbidites on the continental slope during MIS 4 (rate of turbidite emplacement was especially high following the initial retreat of the ice) 32 - 24 cal ka BP ice expansion characterised by laminated and massive mud deposition and turbidite emplacement 24 - 20 cal ka BP advance characterised by glacigenic debris-flow emplacement 20 cal ka BP ? initial retreat of the ice sheet characterised by increased IRD and hemipelagic sedimentation 15.7 - 14.65 cal ka BP ? second phase of retreat characterised by increased IRD <14.65 cal ka BP ? accelerated retreat characterised by deposition of thick, fine-grained laminated mud deposits; rates of sedimentation 1 to 2 orders of magnitude greater than when ice was at the shelf edge **Storfjorden Trough-Mouth Fan:** Northern/Central Fan ? >50 m of glacigenic debris-flow deposits emplaced during MIS 2; gully incision into upper slope Southern Fan ? Multiple submarine landslide scars; interlaminated plumite deposits upto 50 m thick interbedded with discontinuous diamicts **Bear Island Trough-Mouth Fan:** Glacigenic debris-flow emplacement characterises each advance to the shelf edge Gullies are incised into the upper slope at the margins of the trough-mouth fan <1 m of glacimarine sediments recovered from the upper fan 2400 km3 of sediment accumulated at 13 cm/ka

Table 6.3 Summary of the important steps in glacial evolution of the Svalbard/Barents Sea Margin and the resulting record of sedimentation.

6.2.4   Scandinavian Ice Sheet

The following section focusses on the evolution of the Scandinavian Ice Sheet during the Quaternary.

6.2.4.1   2.58 – 1.1 Ma

Of the three major ice sheets, the Scandinavian Ice Sheet was the least extensive during this period (Sejrup et al., 2000; Faleide et al., 2002). The prevalent belief is that the ice sheet remained an intermediate size, rarely extending beyond the fjords of western Norway (Jansen and Sjøholm, 1991; Henrich and Baumann, 1994). Evidence for this comes from the limited IRD delivery to ODP sites on the Vøring Plateau, the Norwegian Basin and cores bordering the Barents Sea as well as

seismic stratigraphy of the continental margin of Norway (Jansen et al., 1988; Henrich, 1989; Haflidason et al., 1991; Sejrup et al., 1996).

An alternative view suggests that ice caps in northern and southern Scandinavia behaved differently from 2.58 – 1.1 Ma. According to this interpretation, at latitudes higher than the Vøring Plateau, the ice sheet regularly advanced to the palaeo-shelf edge between 2.7 and 1.1 Ma (Rokoengen et al., 1995; Henriksen and Vorren, 1996). Meanwhile, south of the Vøring Plateau, the ice sheet remained limited in size (Rise et al., 2005). The different response of ice caps in northern Scandinavia is hypothesised to be a consequence of the greater influence of obliquity forcing at higher latitudes (Mangerud et al., 1996).

6.2.4.1.1 Sedimentary records of ice sheet and submarine mass movement histories

There is little direct evidence of Scandinavian Ice Sheet expansion from 2.58 – 1.1 Ma on the continental shelf beyond IRD records from more distal core sites. There is no evidence of ice sheet sedimentation related submarine mass movement occurrence in any ODP core beyond the shelf break (Jansen and Raymo, 1996; Jansen et al., 2000). It is therefore suggested that from 2.58 – 1.1 Ma sea level change and the related continental shelf exposure was the dominant control on sedimentation along the West Norwegian Margin (Eidvin et al., 2000; Faleide et al., 2002). In spite of the lack of rapid sedimentation, a large submarine landslide (Slide W; Fig. 6.12) is inferred to have occurred in the same area as the Storegga Slide complex between 2.7 and 1.7 Ma remobilising an estimated 24,600 km^3 of sediment (Hjelstuen and Andreassen, 2015). The occurrence of this slide does not appear to be directly related to glacial processes although the imprecise dating makes this conclusion uncertain (Solheim et al., 2005a).
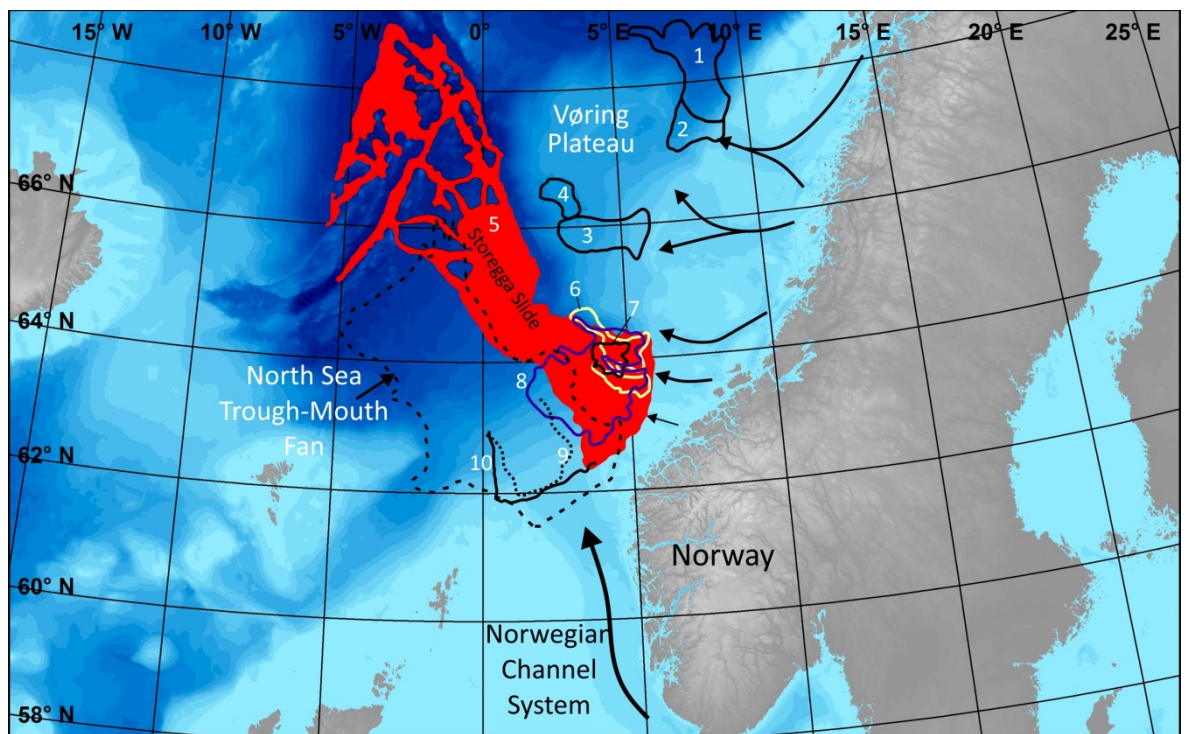
Figure 6.12 Large submarine landslides identified on the Norwegian Continental Margin. 1) Trænadjupet Slide; 2) Nyk Slide; 3) Vigrid Slide; 4) Sklinnadjupet Slide; 5) Storegga Slide; 6) R Slide; 7) W Slide; 8) S Slide; 9) Tampen Slide; 10) Møre Slide. Palaeo-ice stream flow directions indicated by arrows.

The alternative model of Scandinavian Ice Sheet development differing in northern and southern Scandinavia is based primarily on the poorly constrained dating of different seismic packages along the margin (Rise et al., 2005). According to this interpretation limited ice advances in the south had little influence on sedimentary processes along this part of the margin (Rise et al., 2005). However, in the north, where ice is envisaged to have reached the shelf edge on numerous occasions significantly contributing to sediment wedge progradation along the margin; particularly in the Trænabanken/Trænadjupet area (Fig. 6.13b; Henriksen and Vorren, 1996; Rise et al., 2005; Ottesen et al., 2012).
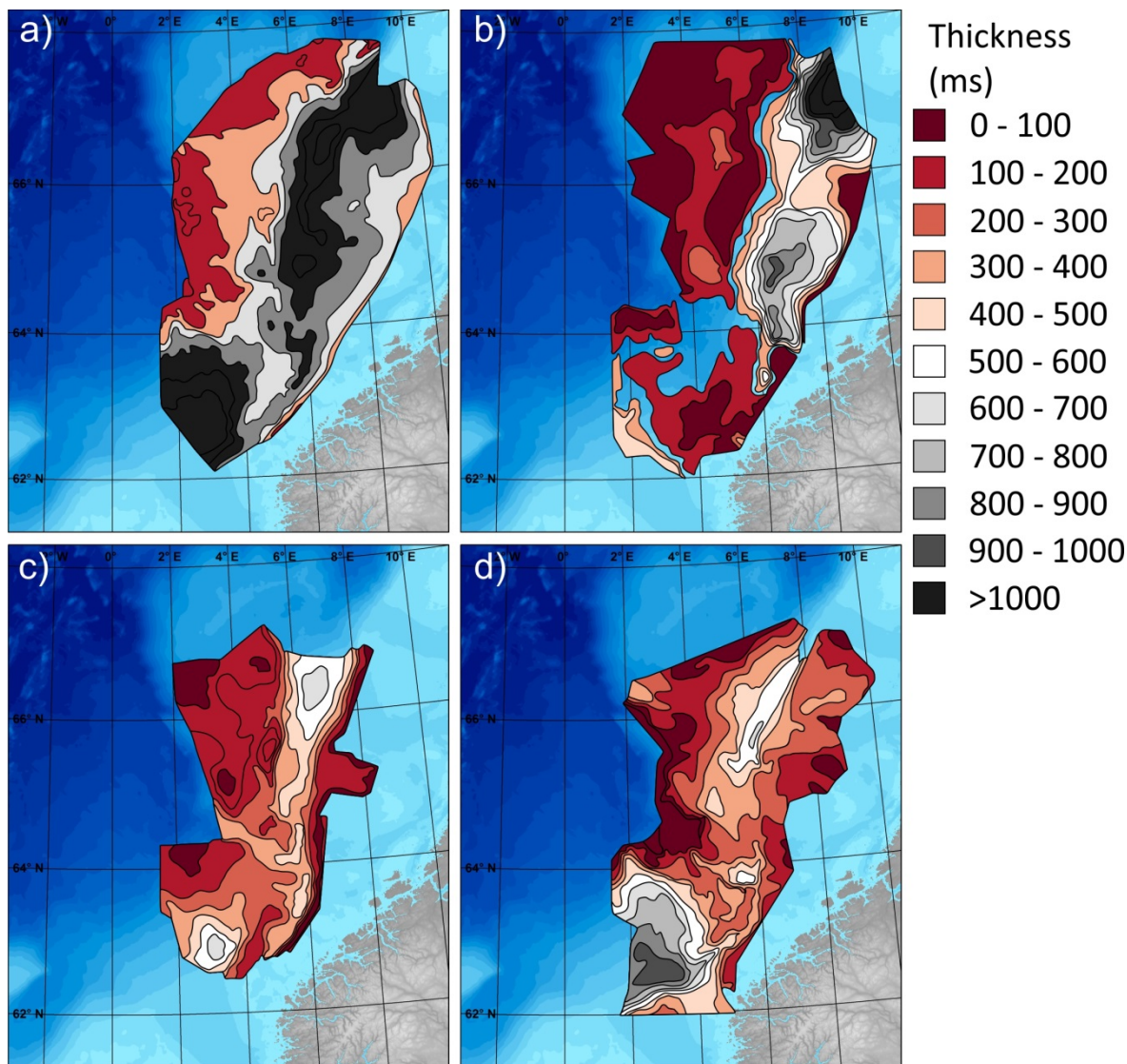
Figure 6.13 Isopach maps of; a) Naust Formation; b) Naust W (deposited from 2.7 – 1.7 Ma); c) Naust U (deposited from 1.7 – 1.1 Ma) and Naust S (deposited from 1.1 – 0.4Ma); d) Naust R (deposited from 0.4 – 0.2 Ma) and O (deposited from 0.2 – 0 Ma). Note that the thicknesses of the deposited material increases to the south with younger ages. Modified from Rise et al. (2005).

6.2.4.2   1.1 – 0.7 Ma

Large scale intensification of glaciation in the Northern Hemisphere is believed to have started after 1.1 Ma (Mudelsee and Schulz, 1997; Mudelsee and Stattegger, 1997). The initial climate step towards a longer glacial/interglacial periodicity is marked by the first definitive expansion of the Scandinavian Ice Sheet to the shelf edge along the entire continental margin (Haflidason et al., 1991; Sejrup et al., 1995; 2000; 2005). The extent of advance is shown by dated till layers

(Haflidason et al., 1991) and IRD records on the Vøring Plateau and in the Norwegian Sea (Baumann and Huber, 1999; Helmke et al., 2003a; 2005). Having retreated the Scandinavian Ice Sheet appears to have reverted to its relatively confined dimensions exhibited from 2.58 – 1.1 Ma until the abrupt adoption of the 100 kyr climatic cycles (Mudelsee and Schulz, 1997; Mudelsee and Stattegger, 1997).

6.2.4.2.1   Sedimentary records of ice sheet and submarine mass movement histories

The extent of the 1.1 Ma Scandinavian Ice Sheet advance is marked by the presence of a nearly continuous till layer across the continental shelf (Sejrup et al., 2004). In the Norwegian Channel this till layer is up to 70 m thick (Haflidason et al., 1991). Indeed, this till layer marks the first evidence of the presence of an ice stream in the Norwegian Channel (Berg et al., 2005). The presence of the Norwegian Channel Ice Stream resulted in the first significant delivery of glacial sediments to the North Sea Trough-Mouth Fan during the Quaternary (Fig. 13c; King et al., 1996). However, despite progradation of the proximal fan and the inferred rapid delivery of glacigenic sediment, there are no recognisable debris-flow lobes associated with this advance in the seismic stratigraphy (King et al., 1996; Faleide et al., 2002). Moreover, the chronological control on the initiation of the Norwegian Channel Ice Stream has been challenged, suggesting it may have first been present no earlier than ~0.5 Ma (Ottesen et al., 2014).

Despite uncertainty over the initiation of the Norwegian Channel Ice Stream, the presence of Cretaceous chalk IRD at Site MD992277 (Fig. 6.3) associated with the 1.1 Ma advance indicates the extension of the Scandinavian/British Ice Sheets into the North Sea (Helmke et al., 2005). The nearest source of chalk extending from the British Isles across the North Sea (Ziegler, 1990), thereby implying a large number of icebergs originated from the North Sea region at this time (Helmke et al., 2003b).

Marine sedimentation returned along the continental margin following the retreat of the ice sheet from its maximum extent (Jansen et al., 1988; Haflidason et al., 1991). The marine sediment package is 40 m thick in the Norwegian Channel above the 1.1 Ma till (Sejrup et al., 1996). During

subsequent glacial periods between 1.1 and 0.7 Ma, it does not appear that the Scandinavian Ice Sheet expanded out onto the continental shelf and thus had little impact on sedimentary processes. Moreover, the sporadic amount of IRD found in marine sequences from this period has been thought to suggest that the ice sheet barely reached the coast (Sejrup et al., 2004; 2005).

6.2.4.3   0.7 – 0.13 Ma

The Scandinavia Ice Sheet remained restricted to alpine settings until ~600 ka (Sejrup et al., 2000; Nygård et al., 2005). IRD records from ODP Sites 643 and 644 show major increases in the amplitude of IRD peaks associated with the adoption of the 100 kyr climatic cycle after ~600 ka (Henrich and Baumann, 1994; Mudelsee and Schulz, 1997).

From 0.7 – 0.13 Ma, 5 major advances are envisaged. Of these, four reached the shelf edge, while one only reached the inner continental shelf (Dahlgren et al., 2002). The four advances of the ice sheet which reached the shelf edge are attributed to MIS 14, MIS 12, MIS 10 and MIS 6. Disagreements exist as to the extent of the MIS 8 advance. Some studies suggest that the ice sheet reached the shelf break across most of the continental shelf (Sejrup et al., 2000; Berg et al., 2005; Nygård et al., 2005; Rise et al., 2005). Others suggest that it only reached the mid-continental shelf (Dahlgren et al., 2002).

The extent of retreat from these glacial maximums is equally varied. Reconstructions suggest that Scandinavia became completely deglaciated during MIS 13 (524 – 478 ka BP), MIS 11 (423 – 362 ka BP) and MIS 5e (128 – 115 ka BP) (Henrich and Baumann, 1994; Hjelstuen et al., 2005; Sejrup et al., 2005). This was a consequence of these interglacials being particularly warm (Helmke and Bauch, 2003; Helmke et al., 2003a). In contrast, during MIS 9 (339 – 303 ka BP) and 7 (245 – 186 ka BP) the Scandinavian Ice Sheet only retreated to fjord and alpine settings (Sejrup et al., 2000) as a consequence of these interglacials being significantly cooler than other interglacials from 0.7 Ma to the present (Helmke and Bauch, 2003).

6.2.4.3.1   Sedimentary records of ice sheet and submarine mass movement histories

The six advances of the Scandinavian Ice Sheet from 0.7 – 0.13 Ma are reflected in the stratigraphic record of the Norwegian continental shelf and its slope deposits (Figs 6.13 - 6.16; Dahlgren et al., 2002; 2005). Until the MIS 14 advance, the continental shelf and slope were dominated by deposition of interbedded hemipelagic and glacimarine sediments reflecting the more withdrawn position of the ice sheet at this time (Sejrup et al., 1989, 2004; King et al., 1996; Nygård et al., 2005). From MIS 14 onwards, continental shelf and slope deposition were dominated by ice sheet sediment delivery (Dahlgren et al., 2005). The change in ice sheet extent at this time is also reflected in the IRD records from the Vøring Plateau and in the Norwegian Basin; larger amounts of IRD from the Scandinavian Ice Sheet penetrating further westward (Krissek, 1989; Helmke et al., 2003b).
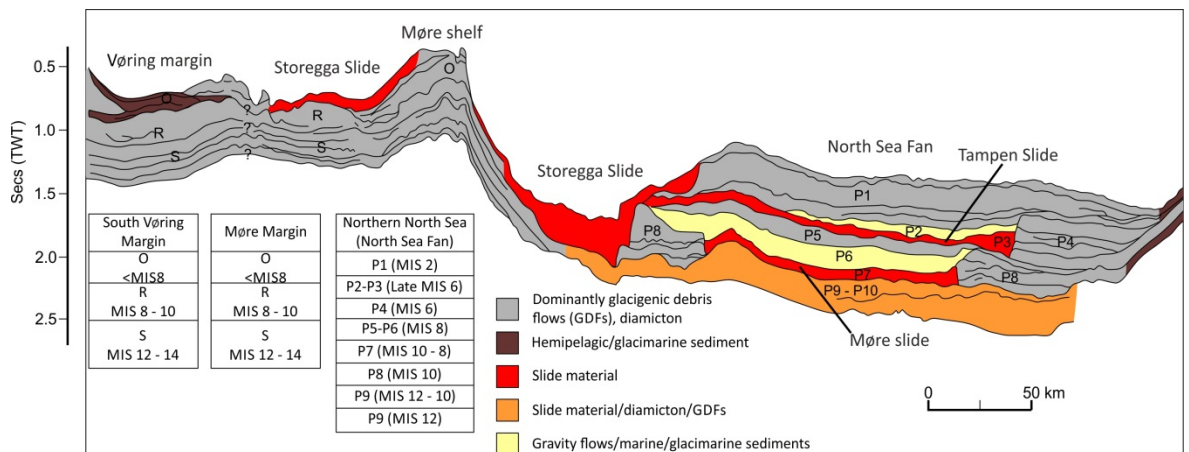
Figure 6.14 Seismic profile crossing the North Sea Trough-Mouth Fan, Storegga Slide and the southern Vøring Margin showing the distribution and correlation of identified Pleistocene units along the Nordic Seas Margin (adapted from Sejrup et al. 2004).

As far south as the Møre Shelf, the MIS 14 advance is marked by the presence of a structureless diamict along the outer shelf of the continental margin (Fig. 6.14; Dahlgren et al., 2002). Beyond the shelf edge, seismic stratigraphy and ODP core records indicate that glacigenic debris-flows were the dominant process by which sediment was re-worked (Talwani et al., 1976; Dahlgren et al., 2002). In contrast, there is no evidence of an ice advance onto the continental shelf in southwestern Norway at this time (Helmke et al., 2003a; Hjelstuen et al., 2005). This may be a

consequence of later reworking of sediment. However, it is unlikely that an advance in this area during MIS 14 was as significant for sediment delivery as later advances.
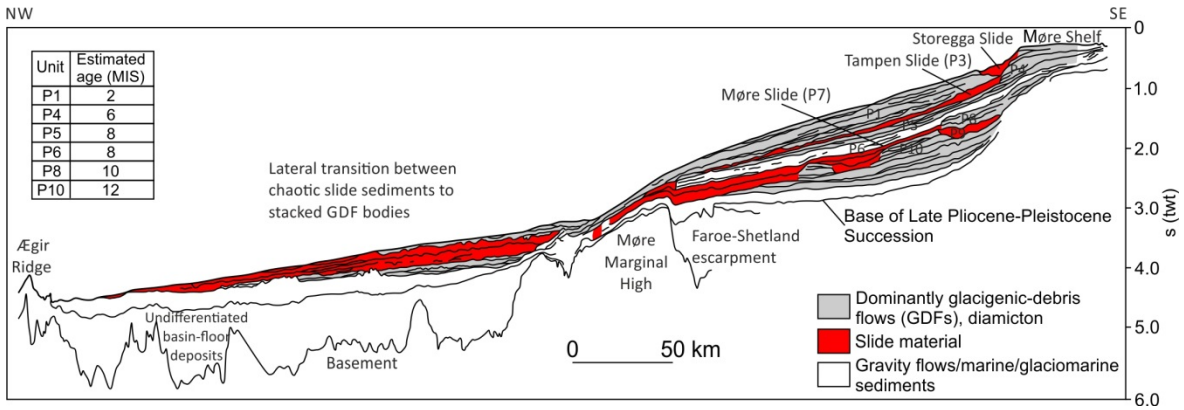
Figure 6.15 Seismic section across the North Sea Trough-Mouth Fan. P1 – P10: identified Late Plio-Pleistocene seismic sequences on the proximal North Sea Trough-Mouth Fan. GDFs = Glacigenic Debris-Flows. Modified from Sejrup et al. (2004).
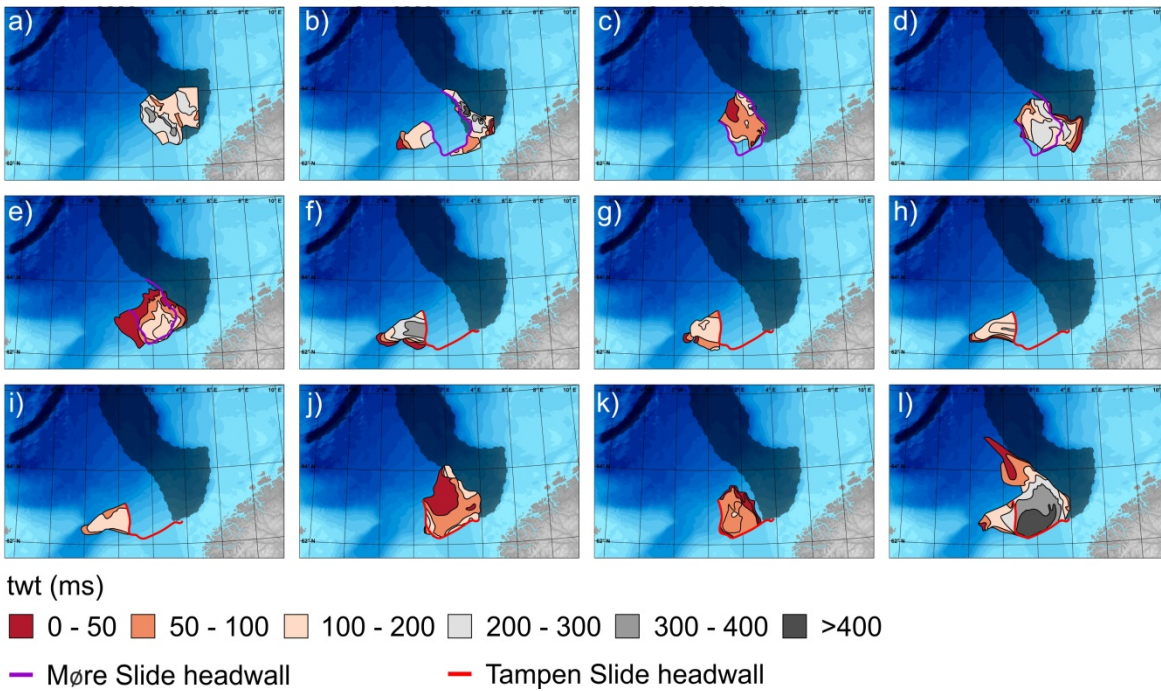
Figure 6.16 Isopach maps for units P1 - P10 identified in Fig. 6.15. a) P10 – P9; b) P8; c) P7; d) P; e) P5; f) P4; g) P4a; h) P4b); i) P4c); j) P3 and Tampen Slide; k) P2; l) P1.

The more extensive MIS 12 advance is marked by a diamict on the shelf along most of the Norwegian Margin (Fig. 6.14; Sejrup et al., 2000; Nygård et al., 2005). Beyond the continental shelf, the sedimentation history is more varied. The outer Møre shelf and the continental slope beyond is characterised by marine/glacimarine deposition (Figs 6.14 and 6.15; STRATAGEM, 2002;

Nygård et al., 2005). In the Møre shelf region, seismic stratigraphy suggests that this unit has primarily infilled the areas between the MIS 14 advance depositional lobes and that the volume of deposited MIS 12 glacimarine sediment may have been greater than that deposited during the earlier advance (Dahlgren et al., 2002). Further south, the North Sea Trough-Mouth Fan underwent a major constructional phase (Fig. 6.16). It is estimated that the Norwegian Channel Ice Stream delivered as much as 3000 km^3 of sediment during this glacial, the majority of which was remobilised as glacigenic debris-flows (King et al., 1996; Nygård et al., 2005). However, subsequent to deglaciation the Møre Submarine Landslide (400 – 380 ka BP) is estimated to have reworked 1200 km^3 of this sediment (Figs 6.15 and 6.16; King et al., 1996; Nygård et al., 2005; Hjelstuen et al., 2007).

On the mid-Norwegian shelf the MIS 10 and MIS 8 are characterised by diamicts on the shelf (Fig. 6.17a; Rise et al., 2005). Beyond the shelf edge seismic data reveals large stacked glacigenic debris-flow lobes and stacked glacigenic debris-flow lenses, related to strong glacial erosion of the shelf (Nygård et al., 2003; Rise et al., 2005). As a consequence of poorly constrained dating of different seismic facies, it is yet unclear as to what deposit thickness is related to the MIS 10 advance and what thickness is related to the MIS 8 advance (Dahlgren et al., 2002; Rise et al., 2005).

In contrast to the mid-Norwegian shelf, MIS 10 and 8 can be clearly differentiated on the southwestern part of the margin. Two distinct glacigenic till units were deposited on the South Vøring Margin and North Sea Margin associated with these two glacials (Figs 6.14, 6.16b-d; King et al., 1996; Haflidason et al., 1998). The MIS 10 and 8 advances are estimated to have delivered approximately 2600 and 3500 km^3 of sediment to the North Sea Trough-Mouth Fan respectively (Nygård et al., 2005). Once deposited by the ice at the shelf edge the MIS 10 glacigenic sediment was remobilised and emplaced down the fan by glacigenic debris-flows (King et al., 1996; Sejrup et al., 2004; 2005; Solheim et al., 2005a). In contrast, the initial phase of MIS 8 deposition (~2100 km^3) was characterised by a combination of glacimarine, marine and gravity-flow processes as a

consequence of ice not reaching the shelf edge (Dahlgren et al., 2002; Sejrup et al., 2004). The

second phase of deposition (~1400 km^3) was dominated by glacigenic debris-flow emplacement

and is thought to represent the period when ice was at the shelf edge of the Norwegian Channel

(Sejrup et al., 2004; Nygård et al., 2005). Two large submarine landslides also occurred during MIS

8. On the South Vøring Margin, the Sklinnadjupet Landslide (Fig. 6.12) is inferred to have occurred

~300 ka BP, the headwall of the slide being based at the mouth of the Sklinnadjupet Trough

(Dahlgren et al., 2002; Solheim et al., 2005a; Hjelstuen et al., 2007). Further to the south at the

mouth of Frøyabankhola Trough, the R Landslide is also inferred to have occurred ~300 ka BP

(Sejrup et al., 2005).
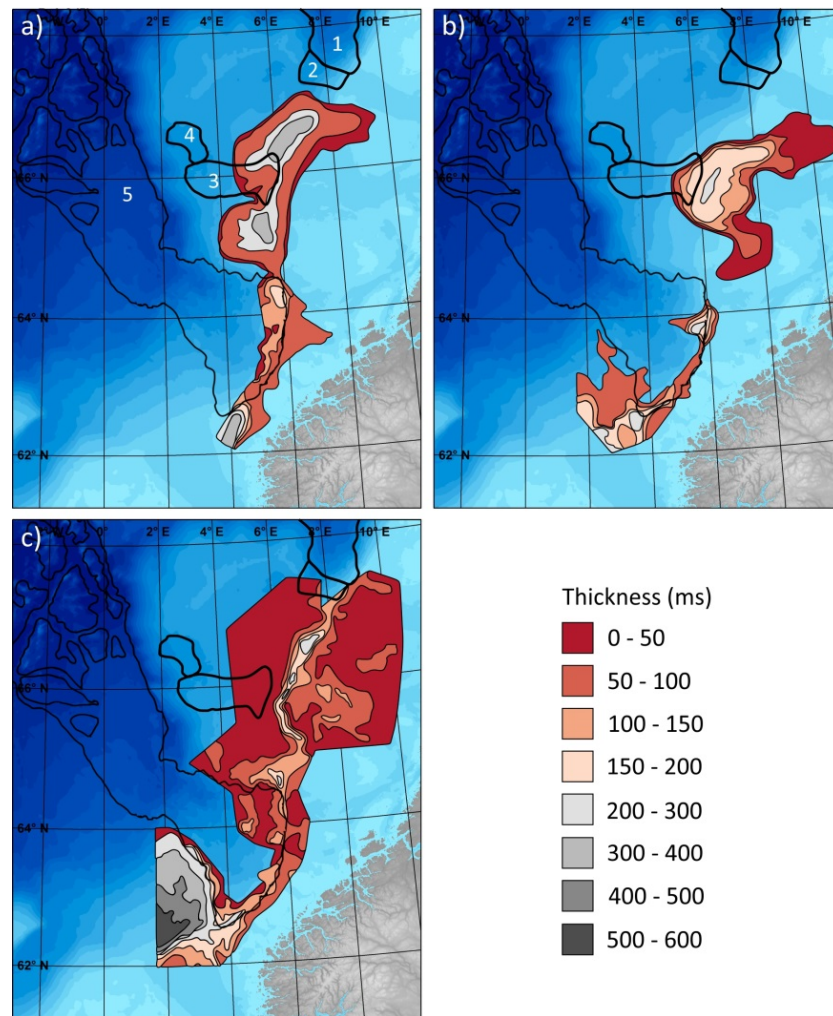
Figure 6.17 Isopach maps of glacigenic deposits along the mid- and southern Norwegian Margins from a) the Elsterian (MIS 10 – 8), b) the Saalian (MIS 6) and c) the Wicheslian (MIS 5d – 2). 1 – 5: Submarine landslide outlines. 1) Trænadjupet Slide; 2) Nyk Slide; 3) Vigrid Slide; 4) Sklinnadjupet Slide; 5) Storegga Slide.

The sedimentary deposits from the mid-Norwegian shelf suggests that the Saalian ice sheet (MIS 6) did not reach the shelf edge (Fig. 6.17b; Rokoengen et al., 1995; Rise et al., 2005). Glacigenic sediments composed of laterally stacked 'till tongues', up to 200 m thick, were deposited on the outer part of the shelf and are inferred to be the result of ice streams flowing out between Haltenbanken and Trænabanken (Fig. 6.17b; Rise et al., 2005). Further south, the Saalian ice sheet did reach the shelf edge. An extensive till layer is found from the South Vøring Margin to the northern North Sea Margin (Fig. 6.14; Sejrup et al., 2004; 2005). Sediment deposited at the shelf edge along these margins has been predominantly reworked by glacigenic debris-flows (Sejrup et al., 2004). During this glacial, it is estimated that 2600 km^3 of sediment was deposited on the

North Sea Trough-Mouth Fan, the majority being reworked by glacigenic debris-flows (King et al., 1996; Nygård et al., 2005). Large amounts of material were also supplied to the area where the Storegga Slide subsequently occurred (Rise et al., 2005). Estimating the volume of sediment delivered to this margin by the Saalian ice sheet is, however, problematic. This is a consequence of the Tampen and Storegga Slides evacuating large volumes of material into the Norwegian Basin (Haflidason et al., 2005; Paull et al., 2007). The Tampen Slide was originally thought to have occurred on the North Sea Trough-Mouth Fan at ~130 ka BP, after the retreat of the Saalian ice sheet (Bryn et al., 2003; Bryn et al., 2005; Solheim et al., 2005a). However, subsequent dating of turbidite deposits in the Norwegian Basin has challenged this original assumption and it will therefore be considered in the following sections (Watts et al., 2016) .

The ice sheet chronology and the associated sedimentary processes that have been described in this section portray a simple pattern of advance, deposition and reworking of sediment and retreat of the ice sheet. This regime depicted is, however, likely to be a simplification of the actual chronology. Reconstructions of ice sheet histories in the Weichselian (following section) show the ice sheet to have undergone multiple advance and retreats during a single glacial. It is therefore likely that diamict and glacigenic debris-flow units which encompass a single glacial cycle could in the future be subdivided to reflect multiple ice sheet fluctuations within one glacial (Dahlgren et al., 2002). This will require higher resolution seismic stratigraphies of the continental shelf and slope combined with higher resolution dating of marine sediments.

6.2.4.4   0.13 – 0 Ma (Weichselian – Present)

As was demonstrated for the Svalbard/Barents Sea region, the higher temporal resolution and more complete records allow us to identify multiple advance and retreat cycles of the Scandinavian Ice Sheet during the Weichselian (Sejrup et al., 2000; Svendsen et al., 2004a; Hughes et al., 2016).

Two advances are proposed during the Early Weichselian. Increased rates of IRD deposition around the Norwegian Sea show the earliest advance to have occurred during MIS 5d (Baumann

et al., 1995; Fronval and Jansen, 1997; Rasmussen et al., 2003). Glacial ice is believed to have expanded sufficiently to reach the coast and its fjords during this period (Sejrup et al., 2004; Lekens et al., 2009). Ice retreated inland during MIS 5c before expanding to reach the outer coastline during MIS 5b. Ice again retreated inland during MIS 5a (Hjelstuen et al., 2005).

The first ice sheet expansion to the shelf edge occurred during MIS 4. During this period ice is hypothesised to have reached the shelf edge between 70 and 60 ka BP (Mangerud, 1991). MIS 3 was predominantly characterised by ice sheet retreat into western Norwegian fjords (Baumann et al., 1995). A minor readvance, the Jæren-Skjonghelleren has been proposed ~42 cal ka BP (Mangerud et al., 2003; Sejrup et al., 2003; Lambeck et al., 2010). This advance is tentatively proposed to have extended beyond the western Norwegian coastline before retreating by 37 cal ka BP (Sejrup et al., 2000). The exact extent of this retreat along the margin is uncertain; however, the minimum retreat scenario suggests that the ice sheet receded to the heads of the Norwegian fjords (Mangerud, 1991, 2004; Svendsen et al., 2004a).

Records of the Last Glacial Maximum Scandinavian Ice Sheet vary depending on location. In northern Norway, in the Andfjorden area, the ice sheet is hypothesised to have expanded from 34 cal ka BP (Vorren and Plassen, 2002), reaching the shelf edge from 24 – 23 cal ka BP. A retreat of up to 100 km occurred between 22 and 20 cal ka BP (Vorren and Plassen, 2002). It then readvanced and was present at the shelf edge from 16 – 14 cal ka BP before retreating. The remainder of the Late Weichselian was characterised by retreat, stillstands and minor readvances (Vorren and Plassen, 2002; Dahlgren and Vorren, 2003).

In mid-Norway reconstruction of the Late Weichselian ice sheet is highly dependent on the type of record used. Solely based on terrestrial data, the main expansion to the shelf edge is interpreted to have begun at ~24 cal ka BP, ice reaching the shelf edge at 23.5 cal ka BP (Olsen et al., 2001a; 2001b). Limited advances had occurred previously between 34 – 32 and 30 – 28 cal ka BP (Olsen et al., 2001b). Terrestrial records suggest the ice retreated from the shelf edge after 23 cal ka BP, which was followed by a short re-advance after 18 cal ka BP until 16 cal ka BP (Olsen et

al., 2001a; Dahlgren and Vorren, 2003). Using marine records (IRD and continental slope deposits) the ice sheet in mid-Norway is interpreted to have advanced to, and retreated from, the shelf edge four times between 21 – 16 cal ka BP (Dahlgren and Vorren, 2003); a retreat occurring, on average, every 2 ka. The marine records suggest that the ice retreated from the shelf edge for the last time at ~16 cal ka BP (Dahlgren and Vorren, 2003).

The glacial history of the Late Weichselian Scandinavian Ice Sheet in southwest Scandinavia is the best constrained as a consequence of numerous studies focussing on the Storegga Slide (Sejrup et al., 1996; 2000; Bryn et al., 2003; Haflidason et al., 2005; Hjelstuen et al., 2005). The ice sheet is interpreted to have expanded from 30 ka BP in this sector and to have reached its first glacial maximum as early as 29 – 27 ka BP (Larsen et al., 2009; Svendsen et al., 2015), remaining on the shelf edge until 23 cal ka BP (Sejrup et al., 1994). Following a retreat from the shelf edge, the ice sheet subsequently readvanced to the shelf edge along the south western Norwegian margin from ~19 – ~15 ka BP after which it retreated. The ice sheet did not, however, advance to the shelf edge of the Norwegian Channel and thus the Norwegian Channel Ice Stream was not present at the shelf edge at this time (Sejrup et al., 2000; Sejrup et al., 2003; Hjelstuen et al., 2005; Svendsen et al., 2015). A more detailed history of the retreat is available from Hughes et al. (2016).

6.2.4.4.1   Sedimentary records of ice sheet and submarine mass movement histories

The record of associated ice sheet sedimentary processes is highly variable along the continental margin of Scandinavia. The completeness of the record and the precision with which it has been dated increases from north to south.

6.2.4.4.1.1   North Norwegian continental shelf

The record of Weichselian sedimentary deposits is least well understood along the northern margin (Lofoten – Vesterålen) of Norway and only extends back to MIS 3. Here, seismic and swath bathymetric mapping of the continental shelf and slope reveal the presence of former areas of fast flowing ice (Ottesen et al., 2005). However, the thickness of glacigenic sediment deposited on

the shelf and upper continental slope is limited (Brendryen et al., 2015). This is thought to be a consequence of relatively small ice stream catchment areas limiting sediment transport volumes (Brendryen et al., 2015) and effective downslope transport of sediment via gullies and canyons on the continental slope (Baeten et al., 2013; Rise et al., 2013). The number and size of submarine canyons in this sector is unique along the Norwegian Margin (Rise et al., 2012; 2013). Moreover, the Andøya Canyon and Lofoten Channel are the only canyon and channel systems of comparable size to the Greenland Submarine Channel system (Ó Cofaigh et al., 2006).

The earliest dated sedimentary deposits on the Lofoten – Vesterålen margin correspond to the hypothesised 34 cal ka BP ice sheet expansion (Vorren and Plassen, 2002). Glacigenic debris-flow deposits and a plumite deposit (dated to 29260 ± 95 cal BP) characterise this advance on the continental slope (Brendryen et al., 2015). The combination of these deposits suggest that the ice was present at the shelf edge prior to 29260 ± 95 cal BP before undergoing a major retreat. Subsequent glacigenic debris-flow deposits, indicative of ice at the shelf edge, are dated to 18470, 22990 and between 25020 and 25660 cal BP (Baeten et al., 2014; Brendryen et al., 2015). Between these deposits, several laminated units interpreted as plumites were deposited (Brendryen et al., 2015). On top of the last glacigenic debris-flow deposits, finely-laminated units and finely-laminated dropstone muds were deposited; the former interpreted to be a plumite (Vorren and Plassen, 2002), the later, deposits beneath an ice shelf (Brendryen et al., 2015).

Beyond the shelf edge, submarine landslide headscars are also visible on bathymetry. The largest is the Andøya Slide headwall. Located to the north of the Andøya Canyon, the Andøya Slide covers ~9700 km^2 with a run-out distance of ~190 km (Laberg et al., 2000). Further south, slide scars from landslides containing between 0.061 and 8.7 km^3 of sediment have also been mapped (Baeten et al., 2013). These landslides are interpreted to be of Holocene age due to a lack of sediment drape and rugged seafloor relief (Laberg et al., 2000; Baeten et al., 2013). However, more accurate dates are yet to be obtained.

6.2.4.4.1.2   Mid-Norwegian Shelf

Studies of the mid-Norwegian Shelf and slope have identified two types of deposits associated with the Weichselian glacial. The MIS 5 and 4 advances are associated with two sets of laminated seismic facies on the continental slope (Henrich and Baumann, 1994; Dahlgren and Vorren, 2003). The MIS 5 sediment package is thickest on the lower to mid-slope and is ~30 m thick (Dahlgren and Vorren, 2003). The MIS 4 deposits are up to 70 m thick and thickest on the southern side of the Sklinnadjupet Slide scar (Dahlgren et al., 2002; Dahlgren and Vorren, 2003). Both deposits are thought to have been emplaced within 10 ka and correspond to marine and glacimarine deposition reflecting a more withdrawn ice sheet position.

In contrast to earlier advances, the MIS 2 ice sheet is thought to have extended to the shelf edge along the entire mid-Norwegian Shelf (Ottesen et al., 2001; Taylor et al., 2002b). Two continental shelf till units can be recognised. These structureless grey diamicts terminate in sediment wedges at the shelf edge (Dahlgren and Vorren, 2003). According to conservative estimates of ice sheet activity along this margin the till layers were deposited from 25900 – 19400 cal BP (Olsen et al., 2001b; Dahlgren and Vorren, 2003). This hypothesised advance is associated with glacigenic debris-flow emplacement on the continental slope (Dahlgren et al., 2002). It has, however, been suggested from IRD records that these till layers may in fact represent up to four advances to the shelf edge between ~27000 ± 101 cal BP and ~18800 ± 39 cal BP (Dokken and Jansen, 1999; Dahlgren and Vorren, 2003). In contrast to other parts of the Norwegian Margin, ice sheet retreat is not associated with plumite deposition (Hjelstuen et al., 2004; 2005).

The preservation of these till layers and glacigenic debris-flows varies from north to south. In the north these sediments have been removed by successive submarine landslides (Laberg and Vorren, 2000; Laberg et al., 2003). Two large submarine landslides have been identified beyond the mouth of the Trænadjupet Trough. The Nyk Slide affects an area of 4,000 – 6,000 km^2 and contained an estimated 400 – 720 km^3 of material (Lindberg et al., 2004; Allin et al., in review). The slide is dated from 21.8 – 19.3 cal ka BP (Allin et al., in review). The Trænadjupet Slide

affected an area of 4,000 – 5,000 km^2 and contained an estimated 500 – 700 km^3 of material (Laberg and Vorren, 2000; Laberg et al., 2002a; Allin et al., in review). The Trænadjupet Slide is dated from 3.5 – 2.8 cal ka BP (Allin et al., in review). The relationship between the timing of these slides and the local sedimentation patterns is significantly different. The Nyk Slide occurred after a period of glacigenic debris-flow emplacement on the continental slope beyond the Trænadjupet Trough when sedimentation rates were as high as 4 m/ka (Baeten et al., 2014; Brendryen et al., 2015; Allin et al., in review). The Trænadjupet Slide occurred ~10 ka after ice retreat from the shelf edge when sedimentation rates were reduced to only a few cm/ka (Baeten et al., 2014; Allin et al., in review).

6.2.4.4.1.3   South Vøring Margin

Little evidence has yet been found that ice reached the shelf break along the South Vøring Margin before the MIS 2 glaciation (Hjelstuen et al., 2005). Instead sedimentation is dominated by marine and glacimarine processes (King et al., 1996; Nygård et al., 2005). Three separate glacigenic units, envisaged to be glacigenic debris-flows, have been identified from MIS 2 (Solheim et al., 2005a). These units are interpreted to have been deposited at ~24840 ± 67, 19020 ± 48, 18580 ± 56 cal BP (Hjelstuen et al., 2005). These units are separated by laminated sequences reflecting a more withdrawn position of the ice sheet.
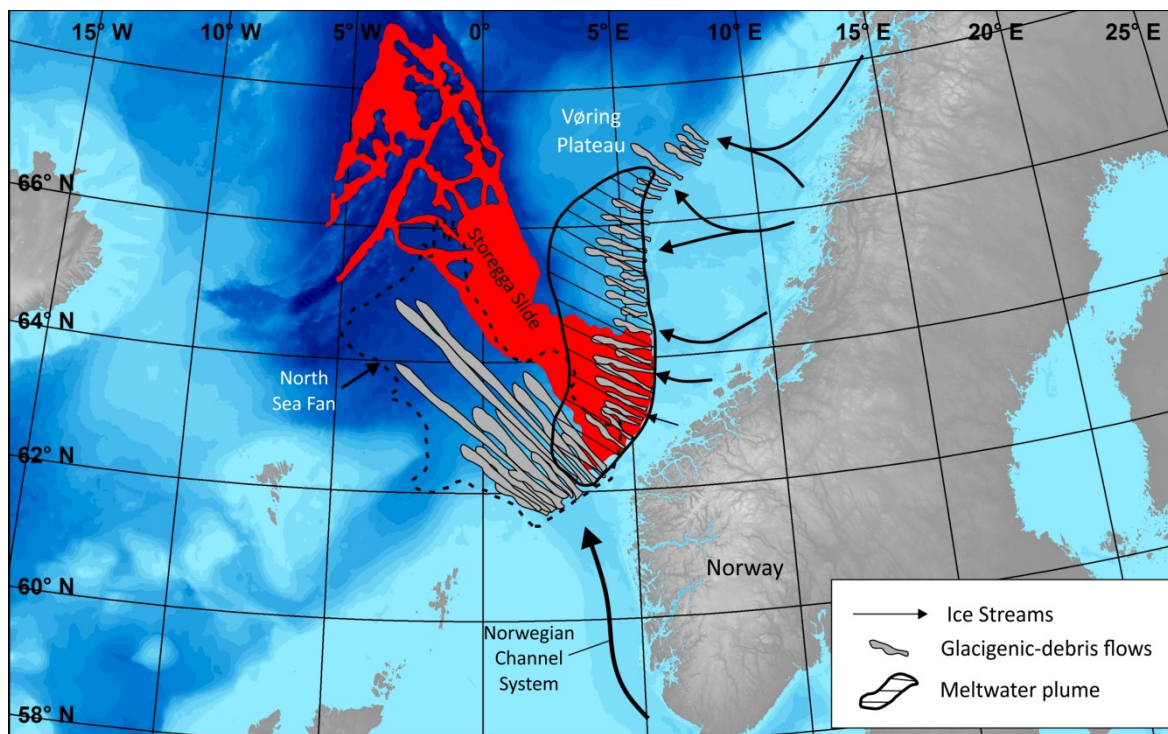
Figure 6.18 Schematic model showing Late Weichselian ice releated deposition across the North Sea and South Vøring Margins. The continental slope is characterised by glacigenic debris-flow emplacement. The disintegration of the Norwegian Channel Ice Stream resulted in the release of a meltwater plume which transported fine-grained material to the Storegga Slide region and the South Vøring margin. Palaeo-ice stream flow directions are indicated by arrows. Adapted from Lekens et al. (2005) and Hjelstuen et al. (2005).

Thin and restricted to the uppermost continental slope, till and debris-flow units on the South Vøring Margin suggest slow rates of sediment delivery during MIS 2. In contrast, the rate of hemipelagic and glacimarine sedimentation which covered the limited glacial deposits was extremely rapid (Hjelstuen et al., 2005). Three periods of plumite deposition are hypothesised; 21.5 – 19.7 cal ka BP, 18.6 – 18.3 cal ka BP and a less northerly extensive period from 18.3 – 18.0 cal ka BP (Fig. 6.18; Lekens et al., 2005; 2009). During the deposition of these deposits it has been calculated that the sedimentation rate over this part of the margin was 1250 cm/ka and was as much as 1750 cm/ka (Lekens et al., 2005). The source of these sediments is inferred to be the Norwegian Channel Ice Stream (Hjelstuen et al., 2004). The greater rate of sediment accumulation in the Storegga Slide area and the South Vøring Margin is hypothesised to be related to slope parallel currents moving suspended sediment northwards from the North Sea Margin.

6.2.4.4.1.4   North Sea Margin

Weichselian sedimentation along the North Sea Margin is dominated by emplacement of diamict layers on the continental shelf and glacigenic debris-flow deposits beyond the shelf edge (Sejrup et al., 2003; Hjelstuen et al., 2005). With the exception of the MIS 2 advance of the Scandinavian Ice Sheet, there is a large amount of uncertainty concerning the extent of the earlier advances. Some authors suggest that there is little/no evidence of an ice advance to the shelf edge in the Norwegian Channel before 28 ka BP (Hjelstuen et al., 2005; Nygård et al., 2005; 2007). According to this interpretation sedimentation up until 28 ka BP was dominated by marine and glacimarine processes. Other studies have suggested that multiple till units exist and are linked to advances during the Karmøy Stadial (~85 to 70 ka BP) and the Skjonghelleren Stadial (~50 to 36 ka BP) (Sejrup et al., 1995; 2003; 2004). These till layers can be traced beyond the shelf break in the form of glacigenic debris-flow deposits on the upper slope (Sejrup et al., 2003).

If it is assumed that ice only reached the shelf edge during MIS 2, 4 oscillations of the ice front are envisaged, although the Norwegian Channel Ice Stream was only present at the shelf edge during the earliest advance from after 30 cal ka BP to 23 cal ka BP (Sejrup et al., 1994; Nygård et al., 2005). Three sequences of glacigenic debris-flow deposits are associated with this advance on the North Sea Trough-Mouth Fan. Each debris-flow sequence is separated by a phase of hemipelagic deposition (Lekens et al., 2009). Individual debris-flows from this period can be mapped out as far as 500 km from the shelf edge (King et al., 1998). The volume of sediment accumulated on the fan during this period is estimated to be up to ~5300 km^3 (Nygård et al., 2005) out of a total of ~5800 km^3 deposited during the entire Weichselian (Nygård et al., 2005).

Following the retreat of the Norwegian Channel Ice Stream at ~23 cal ka BP, the North Sea Trough-Mouth Fan was dominated by marine and glacimarine deposition (Fig. 6.18; Lekens et al., 2005). However, sedimentation rates were an order of magnitude lower compared to the Storegga and South Vøring areas. From 19 – 18 cal ka BP, plumite sedimentation rates were ~60 cm/ka. From 18 – 17 cal ka BP, plumite sedimentation rates were ~30 cm/ka. This rose to ~40

cm/ka until 14.5 cal ka BP before returning to normal sedimentation rates of <10 cm/ka (Sejrup et al., 2000; Lekens et al., 2005; 2009).

During the Weichselian two large submarine landslides are known to have occurred in this region. The earlier slide, the Tampen Slide, is now dated to ~52 – 48 cal ka BP (Watts et al., 2016). It has a volume estimated to be greater than the Storegga Slide (Watts et al., 2016). The headwall of this slide is found on the North Sea Trough-Mouth Fan (Fig. 6.16). The timing of this slide relative to Norwegian Channel Ice Stream activity is uncertain. If the ice stream is assumed to have reached the shelf edge repeatedly during the Weichselian then the slide occurred after the ice stream retreated from the shelf edge at the end of MIS 4. If correct a large volume of material was likely advected to the shelf edge and subsequently remobilised with large volumes of North Sea Trough-Mouth Fan Saalian deposits as part of this slide. If the ice stream is assumed not to have reached the shelf edge until MIS 2/3 then the slide occurred as a consequence of relatively little deposition of material on the trough-mouth fan. In this scenario, the majority of evacuated sediments were derived from the Saalian glaciation.

The Storegga Slide occurred north of the North Sea Trough-Mouth Fan ~8200 BP (Haflidason et al., 2005). The slide evacuated an estimated 3000 km^3 of sediment and affected an area of 95,000 km^2 (Haflidason et al., 2004). The Storegga Slide occurred significantly (6 ka) after the period of high sedimentation had finished. Within the Storegga Slide escarpment additional slides have been identified and dated to 5700 cal BP and 2800 – 2200 cal BP (Haflidason et al., 2005; Lekens et al., 2009).

The history of the Scandinavian Ice Sheet and the related sedimentation processes are summarised in Table 6.4 and Fig. 6.7c.

Period (Ma)	Ice sheet history	Sedimentation record
2.58 - 1.1	*Reconstruction 1:* Intermediate size ice sheet rarely expanding beyond fjords of western Norway *Reconstruction 2:* Glaciers regularly advanced to the shelf edge north of the Vøring Plateau Glaciers remained limited in size south of the Vøring Plateau	Slide W occurred between 2.7 and 1.7 Ma and is estimated to have rembolised 24,600 km3 *Reconstruction 1:* No evidence of ice sheet related submarine mass movements Limited delivery of IRD *Reconstruction 2:* Progradation of sediment wedges in the north where ice reached the shelf edge Little/no influence of ice along southern Norwegian margin
1.1 - 0.7	First expansion to the shelf edge after 1.1 Ma Subsequent reversion to limited ice sheet extent seen previously	1.1 Ma lacial advance marked by near continuous till layer Glacimarine sedimentation associated with 1.1 Ma advance beyond the shelf edge Retreat of ice sheet is marked by a return of marin sedimentation along the entire margin
0.7 - 0.13	Advances to the shelf edge during MIS 14, 12, 10 and 6 Uncertainty over whether MIS 8 advance reached the shelf edge or just the mid-continental shelf	*MIS 14:* Till present on the outer shelf as far south as the Møre Shelf Glacigenic debris-flow emplacement on continental shelf beyond where till is present on the shelf Little/no sedimentary evidence of ice sheet advance south of the Møre Shelf *MIS 12:* Advance is marked by regional till layer Outer Møre Shelf and continental slope is characterised by marine/glacimarine deposition North Sea Trough-Mouth Fan underwent a major construction phase; 3000 km3 of sediment was deposited, mainly in the form of glacigenic debris-flow deposits Møre submarine landslide (400 - 380 ka BP) reworked 1200 km3 of sediment previously deposited on the North Sea Trough-Mouth Fan *MIS 10 - 8:* Mid-Nowegian margin → MIS 10 and 8 cannot be clearly distinguished; sequence characterised by strong shelf erosion and glacigenic debris-flow emplacement on the continental slope South Norwegian margin→ MIS 10 and 8 clearly distinguishable Two distinct glacigenic till units on the south Vøring and North Sea margin 2600 km3 of sediment emplaced as glacigenic debris-flow deposits on the North Sea Trough-Mouth Fan during MIS 10 3500 km3 of sediment emplaced on the North Sea Trough-Mouth Fan during MIS 8; 2100 km3 through glacimarine processes (ice not at the shelf edge), 1400 km3 by glacigenic debris-flows (ice at the shelf edge) Sklinnadjupet (300 ka BP) and R (300 ka BP) landslides occurred during MIS 8 *MIS 6:* Mid-Norwegian margin → deposition of stacked till tongues up to 200 m thick as a result of ice not reaching the shelf edge South Vøring to Northern North Sea margin → extensive till layer deposited to the shelf edge; glacigenic debris-flow emplacement beyond teh shelf edge North Sea Trough-Mouth Fan → 2600 km3 of sediment deposited, predominantly by glacigenic debris-flows
0.13 - 0	MIS 5d (109 - 96 ka BP) advance to coast and into fjords MIS 5b (87 - 82 ka BP) advance to the outer coastline MIS 4 (71 - 57 ka BP) advance to the shelf edge Minor readvance beyond the west Norwegian coastline around (42 cal ka BP) *Northern Norway:* Ice advanced from 34 cal ka BP, reaching the shelf edge from 24 - 23 cal ka BP Retreat of up to 100 km between 22 and 20 cal ka BP Readvance to the shelf edge from 16 - 14 cal ka BP *Mid-Norway:* Main expansion to shelf edge began at 23.5 cal ka BP Retreat from shelf edge afteer 23 cal ka BP Short readvance after 18 cal ka BP until 16 cal ka BP *Southern Norway:* Expansion from 30 cal ka BP At the shelf edge as early as 29 - 27 cal ka BP Ice retreated from the shelf edge after 23 cal ka BP	*North Norwegian Continental Shelf (MIS 3 - 1):* Earliest dated glacigenic debris-flows emplaced around 34 cal ka BP Plumite deposition around 25,590 14C yr BP Additional glacigenic debris-flow sequences dated to 15.6 ka BP, 19.5 ka BP and 21.7 - 21.1 ka BP; laminated plumites interbed glacigenic debris flow deposits Large numbers of submarine landslides during the Holocene including the Andøya Slide **_____** *Mid-Norwegian Continental Shelf (MIS 5 - 1):* MIS 5 and 4 marine and glacimarine deposition on continental slope reflect withdrawn ice sheet position Two till layers associated with the MIS 2 advance from 22 - 16.5 c14a BP; glacigenic debris-flows associated with these advances are found on the continental slope Little/no evidence of plumites Two large submarine landslides (Nyk and Trænadjupet) occurred between 21.8 - 19.3 cal ka BP and 3.5 - 2.8 cal ka BP *South Vøring Margin (MIS 2 - 1):* Three glacigenic units interpreted as glacigenic debris-flows on the continental slope from MIS 2 (21,000, 16,200, 15,700 14C yr BP) Plumite deposits interbed the debris-flow units; deposition rates from Plumites during deglaciation as high as 1750 cm/kyr *North Sea Margin:* MIS 2 glacial advance characterised by a till unt on the continental shelf and glacigenic debris-flows on the continental slope Three sequences of glacigenic debris-flows emplaced on the North Sea Trough-Mouth Fan separated by hemipelagic deposition 5300 km3 of sediment accumulated on the North Sea Trough-Mouth Fan durng MIS (5800 km3 accumulated during the entire Weichselian) North Sea Trough-Mouth Fan was dominated by marine and glacimarine deposition after 23 cal ka BP From 19 - 18 cal ka BP plumite sedimentation rates were 60 cm/ka; 18 - 17 cal ka BP plumite sedimentation rates were 30 cm/ka which rose to 40 cm/ka before returning to background interglacial rates (<10 cm/ka) after 14.5 cal ka BP Tampen and Storegga submarine landslides occurred around 52 - 48 cal ka BP and 8.2 cal ka BP respectively

Table 6.4 Summary of the important steps in glacial evolution of the Norwegian continental margin and the resulting record of sedimentation.

187

6.3   How do the continental margins of the Nordic Seas compare with other glaciated margins?

The previous section outlined the evolution of the continental margins of the Nordic Seas with respect to the histories of three ice sheets. The following section will discuss similarities and differences seen on a range of other glaciated continental margins. The margins we have chosen to include in this comparison reflect the range of environments outlined in the continuum of glacier-influenced settings in Fig. 6.1.

6.3.1   Antarctic continental margin

The continental margins of Antarctica have the coldest climate and should therefore be the least influenced by meltwater processes. Many of the morphological features identified on the margins of the Nordic Seas are present on the Antarctic continental margin. Bathymetric, seismic and sedimentological studies have all identified the presence of trough-mouth fans, submarine channels, gullies and landslides (Kuvaas and Leitchenkov, 1992; Dowdeswell et al., 2008; Amblas and Canals, 2016; Canals et al., 2016; Gales et al., 2016; and references therein). However, there are significant differences in the morphologies of these features, their relative numbers and the relative timescales over which different sedimentation processes operate.

6.3.1.1   Antarctic trough-mouth fans

Despite the number of cross-shelf troughs seen on the continental shelves of Antarctica and the extended period over which glacial processes have operated (Antarctica has been glaciated for about 34 Ma; Zachos et al., 2001), there are relatively few trough-mouth fans (Ó Cofaigh et al., 2003). Nonetheless, three large trough-mouth fans have been recognised; the Crary Trough-Mouth Fan in the Weddell Sea (Kuvaas and Kristoffersen, 1991), the Prydz Bay Trough-Mouth Fan offshore the Lambert-Amery glacial system in East Antarctica (Kuvaas and Leitchenkov, 1992), and the Belgica Trough-Mouth Fan in the Bellingshausen Sea (Dowdeswell et al., 2008).

Of these trough-mouth fans, the morphology and inferred processes of the Belgica Trough-Mouth Fan most clearly resemble those outlined on Nordic Sea trough-mouth fans (Fig. 6.19a). It covers an estimated area of at least 22,000 km^2 and contains ~60,000 km^3 of sediment that has accumulated over the past 5.3 Ma (Scheuer et al., 2006; Dowdeswell et al., 2008). Compared to the Nordic Sea trough-mouth fans it therefore falls between Storfjorden and Scoresby Sund (115,000 and 15,000 km^3 respectively) in terms of volume despite having a palaeo-drainage basin under full-glacial conditions an order of magnitude greater (200,000 km^2 vs 60,000 km^2) than either system from the Nordic Seas (Vorren et al., 1998; Ó Cofaigh et al., 2005; Håkansson et al., 2007). As seen in the Nordic Seas, seismic stratigraphic analysis of the Belgica Trough-Mouth Fan reveals semi-transparent lenses interpreted to be glacigenic debris-flow deposits (Ó Cofaigh et al., 2005; Hillenbrand et al., 2010). Gully and channel systems have been cut into the emplaced deposits (Fig. 6.19a; Dowdeswell et al., 2008). As seen on some trough-mouth fans in the Nordic Seas the density of these features is highest at the margins of the Belgica Trough-Mouth Fan. However, the depth of incision, downslope extent beyond the lower slope and presence across the entire width of the fan contrasts strongly with systems in the Nordic Seas whose gully systems are much less well developed and generally confined to the upper slopes (Dowdeswell et al., 2008; Pedrosa et al., 2011; Lucchi et al., 2013; Llopart et al., 2015). Also unlike the largest fans in the Nordic Seas, there is no evidence of major slides or other mass wasting (Nitsche et al., 1997; Dowdeswell et al., 2008). Unfortunately, no chronologic information is available to date the timing of debris-flow emplacement and channel incision.

The Prydz Bay Trough-Mouth Fan is the best understood of Antarctic trough-mouth fan (Fig. 6.19c). Its development can be divided into three phases. Phase 1 lasted from the Late Miocene until 1.1 Ma. During this period the Lambert Glacier advanced to the shelf edge, depositing diamicts which were subsequently reworked by glacigenic debris-flows (Kuvaas and Leitchenkov, 1992; O'brien and Harris, 1996; Passchier et al., 2003; O'Brien et al., 2007). The volumes of these flows were much lower than those seen on the Bear Island and North Sea Trough-Mouth Fans (O'brien and Harris, 1996). These deposits were interbedded with contouritic sediments and

turbidites (Passchier et al., 2003). During Phase 2 (1.1 – 0.78 Ma), glacial sediment input decreased leading to a reduction in the number and thickness of glacigenic debris-flows (O'Brien et al., 2007). Phase 3 (0.78 Ma – present), coinciding with the adoption of 100 kyr climate cyclicity, was witness to a cessation of debris-flow activity and a growing dominance of glacimarine deposition as the Lambert Glacier failed to reach the shelf edge (Passchier et al., 2003). No evidence yet exists for large scale mass failures (Kuvaas and Leitchenkov, 1992). The volume of sediment which accumulated during the construction of the Prydz Bay Trough-Mouth Fan is comparatively small (27,740 km^3) when the drainage area (3.5 x 10^5 km^2) of the Lambert Glacier under full glacial conditions is considered (Denton and Hughes, 2002).
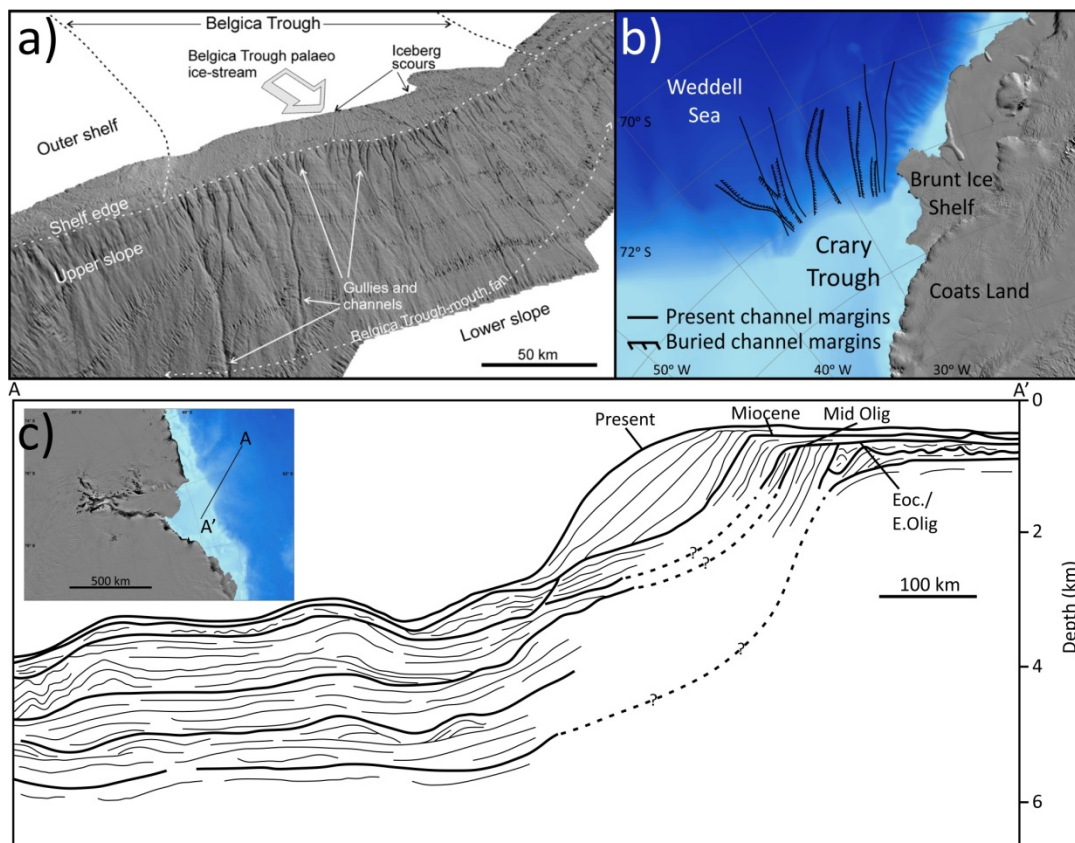
Figure 6.19 Examples of trough-mouth fans from Antarctica with varying morphologies. a) Oblique view (from the north) of sun-illuminated swath bathymetry of the Belgica Trough-Mouth Fan and the major sedimentary features. b) Present and buried channels identified on the Crary Trough-Mouth Fan. c) Bathymetric map and seismic interpretation of the Prydz Bay Trough-Mouth Fan. Modified from Dowdeswell et al. (2008), Kuvass and Kristoffersen (1991) and Passchier et al. (2003).

The Crary-Weddell Sea Fan system of which the Crary Tough-Mouth Fan is part covers an estimated area of 750,000 km^2 (Anderson et al., 1986). Initiation of the fan began ~34 Ma but unlike other trough-mouth fans has been dominated by the presence of large channel-levee complexes (Kuvaas and Kristoffersen, 1991). Three channel-levee complexes have existed during the last 34 Ma (Fig. 6.19b). They are hypothesised as being a result of brine rejection eroding channels during interglacials and depositing winnowed fine sediments from the upper slope and shelf on the levees (Kuvaas and Kristoffersen, 1991). During glacials, glacial meltwater transport of sediment, turbidity currents and downslope evolving submarine slumps and debris-flows result in enhanced channel-levee activity and fan progradation (Kuvaas and Kristoffersen, 1991; Melles and Kuhn, 1993). Dating of material from the levee complexes supports this hypothesis; deposition on the levees in water depths of 2000 – 3000 m ranged from 100 – 200 cm/kyr during the last glacial and has only been a few cm/kyr during the Holocene (Weber et al., 1994). Glacigenic debris-flows and submarine landslides have also been identified (Melles and Kuhn, 1993; Gales et al., 2016). Larger submarine landslides have also been suggested to have occurred on the Crary Trough-Mouth Fan during the Early Pleistocene during the drawdown of East Antarctica (Bart et al., 1999).

6.3.1.2   Antarctic gullies and submarine channels

A large proportion of the mapped Antarctic Margin is dominated by gullies and channel systems and therefore bares a greater similarity to the East Greenland Margin than the Norwegian Margin. The gullies and channels are, however, more numerous and permanent features.

Gullies have been found incised into trough-mouth fans (e.g. the Crary Trough-Mouth Fan) and the continental slope in front and between cross-shelf troughs (Dowdeswell et al., 2004a; 2006a; Gales et al., 2014). Depending on their location, gully formation has been linked to different processes. Along parts of the Antarctic Margin, gully formation is hypothesised to be a consequence of cold-dense water cascading down the continental slope through brine rejection (Noormets et al., 2009). Many are, however, hypothesised to be a consequence of turbidity current activity, sediment-laden subglacial meltwater discharge or small-scale mass failures

(Dowdeswell et al., 2006a; Gales et al., 2016). In many cases gullies feed channel systems or coalesce to form channels themselves further down the continental slope.

Extensive channel networks have been found offshore of the continental shelf around most of the Antarctic Margin. Offshore of the Antarctic Peninsula, dendritic canyon-channel systems are found at the mouths of cross-shelf troughs (Amblas et al., 2006; Amblas and Canals, 2016). These systems are a consequence of intense turbidity current activity which occurs due to ice at the shelf edge delivering large amounts of sediment, subglacial meltwater plumes and the relatively steep continental slope favouring turbidity current formation (Pudsey and Camerlenghi, 1998; Dowdeswell et al., 2004a). Sediment mounds are found between these channels as a consequence of bottom current reworking and deposition of sediment (Amblas et al., 2006).

Other extensive channel/submarine canyon and related submarine fan systems have been found on the Wilkes Land Margin (130 – 145°E) and Queen Maud Land (12 – 18°W) (Escutia et al., 2000; Busetti et al., 2003; Ó Cofaigh et al., 2003). The presence and morphology of these systems is thought to be the result of multiple factors. The ice streams feeding these systems are relatively small, frequently migrate and deliver insufficiently large volumes of sediment when at the shelf edge to build a trough-mouth fan system (Escutia et al., 2000). The proportionally larger volumes of coarse sediment delivered to the top of these systems by ice streams is also thought to be partially responsible for their steep upper and mid- slopes when compared to similar fluvial systems (Escutia et al., 2000).

6.3.1.3   Antarctic submarine landslides

When compared to the margins of the Nordic Seas, the Antarctic continental margin is notable for its lack of submarine landslides. Exceptions exist, the Gebra Slide on the Antarctic Peninsula margin contains ~21 km^3 of sediment (Imbo et al., 2003; Canals et al., 2016) and slides have been identified on the Crary Trough-Mouth Fan (Gales et al., 2014; 2016). However, there is as yet little evidence of frequent mass wasting events with volumes comparable to the Storegga or Trænadjupet Slides despite the clear contrasts in sediment package characteristics that would be

deposited by glacial and contouritic processes that operate around Antarctica (Kuvaas et al., 2005;

Gales et al., 2014).

6.3.2   East Canadian Margin

The continental margin of East Canada was the location of the furthest eastern extension of the

Laurentide Ice Sheet (Fig. 6.20). Running from $\sim 40 - 76^{o}$N, the East Canadian Margin has features

similar to those seen on other glaciated margins but also exhibits features indicative of greater

meltwater influence. This could be a consequence of either the lower latitude of the southern

part of the margin or of the internal dynamics of the Laurentide Ice Sheet (Bond et al., 1992;

Piper, 2005).
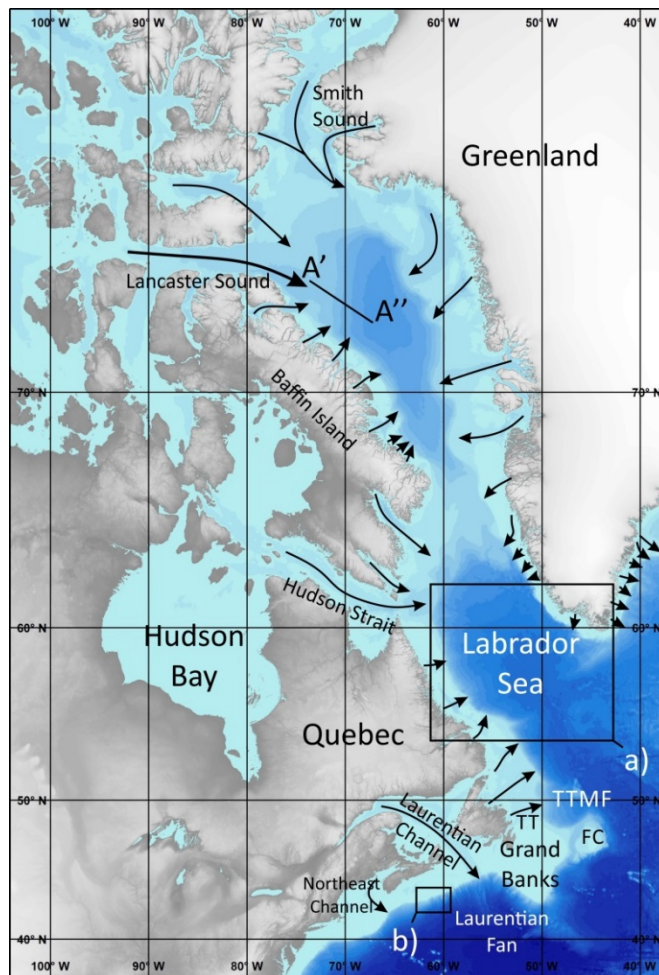
Figure 6.20 Location map of the East Canadian Margin. Cross-shelf troughs inferred to have contained ice streams during the last glacial are illustrated with arrows. Study areas in Fig. 6.21 a), b) and c) are identified.

6.3.2.1   East Canadian trough-mouth fans

Trough-mouth fans have been identified along the entire East Canadian Margin (Aksu and Hiscott, 1989; Piper, 2005; Tripsanas and Piper, 2008; Li et al., 2011). However, their morphology changes with latitude. At the northern end of the East Canadian Margin, trough-mouth fans have similar architectures and sedimentation regimes to those described on the Svalbard/Barents Sea continental margin. For example, the depositional systems operating on Lancaster Sound and Trinity Trough-Mouth Fan are dominated by the emplacement of glacigenic debris-flow units (Fig. 6.21; Tripsanas and Piper, 2008; Li et al., 2011). Originating from till wedges higher on the continental slope, glacigenic debris-flow emplacement is responsible for the majority of progradation of these fans during glacial periods (Piper, 2005).

Further south, the Laurentian and Northeast Trough-Mouth Fans have very different morphologies and thus different sedimentation histories. Both trough-mouth fans are dominated by large channel-levee systems (Piper et al., 2016). Seismic profiles across both fans shows that similar channel systems have previously existed on these fans throughout the Quaternary (Piper et al., 2016). These channel systems and the growth of these fans is hypothesised to have been the result of exceptionally large discharges of sediment-laden meltwater to the slope leading to the formation of hyperpycnal flows or turbidity currents re-working rapidly deposited plume deposits (Piper et al., 2007; Clare et al., 2016). Submarine slump and debris avalanche reworking of deposited material is also thought to play a role in the sedimentation history of these fans (Piper et al., 2012). Critically, there is little evidence of glacigenic debris-flows being important to the development of these trough-mouth fans.

6.3.2.2   East Canadian gullies and submarine channels

Much of the East Canadian Margin is characterised by alternating regions of high and low density gullies and channels (Hesse et al., 1999; Mosher et al., 2004). Where cross-shelf troughs are found, sedimentation is dominated by glacigenic debris-flow emplacement (Hesse et al., 2001; Piper, 2005). Gullies and channels have, however, been incised into the emplaced debris-flow

units by sediment-laden meltwater being discharged from the ice margin and the downslope evolution of glacigenic debris-flows into turbidity currents (Piper, 2005; Dowdeswell et al., 2016a; 2016c). Between the cross-shelf troughs, meltwater processes dominate resulting in the formation of dendritic gully and canyon systems. These systems are hypothesised to be a consequence of hyperpycal flow formation, the re-working of sediment by turbidity currents which has settled out from meltwater plumes that have been entrained southward by the Labrador Current and mass-wasting processes (Fig. 6.21; Hesse et al., 1997; 2001; 2004; Ó Cofaigh et al., 2003). Many of the channel and canyon systems subsequently coalesce to feed deep-sea channels such as the North Atlantic Mid-Ocean Channel (Piper, 2005).

6.3.2.3   East Canadian submarine landslides

The first identified submarine landslide was the Grand Banks landslide in 1929 (Heezen and Ewing, 1952; Piper and Aksu, 1987). Like the Storegga region, these events appear to be relatively common along the East Canadian Margin. Landslide headwalls have been identified on the upper continental slope, in gullies, on canyon flanks, and at the base of the continental slope (Mosher et al., 1994; 2004; Piper, 2005; Dowdeswell et al., 2016a). These landslides therefore likely play an important role in the maintenance and morphology of the channel and gully systems which exist along much of the margin (Piper, 2005; Dowdeswell et al., 2016a; 2016c).

The majority of the landslides within the gully and channel systems north of Orphan Basin have been interpreted to have contained relatively small volumes of sediment. As a consequence these landslides are unlikely to have the geohazard potential of the large submarine landslides seen during the Holocene in the Nordic Seas. In contrast, the south eastern part of the Canadian Margin from the Flemish Cap to Georges Banks has experienced large numbers of large mass failures during the Quaternary (Piper et al., 2003; Piper, 2005). Here, failures with volumes up to ~800 km^3 have been identified (Piper and Ingram, 2003). 10 landslides with volumes >10 km^3 have been identified within Quaternary stratigraphy on this part of the margin suggesting a mean recurrence interval of 0.25 Ma (Piper and Ingram, 2003; Piper et al., 2003). However, the

recurrence times vary between individual basins (Piper et al., 2003) and there are large dating uncertainties on most landslides. The recurrence of smaller, but still >1 km^3, landslides is shorter. For example, 9 turbidite deposits, interpreted to originate from landslides on the Flemish Cap occurred during the last 150 ka (Huppertz and Piper, 2009).
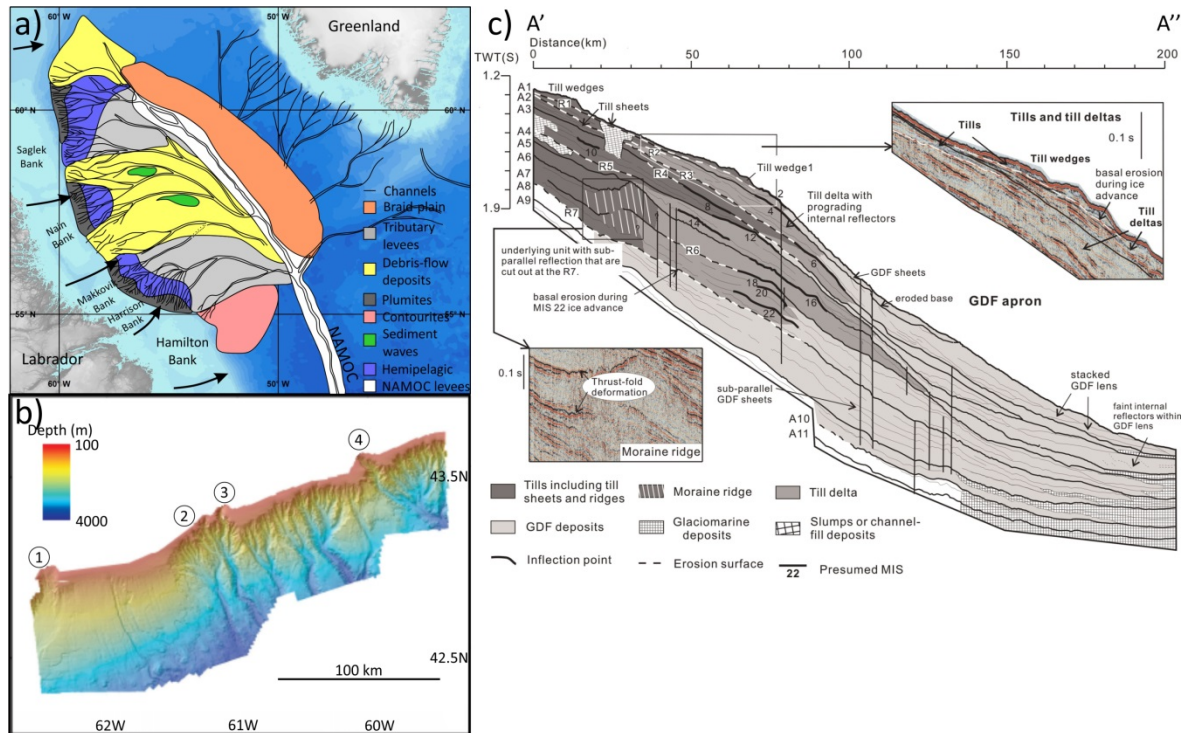
Figure 6.21 Examples of ice sheet influenced sedimentary features on the East Canadian Margin. a) Map of the Labrador Sea showing the upslope branching pattern of tributary channels on the slope and distribution of major sediment facies (redrawn from Hesse et al. (1997) and Ó Cofaigh et al. (2003)). Inferred ice stream positions are marked with arrows. NAMOC = North Atlantic Mid-Ocean Channel. b) Multibeam bathymetric sonar data showing the morphology of the central Scotian Slope. 1 = Mohican Channel; 2 = Verrill Canyon; 3 = Dawson Canyon; 4 = Logan Channel. Modified from Mosher et al. (2004). c) Seismic interpretation of the Lancaster Sound Trough-Mouth Fan from an airgun profile. Detail of stacked structure of till and till delta are shown in the upper insert. A close-up of two moraine ridges is shown in the lower insert. Presumed MIS stages are labelled along their corresponding seismic reflector. Modified from Li et al. (2011).

The identified large submarine landslides on the south eastern part of the Canadian Margin are thought to be directly linked to glaciation of the continental slope. Glacial and pro-glacial

sediment packages have been shown to fail retrogressively along their bedding plane on this section of the margin (Piper et al., 1999; Mosher et al., 2004). Moreover, the most recent failures identified on the Scotian Slope and Grand Banks occurred at or immediately after the Laurentide Ice Sheet reaches its local maximum extent during the last glaciation of the shelf (Piper and Campbell, 2005). Extrapolating further back into the Quaternary, the Laurentide Ice Sheet is interpreted to have reached the shelf edge in this area repeatedly from MIS 12 (0.45 Ma) onwards (Piper et al., 1994). However, the poorly constrained dating of the large mass transport deposits which pre- and post- date MIS 12 prevents any further understanding of the influence that shelf edge glaciations have had on the frequency of large submarine landslides.

6.4   Glaciated margin systems – a new conceptual model

In the following section we develop a new conceptual model of sedimentation on glaciated margins based on the ice sheet histories around the Nordic Seas outlined in Section 6.2 and the comparisons made in Section 6.3 with other margins.

6.4.1   How has ice sheet history and sedimentation changed with climate?

We first address the influence that climate has had in the Nordic Seas on ice sheet and sedimentation histories in reference to the variables outlined in Section 6.1 and in Figs. 6.1 and 6.2. Two key questions have to be addressed. First, do cooler climates result in increased glacial sediment delivery to the continental margin? Second, has the transition between the 41 and 100 kyr climate cycles enhanced glacial delivery of sediment?

If the history of ice sheets and sedimentation around the Nordic Seas is considered as a whole then no clear relationship exists between climate and glacial delivery of sediment. For example, a fundamental contrast exists between the East Greenland and southern Norwegian margins. The delivery of sediment by the Greenland Ice Sheet appears to increase as climate cools until the adoption of the 100 kyr climate cycles at which point it decreases (Table 6.1). In contrast, glacial sedimentation dramatically increases on the southern Norwegian Margin as climate cools and the

100 kyr climatic cycles are adopted (Table 6.4). It is therefore prudent to instead consider the evolution of ice sheet sediment delivery on individual margins of the Nordic Seas related to their climatic setting.

The Nordic Seas margins can be considered to exist within a climatic range. The southern Norwegian section of the margin is the warmest and wettest (Patton et al., 2016). Both the temperature and volume of precipitation are believed to reduce with increasing latitude along this margin; Svalbard therefore having the coolest and driest climate (Patton et al., 2016). The Greenland Margin is the coolest of the margins (Fig. 6.1). For each of these margins the climatic deterioration seen during the Quaternary therefore represents a shift towards a cooler climate (Fronval and Jansen, 1996; Thiede et al., 1998; Jansen et al., 2000). Assuming that this is correct, it therefore appears that a threshold exists, at which point continued cooling of the climate serves to reduce the efficiency of ice sheet sedimentation. This threshold is likely controlled by the comparative areas of cold-based ice and the extent and area of fast flowing ice streams. The sedimentation history offshore Svalbard most clearly illustrates such a relationship (Table 6.3). As climate deteriorated from 2.8 Ma to 1.0 Ma, ice sheet driven sedimentation through glacimarine processes and glacigenic debris-flow emplacement on the continental shelf increased. However, since 1.0 Ma the rate of sedimentation and the thickness of glacigenic debris-flow deposits has decreased (Sættem et al., 1994; Solheim et al., 1998; Knies et al., 2009). Despite the extent and drainage area of the ice sheet being similar it therefore appears that the efficiency of glacial sedimentation decreased following a cooling of the climate and adoption of the 100 kyr climate cycles. Further support for this suggestion is found on the Norwegian Margin where the location of maximum volume of deposited sediment has progressively moved southwards as climate has cooled (Fig. 6.13; Rise et al., 2005).

Analysis of the history of sedimentation offshore Antarctica (Section 6.3.1) supports the idea of a sedimentation tipping point. Since the inception of the Antarctic Ice Sheet, ice sheet related sedimentation has occurred on the continental margin (Kuvaas and Kristoffersen, 1991). Dating of

sediment packages beyond the continental shelf has, however, shown the volume of sediment transported to have decreased in line with cooling climates. For example, sedimentation on the Prydz Bay Trough-Mouth Fan from the Late Miocene to 1.1 Ma was dominated by glacigenic debris-flows (Passchier et al., 2003). As climate continued to cool, the temperature of the East Antarctic interior and precipitation received there were reduced. This led to a hypothesised reduction in the area of fast flowing warm-based ice (Passchier et al., 2003; O'Brien et al., 2004). The reduced sediment transport manifest itself in reduced numbers and thickness of glacigenic debris-flow deposits; emplacement of these deposits eventually ceasing after 0.78 Ma with the adoption of 100 kyr climate cycles.

6.4.2   Trough-mouth fans

The largest sedimentary features on glaciated margins are trough-mouth fans which are of comparable size to deep-sea fans formed offshore the World's largest rivers. They form preferentially in front of cross-shelf troughs as a consequence of fast-flowing ice streams delivering large volumes of sediment to the shelf edge over repeated glacial cycles (Ó Cofaigh et al., 2003; Dowdeswell et al., 2010). The classical trough-mouth fan model was developed from observations in the Nordic Seas (Laberg and Vorren, 1995; Dowdeswell et al., 1996; Vorren and Laberg, 1997). This model was developed by Ó Cofaigh et al. (2003) and recognised the importance of slope setting and hypothetical cases of low sedimentation. Here, we attempt to improve the model of trough-mouth fan processes using the observations outlined in previous sections.

6.4.2.1   Characterisation of trough-mouth fans

Our analysis of trough-mouth fans around the Nordic Seas and on other continental margins identifies four variants of trough-mouth fan depending on the dominant sediment/meltwater environment present in each location (Fig. 6.22). Type 1 trough-mouth fans are dominated almost entirely by glacigenic debris-flow emplacement. During full-glacial conditions, the rate of sediment delivery to the shelf edge is sufficient to trigger multiple glacigenic debris-flows which

dominate the upper slope (Vorren and Laberg, 1997; Laberg and Dowdeswell, 2016). Sufficient

numbers of flows can occur, that they form an apron radiating out from the top of the fan to the

mid/lower slope (Fig. 6.22; King et al., 1998; Taylor et al., 2002a). The lower slope is dominated by

interbedded hemipelagic sediments and distal debris-flow muds and turbidites from the

downslope evolution of glacigenic debris-flows (Laberg and Vorren, 1995). The volume and rate of

sediment delivery to type 1 trough-mouth fans by ice streams is sufficiently large to dampen any

influence that meltwater sedimentation may have on trough-mouth fan evolution.
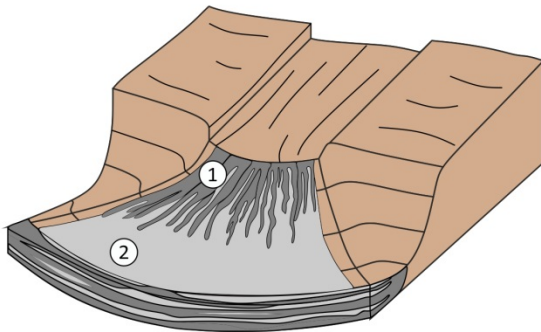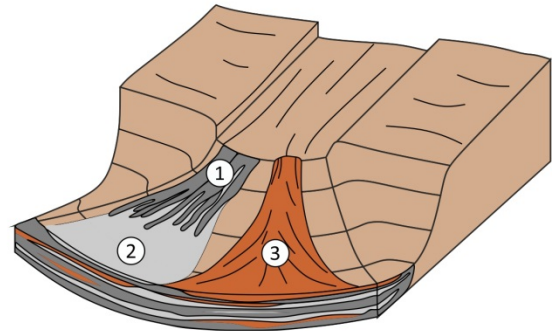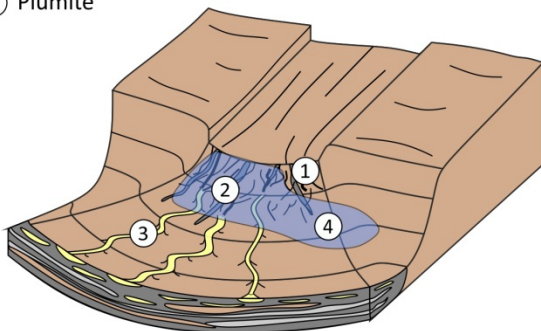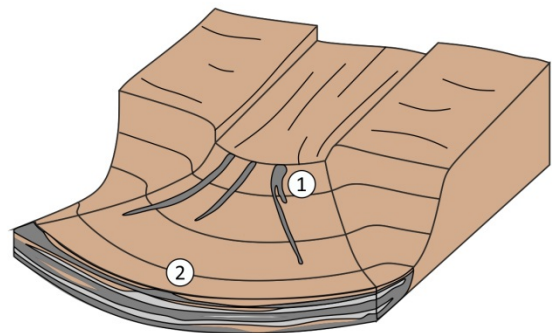
Figure 6.22 Schematic model of trough-mouth fan classification from analysis of glaciated continental margins in this study.

Type 2 trough-mouth fans are dominated by a range of submarine mass movement processes

(Fig. 6.22). As on type 1 trough-mouth fans, these fans are dominated by the emplacement of

glacigenic debris-flow deposits. Where these fans differ to type 1 fans is that the rate of

sedimentation and the emplacement of the debris-flow apron leads to further instabilities within the trough-mouth fan. These instabilities can culminate in submarine slumping and large submarine landslides. Although other processes may play a role in the evolution of these trough-mouth fans (e.g. gully formation or contourite deposition), their sedimentary architecture is dominated by different types of submarine mass movement deposit.

Type 3 trough-mouth fans are characterised by medium rates of sediment delivery but meltwater processes also have a greater influence (Fig. 6.22). As was the case for type 1 and type 2 trough-mouth fans, a significant volume of a type 3 trough-mouth fan may still be made up of glacigenic-debris flow deposits which are emplaced when ice is at the shelf edge. However, the number and volume of these deposits is limited compared to type 1 and type 2 trough-mouth fans. Instead the defining characteristic of these fans is the presence of gullies, channel systems and plumite deposits. Gully incision in the upper slope has been hypothesised as a consequence of sediment-laden subglacial meltwater flow (Lowe and Anderson, 2002; Noormets et al., 2009; Bellec et al., 2016). Alternatively they may by the result of dense water formation related to sea ice production on the shelf which subsequently cascades down the face of the trough-mouth fan. Although relatively rare, in some settings, e.g. Laurentian, Northeast and Crary Trough-Mouth Fans, channel-levee complexes have also been observed (Aksu and Piper, 1987; Piper, 1988; Kuvaas and Kristoffersen, 1991). It is interesting to note the contrasting latitudes where these trough-mouth fans are found; the channel-levee systems perhaps being initiated by different processes. Channel formation is thought to be characteristic of warm-based ice at the shelf edge delivering large amounts of meltwater and sediment. Where sufficient meltwater and sediment is present, turbidity currents and hyperpycnal flows are able to produce channel systems (Aksu and Piper, 1987; Piper and Normark, 2009). It has also been speculated that some of these systems may be associated with catastrophic meltwater discharge; in some cases from subglacial lake drainage. Plumites meanwhile are deposited as a consequence of sediment-laden meltwater plumes (Lucchi et al., 2013). The extent and influence of these processes may, however, be controlled by the rate of retreat of the ice stream from the trough-mouth fan during deglaciation.

Type 4 trough-mouth fans are characterised by low rates of sedimentation (Fig. 6.22). Scoresby Sund and Prydz Bay Trough-Mouth Fan represent type 4 trough-mouth fans. These fans are comparatively sediment starved, even during full-glacials. This reflects a number of factors, either individually or in combination. It can be a consequence of ice delivering little sediment to the fan due to it rarely extending to the shelf edge or to be being present at the shelf edge for only a limited period of time, or to supplying relatively little sediment. Importantly, meltwater processes associated with ice stream advance and retreat also deliver little sediment to the shelf edge. The lack of sediment delivery means that glacigenic debris-flows are infrequent and do not produce the apron of deposits seen on type 1 and 2 trough-mouth fans (Dowdeswell et al., 1997). It is perhaps unlikely that a trough-mouth fan would form under type 4 conditions alone. These systems therefore probably reflect rates of sediment delivery associated with glacials where different ice sheet regimes existed or where margins have evolved and which no longer favour progradation of the trough-mouth fan.

6.4.2.1.1   Can trough-mouth fan characteristics change?

To understand glaciated continental margin evolution it is important to understand whether trough-mouth fans can switch their type characteristics. Fundamental to this question is whether location, e.g. continental shelf geology and catchment area, or climate/ice sheet characteristics control the type of trough-mouth fan which develops. It is clear from the compilation of sedimentary records from the Nordic Seas that location can play a significant role in the type of trough-mouth fan which develops or whether a trough-mouth fan is able to develop at all (Wellner et al., 2001; Ó Cofaigh et al., 2003). For example, there is a clear contrast between East Greenland Margin and Svalbard/Barents Sea Margin trough-mouth fans as a consequence of ice streams overriding sediments and bedrock with contrasting erodibilities (Solheim et al., 1996; 1998; Ó Cofaigh et al., 2003). The position and flow of ice streams is not, however, static. Analysis of buried mega-scale glacial lineations has shown that ice streams frequently migrate between glaciations (Dowdeswell et al., 2006b; Graham et al., 2009). Flow migration may result in the ice

stream flowing over a substrate with contrasting properties and thus changing the input of sediment to a trough-mouth fan. Flow migration of the Lambert-Amery Ice Stream, from an area of readily erodible sediment to hard bedrock, has been cited as one of the main contributing factors for the initial reduction in sediment transport to the Prydz Bay Trough-Mouth Fan (Passchier et al., 2003; O'Brien et al., 2007).

The compilation of ice sheet and sedimentation histories does, however, suggest that climate and its associated impacts on ice sheet characteristics may have a larger impact on controlling temporal switches between trough-mouth fan types. Climatic deterioration can clearly be seen as a driving factor behind the transition of the Scoresby Sund Trough-Mouth Fan between type 1 and type 4. It is also responsible for the shut-off of sediment supply to the Prydz Bay Trough-Mouth Fan after the adoption of 100 kyr climatic cyclicity. Further evidence can also be found in the changing sedimentation regimes seen on trough-mouth fans on the Svalbard margin (Table 3) and the transition in fan type associated with latitudinal change along the East Canadian Margin. Interestingly, it could also be suggested that the Bear Island Trough-Mouth Fan is transitioning between type characteristics. Between 1.3 and 0.2 Ma the Bear Island Trough-Mouth Fan was dominated by glacigenic debris-flow emplacement and large submarine landslide occurrence (i.e. a type 2 trough-mouth fan). However, since at least 0.2 Ma (a consequence of poor age constraints), there is no evidence of large submarine landslide occurrence on the fan itself (Fig. 6.10). It is therefore possible that the trough-mouth fan has transitioned to type 1, characterised predominantly by glacigenic debris-flow emplacement. A possible explanation for this is the continued subsidence of the Barents Sea continental shelf and deepening of the Bear Island Trough which may have reduced the sediment supply (see Fig. 6.10). It may also have led to a reduction in the volume of glacimarine sediment deposition on the fan as the Bear Island Ice stream became more susceptible to rapid retreat due to its deeper water setting. This may have reduced the volume of contrasting sediment packages on the fan hypothesised to be required for large submarine landslide occurrence (Bryn et al., 2005).

6.4.2.1.2   Do trough-mouth fans have characteristic depositional sequences?

The sedimentary sequence of the Late Weichselian advance and retreat has been described on a number of trough-mouth fans around the Nordic Seas, e.g. Isfjorden (Elverhøi et al., 1995; Dowdeswell and Elverhøi, 2002). However, the setting of and sedimentary processes operating on trough-mouth fans are highly variable. For example, the depositional characteristics vary across and between the Storfjorden and Bear Island Trough-Mouth Fans during the Late Weichselian advance and retreat alone (Laberg and Vorren, 1995; Pedrosa et al., 2011; Lucchi et al., 2013). It is therefore difficult if not problematic to describe a characteristic depositional sequence for a trough-mouth fan type.

6.4.2.2   How can we better understand trough-mouth fans?

Understanding the controls on trough-mouth fan morphologies and processes remains challenging. Fundamentally this stems from there being very few/no observations of sediment transport by ice streams and submarine mass movements on trough-mouth fans and thus estimating sediment accumulation across a single trough-mouth fan during a full glacial period is very difficult. This is the case even when using the sedimentary record; there are very few studies which have been able to produce estimates of sediment accumulation (Laberg and Vorren, 1996; Nygård et al., 2005). Crucially, the precise timing of sediment delivery is usually uncertain in these studies. Fewer studies still have been able to model the delivery of sediment by ice streams to trough-mouth fans (Dowdeswell et al., 1999; Dowdeswell et al., 2010). Future efforts to understand trough-mouth fans should therefore follow two separate lines. First, understanding of ice stream transfer of sediment needs to be improved and how this can be impacted by meltwater drainage system evolution. Achieving this will likely require observations from currently deforming glacier beds and proglacial environments in marine settings (Hart et al., 2011; Dowdeswell et al., 2015). Second, additional high resolution seismic and sedimentary records are needed on trough-mouth fans in order to precisely constrain the timing and volume of sediment delivery by ice streams.

6.4.3   Glaciated continental margins

In addition to the multiple types of trough-mouth fan that have been identified, our records also indicate that there are multiple types of glaciated margins (Fig. 6.23). We recognise three characteristic margin types. The first is characterised by high sediment inputs by ice streams and by the formation of trough-mouth fans (Dowdeswell et al., 1996). Along these margins, ice stream sedimentation is sufficiently high or has been sufficiently high in the past to allow trough-mouth fans to form even when conditions appear unfavourable such as seismically active or steep margins, e.g. the Bering Trough-Mouth Fan formation over the Aleutian Trench (Montelli et al., 2017).

The second margin type is characterised by high sediment inputs but which are insufficient to lead to the formation of trough-mouth fans. Along these margins, large volumes of sediment are delivered by a range of mechanisms. First, ice sheet flow delivers sediment at an enhanced rate compared to rates of interglacial sedimentation (Dowdeswell and Elverhøi, 2002). Second, ice streams may still be present and deliver large volumes of sediment. Third, sediment is delivered by glacial meltwater in addition to glacigenic debris-flows (Lekens et al., 2005; 2006). Fourth, ocean currents may deposit significant contourite deposits. The interbedding of the multiple types of sediment and the contrasting properties of these packages can lead to instabilities within the sediment stack (Baeten et al., 2013; 2014). As a consequence these margin types are often characterised by the occurrence of submarine slumps and landslides. The Storegga region is the type example for this margin type.

The third margin type is characterised by low sediment input (Dowdeswell et al., 1996; Ó Cofaigh et al., 2003). Here, ice may not always reach the shelf edge during full glacials and thus direct delivery of sediment by ice is temporally limited. Alternatively, where ice regularly reaches the shelf edge, it may not transport large volumes of sediment. As a consequence the number and extent of glacigenic debris-flows is limited, as is the progradation of glacigenic structures. The development of these features will be further hindered if the continental slope is steep or the

margin is tectonically active. The continental shelf and slope are, thus dominated by glacimarine and marine processes. As a result the dominant sediment transport process which dominates margin characteristics is turbidity currents which often result in the formation of channels.

Margin 1 - Trough-mouth fans

① Glacigenic debris-flows
② Distal debris-flow muds/
   Turbidites
③ Large submarine landslides
④ Plumite
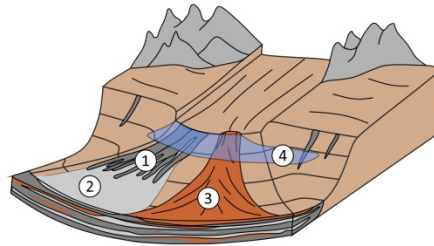
Margin 2 - High sediment/High meltwater input

① Glacigenic debris-flows
② Plumite
③ Submarine landslides
④ Contourite
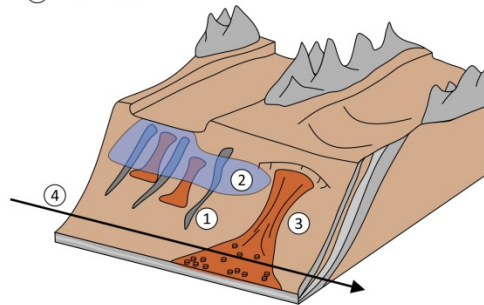
Margin 3 - Low sediment input

① Glacigenic debris-flows
② Turbidity currents
③ Sediment waves
④ Channel-levee system
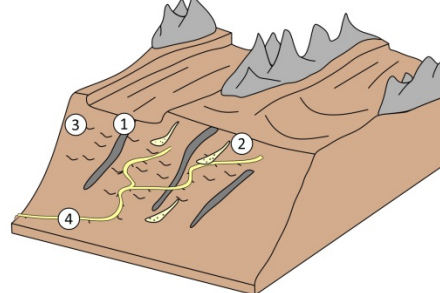
Figure 6.23 Schematic model of glaciated margin classification from analysis of glaciated continental margins in this study.

6.4.4   Submarine landslides

Submarine landslides are considered to be one of the main morphological features of glaciated margins and a common feature on trough-mouth fans. In the following section we will therefore discuss the history of submarine landslides and their connection to ice sheet histories.

6.4.4.1   Distribution of large submarine landslides

The global distribution of known large submarine landslides on glaciated margins is very uneven. Where large submarine landslides have been identified, these locations appear to favour recurrent mass-failures of this scale. In other areas they are extremely rare or have yet to be identified as a consequence of globally uneven data coverage. The frequency of these events in two regions standout; they are especially common on the Norwegian/Barents Sea Margin and the South East Canadian Margin. They are conspicuously absent from several other glaciated margins. The following section will discuss the likely causes of this distribution.

6.4.4.1.1   Sediment supply

Sediment supply appears to be crucial for submarine landslide occurrence on glaciated margins. Previous models based on the Storegga Slide suggested that ice stream driven rapid sedimentation could generate overpressure or increased pore pressures (Bryn et al., 2003; Haflidason et al., 2003). Indeed sedimentary evidence from this part of the Norwegian Margin suggests that sedimentation rates were as high as 1750 cm/ka during deglaciation (Lekens et al., 2005; 2009). However, slope failure was not caused by the rate of sedimentation alone but by the contrasting strength and porosity profiles of soft marine clays and glacigenic sediments (Bryn et al., 2005; Kvalstad et al., 2005). The boundary between the two sediment packages provided the plane along which slope failure occurred. Geotechnical investigations of other sections of the Norwegian Margin where submarine landslides are common has revealed similar site characteristics. In the Trænadjupet region, the contrast is provided by glacigenic sediments, and coutouritic and marine clays (Laberg et al., 2003; Baeten et al., 2014). The south east Canadian Margin also experiences similarly rapid sedimentation (4 m/ka) from meltwater plumes (Mosher

et al., 1989; Piper and Ingram, 2003). We therefore suggest that the Bryn et al. (2005) model for large submarine landslide occurrence of rapid ice sheet controlled sedimentation combined with the presence of pre-existing 'weak' layers is applicable to other glaciated continental margins (Fig. 6.24).
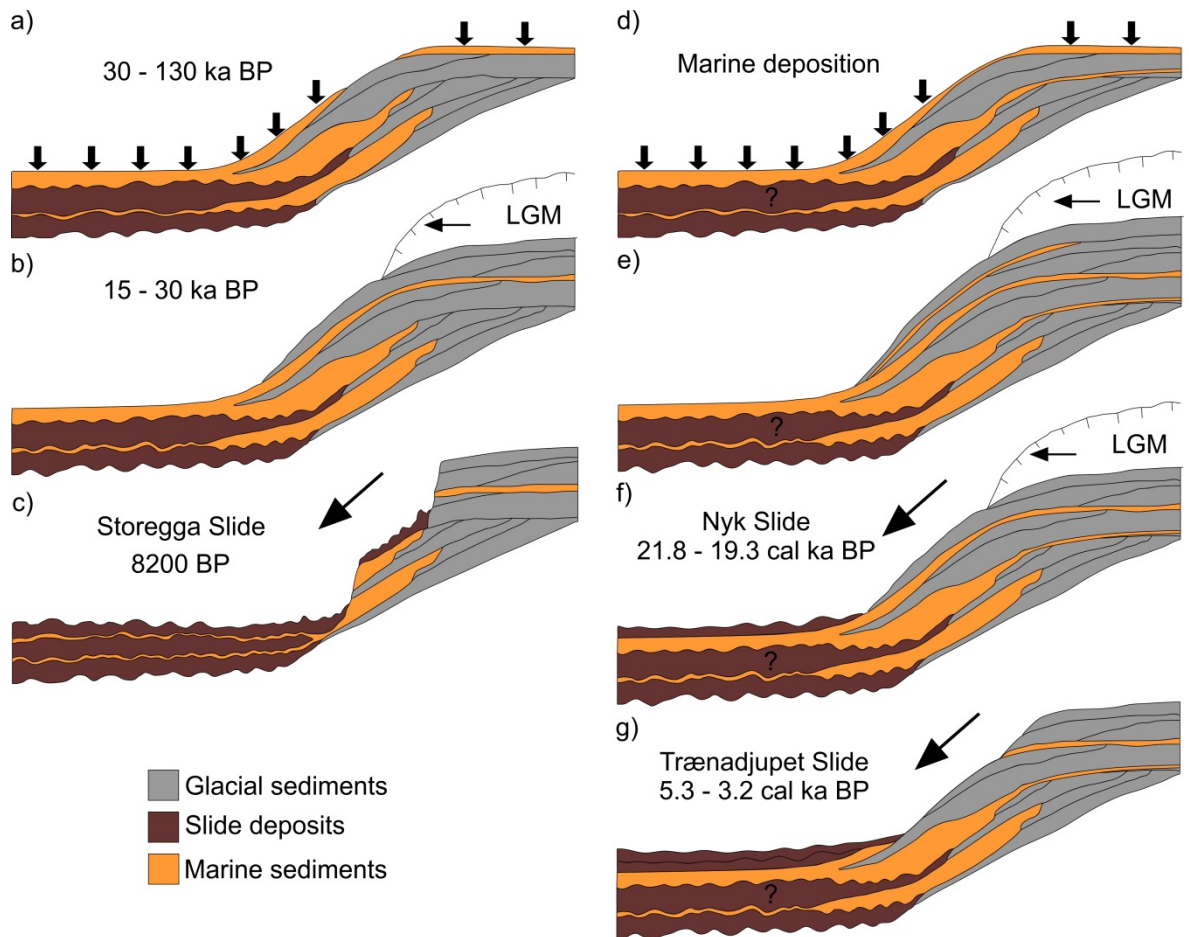
Figure 6.24 Illustration of the proposed depositional and slide processes that occur in the Storegga Slide (a – c) and the Trænadjupet Slide (d – g) areas. a) Deposition of soft marine clays during the last interglacial. b) Ice at the shelf edge during the Last Glacial Maximum and the deposition of glacial sediments. c) The Storegga Slide. Two older slides scars are filled with marine clays below the Storegga Slide scar. Adapted from Bryn et al. (2005). d) Deposition of soft marine clays and contouritic sediments. e) Ice at the shelf edge and the deposition of glacial sediments. f) Nyk Slide occurs altering the properties of the sediment package on the continental slope. g) The Trænadupet Slide.

6.4.4.1.2   Passive vs. active margins

Earthquakes are often cited as the triggering mechanism for submarine mass movements (Stigall and Dugan, 2010; Masson et al., 2011). Indeed, the Grand Banks submarine landslide is evidence that large earthquakes can trigger large submarine landslides on glaciated margins (Piper et al., 1999). However, as has been identified on non-glaciated margins there is a significant contrast between submarine landslide occurrence on passive and active margins. The multiple large submarine landslides on the south east Canadian and Norwegian margins are thought to have been triggered by earthquakes related to isostatic adjustment following ice sheet retreat (Piper and Ingram, 2003; Bryn et al., 2005; Piper, 2005; Allin et al., in review). The passive nature of both of these margins means that sediments deposited by the ice sheets were rarely subject to seismic shaking. Sufficient sediment was therefore able to accumulate in both regions before failure was triggered by the increased seismicity associated with deglaciation. In contrast, no large submarine landslides have been identified on the South Alaskan Margin during the Quaternary (Gulick, *pers comms*). Here, ice sheet deposited sediments are exposed to repeated strong ground-shaking. Subduction zone shaking has been shown to lead to enhanced consolidation and strengthening of seafloor sediment (Sultan et al., 2004; Völker et al., 2011; Pope et al., 2017). This, combined with the triggering of smaller scale submarine mass movements removing weaker sediments, likely prevents large submarine landslides occurring on these active margins.

6.4.4.1.3   A consolidated model of submarine landslides on glaciated margins?

The Bryn et al. (2005) model of large submarine landslide occurrence was used in geohazard assessment for the development of the Ormen Lange gas field (Solheim et al., 2005b) and has since been used to inform tsunami hazard assessment on the margins of the Nordic Seas (e.g. Tsunami risk and strategies for the European region Project). Hazard assessment for submarine landslides requires the likely triggering mechanism, failure dynamics and frequency of events to be identified (Talling et al., 2014; Pope et al., 2015). However, our increasing understanding of

landslides along the Norwegian Margin has shown significant differences between landslides on different parts of the margin.

In terms of frequency, the Bryn et al. (2005) model suggests that each submarine landslide requires a separate ice stream advance to the shelf edge; each advance delivering sediment to fill the slide scar from the previous event and recharge the slope for failure (Fig. 6.24). However, dating of other landslides along this margin shows that landslide recurrence does not correlate simply with each ice advance. The Nyk and Trænadjupet Slides were separated by 14 ka (Allin et al., in review). A short lived glacial advance occurred between the two events but it did not reach the shelf edge nor did it result in a large increase in sedimentation (Fig. 6.25; Olsen et al., 2001b). Even in the Storegga area the recurrence rate for the three submarine landslides that occurred here (Storegga, R and S) was 200 kyr representing multiple ice stream advances to the shelf edge (Hjelstuen et al., 2005; Watts et al., 2016).
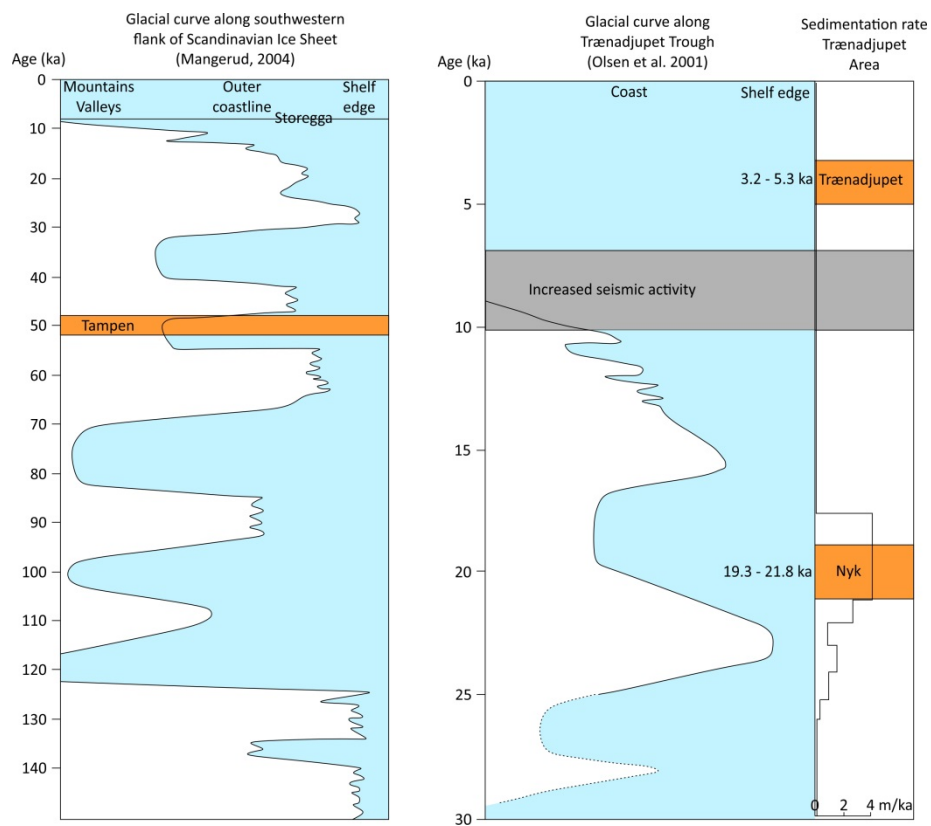
Figure 6.25 Timing of large submarine landslides in the Norwegian Basin and the Trænadjupet area relative to local ice sheet activity. Sedimentation rate beyond the Trænadjupet Trough and local seismicity are also shown (modified from Allin et al., in review).

A contrast between the failure dynamics also exists. Analysis of the Storegga Slide deposits has led to the interpretation that the slide was a retrogressive failure during which the slide mass disintegrated forming a large turbidite (Haflidason et al., 2004; Bondevik et al., 2005; Masson et al., 2006). In contrast, detailed analysis of the Trænadjupet Slide has led to the hypothesis that the Trænadjupet Slide occurred top-down due to the presence of three progressively deeper headwalls and that the slide mass largely failed to disintegrate as shown by the presence of large block fields (Laberg et al., 2002b; Allin et al., in review). Progressive subaerial landslides have been recognised in a number of locations, notably Norway and Quebec (Locat et al., 2008; Quinn et al., 2012). These landslides are generally a consequence of strain induced loss of structure in clays resulting in slope failure (Urciuoli et al., 2007). In the submarine environment, top-down slope failure would likely have been initiated as a consequence of pore pressure build-up along a 'weak' layer. This is likely to have been a contouritic deposit in the Trænadjupet case (Sultan et al., 2004; Baeten et al., 2014). Failure of the initial sediment package and its downslope progression resulted in the subsequent failure of deeper 'weak' layers due to shearing or rapid increases in overburden pressure. It is possible that the occurrence of the Nyk Slide played a significant role in the triggering of the Trænadjupet Slide either through unloading of the seafloor or as a consequence of deformation of seafloor sediments due to overriding slide material (Fig. 6.24). The different failure dynamics means that the tsunamigenic potential of landslides from the two regions is probably different (Løvholt et al., 2005; 2016).

Despite the clear similarities identified in terms of preconditioning and triggering mechanisms in the Storegga and Trænadjupet regions (see Section 6.4.3.1.1.) clear differences exist which are important for understanding landslide processes on glaciated margins. This suggests that one model of landslide occurrence may not be appropriate. Further work is therefore needed in order to understand whether the close temporal association of the Nyk and Trænadjupet Slides is unique or whether this can be a common feature on these margins.

6.5   Conclusions

Our understanding of glaciated continental margin processes and evolution has come predominantly from studies of the Nordic Seas during the last glacial period. Using a combination of geophysical and sedimentological records, these studies have produced conceptual models for processes associated with different morphological features, continental slope architecture and the primary drivers (e.g. climate) behind these observations. Here, we have reviewed the current understanding of ice sheet growth and decay around the Nordic Seas and how this is related to the history of sedimentation and margin architecture. These histories have then been compared with other glaciated margins in order to identify unified models of glaciated continental margin evolution. This contribution achieves the following:

1) A comprehensive record of Greenland, Barents Sea and Scandinavian Ice Sheet growth and decay on the margins of the Nordic Seas over the last 2.58 Ma is provided.

2) The record of sedimentation and submarine mass movements which have occurred as a consequence of the growth and decay of the reconstructed ice sheets has been compiled.

3) However, the completeness of ice sheet growth and decay records and the record of sedimentary processes is shown to be temporally and spatially highly variable.

4) From the records of ice sheet growth and decay and the associated sedimentation, we have been able to review the first order controls on sediment delivery to the continental margin at the scale of an ice sheet.

5) We have identified a new conceptual model of trough-mouth fans and glaciated margins worldwide according to the driving factors behind their associated sedimentary processes.

6) We have provided a review of the relationship between ice sheets and large submarine landslides on glaciated margins. We have tested previous models of submarine landslide occurrence on glaciated margins using this information and hence proposed an additional model to explain some large submarine landslides.

Chapter 7:   Summary and future work

7.1   Overview

This thesis explores the frequency and triggering mechanisms of submarine mass movements around the world and addresses their geohazard implications and their possible relationship with climate change. To achieve this a variety of different methods and data types were used.

7.2   Responses to initial questions posed in this thesis

The following section outlines the responses to the overarching questions raised in **Chapter 1**.

1)   **Are large submarine landslides temporally random or do uncertainties in available age constraints make it impossible to tell?**

First, this thesis focussed on large submarine landslide occurrence. Previous work had concluded that these $>\sim 1$ km^3 submarine landslides were temporally random (Urlaub et al., 2013). This conclusion was made on the basis of the most complete compilation of submarine landslide ages (41 events) in the last 30 ka. It was, however, unclear from this study whether the landslides were indeed temporally random or whether considerable uncertainties on most landslide ages made it impossible to tell. To address this question multiple artificially generated datasets of landslide ages with known distributions were tested using the same statistical methodologies used in the Urlaub et al. (2013) study.

The primary conclusion of this chapter was that there are currently too few, sufficiently well-dated large submarine landslides to know whether these large landslides are indeed temporally random. Second, it demonstrated that the use of global datasets, i.e. the combination of landslide ages from multiple settings around the world, would likely appear random to statistical tests. This is a result of environmental settings having different preconditioning and triggering factors as no single environmental variable is likely to be globally consistent. Global environmental variables, such as sea level, will also likely be offset in time at different locations. Third, the number of submarine landslides that would be needed to test whether there is a significant correlation between landslide frequency and global sea level was calculated. Using simulated landslide ages that correlated perfectly with sea level, the number of landslides needed to test for a significant correlation with sea level ranged from 10 to 53. The mean was 38, even with no age uncertainties. The number of well dated landslides within the current global catalogue of large landslides is much lower.

Using artificial datasets this study has indicated many of the issues inherent with using a global record of submarine landslides in its current form. The results indicated that both age uncertainties associated with most of the large submarine landslides and the combination of data from multiple settings makes it hard to test for links between a single global environmental factor and event triggering. Ultimately, this study suggests that it may indeed be highly unlikely that a global database of landslide ages could be used to identify a triggering/preconditioning mechanism. As a result, the chapter provides some suggestions for a best future strategy to test for links between environmental factors and landslide frequency. The best future strategy identified is the use of landslide frequency records from local studies, with numerous recurrence intervals, in conjunction with detailed records of local environmental change. By carrying out analysis of local records, the impact of uncertainties are minimised as the relationship/order of events is clear as is the local variability of any given factor such as sea level. This method provides the basis for the study that was carried out on the Bear Island Trough-Mouth Fan in **Chapter 5**.

2)   Which earthquakes trigger damaging submarine mass movements?

Having identified the possible pitfalls associated with statistical analysis of global records of submarine landslides, the next chapter focussed on a form of indirect monitoring to investigate the triggering of submarine mass movements. Using a global dataset of subsea fibre-optic cable breaks from 1989 to 2015, **Chapter 3** focussed on the triggering of submarine mass movements by earthquakes. It focussed on two main questions. First, which magnitude earthquakes do (and do not) trigger submarine mass movements that break cables and does this vary on a regional basis? Second, for turbidite palaeoseismology (the use of turbidite deposits along specific margins (Adams, 1990; Gràcia et al., 2013) to reconstruct large earthquake histories to be applied appropriately, do other parameters such as local sediment supply need to be assessed as part of turbidite palaeoseismology rather than just ground shaking? However, it did provide the first chance to identify earthquake triggering and non-triggering of submarine mass movements worldwide.

The primary conclusion of this chapter was that there is no obvious earthquake magnitude, which will consistently trigger a submarine mass flow. The only possible exception is that all M_w 9.0 earthquakes trigger mass flows. However, the small number of observations (N = 2) is too small to make a robust conclusion. Second, the relationship between earthquake magnitude and the trigger of a submarine mass movement which breaks a cable varies on a regional basis. In some regions (e.g. Taiwan) small earthquakes (M_w 3.0 to 5.0) can trigger sediment flows whilst in others (e.g. Japan) only large earthquakes ($\geq M_w$ 7.0) can trigger sediment flows. The different response to earthquake magnitudes is a response to regional sediment supply, submarine topography,

seismic regimes and their temporal variability. Thus, in order for turbidite palaeoseismology to be robust for specific regions, local sediment supply and slope response to earthquake shaking therefore needs to be quantified. Last, not all earthquakes above a certain magnitude generate powerful (cable breaking) submarine mass movements. Globally, during the study period, only 15 of 56 (27%) earthquakes above M_w 7.0 produced submarine mass movements that broke cables.

Access to the cable break database has been shown to be extremely valuale for identifying which earthquakes did, and did not trigger submarine mass movements. However, it is important to acknowledge a number of issues inherent within the cable break analysis of mass flow occurrence. First, the distribution and age of cables (older cables being more susceptible to damage) throughout the World's oceans is uneven. Uneven cable coverage means the likelihood of a flow being detected varies between different regions. Comparison of flow triggering using the cable break database in different regions must therefore acknowledge the uncertainty created by variable detection probabilities. Second, even where cables are present, not every submarine mass movement may be detected. This is a consequence of flows needing to impart sufficient force to cause a cable break. The required force to achieve this varies according to flow type, cable type (i.e. armoured vs. Nor armoured), cable age, orientation to the mass flow, the amount of slack or whether the flow buries a cable rather than breaks it. Even where flows have been sufficiently powerful to break a cable, it has been shown that it may not break all adjacent cables (e.g. Gavey et al., 2017). Thus where only a single cable crosses the flow path, the likelihood of detection is severely reduced. Third, no fully comprehensive universal cable break database exists. The database presented here is a compilation of breaks repaired by Global Marine Systems Ltd and collaborators. There may be breaks and cables that are unreported. However, despite these caveats, the cable break database has provided the first chance to identify which earthquakes did and did not trigger submarine mass movements worldwide.

3) How do tropical cyclones trigger damaging sediment density flows?

Having used subsea fibre-optic cable breaks to test the links between earthquake occurrence, magnitude and the generation of submarine mass movements, **Chapter 4** focusses on using the same database of cable breaks to investigate tropical cyclone triggering of submarine mass movements. This chapter focussed on three main questions. First, how important are tropical cyclones for triggering submarine mass movements which break subsea cables? Second, can the mechanisms by which tropical cyclones trigger submarine mass movements be identified from the cable break data? Third, is the frequency of tropical cyclone related submarine mass movements likely to change due to projected climate change?

The primary conclusion of this chapter was that tropical cyclones trigger submarine mass movements which break cables in almost all areas of the world where they are found from depths of 20 m to over 6200 m. Even in areas where cable breaks were not observed (the Bay of Bengal and the Arabian Sea) this was likely a consequence of the sparse cable network in these areas. However, in comparison to earthquake triggered submarine mass movements which break cables, the absolute number of submarine mass movements related to tropical cyclones was significantly lower. Individual earthquakes triggered at least 57 submarine mass movements compared to tropical cyclones triggering at least 22 submarine mass movements. In both cases flows were particularly prevalent around South East Asia.

Second, three sets of triggering mechanisms related to tropical cyclones were identified from the cable break data. Tropical cyclones can initially trigger submarine mass movements through dynamic loading of the seabed due to storm surge, storm and internal wave processes. Submarine mass movements triggered by dynamic loading are rare compared to those triggered by other mechanisms. Mass movements are more commonly triggered by as a consequence of flood discharges from rivers, through the formation of hyperpycnal flows, and as a consequence of delayed failure of recently deposited large volumes of sediments.

Last, it is yet unclear whether the global frequency of submarine mass movements triggered by tropical cyclones is likely to change. This uncertainty is driven primarily by two factors. First, increases to the number and density of subsea cables makes identification of any trends in the number and location of cable breaks difficult to identify. Second, global trends in tropical cyclone activity are uncertain. However, it is likely that the number of sediment density flows in South East Asia, and in particular offshore Taiwan are likely to increase.

4) Can we identify the frequency and triggering mechanisms of glacigenic debris-flows?

Having investigated specific triggering processes for submarine mass movement initiation in **Chapters 3** and **4**, **Chapter 5** focussed on the triggering of a specific type of submarine mass movement. Here, methodologies identified as the best means for understanding the triggering processes from deposits identified in **Chapter 2**, were applied to deposits from glacigenic debris-flows in a series of piston cores. These cores were located on the distal northern end of the Bear Island Trough-Mouth Fan. The main aims of this chapter were; first, can multiple glacigenic debris-flows on the Bear Island Trough-Mouth Fan be dated? Second, how is glacigenic debris-flow occurrence related to ice sheet processes?

59 glacigenuc debris-flow muds were dated in a single piston core on the distal northern end of the Bear Island Trough-Mouth Fan using a combination of radiocarbon dating, coccolithophore

biostratigraphy and µXRF geochemistry. This study therefore represents the first to date multiple glacigenic debris-flows on the Bear Island Trough-Mouth Fan. These deposits were interpreted as corresponding to glacigenic debris-flows further upslope on the fan. This interpretation was made on the basis of similar geochemical compositions, average grain-sizes and sediment colour. Both the large debris-flow deposits and thin distal debris-flow muds also have low magnetic susceptibility records implying that they were flow deposits. Stratigraphically the glacigenic debris-flow visible in core PE75 and the shallow seismic data corresponded to thin mud layers in nearby cores.

Statistical analysis of the recurrence intervals for flow deposit emplacement shows that the flows were statistically clustered in time and thus likely have a common trigger. The temporal clustering of these flows and the coincidental dates for the youngest set of flows with the known maximum extent of the Barents Sea Ice Sheet during the Late Weichselian shows that debris-flow occurrence is a consequence of ice being present at the continental shelf edge. Despite this, a precise triggering mechanism for these flows cannot be identified and thus we are only able to suggest possible triggers. The glacigenic debris-flows may have been triggered as a consequence of; (1) earthquakes relating to isostatic adjustment; (2) the build-up of excess pore pressures due to high rates of sediment deposition; (3) oversteepening; or (4) small ice-front oscillations. However, despite not being able to identify a precise trigger, the record of glacigenic debris-flows on the Bear Island Trough-Mouth Fan in the presented cores suggests that these deposits can be used to reconstruct the history of the Bear Island Ice Stream in the Bear Island Trough.

Analysis of the glacigenic debris-flow deposits also identified two significant variations in ice sheet processes. First, the number and thickness of the older deposit cluster was significantly different to those from younger sets of deposits. If the number and thickness of deposits is representative of the volume of sediment advected to the shelf edge by the Bear Island Ice Stream, then the duration or rate of sediment delivery was far greater during the Saalian than the Weichselian glacial interval. This could be a consequence of the Saalian ice sheet thickness being greater than that of the Weichselian ice sheet leading to higher ice sheet velocities and a more stable ice-front position at the shelf edge. If the number of deposits relates to a specific triggering mechanism, i.e. small ice-front oscillations or earthquakes, then the number of oscillations/earthquakes during the Saalian was also greater than any of the advances during the Weichselian. However, in both scenarios the frequency of glacigenic debris-flow triggering is much greater than the total number of advances. Second, the geochemical composition of debris-flows in the oldest advance was different to younger deposits. From this, it is inferred that the sediment making up the debris-flows was sourced from a different region during the Saalian advance. As a result we suggest that the configuration of the Barents Sea Ice Sheet changed between the glacial cycles.

5) **What is the relationship between ice sheets and submarine mass movement occurrence?**

Whilst **Chapters 3** and **4** analysed the role that specific phenomena have played in triggering submarine mass movements capable of breaking submarine cables over the last 25 years and **Chapter 5** analysed glacigenic debris-flow recurrence, **Chapter 6** focussed on the general relationship between ice sheets and submarine mass movements. First, the chapter aimed to use published data to reconstruct ice sheet and sedimentation histories around the Nordic Seas during the Quaternary. Second, it aimed to use these reconstructions to analyse how changes in climate may impact upon the relationship between ice sheet growth and the occurrence of different types of submarine mass movement. Last, it aimed to test previously published conceptual models of glaciated margin processes and evolution, and submarine landslide occurrence against the present understanding of these margins.

The reconstructions presented in **Chapter 6** using geophysical and sedimentological data from around the Nordic Seas showed the completeness of records and understanding of ice sheet histories to be highly variable. Records of the Greenland, Barents Sea and Scandinavian Ice Sheets were most complete for the most recent glacial and became poorer towards the start of the Quaternary. Comparison of the records related to the different ice sheets also showed that the records of the Greenland Ice Sheet and its related sedimentation were the least comprehensive while those of the Scandinavian Ice Sheet were the most comprehensive.

Changes to climate and climate cyclicity were shown to have significant impacts on ice sheet and sedimentation histories around the Nordic Seas. By combining observations from around the Nordic Seas with others from different glaciated continental margins, it was suggested that a climatic threshold exists beyond which the efficiency of ice sheet driven sedimentation is reduced. The threshold is likely controlled by the comparative areas of cold-based ice and the extent and area of warm-based fast-flowing ice streams. It may also be a consequence of the removal of more easily erodible substrate by earlier glaciations. Reductions in the volume of sediment transport was shown to limit the number and thickness of submarine mass movement events such as glaicgenic debris-flows.

Using published records from around the Nordic Seas improvements to models for trough-mouth fan and glaciated margin processes were proposed in **Chapter 6**. 4 types of trough-mouth fan were identified, corresponding to the dominant sediment/meltwater environment present at each locations. Those dominated by high rates of ice sheet sediment delivery were characterised by turbidity current, glacigenic debris-flow and submarine landslide occurrence. Where sedimentation rates were lower but large volumes of meltwater were supplied, trough-mouth

fans were dominated by glacigenic debris-flows, turbidity currents, plumites and the presence of channel-levee systems. Other trough-mouth fans which were sediment starved were characterised by infrequent and small glacigenic debris-flows.

Building on the model of glaciated continental margins by Dowdeswell et al. (1996), 3 types of glaciated margin were identified with the most common types of submarine mass movement. Margin type 1 was defined by the presence of trough-mouth fans and was thus associated with glacigenic debris-flows etc. Second, margins on which ice sheet delivered large volumes and sediment and maltwater but trough-mouth fans failed to develop. Along these margins, glacigenic debris-flows, submarine landslides and plumites were also common. Last, margins where ice sheets delivered small volumes of sediment. Here, glacigenci debris-flows occur but are less common and volumetrically large. Instead, these margins are dominated by turbidity currents and the resulting sediment wave fields and channel systems.

Last, **Chapter 6** provided a review of previous models of large submarine landslide occurrence on glaciated margins. The distribution of these submarine mass movements was shown to be highly uneven. It was suggested that this was a consequence of a combination of the need for sufficiently high rates of ice sheet driven sedimentation, the presence of 'weak' layers (contoritic or plumite deposits) and low average seismicity. Analysis of the frequency of large submarine landslides also showed that the rate of recurrence on different sections of the margin (e.g. Storegga vs. Trænadjupet) is highly variable with apparent differences in the timing between high sedimentation and the eventual triggering of the landslide. Landslides were also shown to disintergrate along some sections of glaciated margins whilst remaining as large blocks on others. In both cases, further work is needed to understand the triggering mechanism and slide dynamics of these large slides.

7.3   Future research

The following section poses some future research questions and outlines proposed directions which can improve our understanding of submarine mass movement frequency and the geohazards they represent. The questions asked are:

1) *Will short-term climate change impact upon the hazard posed to seafloor infrastructure by submarine mass movements?*

2) *Can the record of submarine mass movements be used to better constrain the history of ice sheets?*

7.3.1   Will short-term climate change impact upon the hazard posed to seafloor infrastructure by submarine mass movements?

Long-term cyclic changes to climate over thousands of years related to glacial-interglacial cycles are thought to impart a strong control on submarine mass movement recurrence (Bryn et al., 2003; Bryn et al., 2005; Covault et al., 2007; Covault and Graham, 2010; Tappin, 2010). However, of more immediate concern for seafloor infrastructure and surrounding coastal communities is whether forecast global warming will have a significant impact on the frequency and magnitude of submarine mass movements (Stocker, 2014).

7.3.1.1   The basic problem

As outlined in **Chapter 2** it may not be possible to discern whether short-term rapid climate change impacts upon the frequency of submarine mass movements from the geological record alone. This is a consequence of the poor temporal resolution of geological records (Urlaub et al., 2013; Pope et al., 2015), signal shredding and the interaction of multiple factors (Jerolmack and Paola, 2010; Pope et al., 2015; Allin et al., 2016; Romans et al., 2016) preventing the identification of precise causes for changes to mass movement frequency. It may, however, be possible to use a combination of direct monitoring of the seafloor, river catchments, damage to infrastructure, meteorological observations and future climate predictions to investigate how global warming may contribute to submarine mass movement frequency.

7.3.1.2   Possible climatic controls on the frequency of submarine mass movements over short-time scales

7.3.1.2.1   Seasonal temperature variations

Seasonal temperature changes in mountainous and higher latitude regions often exhibit a strong control on submarine mass movement occurrence. This control is a result of enhanced river discharges resulting from snow and glacier melt associated with higher spring and summer temperatures (Woo and McCann, 1994; Forbes and Lamoureux, 2005). The increased river discharges can influence the frequency of submarine mass movements if these discharges are linked to greater volumes and rates of sediment accumulation in marine systems.

Temperature changes may affect these systems in a number of ways. First, unseasonably warm weather may lead to an early onset of melting. Early periods of melting can lead to reduced storage of water within the overall system and as a consequence the peak river discharge and thus sediment delivery may be reduced (see Fig. 7.1; Hughes Clarke et al., 2014; Clare et al., 2016). Second, increased temperatures can lead to unseasonal occurrences of rainfall and thus enhanced runoff during winter months. Pulses of rainfall related discharge may result in enhanced sediment transport during the winter, thus possibly reducing the volumes arriving during the spring melt season.
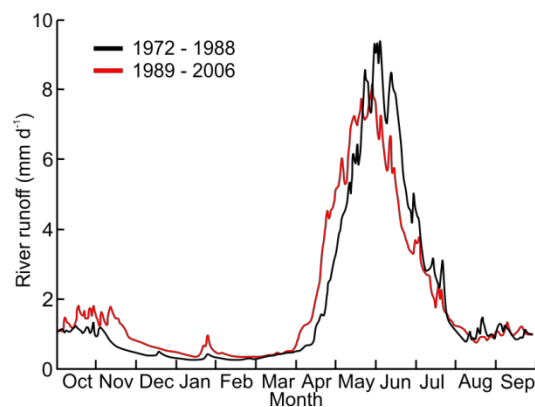
Figure 7.1 Mean annual cycle of daily runoff in the Little Swift River, BC Canada, for 1972 – 1988 and 1989 – 2006 (adapted from Déry et al., 2009). The change in cycles demonstrates the impacts of changing climate regime for snow and glacier melt fed rivers.

In both scenarios temperature changes will lead to alterations in the sedimentary delivery regime to offshore sediment transport systems. Possible consequences include; (1) decreases to the frequency of smaller submarine mass movements as a consequence of reductions to the volume of rapidly deposited sediment; (2) increases to the number of larger less frequent submarine mass movements due to increased sediment storage in pro-river areas due to fewer small volume

flows; (3) an overall decrease in the number of submarine mass movements due to reductions in sediment delivery to pro-river areas.

7.3.1.2.2   Changes to meteorological phenomenon

Where offshore sedimentary systems are less influenced by changes to snow and melt regimes, the largest controls on submarine mass movement frequency will likely result from changes to meteorological phenomena. The possible role which meteorological events can play in the preconditioning and triggering of submarine mass movements have been outlined to a certain extent in **Chapters 3** and **4**. Changes to rainfall intensity, volume, and storm number and track may all impact sediment delivery to a variety of systems.

Sediment systems dominated by surface gravity waves represent the simplest example of how sedimentary systems may be influenced by changes to meteorological phenomena. The size and direction of travel of waves is controlled by the fetch length and strength of surface winds (Bretschneider, 1951). Changes to the number, track and intensity of storms as well as average wind strengths will likely therefore influence wave climates (Mori et al., 2010; Hemer et al., 2013). This will affect sediment transport in these systems.

Where sedimentary systems are not merely dominated by surface waves, changes to storms can have more varied impacts. First, as has been outlined in **Chapters 3** and **4**, intensification of rainfall related to individual storms can lead to enhanced onshore erosion and thus greater volumes of sediment being transported offshore (Kao and Milliman, 2008; Lee et al., 2015). The delivery of sediment-laden river water is then able to trigger submarine mass movements through the occurrence of hyperpycnal flows or as a consequence of rapid deposition of sediment (**see Chapter 4**; Mulder and Moran, 1995; Mulder et al., 2003; Piper and Normark, 2009; Carter et al., 2012; Clare et al., 2016).

Second, changes to the speed of passage of a storm and storm tracks can impact sediment delivery. Slower passage of storm systems will likely increase the amount of rainfall received; thus having a similar impact as rainfall intensification within a given system. In contrast, changes to storm tracks, could have variable impacts. The movement of storm track, as has been indicated by poleward migration of tropical cyclone activity (Kossin et al., 2014; Mei and Xie, 2016), may lead to more intense storm systems impacting areas which have experienced relatively few intense storms. The intense storms may then lead to landscape evolution and adjustment in these areas leading to enhanced sediment transport to offshore systems (Stone et al., 2004; Lin et al., 2008; Gavey et al., 2017). Equally, regions which frequently experienced major storms may now be

impacted by relatively few, leading to reduced sediment transport. Both scenarios would impact upon the frequency of submarine mass movements.

7.3.1.3   Possible future directions

Understanding whether short-term climate change will alter the frequency of submarine mass movements requires a number of variables to be constrained. First, it is necessary to obtain a basic understanding of the frequency of flows in different types of settings which can be applied to other areas. For example, the frequency of events offshore a river delta (Hughes Clarke et al., 2014; Hughes Clarke, 2016) is likely very different from a gravity wave dominated canyon system (Paull et al., 2002; Smith et al., 2007).

To achieve this long-term monitoring of flows in these systems is necessary and fulfils two goals (Talling et al., 2015). (1) Long-term monitoring can reveal how active sedimentary systems are. This can provide information relevant for both geohazard analysis and for analysis of the delivery of organic carbon to deeper water (Galy et al., 2007; Thomas et al., 2010). For example, recent monitoring work offshore the Congo Canyon has demonstrated that the canyon was active 25% of the time that monitoring equipment was present (Cooper et al., 2013). Submarine mass movements thus likely represent a key process for the transport and burial of organic carbon in this location. (2) Individual triggering mechanisms can be identified for specific submarine mass movements and not just those that damage subsea fibre-optic cables. This has already been achieved on the Squamish Prodelta in British Colombia, Canada (Hughes Clarke et al., 2012; Clare et al., 2016) but needs to be expanded into other types of system (see Fig. 7.2). Understanding the precise triggering mechanisms for mass movement events can facilitate future modelling and prediction studies allowing the possible impacts of future short-term changes to weather patterns on specific sedimentary systems to be predicted.
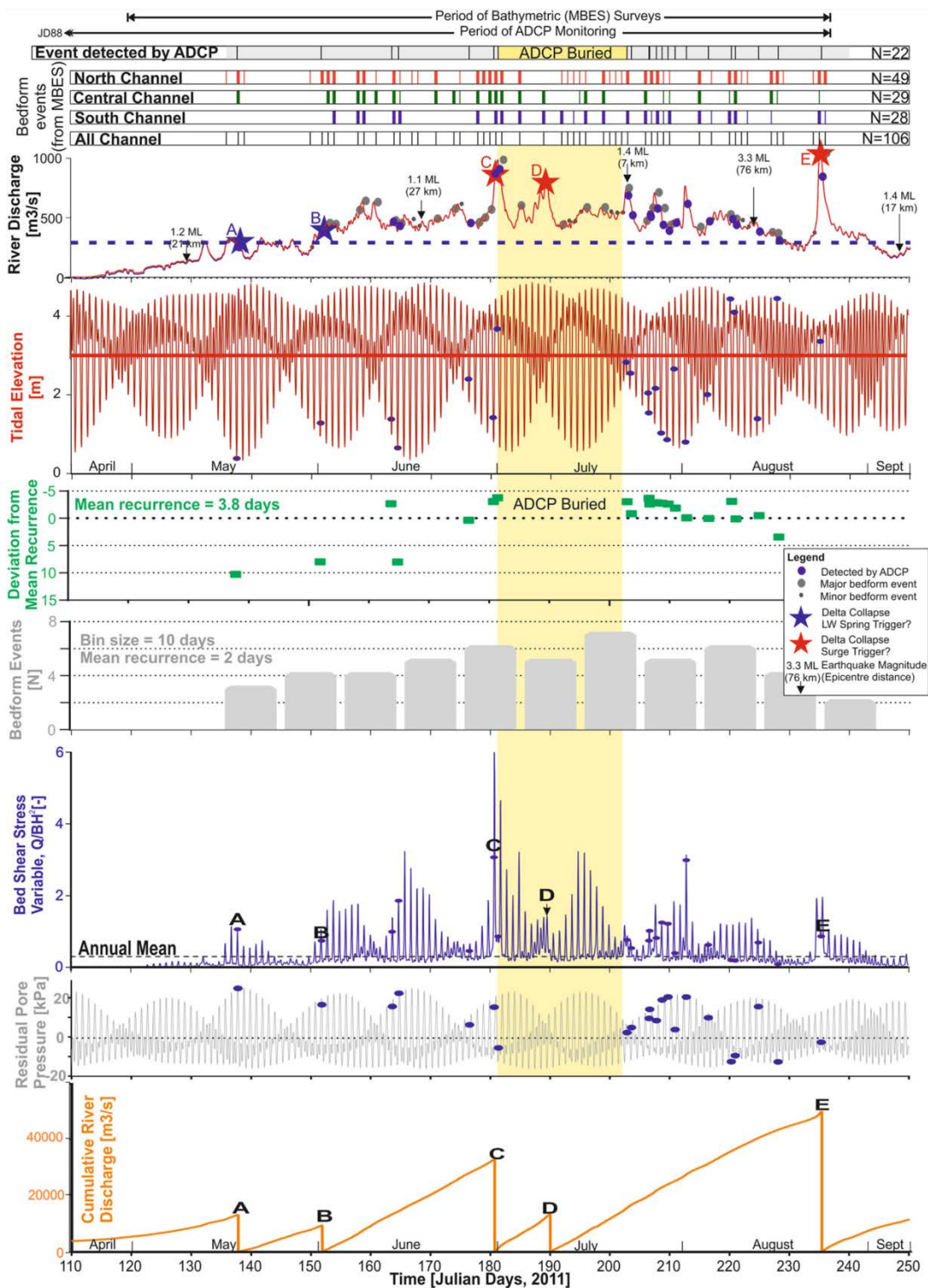
Figure 7.2 Time series of submarine mass movement occurrence and possible controlling variables. Top four staves show timing of turbidity currents recorded by an ADCP and bedform events detected from bathymetric surveys, river discharge and earthquakes, tidal elevation, recurrence of turbidity currents detected at ADCP location, bedform event frequency per 10 day bins, delta-top bed shear stress variable, residual pore pressure at 10 m below seafloor and cumulative river discharge leading up to delta-lip collapses A to E (from Clare et al., 2016).

A second alternative is the construction of high resolution sediment delivery budgets to offshore areas in combination with evidence of previous submarine mass movements. Although challenging, building up these records may help generate a longer-term record of the relationship of environmental variables to submarine mass movement occurrence. Perhaps the best example of where this could be achieved is offshore Taiwan (see Fig. 7.3). Here, the large number of monitored rivers (Agency, 2010), combined with the high number and density of offshore cables may allow the comparison of sediment budgets with the occurrence damaging submarine mass movements in relation to atmospheric forcing.
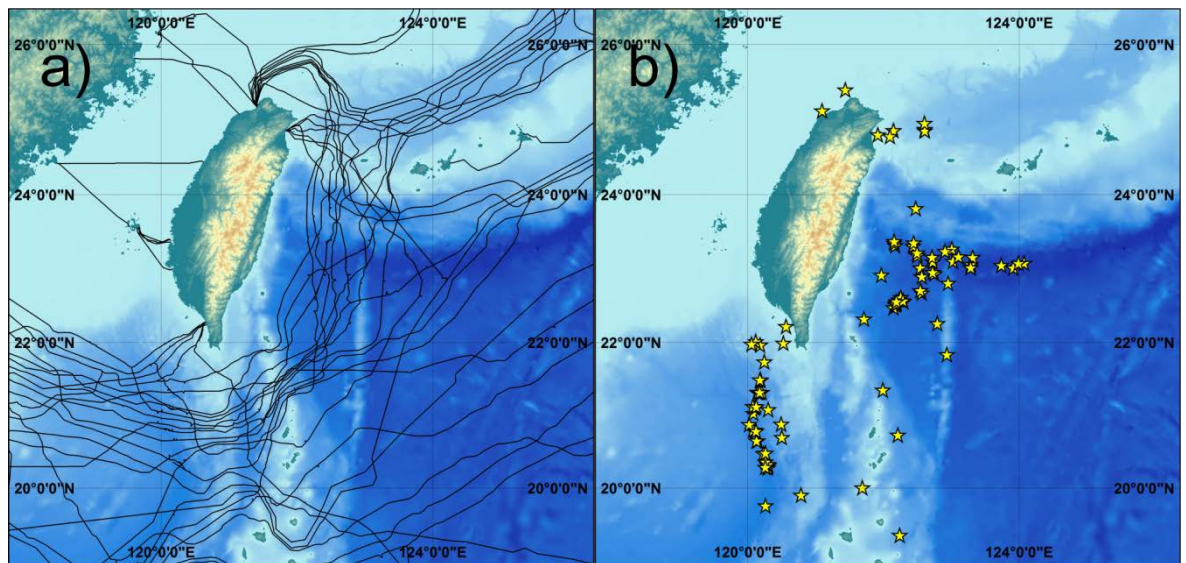
Figure 7.3 a) Subsea fibre-optic around Taiwan. b) Cable breaks caused by submarine mass movements triggered.

7.3.2   Can the record of submarine mass movements be used to better constrain the history of ice sheets?

Understanding glacier and ice sheet mass balance, dynamics and how they change over different timescales is important for predicting future contributions to sea level change as a consequence of sustained climatic forcing (Quincey et al., 2009). Settings where glacier ice is no longer present, but a record of the ice-bed interface, landforms and the sediments lying immediately beneath it are preserved without significant modification can therefore provide an important archive of past glacial activity. They can also illustrate ice sheet response to climatic forcing (Ó Cofaigh et al., 2003; Ottesen et al., 2005; Ottesen et al., 2007). The marine record often provides such an archive.

7.3.2.1   Reconstruction of ice sheet histories in this thesis

Ice dynamics and the retreat of the Late Weichselian ice sheets are well constrained because of relatively well-preserved and dated sediments (Sættem et al., 1994; Vorren and Laberg, 1997; Landvik et al., 1998; Solheim et al., 1998) and submarine geomorphology (Ottesen et al., 2005; Andreassen et al., 2008; Hillenbrand et al., 2010; Winsborrow et al., 2012) allow the ice sheet history to be reconstructed. However, the most recent glacial advance and retreat has reworked earlier sediments and has overprinted older geomorphology, thereby obscuring the record of past ice behaviour. This thesis has demonstrated that sedimentary archives on the continental slope can extend the record of ice sheet history beyond the Late Weichselian to encompass multiple advance and retreat cycles.

Chapter 5 showed that it was possible to use the record of glacigenic debris-flow deposits to reconstruct the timing of when ice was at the shelf edge. Moreover, it was also shown that it was possible to use the number and thickness of deposits to infer differences in ice sheet stability and possible flow velocities. Analysis of the geochemical composition of the debris-flow deposits alos revealed changed to the flow configuration of the Barents Sea Ice Sheet between different glacial periods. Using geophysical and sedimentological data from around the Nordic Seas, **Chapter 6** reconstructed the history of the Greenland Ice Sheet, Barents Sea Ice Sheet and Scandinavian Ice Sheet through the Quaternary. Using sedimentary archives, this chapter showed that changes to climate and climate cyclicity could have significant impacts on ice sheet delivery of sediment and thus the type, thickness and frequency of submarine mass movements. It subsequently used the record of the presence/absence of these deposits and their associated landforms to define characteristics margin types worldwide according to the driving factors behind the observed sedimentation processes. However, the conclusions of both **Chapters 5** and **6** and the ability of future studies to use submarine mass movements to reconstruct ice sheet histories are perhaps limited by our current lack of observations of these flows occurring in contemporary environments.

7.3.2.2   Possible future directions of research

Improvements to our understanding of ice sheet histories using sedimentary archives and particularly the record of submarine mass movements can be made through direct monitoring of contemporary glaciated environments.

7.3.2.2.1   Direct monitoring of submarine mass movements in proglacial environments

To date, very little monitoring data from subaqueous proglacial environments exists. Primarily this is a consequence of these areas often being remote and hazardous, whilst any deployment of

equipment faces the additional hazard posed by icebergs. As a consequence the majority of monitoring data is in the form of fjord circulation patterns and remote sensing observations of meltwater plumes (MacAyeal, 1985; Powell, 1990; Hunter et al., 1996; Cowan et al., 1997; Straneo et al., 2010; Jiskoot et al., 2012; Dowdeswell et al., 2015). In terms of submarine mass movements, we therefore have very little understanding of their triggers, frequency, flow characteristics or their relative roles in sediment budgets in contemporary environments.

Recent advances in understanding submarine mass movements and other sedimentation processes in pro-delta and submarine canyon settings at low-latitudes have come from direct monitoring studies (Khripounoff et al., 2003; 2012; Hughes Clarke et al., 2012; 2014; 2016; Cooper et al., 2013; Xu et al., 2014; Clare et al., 2016; Azpiroz-Zabala et al., 2017; Symons et al., 2017). Specifically these studies have been able to analyse the triggers, frequency, volumes and flow characteristics of turbidity currents in these locations. By carrying out direct monitoring studies in front of marine terminating glaciers across a range of climatic settings, i.e. Alaska, Svalbard, Greenland, Antarctica (see Fig. 6.1), we would greatly increase our understanding of submarine mass movements and sedimentation processes in pro-glacial environments. At the very least by carrying out repeat multibeam bathymetry surveys in from of a range of marine terminating glaciers it would be possible to estimate the annual volume of discharged sediment and possible frequencies of submarine mass movements in these different settings. These measurements would also contribute to our understanding of the rate at which sub- and proglacial landforms are formed and thus improve interpretations of the glacimarine marine record.

7.4 Concluding remarks

This thesis presented a range of different methods for the determination and analysis of submarine mass movement frequency, triggering and geohazard implications. Using different types of data we have demonstrated:

- That event datasets of limited size make identifying a common trigger using statistical analyses extremely difficult.
- Even small uncertainties can prevent the identification of non-random distributions of events thus making identification of a trigger difficult.
- Global compilations of event data should not generally be used to identify a common trigger due to differences in local environmental variables.
- Earthquakes magnitudes as low as M_w 3.0 were shown to be capable of triggering submarine mass movements if local tectonic and sedimentary regimes were favourable.

- Tropical cyclones can trigger sediment density flows through three mechanisms; (1) directly in response to dynamic loading of the seafloor; (2) as a response to a fluvial flood discharge of sediment or; (3) after a delay as a consequence of dynamic loading of the seabed and rapidly deposited sediment. Flows were most commonly triggered by the last mechanism.

- Sediment density flow frequency is likely to increase around South East Asia as a consequence of increased tropical cyclone intensities, slower tropical cyclone passage and poleward migration of storm tracks increasing sediment discharge to the continental shelf.

- The timing, number and thickness of glacigenic debris-flow deposits can be used to reconstruct ice stream advances to the shelf edge and their dynamics.

- The geochemical composition of glacigenic debris-flows can be used to reconstruct palaeo-ice flow directions/ice sheet configurations.

- New conceptual models of trough-mouth fans and glaciated margins have been presented according to the driving factors (ice sheet sediment/meltwater delivery etc.) behind their dominant sedimentary processes.

- Having tested the old model of large submarine landslide occurrence on glaciated margins which is based on the Storegga Slide Complex, an additional model to explain some large submarine landslides (Nyk and Trænadjupet Slides) has been presented.

The breath of different methods used during this thesis in order to improve our understanding of the frequency and triggering of submarine mass movements reflects the number of challenges that need to be overcome. However, principle among these is the lack of direct observation either of the flows themselves or of how properties in the subsurface change prior to triggering. The use of direct monitoring technologies such as ADCPs is beginning to address this problem. However, they have primarily been used to monitor turbidity currents. Future studies directed at monitoring different types of submarine mass movement as well as linking changing subsurface properties to triggering mechanisms will therefore greatly aid our understanding of submarine mass movements and their geohazard potential.

List of References

Adams, J., 1990. Paleoseismicity of the Cascadia subduction zone: Evidence from turbidites off the Oregon-Washington margin. Tectonics 9, 569-583.

Adrielsson, L., Alexanderson, H., 2005. Interactions between the Greenland Ice Sheet and the Liverpool Land coastal ice cap during the last two glaciation cycles. Journal of Quaternary Science 20, 269-283.

Agency, W.R., 2010. Hydrological Year Book of Taiwan, Republic of China 2009. Part II-River Stage and Discharge, Taipei.

Aksu, A.E., Hiscott, R.N., 1989. Slides and debris flows on the high-latitude continental slopes of Baffin Bay. Geology 17, 885-888.

Aksu, A.E., Piper, D.J.W., 1987. Late Quaternary sedimentation in Baffin Bay. Canadian Journal of Earth Sciences 24, 1833-1846.

Alford, M.H., 2003. Redistribution of energy available for ocean mixing by long-range propagation of internal waves. Nature 423, 159-162.

Allen, T.I., Wald, D.J., Earle, P.S., Marano, K.D., Hotovec, A.J., Lin, K., Hearne, M.G., 2009. An Atlas of ShakeMaps and population exposure catalog for earthquake loss modeling. Bulletin of Earthquake Engineering 7, 701-718.

Alley, R.B., Blankenship, D.D., Rooney, S.T., Bentley, C.R., 1989. Sedimentation beneath ice shelves—the view from ice stream B. Mar Geol 85, 101-120.

Allin, J.R., Hunt, J.E., Talling, P.J., Clare, M.A., Pope, E., Masson, D.G., 2016. Different frequencies and triggers of canyon filling and flushing events in Nazaré Canyon, offshore Portugal. Mar Geol 379, 89-105.

Allin, J.R., Mozzato, A., Talling, P.J., Hunt, J.E., Tappin, D.R., Cartigny, M.J.B., Pope, E.L., Watts, M., Clare, M.A., Haflidason, H., Baeten, N.J., Dowdeswell, J.A., in review. A new view of large (>100 km3) submarine landslides: triggered from the top down, weakly tsunamigenic, and occurring twice in a glacial cycle.

Alvarado, A., 2006. Updates on MMS (Minerals Management Service) regulatory issues for offshore operators. Uniform Resource Locator (URL): http://www.southerngas.org/EVENTS/documents/SGAOGO06Alvarado.pdf (accessed 13 March, 2007).

Amblas, D., Canals, M., 2016. Contourite drifts and canyon-channel systems on the Northern Antarctic Peninsula Pacific margin. Geological Society, London, Memoirs 46, 393-394.

Amblas, D., Urgeles, R., Canals, M., Calafat, A.M., Rebesco, M., Camerlenghi, A., Estrada, F., De Batist, M., Hughes-Clarke, J.E., 2006. Relationship between continental rise development and palaeo-ice sheet dynamics, Northern Antarctic Peninsula Pacific margin. Quaternary Sci Rev 25, 933-944.

Ambraseys, N.N., Simpson, K.A., Bommer, J., 1996. Prediction of horizontal response spectra in Europe. Earthq Eng Struct D 25, 371-400.

Amundson, J.M., Fahnestock, M., Truffer, M., Brown, J., Lüthi, M.P., Motyka, R.J., 2010. Ice mélange dynamics and implications for terminus stability, Jakobshavn Isbræ, Greenland. Journal of Geophysical Research: Earth Surface (2003–2012) 115.

Andersen, E.S., Dokken, T.M., Elverhoi, A., Solheim, A., Fossen, I., 1996. Late Quaternary sedimentation and glacial history of the western Svalbard continental margin. Mar Geol 133, 123-156.

Andersen, E.S., Solheim, A., Elverhøi, A., 1994. Development of a high Arctic margin, exemplified by the western margin of Svalbard, International Conference on Arctic Margins, Alaska, pp. 155 - 160.

Anderson, J.B., Wright, R., Andrews, B., 1986. Weddell Fan and associated abyssal plain, Antarctica: morphology, sediment processes, and factors influencing sediment supply. Geo-Mar Lett 6, 121-129.

Andreassen, K., Laberg, J.S., Vorren, T.O., 2008. Seafloor geomorphology of the SW Barents Sea and its glaci-dynamic implications. Geomorphology 97, 157-177.

Andreassen, K., Nilssen, L.C., Rafaelsen, B., Kuilman, L., 2004. Three-dimensional seismic data from the Barents Sea margin reveal evidence of past ice streams and their dynamics. Geology 32, 729-732.

Andreassen, K., Ødegaard, C.M., Rafaelsen, B., 2007. Imprints of former ice streams, imaged and interpreted using industry three-dimensional seismic data from the south-western Barents Sea. Geological Society, London, Special Publications 277, 151-169.

Andreassen, K., Winsborrow, M.C.M., Bjarnadóttir, L.R., Rüther, D.C., 2014. Ice stream retreat dynamics inferred from an assemblage of landforms in the northern Barents Sea. Quaternary Sci Rev 92, 246-257.

Andrieux, O., Cooper, C.K., Wood, J., 2013. Turbidity Current Measurements in the Congo Canyon, Offshore Technology Conference. Offshore Technology Conference.

Arai, K., Naruse, H., Miura, R., Kawamura, K., Hino, R., Ito, Y., Inazu, D., Yokokawa, M., Izumi, N., Murayama, M., Kasaya, T., 2013. Tsunami-generated turbidity current of the 2011 Tohoku-Oki earthquake. Geology 41, 1195-1198.

Aspinall, W.P., Woo, G., Voight, B., Baxter, P.J., 2003. Evidence-based volcanology: application to eruption crises. Journal of Volcanology and Geothermal Research 128, 273-285.

Atwater, B.F., Carson, B., Griggs, G.B., Johnson, H.P., Salmi, M.S., 2014. Rethinking turbidite paleoseismology along the Cascadia subduction zone. Geology 42, 827-830.

Atwater, B.F., Griggs, G.B., 2012. Deep-sea turbidites as guides to Holocene earthquake history at the Cascadia Subduction Zone—Alternative views for a seismic-hazard workshop. US Geological Survey Open-File Report 1043, 58.

Azpiroz-Zabala, M., Cartigny, M.J.B., Talling, P.J., Parsons, D.R., Sumner, E.J., Clare, M.A., Simmons, S.M., Cooper, C., Pope, E.L., 2017. Newly recognised turbidity current structure can explain prolonged flushing of submarine canyons. Science Advances 3, e1700200.

Backman, J., Fornaciari, E., Rio, D., 2009. Biochronology and paleoceanography of late Pleistocene and Holocene calcareous nannofossil abundances across the Arctic Basin. Marine Micropaleontology 72, 86-98.

Baeten, N.J., Laberg, J.S., Forwick, M., Vorren, T.O., Vanneste, M., Forsberg, C.F., Kvalstad, T.J., Ivanov, M., 2013. Morphology and origin of smaller-scale mass movements on the continental slope off northern Norway. Geomorphology 187, 122-134.

Baeten, N.J., Laberg, J.S., Vanneste, M., Forsberg, C.F., Kvalstad, T.J., Forwick, M., Vorren, T.O., Haflidason, H., 2014. Origin of shallow submarine mass movements and their glide planes—Sedimentological and geotechnical analyses from the continental slope off northern Norway. Journal of Geophysical Research: Earth Surface 119, 2335-2360.

Barkoulas, J.T., Baum, C.F., Travlos, N., 2000. Long memory in the Greek stock market. Applied Financial Economics 10, 177-184.

Bart, P.J., De Batist, M., Jokat, W., 1999. Interglacial collapse of Crary Trough-mouth fan, Weddell Sea, Antarctica: implications for Antarctic glacial history. Journal of Sedimentary Research 69.

Batchelor, C., Dowdeswell, J., 2014. The physiography of High Arctic cross-shelf troughs. Quaternary Sci Rev 92, 68-96.

Baumann, K.-H., Lackschewitz, K.S., Mangerud, J., Spielhagen, R.F., Wolf-Welling, T.C.W., Henrich, R., Kassens, H., 1995. Reflection of Scandinavian ice sheet fluctuations in Norwegian Sea sediments during the past 150,000 years. Quaternary Res 43, 185-197.

Baumann, K.H., Huber, R., 1999. 12. Sea-surface gradients between the North Atlantic and the Norwegian Sea during the last 3.1 MY: Comparison of Sites 982 and 985, Proceedings of the Ocean Drilling Program: Scientific Results. The Program, p. 179.

Baxter, P.J., Aspinall, W.P., Neri, A., Zuccaro, G., Spence, R.J.S., Cioni, R., Woo, G., 2008. Emergency planning and mitigation at Vesuvius: A new evidence-based approach. Journal of Volcanology and Geothermal Research 178, 454-473.

Bea, R.G., Wright, S.G., Sircar, P., Niedoroda, A.W., 1983. Wave-Induced Slides in South Pass Block 70, Mississippi Delta. J Geotech Eng-Asce 109, 619-644.

Beck, C., De Lépinay, B.M., Schneider, J.-L., Cremer, M., Çağatay, N., Wendenbaum, E., Boutareaud, S., Ménot, G., Schmidt, S., Weber, O., 2007. Late Quaternary co-seismic sedimentation in the Sea of Marmara's deep basins. Sediment Geol 199, 65-89.

Becker, J.J., Sandwell, D.T., Smith, W.H.F., Braud, J., Binder, B., Depner, J., Fabre, D., Factor, J., Ingalls, S., Kim, S.H., 2009. Global bathymetry and elevation data at 30 arc seconds resolution: SRTM30_PLUS. Marine Geodesy 32, 355-371.

Beget, J.E., Addison, J.A., 2007. Methane gas release from the storegga submarine landslide linked to early-Holocene climate change: a speculative hypothesis. Holocene 17, 291-295.

Bellec, V.K., Rise, L., Bøe, R., Dowdeswell, J.A., 2016. Glacially related gullies on the upper continental slope, SW Barents Sea margin. Geological Society, London, Memoirs 46, 381-382.

Benn, D.I., Hulton, N.R.J., Mottram, R.H., 2007a. 'Calving laws','sliding laws' and the stability of tidewater glaciers. Annals of glaciology 46, 123-130.

Benn, D.I., Warren, C.R., Mottram, R.H., 2007b. Calving processes and the dynamics of calving glaciers. Earth-Sci Rev 82, 143-179.

Bennett, M.R., 2003. Ice streams as the arteries of an ice sheet: their mechanics, stability and significance. Earth-Sci Rev 61, 309-339.

Berg, K., Solheim, A., Bryn, P., 2005. The Pleistocene to recent geological development of the Ormen Lange area. Mar Petrol Geol 22, 45-56.

Bernard, E., Titov, V., 2006. Improving tsunami forecast skill using deep ocean observations. Mar Technol Soc J 40, 86-89.

Bernard, E.N., 2008. The Tsunami-Resilient Coastal Community. J Earthq Tsunami 2, 279-285.

Bernard, E.N., Mofjeld, H.O., Titov, V., Synolakis, C.E., Gonzalez, F.I., 2006. Tsunami: scientific frontiers mitigation, forecasting and policy implications. Philos T R Soc A 364, 1989-2006.

Berndt, C., 2005. Focused fluid flow in passive continental margins. Philosophical Transactions of the Royal Society of London A: Mathematical, Physical and Engineering Sciences 363, 2855-2871.

Berné, S., Rabineau, M., Flores, J.A., Sierro, F., 2004. The impact of Quaternary global changes on strata formation: exploration of the shelf edge in the NW Mediterranean Sea. Oceanography 17, 92-103.

Biscontin, G., Pestana, J.M., 2006. Factors affecting seismic response of submarine slopes. Natural Hazards and Earth System Science 6, 97-107.

Biscontin, G., Pestana, J.M., Nadim, F., 2004. Seismic triggering of submarine slides in soft cohesive soil deposits. Mar Geol 203, 341-354.

Björck, S., Bennike, O., Ingólfsson, Ó., Barnekow, L., Penney, D.N., 1994a. Lake Boksehandsken's earliest postglacial sediments and their palaeoenvironmental implications, Jameson Land, East Greenland. Boreas 23, 459-472.

Björck, S., Wohlfarth, B., Bennike, O., Hjort, C., Persson, T., 1994b. Revision of the early Holocene lake sediment based chronology and event stratigraphy on Hochstetter Forland, NE Greenland. Boreas 23, 513-523.

Boe, R., Prosch-Danielsen, L., Lepland, A., Harbitz, C.B., Gauer, P., Lovholt, F., Hogestol, M., 2007. An early Holocene submarine slide in Boknafjorden and the effect of a slide-triggered tsunami on Stone Age settlements at Rennesoy, SW Norway. Mar Geol 243, 157-168.

Bond, G., Heinrich, H., Broecker, W., Labeyrie, L., McManus, J.F., Andrews, J., Huon, S., Jantschik, R., Clasen, S., Simet, C., 1992. Evidence for massive discharges of icebergs into the North Atlantic ocean during the last glacial period.

Bond, G.C., Showers, W., Elliot, M., Evans, M., Lotti, R., Hajdas, I., Bonani, G., Johnson, S., 1999. The North Atlantic's 1-2 Kyr Climate Rhythm: Relation to Heinrich Events, Dansgaard/Oeschger Cycles and the Little Ice Age. Mechanisms of global climate change at millennial time scales, 35-58.

Bondevik, S., Løvholt, F., Harbitz, C.B., Mangerud, J., Dawson, A., Inge Svendsen, J., 2005. The Storegga Slide tsunami—comparing field observations with numerical simulations. Mar Petrol Geol 22, 195-208.

Bondevik, S., Mangerud, J., Dawson, S., Dawson, A., Lohne, Ø., 2003. Record-breaking height for 8000-year-old tsunami in the North Atlantic. Eos, Transactions American Geophysical Union 84, 289-293.

Bondevik, S., Stormo, S.K., Skjerdal, G., 2012. Green mosses date the Storegga tsunami to the chilliest decades of the 8.2 ka cold event. Quaternary Sci Rev 45, 1-6.

Bondevik, S., Svendsen, J.I., Johnson, G., Mangerud, J., Kaland, P.E., 1997. The Storegga tsunami along the Norwegian coast, its age and run up. Boreas 26, 29-53.

Boore, D.M., Atkinson, G.M., 2008. Ground-motion prediction equations for the average horizontal component of PGA, PGV, and 5%-damped PSA at spectral periods between 0.01 s and 10.0 s. Earthquake Spectra 24, 99-138.

Boulton, G.S., 1978. Boulder shapes and grain-size distributions of debris as indicators of transport paths through a glacier and till genesis. Sedimentology 25, 773-799.

Bourget, J., Zaragosi, S., Ellouz-Zimmermann, N., Mouchot, N., Garlan, T., Schneider, J.L., Lanfumey, V., Lallemant, S., 2011. Turbidite system architecture and sedimentary processes along topographically complex slopes: the Makran convergent margin. Sedimentology 58, 376-406.

Brendryen, J., Haflidason, H., Rise, L., Chand, S., Vanneste, M., Longva, O., L'Heureux, J.S., Forsberg, C.F., 2015. Ice sheet dynamics on the Lofoten–Vesterålen shelf, north Norway, from Late MIS-3 to Heinrich Stadial 1. Quaternary Sci Rev 119, 136-156.

Bretschneider, C.L., 1951. Revised wave forecasting relationships. Coastal Engineering Proceedings 1, 1.

Broecker, W.S., Denton, G.H., 1990. The role of ocean-atmosphere reorganizations in glacial cycles. Quaternary Sci Rev 9, 305-341.

Brothers, D.S., Luttrell, K.M., Chaytor, J.D., 2013. Sea-level-induced seismicity and submarine landslide occurrence. Geology 41, 979-982.

Bruschi, R., Bughi, S., Spinazzè, M., Torselletti, E., Vitali, L., 2006. Impact of debris flows and turbidily currents on seafloor structures. NORSK GEOLOGISK TIDSSKRIFT 86, 317.

Bryn, P., Berg, K., Forsberg, C.F., Solheim, A., Kvalstad, T.J., 2005. Explaining the Storegga slide. Mar Petrol Geol 22, 11-19.

Bryn, P., Solheim, A., Berg, K., Lien, R., Forsberg, C.F., Haflidason, H., Ottesen, D., Rise, L., 2003. The Storegga Slide complex; repeated large scale sliding in response to climatic cyclicity, Adv Nat Tech Haz Res. Springer, pp. 215-222.

Bugge, T., 1983. Submarine slides on the Norwegian continental margin, with special emphasis on the Storegga area, vol. 110. Trondheim, Norway: Continental Shelf and Petroleum Technology Research Institute, A/S publication.

Bugge, T., Befring, S., Belderson, R.H., Eidvin, T., Jansen, E., Kenyon, N.H., Holtedahl, H., Sejrup, H.P., 1987. A giant three-stage submarine slide off Norway. Geo-Mar Lett 7, 191-198.

Burke, K., 1967. The Yallahs Basin: a sedimentary basin southeast of Kingston, Jamaica. Mar Geol 5, 45-60.

Burnett, D.R., Beckman, R., Davenport, T.M., 2013. Submarine Cables: the handbook of Law and Policy. Martinus Nijhoff Publishers.

Busetti, M., Caburlotto, A., Armand, L., Damiani, D., Giorgetti, G., Lucchi, R.G., Quilty, P.G., Villa, G., 2003. Plio-Quaternary sedimentation on the Wilkes Land continental rise: preliminary results. Deep Sea Research Part II: Topical Studies in Oceanography 50, 1529-1562.

Butt, F.A., Drange, H., Elverhøi, A., Otterå, O.H., Solheim, A., 2002. Modelling Late Cenozoic isostatic elevation changes in the Barents Sea and their implications for oceanic and climatic regimes: preliminary results. Quaternary Sci Rev 21, 1643-1660.

Butt, F.A., Elverhøi, A., Forsberg, C.F., Solheim, A., 2001. Evolution of the Scoresby Sund Fan, central East Green land-evidence from ODP Site 987. NORSK GEOLOGISK TIDSSKRIFT 81, 3-15.

Camerlenghi, A., Urgeles, R., Fantoni, L., 2010. A database on submarine landslides of the Mediterranean Sea, Adv Nat Tech Haz Res. Springer, pp. 503-513.

Campbell, K.W., 1997. Empirical near-source attenuation relationships for horizontal and vertical components of peak ground acceleration, peak ground velocity, and pseudo-absolute acceleration response spectra. Seismological Research Letters 68, 154-179.

Campbell, K.W., 2003. Prediction of strong ground motion using the hybrid empirical method and its use in the development of ground-motion (attenuation) relations in eastern North America. B Seismol Soc Am 93, 1012-1033.

Canals, M., Amblas, D., Casamor, J.L., Lastras, G., 2016. Gebra Slide: glacial and tectonic controls on recurrent submarine landsliding off the northern tip of the Antarctic Peninsula. Geological Society, London, Memoirs 46, 417-418.

Canals, M., Calafat, A., Camerlenghi, A., De Batist, M., Urgeles, R., Farran, M., Geletti, R., Versteeg, W., Amblas, D., Rebesco, M., 2003. Uncovering the footprint of former ice streams off Antarctica. EOS: TRANSACTIONS AMERICAN GEOPHYSICAL UNION 84, 97-103.

Canals, M., Danovaro, R., Heussner, S., Lykousis, V., Puig, P., Trincardi, F., Calafat, A., Durrieu de Madron, X., Palanques, A., Sànchez-Vidal, A., 2009. Cascades in Mediterranean submarine grand canyons. Oceanography 22, 26-43.

Carter, L., Burnett, D., Drew, S., Hagadorn, L., Marle, G., Bertlett-McNeil, D., Irvine, N., 2009. Submarine cables and the oceans- connecting the world: UNEP-WCMC Biodiversity Series 31. ICPC/UNEP/UNEP-WCMC. 64.

Carter, L., Gavey, R., Talling, P.J., Liu, J.T., 2014. Insights into submarine geohazards from breaks in subsea telecommunication cables. Oceanography 27, 58-67.

Carter, L., Milliman, J.D., Talling, P.J., Gavey, R., Wynn, R.B., 2012. Near-synchronous and delayed initiation of long run-out submarine sediment flows from a record-breaking river flood, offshore Taiwan. Geophys Res Lett 39.

Cassidy, M., Watt, S.F.L., Talling, P.J., Palmer, M.R., Edmonds, M., Jutzeler, M., Wall-Palmer, D., Manga, M., Coussens, M., Gernon, T., 2015. Rapid onset of mafic magmatism facilitated by volcanic edifice collapse. Geophys Res Lett 42, 4778-4785.

Catania, G.A., Scambos, T.A., Conway, H., Raymond, C.F., 2006. Sequential stagnation of Kamb ice stream, West Antarctica. Geophys Res Lett 33.

Cattaneo, A., Babonneau, N., Ratzov, G., Dan-Unterseh, G., Yelles, K., Bracene, R., De Lepinay, B.M., Boudiaf, A., Déverchere, J., 2012. Searching for the seafloor signature of the 21 May 2003 Boumerdes earthquake offshore central Algeria. Nat Hazard Earth Sys 12, 2159-2172.

Channell, J.E.T., Smelror, M., Jansen, E., Higgins, S.M., Lehman, B., Eidvin, T., Solheim, A., 1999. 10. Age models for glacial fan deposits off East Greenland and Svalbard (Sites 986 and 987), Proceedings of the Ocean Drilling Program: Scientific results. The Program, p. 149.

Chaytor, J.D., Uri, S., Solow, A.R., Andrews, B.D., 2009. Size distribution of submarine landslides along the US Atlantic margin. Mar Geol 264, 16-27.

Chen, C., Hiscott, R.N., 1999. Statistical analysis of facies clustering in submarine-fan turbidite successions. Journal of Sedimentary Research 69, 505-517.

Chen, J.C., Huang, W.S., Jan, C.D., Yang, Y.H., 2012. Recent changes in the number of rainfall events related to debris-flow occurrence in the Chenyulan Stream Watershed, Taiwan. Natural Hazards and Earth System Science 12, 1539-1549.

Cheshire, H., Thurow, J., Nederbragt, A.J., 2005. Late Quaternary climate change record from two long sediment cores from Guaymas Basin, Gulf of California. Journal of Quaternary Science 20, 457-469.

Chevron, 2014. Angola Fact Sheet.

Christoffersen, P., Tulaczyk, S., Behar, A., 2010. Basal ice sequences in Antarctic ice stream: Exposure of past hydrologic conditions and a principal mode of sediment transfer. Journal of Geophysical Research: Earth Surface (2003–2012) 115.

Chronis, G., Lykousis, V., Georgopoulos, D., Zervakis, V., Stavrakakis, S., Poulos, S., 2000. Suspended particulate matter and nepheloid layers over the southern margin of the Cretan Sea (NE Mediterranean): seasonal distribution and dynamics. Progress in oceanography 46, 163-185.

Clare, M.A., Hughes Clarke, J.E., Talling, P.J., Cartigny, M.J.B., Pratomo, D.G., 2016. Preconditioning and triggering of offshore slope failures and turbidity currents revealed by most detailed monitoring yet at a fjord-head delta. Earth and Planetary Science Letters 450, 208-220.

Clare, M.A., Talling, P.J., Challenor, P., Malgesini, G., Hunt, J.E., 2014. Distal turbidites reveal a common distribution for large (>0.1 km3) submarine landslide recurrence. Geology 42, 263-266.

Clare, M.A., Talling, P.J., Hunt, J.E., 2015. Implications of reduced turbidity current and landslide activity for the Initial Eocene Thermal Maximum–evidence from two distal, deep-water sites. Earth and Planetary Science Letters 420, 102-115.

Clark, C.D., 1993. Mega-scale glacial lineations and cross-cutting ice-flow landforms. Earth Surf Proc Land 18, 1-29.

Clarke, S., Hubble, T., Airey, D., Yu, P., Boyd, R., Keene, J., Exon, N., Gardner, J., 2012. Submarine Landslides on the Upper Southeast Australian Passive Continental Margin–Preliminary Findings, Adv Nat Tech Haz Res. Springer, pp. 55-66.

Colleoni, F., Krinner, G., Jakobsson, M., Peyaud, V., Ritz, C., 2009. Influence of regional parameters on the surface mass balance of the Eurasian ice sheet during the peak Saalian (140 kya). Global and Planetary Change 68, 132-148.

Cooper, C., Wood, J., Andrieux, O., 2013. Turbidity current measurements in the Congo Canyon, Offshore Technology Conference, May, pp. 06-09.

Covault, J.A., Graham, S.A., 2010. Submarine fans at all sea-level stands: Tectono-morphologic and climatic controls on terrigenous sediment delivery to the deep sea. Geology 38, 939-942.

Covault, J.A., Normark, W.R., Romans, B.W., Graham, S.A., 2007. Highstand fans in the California borderland: The overlooked deep-water depositional systems. Geology 35, 783-786.

Cowan, E.A., Cai, J., Powell, R.D., Clark, J.D., Pitcher, J.N., 1997. Temperate glacimarine varves: an example from Disenchantment Bay, southern Alaska. Journal of Sedimentary Research 67.

Croudace, I.W., Rindby, A., Rothwell, R.G., 2006. ITRAX: description and evaluation of a new multi-function X-ray core scanner. Special publication-geological society of London 267, 51.

Cuffey, K.M., Paterson, W.S.B., 2010. The physics of glaciers. Academic Press.

Dadson, S.J., Hovius, N., Chen, H., Dade, W.B., Lin, J.-C., Hsu, M.-L., Lin, C.-W., Horng, M.-J., Chen, T.-C., Milliman, J.D., 2004. Earthquake-triggered increase in sediment delivery from an active mountain belt. Geology 32, 733-736.

Dahlgren, K.I.T., Vorren, T.O., 2003. Sedimentary environment and glacial history during the last 40 ka of the Vøring continental margin, mid-Norway. Mar Geol 193, 93-127.

Dahlgren, K.I.T., Vorren, T.O., Laberg, J.S., 2002. Late Quaternary glacial development of the mid-Norwegian margin—65 to 68 N. Mar Petrol Geol 19, 1089-1113.

Dahlgren, K.I.T., Vorren, T.O., Stoker, M.S., Nielsen, T., Nygård, A., Sejrup, H.P., 2005. Late Cenozoic prograding wedges on the NW European continental margin: their formation and relationship to tectonics and climate. Mar Petrol Geol 22, 1089-1110.

Dan, G., Sultan, N., Savoye, B., Deverchere, J., Yelles, K., 2009. Quantifying the role of sandy–silty sediments in generating slope failures during earthquakes: Example from the Algerian margin. International Journal of Earth Sciences 98, 769-789.

Das, R., Wason, H.R., Sharma, M.L., 2011. Global regression relations for conversion of surface wave and body wave magnitudes to moment magnitude. Nat Hazards 59, 801-810.

Daub, E.G., Ben-Naim, E., Guyer, R.A., Johnson, P.A., 2012. Are megaquakes clustered? Geophys Res Lett 39.

Dawson, A., Bondevik, S., Teller, J., 2011. Relative timing of the Storegga submarine slide, methane release, and climate change during the 8.2 ka cold event. The Holocene 21, 1167-1171.

Dawson, A., Long, D., Smith, D., 1988. The Storegga slides: evidence from eastern Scotland for a possible tsunami. Mar Geol 82, 271-276.

Dee, D.P., Uppala, S.M., Simmons, A.J., Berrisford, P., Poli, P., Kobayashi, S., Andrae, U., Balmaseda, M.A., Balsamo, G., Bauer, P., Bechtold, P., Beljaars, A.C.M., van de Berg, L., Bidlot, J., Bormann, N., Delsol, C., Dragani, R., Fuentes, M., Geer, A.J., Haimberger, L., Healy, S.B., Hersbach, H., Hólm, E.V., Isaksen, L., Kållberg, P., Köhler, M., Matricardi, M., McNally, A.P., Monge-Sanz, B.M., Morcrette, J.J., Park, B.K., Peubey, C., de Rosnay, P., Tavolato, C., Thépaut, J.N., Vitart, F., 2011. The ERA-Interim reanalysis: configuration and performance of the data assimilation system. Quarterly Journal of the Royal Meteorological Society 137, 553-597.

Dengler, A.T., Wilde, P., Noda, E.K., Normark, W.R., 1984. Turbidity currents generated by Hurricane Iwa. Geo-Mar Lett 4, 5-11.

Denton, G.H., Hughes, T.J., 2002. Reconstructing the Antarctic Ice Sheet at the Last Glacial Maximum. Quaternary Sci Rev 21, 193-202.

Déry, S.J., Stahl, K., Moore, R.D., Whitfield, P.H., Menounos, B., Burford, J.E., 2009. Detection of runoff timing changes in pluvial, nival, and glacial rivers of western Canada. Water Resour Res 45.

Di Giacomo, D., Bondár, I., Storchak, D.A., Engdahl, E.R., Bormann, P., Harris, J.C., 2015. ISC-GEM: Global Instrumental Earthquake Catalogue (1900–2009), III. Re-computed MS and mb, proxy MW, final magnitude composition and completeness assessment. Physics of the Earth and Planetary Interiors 239, 33-47.

Dokken, T.M., Jansen, E., 1999. Rapid changes in the mechanism of ocean convection during the last glacial period. Nature 401, 458-461.

Dowdeswell, E.K., Todd, B.J., Dowdeswell, J.A., 2016a. Canyons and slides on the continental slope seaward of a shallow bank, Labrador margin, eastern Canada. Geological Society, London, Memoirs 46, 405-406.

Dowdeswell, J.A., Canals, M., Jakobsson, M., Todd, B.J., Dowdeswell, E.K., Hogan, K.A., 2016b. Introduction: an Atlas of Submarine Glacial Landforms. Geological Society, London, Memoirs 46, 3-14.

Dowdeswell, J.A., Dowdeswell, E.K., Todd, B.J., Saint-Ange, F., Piper, D.J.W., 2016c. Channels and gullies on the continental slope seaward of a cross-shelf trough, Labrador margin, eastern Canada. Geological Society, London, Memoirs 46, 385-386.

Dowdeswell, J.A., Elverhøi, A., 2002. The timing of initiation of fast-flowing ice streams during a glacial cycle inferred from glacimarine sedimentation. Mar Geol 188, 3-14.

Dowdeswell, J.A., Elverhøi, A., Andrews, J.T., Hebbeln, D., 1999. Asynchronous deposition of ice-rafted layers in the Nordic seas and North Atlantic Ocean. Nature 400, 348-351.

Dowdeswell, J.A., Elverhoi, A., Spielhagen, R., 1998. Glacimarine sedimentary processes and facies on the Polar North Atlantic margins. Quaternary Sci Rev 17, 243-272.

Dowdeswell, J.A., Evans, J., Ó Cofaigh, C., Anderson, J.B., 2006a. Morphology and sedimentary processes on the continental slope off Pine Island Bay, Amundsen Sea, West Antarctica. Geological Society of America Bulletin 118, 606-619.

Dowdeswell, J.A., Hogan, K.A., Arnold, N.S., Mugford, R.I., Wells, M., Hirst, J.P.P., Decalf, C., 2015. Sediment-rich meltwater plumes and ice-proximal fans at the margins of modern and ancient tidewater glaciers: Observations and modelling. Sedimentology 62, 1665-1692.

Dowdeswell, J.A., Kenyon, N.H., Elverhøi, A., Laberg, J.S., Hollender, F.J., Mienert, J., Siegert, M.J., 1996. Large-scale sedimentation on the glacier-influenced polar North Atlantic Margins: Long-range side-scan sonar evidence. Geophys Res Lett 23, 3535-3538.

Dowdeswell, J.A., Kenyon, N.H., Laberg, J.S., 1997. The glacier-influenced Scoresby Sund Fan, East Greenland continental margin: evidence from GLORIA and 3.5 kHz records. Mar Geol 143, 207-221.

Dowdeswell, J.A., Maslin, M.A., Andrews, J.T., McCave, I.N., 1995. Iceberg production, debris rafting, and the extent and thickness of Heinrich layers (H-1, H-2) in North Atlantic sediments. Geology 23, 301-304.

Dowdeswell, J.A., Ó Cofaigh, C., Noormets, R., Larter, R.D., Hillenbrand, C.-D., Benetti, S., Evans, J., Pudsey, C.J., 2008. A major trough-mouth fan on the continental margin of the Bellingshausen Sea, West Antarctica: the Belgica Fan. Mar Geol 252, 129-140.

Dowdeswell, J.A., Ó Cofaigh, C., Pudsey, C.J., 2004a. Continental slope morphology and sedimentary processes at the mouth of an Antarctic palaeo-ice stream. Mar Geol 204, 203-214.

Dowdeswell, J.A., Ó Cofaigh, C., Pudsey, C.J., 2004b. Thickness and extent of the subglacial till layer beneath an Antarctic paleo–ice stream. Geology 32, 13-16.

Dowdeswell, J.A., Ottesen, D., Rise, L., 2006b. Flow switching and large-scale deposition by ice streams draining former ice sheets. Geology 34, 313-316.

Dowdeswell, J.A., Ottesen, D., Rise, L., 2010. Rates of sediment delivery from the Fennoscandian Ice Sheet through an ice age. Geology 38, 3-6.

Dowdeswell, J.A., Siegert, M.J., 1999. Ice-sheet numerical modeling and marine geophysical measurements of glacier-derived sedimentation on the Eurasian Arctic continental margins. Geological Society of America Bulletin 111, 1080-1097.

Dreger, D., 1999. Decadal to Centennial Scale Sediment Records of Ice Advance on the Barents Shelf and Meltwater Discharge Into the Northeastern Norwegian Sea Over the Last 40 Kyr: Dekadische Bis Jahrhundert-Variabilität Von Eisvorstößen Auf Dem Barentsschelf und Schmelzwasserschüben in Die Nordöstliche Norwegensee Während Der Letzten 40 Ka. Inst. für Geowiss., pp. 1 - 79.

Dugan, B., Flemings, P.B., 2000. Overpressure and fluid flow in the New Jersey continental slope: implications for slope failure and cold seeps. Science 289, 288-291.

Dugan, B., Sheahan, T.C., 2012. Offshore sediment overpressures of passive margins: Mechanisms, measurement, and models. Rev Geophys 50.

Egholm, D.L., Pedersen, V.K., Knudsen, M.F., Larsen, N.K., 2012. Coupling the flow of ice, water, and sediment in a glacial landscape evolution model. Geomorphology 141, 47-66.

Ehlers, J., Gibbard, P.L., 2004. Quaternary Glaciations-Extent and Chronology: Part I: Europe. Elsevier.

Eidvin, T., Jansen, E., Rundberg, Y., Brekke, H., Grogan, P., 2000. The upper Cainozoic of the Norwegian continental shelf correlated with the deep sea record of the Norwegian Sea and the North Atlantic. Mar Petrol Geol 17, 579-600.

Einsele, G., 2013. Sedimentary basins: evolution, facies, and sediment budget. Springer Science & Business Media.

El-Robrini, M., Gennesseaux, M., Mauffret, A., 1985. Consequences of the El-Asnam earthquakes: Turbidity currents and slumps on the Algerian margin (Western Mediterranean). Geo-Mar Lett 5, 171-176.

Elverhøi, A., Andersen, E.S., Dokken, T., Hebbeln, D., Spielhagen, R., Svendsen, J.I., Sorflaten, M., Rornes, A., Hald, M., Forsberg, C.F., 1995. The growth and decay of the late weichselian ice sheet in western Svalbard and adjacent areas based on provenance studies of marine sediments. Quaternary Res 44, 303-316.

Elverhøi, A., Hooke, R.L.B., Solheim, A., 1998. Late Cenozoic erosion and sediment yield from the Svalbard–Barents Sea region: Implications for understanding erosion of glacierized basins. Quaternary Sci Rev 17, 209-241.

Emanuel, K., 2005. Increasing destructiveness of tropical cyclones over the past 30 years. Nature 436, 686-688.

Engelhardt, H., Kamb, B., 1998. Basal sliding of ice stream B, West Antarctica. J Glaciol 44, 223-230.

Ercilla, G., Alonso, B., Estrada, F., Chiocci, F.L., Baraza, J., li Farran, M., 2002a. The Magdalena Turbidite System (Caribbean Sea): present-day morphology and architecture model. Mar Geol 185, 303-318.

Ercilla, G., Wynn, R.B., Alonso, B., Baraza, J., 2002b. Initiation and evolution of turbidity current sediment waves in the Magdalena turbidite system. Mar Geol 192, 153-169.

Escutia, C., Eittreim, S.L., Cooper, A.K., Nelson, C.H., 2000. Morphology and acoustic character of the Antarctic Wilkes Land turbidite systems: ice-sheet-sourced versus river-sourced fans. Journal of Sedimentary Research 70, 84-93.

Evans, J., Ó Cofaigh, C., Dowdeswell, J.A., Wadhams, P., 2009. Marine geophysical evidence for former expansion and flow of the Greenland Ice Sheet across the north-east Greenland continental shelf. Journal of Quaternary Science 24, 279-293.

Faleide, J.I., Kyrkjebø, R., Kjennerud, T., Gabrielsen, R.H., Jordt, H., Fanavoll, S., Bjerke, M.D., 2002. Tectonic impact on sedimentary processes during Cenozoic evolution of the northern North Sea and surrounding areas. Geological Society, London, Special Publications 196, 235-269.

Faleide, J.I., Solheim, A., Fiedler, A., Hjelstuen, B.O., Andersen, E.S., Vanneste, K., 1996. Late Cenozoic evolution of the western Barents Sea-Svalbard continental margin. Global and Planetary Change 12, 53-74.

Felix, M., Peakall, J., McCaffrey, W.D., 2006. Relative importance of processes that govern the generation of particulate hyperpycnal flows. Journal of Sedimentary Research 76, 382-387.

Fiedler, A., Faleide, J.I., 1996. Cenozoic sedimentation along the southwestern Barents Sea margin in relation to uplift and erosion of the shelf. Global and Planetary Change 12, 75-93.

Flemings, P.B., Long, H., Dugan, B., Germaine, J., John, C.M., Behrmann, J.H., Sawyer, D., Scientists, I.E., 2008. Erratum to "Pore pressure penetrometers document high overpressure near the seafloor where multiple submarine landslides have occurred on the continental slope, offshore Louisiana, Gulf of Mexico" (vol 269, pg 309, 2008). Earth and Planetary Science Letters 274, 269-283.

Flood, R.D., Hiscott, R.N., Aksu, A.E., 2009. Morphology and evolution of an anastomosed channel network where saline underflow enters the Black Sea. Sedimentology 56, 807-839.

Forbes, A.C., Lamoureux, S.F., 2005. Climatic controls on streamflow and suspended sediment transport in three large middle arctic catchments, Boothia Peninsula, Nunavut, Canada. Arctic, Antarctic, and Alpine Research 37, 304-315.

Forsberg, C.F., Solheim, A., Elverhøi, A., Jansen, E., Channell, J.E.T., Andersen, E.S., 1999. 17. The depositional environment of the Western Svalbard margin during the Late Pliocene and the Pleistocene: Sedimentary facies changes at Site 986, Proceedings of the Ocean Drilling Program: Scientific results. The Program, p. 233.

Frenkel, M.C., Wright, S.G., Gilbert, R.B., Ward, E.G., 2006. Mudflows and Mudslides During Hurricane Ivan, Offshore Technology Conference, Houston, Texas, May 1-4, 2006. Offshore Technology Conference.

Fronval, T., Jansen, E., 1996. Late Neogene paleoclimates and paleoceanography in the Iceland-Norwegian Sea: evidence from the Iceland and Vøring Plateaus, Proceedings of the Ocean Drilling Program. Scientific Results. Ocean Drilling Program, pp. 455-468.

Fronval, T., Jansen, E., 1997. Eemian and early Weichselian (140–60 ka) paleoceanography and paleoclimate in the Nordic seas with comparisons to Holocene conditions. Paleoceanography 12, 443-462.

Fryer, G.J., Watts, P., Pratson, L.F., 2004. Source of the great tsunami of 1 April 1946: a landslide in the upper Aleutian forearc. Mar Geol 203, 201-218.

Funder, S., Hansen, L., 1996. The Greenland ice sheet-a model for its culmination and decay during and after the last glacial maximum. Geological Society of Denmark.

Funder, S., Hjort, C., Landvik, J.Y., 1994. The last glacial cycles in East Greenland, an overview. Boreas 23, 283-293.

Funder, S., Hjort, C., Landvik, J.Y., Nam, S.-I., Reeh, N., Stein, R., 1998. History of a stable ice margin—East Greenland during the middle and upper Pleistocene. Quaternary Sci Rev 17, 77-123.

Funder, S., Kjeldsen, K.K., Kjær, K.H., Ó Cofaigh, C., 2011. The Greenland Ice Sheet during the past 300,000 years: A review. Developments in Quaternary Science 15, 699-713.

Gales, J.A., Larter, R.D., Leat, P.T., Jokat, W., 2016. Components of an Antarctic trough-mouth fan: examples from the Crary Fan, Weddell Sea. Geological Society, London, Memoirs 46, 377-378.

Gales, J.A., Leat, P.T., Larter, R.D., Kuhn, G., Hillenbrand, C.-D., Graham, A.G.C., Mitchell, N.C., Tate, A.J., Buys, G.B., Jokat, W., 2014. Large-scale submarine landslides, channel and gully systems on the southern Weddell Sea margin, Antarctica. Mar Geol 348, 73-87.

Galy, V., France-Lanord, C., Beyssac, O., Faure, P., Kudrass, H., Palhol, F., 2007. Efficient organic carbon burial in the Bengal fan sustained by the Himalayan erosional system. Nature 450, 407-410.

Gard, G., 1988. Late Quaternary calcareous nannofossil biozonation, chronology and palaeo-oceanography in areas north of the Faeroe-Iceland Ridge. Quaternary Sci Rev 7, 65-78.

Garziglia, S., Migeon, S., Ducassou, E., Loncke, L., Mascle, J., 2008. Mass-transport deposits on the Rosetta province (NW Nile deep-sea turbidite system, Egyptian margin): characteristics, distribution, and potential causal processes. Mar Geol 250, 180-198.

Gavey, R., Carter, L., Liu, J.T., Talling, P.J., Hsu, R.T., Pope, E.L., Evans, G., 2017. Frequent sediment density flows during 2006 to 2015, triggered by competing seismic and weather events: Observations from subsea cable breaks off southern Tawain. Mar Geol 384, 147-158.

Geist, E.L., 2000. Origin of the 17 July 1998 Papua New Guinea tsunami: earthquake or landslide. Seismological Research Letters 71, 344-351.

Geist, E.L., Chaytor, J.D., Parsons, T., ten Brink, U., 2013. Estimation of submarine mass failure probability from a sequence of deposits with age dates. Geosphere 9, 287-298.

Geist, E.L., Parsons, T., 2009. Assessment of source probabilities for potential tsunamis affecting the US Atlantic coast. Mar Geol 264, 98-108.

Goldacre, B., 2010. Bad science: quacks, hacks, and big pharma flacks. McClelland & Stewart.

Goldfinger, C., 2011. Submarine Paleoseismology Based on Turbidite Records. Annu Rev Mar Sci 3, 35-66.

Goldfinger, C., Nelson, C.H., Johnson, J.E., 2003. Holocene earthquake records from the Cascadia subduction zone and northern San Andreas fault based on precise dating of offshore turbidites. Annual Review of Earth and Planetary Sciences 31, 555-577.

Goldfinger, C., Nelson, C.H., Morey, A.E., Johnson, J.E., Patton, J.R., Karabanov, E., Gutierrez-Pastor, J., Eriksson, A.T., Gracia, E., Dunhill, G., 2012. Turbidite event history: Methods and implications for Holocene paleoseismicity of the Cascadia subduction zone. US Department of the Interior, US Geological Survey.

Gràcia, E., Lamarche, G., Nelson, H., Pantosti, D., 2013. Preface: marine and Lake paleoseismology. Natural Hazards and Earth System Science 13, 3469-3478.

Gracia, E., Vizcaino, A., Escutia, C., Asioli, A., Rodes, A., Pallas, R., Garcia-Orellana, J., Lebreiro, S.M., Goldfinger, C., 2010. Holocene earthquake record offshore Portugal (SW Iberia): testing turbidite paleoseismology in a slow-convergence margin. Quaternary Sci Rev 29, 1156-1172.

Graham, A.G.C., Larter, R.D., Gohl, K., Hillenbrand, C.-D., Smith, J.A., Kuhn, G., 2009. Bedform signature of a West Antarctic palaeo-ice stream reveals a multi-temporal record of flow and substrate control. Quaternary Sci Rev 28, 2774-2793.

Grauert, M., BJÖRCK, S., Bondevik, S., 2001. Storegga tsunami deposits in a coastal lake on Suouroy, the Faroe Islands. Boreas 30, 263-271.

Greenwood, S.L., Clark, C.D., 2009. Reconstructing the last Irish Ice Sheet 1: changing flow geometries and ice flow dynamics deciphered from the glacial landform record. Quaternary Sci Rev 28, 3085-3100.

Greenwood, S.L., Clason, C.C., Jakobsson, M., 2016. Ice-flow and meltwater landform assemblages in the Gulf of Bothnia, in: Dowdeswell, J.A., Canals, M., Jakobsson, M., Todd, B.J., Dowdeswell, E.K., Hogan, K.A. (Eds.), Geological Society, London, Memoirs. Geological Society, London, pp. 321-324.

Gulick, S.P.S., Jaeger, J.M., Mix, A.C., Asahi, H., Bahlburg, H., Belanger, C.L., Berbel, G.B.B., Childress, L., Cowan, E., Drab, L., Forwick, M., Fukumura, A., Ge, S., Gupta, S., Kioka, A., Konno, S., LeVay, L.J., März, C., Matsuzaki, K.M., McClymont, E.L., Moy, C., Müller, J., Nakamura, A., Ojima, T., Ribeiro, F.R., Ridgway, K.D., Romero, O.E., Slagle, A.L., Stoner, J.S., St-Onge, G., Suto, I., Walczak, M.D., Worthington, L.L., Bailey, I., Enkelmann, E., Reece, R., Swartz, J.M., 2015. Mid-Pleistocene climate transition drives net mass loss from rapidly uplifting St. Elias Mountains, Alaska. Proceedings of the National Academy of Sciences 112, 15042-15047.

Haflidason, H., Aarseth, I., Haugen, J.-E., Sejrup, H.P., Løvlieb, R., Reither, E., 1991. Quaternary stratigraphy of the Draugen area, mid-Norwegian shelf. Mar Geol 101, 125-146.

Haflidason, H., Iversen, M., Løvlie, R., 1998. Møre and Vøring Basin Geological Investigation: lithological and chronological analyses of the geotechnical borings. Unpublished Report, Department of Geology, University of Bergen, Norway, 50pp.

Haflidason, H., Lien, R., Sejrup, H.P., Forsberg, C.F., Bryn, P., 2005. The dating and morphometry of the Storegga Slide. Mar Petrol Geol 22, 123-136.

Haflidason, H., Sejrup, H.P., Berstad, I.M., Nygård, A., Richter, T.O., Bryn, P., Lien, R., Berg, K., 2003. A weak layer feature on the Northern Storegga Slide escarpment, European Margin Sediment Dynamics. Springer, pp. 55-62.

Haflidason, H., Sejrup, H.P., Nygard, A., Mienert, J., Bryn, P., Lien, R., Forsberg, C.F., Berg, K., Masson, D., 2004. The Storegga Slide: architecture, geometry and slide development. Mar Geol 213, 201-234.

Håkansson, L., Alexanderson, H., Hjort, C., Möller, P., Briner, J.P., Aldahan, A., Possnert, G., 2009. Late Pleistocene glacial history of Jameson Land, central East Greenland, derived from cosmogenic 10Be and 26Al exposure dating. Boreas 38, 244-260.

Håkansson, L., Briner, J., Alexanderson, H., Aldahan, A., Possnert, G., 2007. 10 Be ages from central east Greenland constrain the extent of the Greenland ice sheet during the Last Glacial Maximum. Quaternary Sci Rev 26, 2316-2321.

Hallam, A., 1989. Great geological controversies. Oxford University Press.

Hallet, B., Hunter, L., Bogen, J., 1996. Rates of erosion and sediment evacuation by glaciers: A review of field data and their implications. Global and Planetary Change 12, 213-235.

Hampton, M.A., Lee, H.J., Locat, J., 1996. Submarine landslides. Rev Geophys 34, 33-59.

Hansen, L., Funder, S., Murray, A.S., Mejdahl, V., 1999. Luminescence dating of the last Weichselian glacier advance in East Greenland. Quaternary Sci Rev 18, 179-190.

Harbitz, C.B., Løvholt, F., Bungum, H., 2014. Submarine landslide tsunamis: how extreme and how likely? Nat Hazards 72, 1341-1374.

Hart, J.K., Rose, K.C., Martinez, K., 2011. Subglacial till behaviour derived from in situ wireless multi-sensor subglacial probes: Rheology, hydro-mechanical interactions and till formation. Quaternary Sci Rev 30, 234-247.

Hebbeln, D., Dokken, T., Andersen, E.S., Hald, M., Elverhøi, A., 1994. Moisture supply for northern ice-sheet growth during the Last Glacial Maximum. Nature 370, 357-360.

Heezen, B.C., 1956. Corrientes de turbidez del Rio Magdalena. Bol. Soc. Geol. Colombia

 51/52, 135 - 143.

Heezen, B.C., Ewing, M., 1955. Orleansville earthquake and turbidity currents. AAPG Bulletin 39, 2505-2514.

Heezen, B.C., Ewing, W.M., 1952. Turbidity currents and submarine slumps, and the 1929 Grand Banks [Newfoundland] earthquake. American Journal of Science 250, 849-873.

Heezen, B.C., Hollister, C.D., 1971. Face of the deep. Oxford University Press.

Heezen, B.C., Johnson, G.L., 1969. Alaskan submarine cables: A struggle with a harsh environment. Arctic, 413-424.

Heezen, B.C., Menzies, R.J., Schneider, E.D., Ewing, W.M., Granelli, N.C.L., 1964. Congo submarine canyon. AAPG Bulletin 48, 1126-1149.

Helmke, J.P., Bauch, H.A., 2003. Comparison of glacial and interglacial conditions between the polar and subpolar North Atlantic region over the last five climatic cycles. Paleoceanography 18.

Helmke, J.P., Bauch, H.A., Erlenkeuser, H., 2003a. Development of glacial and interglacial conditions in the Nordic seas between 1.5 and 0.35 Ma. Quaternary Sci Rev 22, 1717-1728.

Helmke, J.P., Bauch, H.A., Mazaud, A., 2003b. Evidence for a mid-Pleistocene shift of ice-drift pattern in the Nordic seas. Journal of Quaternary Science 18, 183-191.

Helmke, J.P., Bauch, H.A., Röhl, U., Mazaud, A., 2005. Changes in sedimentation patterns of the Nordic seas region across the mid-Pleistocene. Mar Geol 215, 107-122.

Helsen, M.M., van den Broeke, M.R., van de Wal, R.S.W., van de Berg, W.J., van Meijgaard, E., Davis, C.H., Li, Y., Goodwin, I., 2008. Elevation changes in Antarctica mainly determined by accumulation variability. Science 320, 1626-1629.

Hemer, M.A., Fan, Y., Mori, N., Semedo, A., Wang, X.L., 2013. Projected changes in wave climate from a multi-model ensemble. Nature climate change 3, 471-476.

Henrich, R., 1989. Glacial/interglacial cycles in the Norwegian Sea: sedimentology, paleoceanography, and evolution of Late Pliocene to Quaternary northern hemisphere climate, Proceedings of the Ocean Drilling Program, scientific results, pp. 189-232.

Henrich, R., Baumann, K.-H., 1994. Evolution of the Norwegian Current and the Scandinavian Ice Sheets during the past 2.6 my: evidence from ODP Leg 104 biogenic carbonate and terrigenous records. Palaeogeography, Palaeoclimatology, Palaeoecology 108, 75-94.

Henriksen, S., Vorren, T.O., 1996. Late Cenozoic sedimentation and uplift history on the mid-Norwegian continental shelf. Global and Planetary Change 12, 171-199.

Herman, F., Beaud, F., Champagnac, J.-D., Lemieux, J.-M., Sternai, P., 2011. Glacial hydrology and erosion patterns: a mechanism for carving glacial valleys. Earth and Planetary Science Letters 310, 498-508.

Hesse, R., Klauck, I., Khodabakhsh, S., Piper, D., 1999. Continental slope sedimentation adjacent to an ice margin. III. The upper Labrador Slope. Mar Geol 155, 249-276.

Hesse, R., Klaucke, I., Khodabakhsh, S., Piper, D.J.W., Ryan, W.B.F., Group, N.S., 2001. Sandy submarine braid plains: potential deep-water reservoirs. AAPG bulletin 85, 1499-1521.

Hesse, R., Klaucke, I., Khodabakhsh, S., Ryan, W.B.F., 1997. Glacimarine Drainage Systems in Deep-sea: The NAMOC System of the Labrador Sea and its Sibling, in: Davies, T.A., al., e. (Eds.), Glaciated Continental Margins. Springer, pp. 286-289.

Hesse, R., Rashid, H., Khodabakhsh, S., 2004. Fine-grained sediment lofting from meltwater-generated turbidity currents during Heinrich events. Geology 32, 449-452.

Hibbert, F.D., Austin, W.E.N., Leng, M.J., Gatliff, R.W., 2010. British Ice Sheet dynamics inferred from North Atlantic ice-rafted debris records spanning the last 175 000 years. Journal of Quaternary Science 25, 461-482.

Hill, P., 2012. Changes in submarine channel morphology and slope sedimentation patterns from repeat multibeam surveys in the Fraser River delta, western Canada. Int Assoc Sedimentol Spec Publ 44, 47-70.

Hillenbrand, C.-D., Larter, R.D., Dowdeswell, J.A., Ehrmann, W., Ó Cofaigh, C., Benetti, S., Graham, A.G.C., Grobe, H., 2010. The sedimentary legacy of a palaeo-ice stream on the shelf of the southern Bellingshausen Sea: Clues to West Antarctic glacial history during the Late Quaternary. Quaternary Sci Rev 29, 2741-2763.

Hjelstuen, B.O., Andreassen, E.V., 2015. North Atlantic Ocean deep-water processes and depositional environments: A study of the Cenozoic Norway Basin. Mar Petrol Geol 59, 429-441.

Hjelstuen, B.O., Eldholm, O., Faleide, J.I., 2007. Recurrent Pleistocene mega-failures on the SW Barents Sea margin. Earth and Planetary Science Letters 258, 605-618.

Hjelstuen, B.O., Elverhøi, A., Faleide, J.I., 1996. Cenozoic erosion and sediment yield in the drainage area of the Storfjorden Fan. Global and Planetary Change 12, 95-117.

Hjelstuen, B.O., Sejrup, H.P., Haflidason, H., Nygård, A., Berstad, I.M., Knorr, G., 2004. Late Quaternary seismic stratigraphy and geological development of the south Vøring margin, Norwegian Sea. Quaternary Sci Rev 23, 1847-1865.

Hjelstuen, B.O., Sejrup, H.P., Haflidason, H., Nygard, A., Ceramicola, S., Bryn, P., 2005. Late Cenozoic glacial history and evolution of the Storegga Slide area and adjacent slide flank regions, Norwegian continental margin. Mar Petrol Geol 22, 57-69.

Hoffman, P.F., Kaufman, A.J., Halverson, G.P., Schrag, D.P., 1998. A Neoproterozoic snowball earth. Science 281, 1342-1346.

Hogan, K.A., Dowdeswell, J.A., Mienert, J., 2013. New insights into slide processes and seafloor geology revealed by side-scan imagery of the massive Hinlopen Slide, Arctic Ocean margin. Geo-Mar Lett 33, 325-343.

Hogan, K.A., Dowdeswell, J.A., Noormets, R., Evans, J., Cofaigh, C.Ó., 2010. Evidence for full-glacial flow and retreat of the Late Weichselian Ice Sheet from the waters around Kong Karls Land, eastern Svalbard. Quaternary Sci Rev 29, 3563-3582.

Hogan, K.A., Ó Cofaigh, C., Jennings, A.E., Dowdeswell, J.A., Hiemstra, J.F., 2016. Deglaciation of a major palaeo-ice stream in Disko Trough, West Greenland. Quaternary Sci Rev 147, 5-26.

Holzer, T.L., Savage, J.C., 2013. Global earthquake fatalities and population. Earthquake Spectra 29, 155-175.

Hormes, A., Gjermundsen, E.F., Rasmussen, T.L., 2013. From mountain top to the deep sea– Deglaciation in 4D of the northwestern Barents Sea ice sheet. Quaternary Sci Rev 75, 78-99.

Hornbach, M.J., Lavier, L.L., Ruppel, C.D., 2007. Triggering mechanism and tsunamogenic potential of the Cape Fear Slide complex, US Atlantic margin. Geochemistry, Geophysics, Geosystems 8.

Hsu, S.K., Kuo, J., Lo, C.L., Tsai, C.H., Doo, W.B., Ku, C.Y., Sibuet, J.C., 2008. Turbidity Currents, Submarine Landslides and the 2006 Pingtung Earthquake off SW Taiwan. Terr Atmos Ocean Sci 19, 767-772.

Hughes, A.L.C., Gyllencreutz, R., Lohne, Ø.S., Mangerud, J., Svendsen, J.I., 2016. The last Eurasian ice sheets–a chronological database and time-slice reconstruction, DATED-1. Boreas 45, 1-45.

Hughes Clarke, J.E., 2016. First wide-angle view of channelized turbidity currents links migrating cyclic steps to flow characteristics. Nature communications 7, 11896.

Hughes Clarke, J.E., Brucker, S., Muggah, J., Hamilton, T., Cartwright, D., Church, I., Kuus, P., 2012. Temporal progression and spatial extent of mass wasting events on the Squamish prodelta slope, Proceedings of Canadian Hydrographic Conference 2012, p. 15.

Hughes Clarke, J.E., Marques, C.R.V., Pratomo, D., 2014. Imaging Active Mass-Wasting and Sediment Flows on a Fjord Delta, Squamish, British Columbia, Adv Nat Tech Haz Res. Springer, pp. 249-260.

Hühnerbach, V., Masson, D.G., 2004. Landslides in the North Atlantic and its adjacent seas: an analysis of their morphology, setting and behaviour. Mar Geol 213, 343-362.

Hunt, J.E., Wynn, R.B., Talling, P.J., Masson, D.G., 2013. Frequency and timing of landslide-triggered turbidity currents within the Agadir Basin, offshore NW Africa: Are there associations with climate change, sea level change and slope sedimentation rates? Mar Geol 346, 274-291.

Hunter, L.E., Powell, R.D., Lawson, D.E., 1996. Morainal-bank sediment budgets and their influence on the stability of tidewater termini of valley glaciers entering Glacier Bay, Alaska, USA. Annals of Glaciology 22, 211-216.

Huppertz, T.J., Piper, D.J.W., 2009. The influence of shelf-crossing glaciation on continental slope sedimentation, Flemish Pass, eastern Canadian continental margin. Mar Geol 265, 67-85.

Hürlimann, M., Turon, E., Marti, J., 1999. Large landslides triggered by caldera collapse events in Tenerife, Canary Islands. Physics and Chemistry of the Earth, Part A: Solid Earth and Geodesy 24, 921-924.

Hurst, H.E., 1951. Long-term storage capacity of reservoirs. Trans. Amer. Soc. Civil Eng. 116, 770-808.

Imbo, Y., De Batist, M., Canals, M., Prieto, M.J., Baraza, J., 2003. The Gebra slide: a submarine slide on the Trinity Peninsula Margin, Antarctica. Mar Geol 193, 235-252.

Ingólfsson, Ó., Landvik, J.Y., 2013. The Svalbard–Barents Sea ice-sheet–Historical, current and future perspectives. Quaternary Sci Rev 64, 33-60.

Inman, D.L., Nordstrom, C.E., Flick, R.E., 1976. Currents in submarine canyons: An air-sea-land interaction. Annual Review of Fluid Mechanics 8, 275-310.

Jakobsson, M., Andreassen, K., Bjarnadóttir, L.R., Dove, D., Dowdeswell, J.A., England, J.H., Funder, S., Hogan, K.A., Ingólfsson, Ó., Jennings, A., 2014. Arctic Ocean glacial history. Quaternary Sci Rev 92, 40-67.

Jansen, E., Bleil, U., Henrich, R., Kringstad, L., Slettemark, B., 1988. Paleoenvironmental changes in the Norwegian Sea and the northeast Atlantic during the last 2.8 my: Deep Sea Drilling Project/Ocean Drilling Program sites 610, 642, 643 and 644. Paleoceanography 3, 563-581.

Jansen, E., et al., 1996. 8. Site 985, Proc. Ocean Drill. Program Initial Rep, pp. 253-283.

Jansen, E., Fronval, T., Rack, F., Channell, J.E.T., 2000. Pliocene-Pleistocene ice rafting history and cyclicity in the Nordic Seas during the last 3.5 Myr. Paleoceanography 15, 709-721.

Jansen, E., Raymo, M.E., 1996. 1. Leg 162: New Frontiers on Past Climates, in: Jansen, E., Raymo, M.E., Blum, P., et al. (Eds.), Proceedings Ocean Drilling Program Initial Reports, vol. 162.

Jansen, E., Sjøholm, J., 1991. Reconstruction of glaciation over the past 6 Myr from ice-borne deposits in the Norwegian Sea. Nature 349, 600-603.

Jeng, D.-S., Cha, D.H., 2003. Effects of dynamic soil behavior and wave non-linearity on the wave-induced pore pressure and effective stresses in porous seabed. Ocean Engineering 30, 2065-2089.

Jeng, D.-S., Seymour, B.R., 2007. Simplified analytical approximation for pore-water pressure buildup in marine sediments. J Waterw Port C-Asce 133, 309-312.

Jerolmack, D.J., Paola, C., 2010. Shredding of environmental signals by sediment transport. Geophys Res Lett 37.

Jessen, S.P., Rasmussen, T.L., Nielsen, T., Solheim, A., 2010. A new Late Weichselian and Holocene marine chronology for the western Svalbard slope 30,000–0 cal years BP. Quaternary Sci Rev 29, 1301-1312.

Jiskoot, H., Juhlin, D., St Pierre, H., Citterio, M., 2012. Tidewater glacier fluctuations in central East Greenland coastal and fjord regions (1980s–2005). Annals of Glaciology 53, 35-44.

Kao, S.-J., Dai, M., Selvaraj, K., Zhai, W., Cai, P., Chen, S.-N., Yang, J., Liu, J., Liu, C., Syvitski, J.P., 2010. Cyclone-driven deep sea injection of freshwater and heat by hyperpycnal flow in the subtropics. Geophys Res Lett 37.

Kao, S.J., Milliman, J.D., 2008. Water and sediment discharge from small mountainous rivers, Taiwan: The roles of lithology, episodic events, and human activities. The Journal of Geology 116, 431-448.

Karim, M.F., Mimura, N., 2008. Impacts of climate change and sea-level rise on cyclonic storm surge floods in Bangladesh. Global Environmental Change 18, 490-500.

Kayen, R.E., Lee, H.J., 1991. Pleistocene slope instability of gas hydrate-laden sediment on the Beaufort sea margin. Marine Georesources & Geotechnology 10, 125-141.

Keefer, D.K., 1984. Landslides caused by earthquakes. Geological Society of America Bulletin 95, 406-421.

Keefer, D.K., 2002. Investigating landslides caused by earthquakes–a historical review. Surveys in Geophysics 23, 473-510.

Kendall, M., Stuart, A., Ord, J., Arnold, S., 1999. Vol. 2A: Classical inference and the linear model. London [etc.]: Arnold [etc.].

Kennett, J.P., Cannariato, K.G., Hendy, I.L., Behl, R.J., 2000. Carbon isotopic evidence for methane hydrate instability during quaternary interstadials. Science 288, 128-133.

Kennett, J.P., Cannariato, K.G., Hendy, I.L., Behl, R.J., 2003. Methane hydrates in Quaternary climate change: The clathrate gun hypothesis. American Geophysical Union.

Khripounoff, A., Crassous, P., Lo Bue, N., Dennielou, B., Silva Jacinto, R., 2012. Different types of sediment gravity flows detected in the Var submarine canyon (northwestern Mediterranean Sea). Progress in Oceanography 106, 138-153.

Khripounoff, A., Vangriesheim, A., Babonneau, N., Crassous, P., Dennielou, B., Savoye, B., 2003. Direct observation of intense turbidity current activity in the Zaire submarine valley at 4000 m water depth. Mar Geol 194, 151-158.

King, E.L., Haflidason, H., Sejrup, H.P., Løvlie, R., 1998. Glacigenic debris flows on the North Sea Trough Mouth Fan during ice stream maxima. Mar Geol 152, 217-246.

King, E.L., Sejrup, H.P., Haflidason, H., Elverhøi, A., Aarseth, I., 1996. Quaternary seismic stratigraphy of the North Sea Fan: glacially-fed gravity flow aprons, hemipelagic sediments, and large submarine slides. Mar Geol 130, 293-315.

Kleiven, H.F., Jansen, E., Fronval, T., Smith, T.M., 2002. Intensification of Northern Hemisphere glaciations in the circum Atlantic region (3.5–2.4 Ma)–ice-rafted detritus evidence. Palaeogeography, Palaeoclimatology, Palaeoecology 184, 213-223.

Kleman, J., Hättestrand, C., Borgström, I., Stroeven, A., 1997. Fennoscandian palaeoglaciology reconstructed using a glacial geological inversion model. J Glaciol 43, 283-299.

Knies, J., Kleiber, H.-P., Matthiessen, J., Müller, C., Nowaczyk, N., 2001. Marine ice-rafted debris records constrain maximum extent of Saalian and Weichselian ice-sheets along the northern Eurasian margin. Global and Planetary Change 31, 45-64.

Knies, J., Matthiessen, J., Vogt, C., Laberg, J.S., Hjelstuen, B.O., Smelror, M., Larsen, E., Andreassen, K., Eidvin, T., Vorren, T.O., 2009. The Plio-Pleistocene glaciation of the Barents Sea–Svalbard region: a new model based on revised chronostratigraphy. Quaternary Sci Rev 28, 812-829.

Knies, J., Vogt, C., Stein, R., 1998. Late Quaternary growth and decay of the Svalbard/Barents Sea ice sheet and paleoceanographic evolution in the adjacent Arctic Ocean. Geo-Mar Lett 18, 195-202.

Knutson, T.R., McBride, J.L., Chan, J., Emanuel, K., Holland, G., Landsea, C., Held, I., Kossin, J.P., Srivastava, A.K., Sugi, M., 2010. Tropical cyclones and climate change. Nat Geosci 3, 157-163.

Kokusho, T., Kojima, T., 2002. Mechanism for postliquefaction water film generation in layered sand. Journal of geotechnical and geoenvironmental engineering 128, 129-137.

Koppes, M., Hallet, B., Rignot, E., Mouginot, J., Wellner, J.S., Boldt, K., 2015. Observed latitudinal variations in erosion as a function of glacier dynamics. Nature 526, 100-103.

Korup, O., 2012. Earth's portfolio of extreme sediment transport events. Earth-Sci Rev 112, 115-125.

Kossin, J.P., Emanuel, K.A., Vecchi, G.A., 2014. The poleward migration of the location of tropical cyclone maximum intensity. Nature 509, 349-352.

Krause, D.C., White, W.C., Piper, D.J.W., Heezen, B.C., 1970. Turbidity currents and cable breaks in the western New Britain Trench. Geological Society of America Bulletin 81, 2153-2160.

Krissek, L.A., 1989. Late Cenozoic records of ice-rafting at ODP Sites 642, 643, and 644, Norwegian Sea: onset, chronology, and characteristics of glacial/interglacial fluctuations, Proceedings of the Ocean Drilling Project. Scientific Results. Texas A&M University College Station, TX, pp. 61-69.

Kuvaas, B., Kristoffersen, Y., 1991. The Crary Fan: a trough-mouth fan on the Weddell Sea continental margin, Antarctica. Mar Geol 97, 345-362.

Kuvaas, B., Kristoffersen, Y., 1996. Mass movements in glaciomarine sediments on the Barents Sea continental slope. Global and Planetary Change 12, 287-307.

Kuvaas, B., Kristoffersen, Y., Guseva, J., Leitchenkov, G., Gandjukhin, V., Løvås, O., Sand, M., Brekke, H., 2005. Interplay of turbidite and contourite deposition along the Cosmonaut Sea/Enderby Land margin, East Antarctica. Mar Geol 217, 143-159.

Kuvaas, B., Leitchenkov, G., 1992. Glaciomarine turbidite and current controlled deposits in Prydz Bay, Antarctica. Mar Geol 108, 365-381.

Kvalstad, T.J., Andresen, L., Forsberg, C.F., Berg, K., Bryn, P., Wangen, M., 2005. The Storegga slide: evaluation of triggering sources and slide mechanics. Mar Petrol Geol 22, 245-256.

L'Heureux, J.S., Vanneste, M., Rise, L., Brendryen, J., Forsberg, C.F., Nadim, F., Longva, O., Chand, S., Kvalstad, T.J., Haflidason, H., 2013. Stability, mobility and failure mechanism for landslides at the upper continental slope off Vesterålen, Norway. Mar Geol 346, 192-207.

Laberg, J.S., Andreassen, K., Knies, J., Vorren, T.O., Winsborrow, M., 2010. Late Pliocene–Pleistocene development of the Barents Sea ice sheet. Geology 38, 107-110.

Laberg, J.S., Dowdeswell, J.A., 2016. Glacigenic debris-flows on the Bear Island Trough-Mouth Fan, Barents Sea margin, in: Dowdeswell, J.A., Canals, M., Jakobsson, M., Todd, B.J., Dowdeswell, E.K., Hogan, K.A. (Eds.), Atlas of Submarine Glacial Landforms: Modern, Quaternary and Ancient. Geological Society, Geological Society, London, Memoirs, v. 46.

Laberg, J.S., Forwick, M., Husum, K., Nielsen, T., 2013. A re-evaluation of the Pleistocene behavior of the Scoresby Sund sector of the Greenland Ice Sheet. Geology 41, 1231-1234.

Laberg, J.S., Vorren, T.O., 1995. Late Weichselian submarine debris flow deposits on the Bear Island Trough mouth fan. Mar Geol 127, 45-72.

Laberg, J.S., Vorren, T.O., 1996. The Middle and Late Pleistocence evolution and the Bear Island Trough Mouth Fan. Global and Planetary Change 12, 309-330.

Laberg, J.S., Vorren, T.O., 2000. The Trænadjupet Slide, offshore Norway—morphology, evacuation and triggering mechanisms. Mar Geol 171, 95-114.

Laberg, J.S., Vorren, T.O., Dowdeswell, J.A., Kenyon, N.H., Taylor, J., 2000. The Andoya Slide and the Andoya Canyon, north-eastern Norwegian-Greenland Sea. Mar Geol 162, 259-275.

Laberg, J.S., Vorren, T.O., Mienert, J., Bryn, P., Lien, R., 2002a. The Trænadjupet Slide: a large slope failure affecting the continental margin of Norway 4,000 years ago. Geo-Mar Lett 22, 19-24.

Laberg, J.S., Vorren, T.O., Mienert, J., Evans, D., Lindberg, B., Ottesen, D., Kenyon, N.H., Henriksen, S., 2002b. Late Quaternary palaeoenvironment and chronology in the Trænadjupet Slide area offshore Norway. Mar Geol 188, 35-60.

Laberg, J.S., Vorren, T.O., Mienert, J., Haflidason, H., Bryn, P., Lien, R., 2003. Preconditions Leading to the Holocene Trænadjupet Slide Offshore Norway, in: Locat, J., Mienert, J., Boisvert, L. (Eds.), Adv Nat Tech Haz Res. Springer Netherlands, pp. 247-254.

Lamb, M.P., Parsons, J.D., 2005. High-density suspensions formed under waves. Journal of Sedimentary Research 75, 386-397.

Lambeck, K., Purcell, A., Zhao, J., Svensson, N.O., 2010. The Scandinavian ice sheet: from MIS 4 to the end of the Last Glacial Maximum. Boreas 39, 410-435.

Lambeck, K., Smither, C., Johnston, P., 1998. Sea-level change, glacial rebound and mantle viscosity fornorthern Europe. Geophys J Int 134, 102-144.

Lambrechts, J., Humphrey, C., McKinna, L., Gourge, O., Fabricius, K.E., Mehta, A.J., Lewis, S., Wolanski, E., 2010. Importance of wave-induced bed liquefaction in the fine sediment budget of Cleveland Bay, Great Barrier Reef. Estuarine, Coastal and Shelf Science 89, 154-162.

Landsea, C., Franklin, J., Beven, J., 2013. The revised Atlantic hurricane database (HURDAT2). United States National Oceanic and Atmospheric Administration's.

Landvik, J.Y., 1994. The last glaciation of Germania Land and adjacent areas, northeast Greenland. Journal of Quaternary Science 9, 81-92.

Landvik, J.Y., Bolstad, M., Lycke, A.K., Mangerud, J., Sejrup, H.P., 1992. Weichselian stratigraphy and palaeoenvironments at Bellsund, western Svalbard. Boreas 21, 335-358.

Landvik, J.Y., Bondevik, S., Elverhøi, A., Fjeldskaar, W., Mangerud, J., Salvigsen, O., Siegert, M.J., Svendsen, J.-I., Vorren, T.O., 1998. The last glacial maximum of Svalbard and the Barents Sea area: ice sheet extent and configuration. Quaternary Sci Rev 17, 43-75.

Landvik, J.Y., Ingolfsson, O., Mienert, J., Lehman, S.J., Solheim, A., Elverhøi, A., Ottesen, D., 2005. Rethinking Late Weichselian ice-sheet dynamics in coastal NW Svalbard. Boreas 34, 7-24.

Larsen, H., Saunders, A., Clift, P., Beget, J., Wei, W., Spezzaferri, S., Party, a.O.L.S., 1994. Seven million years of glaciation in Greenland. Science 264, 952 - 955.

Larsen, H.C., 1990. The East Greenland shelf. The Geology of North America 50, 185-210.

Larsen, N.K., Knudsen, K.L., Krohn, C.F., Kronborg, C., Murray, A.S., Nielsen, O.B., 2009. Late Quaternary ice sheet, lake and sea history of southwest Scandinavia–a synthesis. Boreas 38, 732-761.

Lastras, G., Canals, M., Urgeles, R., De Batist, M., Calafat, A., Casamor, J., 2004. Characterisation of the recent BIG'95 debris flow deposit on the Ebro margin, Western Mediterranean Sea, after a variety of seismic reflection data. Mar Geol 213, 235-255.

Lebreiro, S.M., Voelker, A.H.L., Vizcaino, A., Abrantes, F.G., Alt-Epping, U., Jung, S., Thouveny, N., Gracia, E., 2009. Sediment instability on the Portuguese continental margin under abrupt glacial climate changes (last 60 kyr). Quaternary Sci Rev 28, 3211-3223.

Lee, H.J., 2009. Timing of occurrence of large submarine landslides on the Atlantic Ocean margin. Mar Geol 264, 53-64.

Lee, H.J., Chough, S.K., Yoon, S.H., 1996. Slope-stability change from late pleistocene to holocene in the Ulleung Basin, East Sea (Japan Sea). Sediment Geol 104, 39-51.

Lee, H.J., Locat, J., Dartnell, P., Israel, K., Wong, F., 1999. Regional variability of slope stability: application to the Eel margin, California. Mar Geol 154, 305-321.

Lee, H.J., Schwab, W.C., Booth, J.S., 1993. Submarine landslides: An introduction. Submarine Landslides: Selected Studies in the US Exclusive Economic Zone, 1-1.

Lee, I.-H., Lien, R.-C., Liu, J.T., Chuang, W.S., 2009. Turbulent mixing and internal tides in Gaoping (Kaoping) submarine canyon, Taiwan. Journal of Marine Systems 76, 383-396.

Lee, J.R., Busschers, F.S., Sejrup, H.P., 2012. Pre-Weichselian Quaternary glaciations of the British Isles, The Netherlands, Norway and adjacent marine areas south of 68 N: implications for long-term ice sheet development in northern Europe. Quaternary Sci Rev 44, 213-228.

Lee, T.-Y., Huang, J.-C., Lee, J.-Y., Jien, S.-H., Zehetner, F., Kao, S.-J., 2015. Magnified Sediment Export of Small Mountainous Rivers in Taiwan: Chain Reactions from Increased Rainfall Intensity under Global Warming. PloS one 10, e0138283.

Lekens, W.A.H., Haflidason, H., Sejrup, H.P., Nygård, A., Richter, T., Vogt, C., Frederichs, T., 2009. Sedimentation history of the northern North Sea Margin during the last 150 ka. Quaternary Sci Rev 28, 469-483.

Lekens, W.A.H., Sejrup, H.P., Haflidason, H., Knies, J., Richter, T., 2006. Meltwater and ice rafting in the southern Norwegian Sea between 20 and 40 calendar kyr BP: Implications for Fennoscandian Heinrich events. Paleoceanography 21.

Lekens, W.A.H., Sejrup, H.P., Haflidason, H., Petersen, G.Ø., Hjelstuen, B.O., Knorr, G., 2005. Laminated sediments preceding Heinrich event 1 in the Northern North Sea and Southern Norwegian Sea: origin, processes and regional linkage. Mar Geol 216, 27-50.

Leynaud, D., Mienert, J., Vanneste, M., 2009. Submarine mass movements on glaciated and non-glaciated European continental margins: A review of triggering mechanisms and preconditions to failure. Mar Petrol Geol 26, 618-632.

Leynaud, D., Sultan, N., Mienert, J., 2007. The role of sedimentation rate and permeability in the slope stability of the formerly glaciated Norwegian continental margin: the Storegga slide model. Landslides 4, 297-309.

Li, G., Piper, D.J.W., Calvin Campbell, D., 2011. The Quaternary Lancaster Sound trough-mouth fan, NW Baffin Bay. Journal of Quaternary Science 26, 511-522.

Lin, G.W., Chen, H., Hovius, N., Horng, M.J., Dadson, S.J., Meunier, P., Lines, M., 2008. Effects of earthquake and cyclone sequencing on landsliding and fluvial sediment transfer in a mountain catchment. Earth Surf Proc Land 33, 1354-1373.

Lindberg, B., Laberg, J.S., Vorren, T.O., 2004. The Nyk Slide—morphology, progression, and age of a partly buried submarine slide offshore northern Norway. Mar Geol 213, 277-289.

Lisiecki, L.E., Raymo, M.E., 2007. Plio–Pleistocene climate evolution: trends and transitions in glacial cycle dynamics. Quaternary Sci Rev 26, 56-69.

Liu, J.T., Hung, J.J., Lin, H.L., Huh, C.A., Lee, C.L., Hsu, R.T., Huang, Y.W., Chu, J.C., 2009. From suspended particles to strata: The fate of terrestrial substances in the Gaoping (Kaoping) submarine canyon. Journal of Marine Systems 76, 417-432.

Liu, J.T., Kao, S.-J., Huh, C.-A., Hung, C.-C., 2013. Gravity flows associated with flood events and carbon burial: Taiwan as instructional source area. Annual review of marine science 5, 47-68.

Liu, J.T., Wang, Y.H., Yang, R.J., Hsu, R.T., Kao, S.J., Lin, H.L., Kuo, F.H., 2012. Cyclone-induced hyperpycnal turbidity currents in a submarine canyon. Journal of Geophysical Research: Oceans 117.

Llopart, J., Urgeles, R., Camerlenghi, A., Lucchi, R.G., Mol, B., Rebesco, M., Pedrosa, M.T., 2014. Slope Instability of Glaciated Continental Margins: Constraints from Permeability-Compressibility Tests and Hydrogeological Modeling Off Storfjorden, NW Barents Sea, in: Krastel, S., Behrmann, J.-H., Völker, D., Stipp, M., Berndt, C., Urgeles, R., Chaytor, J., Huhn, K., Strasser, M., Harbitz, C.B. (Eds.), Adv Nat Tech Haz Res. Springer International Publishing, pp. 95-104.

Llopart, J., Urgeles, R., Camerlenghi, A., Lucchi, R.G., Rebesco, M., De Mol, B., 2015. Late Quaternary development of the Storfjorden and Kveithola Trough Mouth Fans, northwestern Barents Sea. Quaternary Sci Rev 129, 68-84.

Locat, A., Leroueil, S., Bernander, S., Demers, D., Locat, J., Ouehb, L., 2008. Study of a lateral spread failure in an eastern Canada clay deposit in relation with progressive failure: the Saint-Barnabé-Nord slide, Proceedings of the 4th Canadian conference on geohazards: from causes to management, pp. 20-24.

Lorenzoni, L., Benitez-Nelson, C.R., Thunell, R.C., Hollander, D., Varela, R., Astor, Y., Audemard, F.A., Muller-Karger, F.E., 2012. Potential role of event-driven sediment transport on sediment accumulation in the Cariaco Basin, Venezuela. Mar Geol 307, 105-110.

Løvholt, F., Harbitz, C.B., Haugen, K.B., 2005. A parametric study of tsunamis generated by submarine slides in the Ormen Lange/Storegga area off western Norway. Mar Petrol Geol 22, 219-231.

Løvholt, F., Pedersen, G., Gisler, G., 2008. Oceanic propagation of a potential tsunami from the La Palma Island. Journal of Geophysical Research: Oceans 113.

Løvholt, F., Pedersen, G., Harbitz, C.B., 2016. Tsunami-Genesis Due to Retrogressive Landslides on an Inclined Seabed, in: Lamarche, G., Mountjoy, J., Bull, S., Hubble, T., Krastel, S., Lane, E., Micallef, A., Moscardelli, L., Mueller, C., Pecher, I., Woelz, S. (Eds.), Adv Nat Tech Haz Res. Springer, pp. 569-578.

Lowe, A.L., Anderson, J.B., 2002. Reconstruction of the West Antarctic ice sheet in Pine Island Bay during the Last Glacial Maximum and its subsequent retreat history. Quaternary Sci Rev 21, 1879-1897.

Lu, J.Y., Hong, J.H., Su, C.C., Wang, C.Y., Lai, J.S., 2008. Field measurements and simulation of bridge scour depth variations during floods. Journal of Hydraulic Engineering 134, 810-821.

Lucchi, R.G., Camerlenghi, A., Rebesco, M., Colmenero-Hidalgo, E., Sierro, F.J., Sagnotti, L., Urgeles, R., Melis, R., Morigi, C., Bárcena, M.-A., 2013. Postglacial sedimentary processes on the Storfjorden and Kveithola trough mouth fans: Significance of extreme glacimarine sedimentation. Global and planetary change 111, 309-326.

Lucchi, R.G., Pedrosa, M.T., Camerlenghi, A., Urgeles, R., De Mol, B., Rebesco, M., 2012. Recent submarine landslides on the continental slope of Storfjorden and Kveithola Trough-Mouth Fans (north west Barents Sea), Adv Nat Tech Haz Res. Springer, pp. 735-745.

Lykousis, V., Roussakis, G., Alexandri, M., Pavlakis, P., Papoulia, I., 2002. Sliding and regional slope stability in active margins: North Aegean Trough (Mediterranean). Mar Geol 186, 281-298.

MacAyeal, D.R., 1985. Evolution of tidally triggered meltwater plumes below ice shelves. Oceanology of the Antarctic continental shelf, 133-143.

Mackiewicz, N.E., Powell, R.D., Carlson, P.R., Molnia, B.F., 1984. Interlaminated ice-proximal glacimarine sediments in Muir Inlet, Alaska. Mar Geol 57, 113-147.

Maizels, J., 1991. The origin and evolution of Holocene sandur deposits in areas of jökulhlaup drainage, Iceland, Environmental Change in Iceland: Past and Present. Springer, pp. 267-302.

Maizels, J., 1993. Lithofacies variations within sandur deposits: the role of runoff regime, flow dynamics and sediment supply characteristics. Sediment Geol 85, 299-325.

Makdisi, F.I., Seed, H.B., 1977. Simplified procedure for estimating dam and embankment earthquake-induced deformations, ASAE Publication No. 4-77. Proceedings of the National Symposium on Soil Erosion and Sediment by Water, Chicago, Illinois, December 12-13, 1977.

Mandelbrot, B.B., Van Ness, J.W., 1968. Fractional Brownian motions, fractional noises and applications. SIAM review 10, 422-437.

Mangerud, J., 1991. The last interglacial/glacial cycle in northern Europe. Quaternary landscapes 38, 75.

Mangerud, J., 2004. Ice sheet limits in Norway and on the Norwegian continental shelf. Developments in Quaternary Sciences 2, 271-294.

Mangerud, J., Astakhov, V.I., Murray, A., Svendsen, J.I., 2001. The chronology of a large ice-dammed lake and the Barents–Kara Ice Sheet advances, Northern Russia. Global and Planetary Change 31, 321-336.

Mangerud, J., Dokken, T., Hebbeln, D., Heggen, B., Ingolfsson, O., Landvik, J.Y., Mejdahl, V., Svendsen, J.I., Vorren, T.O., 1998. Fluctuations of the Svalbard–Barents Sea Ice Sheet during the last 150 000 years. Quaternary Sci Rev 17, 11-42.

Mangerud, J., Jansen, E., Landvik, J.Y., 1996. Late Cenozoic history of the Scandinavian and Barents Sea ice sheets. Global and Planetary Change 12, 11-26.

Mangerud, J., Løvlie, R., Gulliksen, S., Hufthammer, A.-K., Larsen, E., Valen, V., 2003. Paleomagnetic correlations between scandinavian ice-sheet fluctuations and greenland dansgaard–oeschger events, 45,000–25,000 yr BP. Quaternary Res 59, 213-222.

Mangerud, J., Svendsen, J.I., 1992. The last interglacial-glacial period on Spitsbergen, Svalbard. Quaternary Sci Rev 11, 633-664.

Manyika, J., Chui, M., Bughin, J., Dobbs, R., Bisson, P., Marrs, A., 2013. Disruptive technologies: Advances that will transform life, business, and the global economy. McKinsey Global Institute New York.

Marshall, N.F., 1978. Large storm-induced sediment slump reopens an unknown Scripps submarine canyon tributary. Sedimentation in Submarine Canyons, Fans, and Trenches: Stroudsburg, Pennsylvania, Hutchinson & Ross, 73-84.

Martí, J., Hurlimann, M., Ablay, G.J., Gudmundsson, A., 1997. Vertical and lateral collapses on Tenerife (Canary Islands) and other volcanic ocean islands. Geology 25, 879-882.

Martin, D.M., 1999. Depositional setting and implications of Paleoproterozoic glaciomarine sedimentation in the Hamersley Province, Western Australia. Geological Society of America Bulletin 111, 189-203.

Maslin, M., Mikkelsen, N., Vilela, C., Haq, B., 1998. Sea-level- and gas-hydrate-controlled catastrophic sediment failures of the Amazon Fan. Geology 26, 1107-1110.

Maslin, M., Owen, M., Day, S., Long, D., 2004. Linking continental-slope failures and climate change: Testing the clathrate gun hypothesis. Geology 32, 53-56.

Maslin, M., Vilela, C., Mikkelsen, N., Grootes, P., 2005. Causes of catastrophic sediment failures of the Amazon Fan. Quaternary Sci Rev 24, 2180-2193.

Masson, D.G., Arzola, R.G., Wynn, R.B., Hunt, J.E., Weaver, P.P.E., 2011. Seismic triggering of landslides and turbidity currents offshore Portugal. Geochem Geophy Geosy 12.

Masson, D.G., Harbitz, C.B., Wynn, R.B., Pedersen, G., Lovholt, F., 2006. Submarine landslides: processes, triggers and hazard prediction. Philos T R Soc A 364, 2009-2039.

Masson, D.G., Watts, A.B., Gee, M.J.R., Urgeles, R., Mitchell, N.C., Le Bas, T.P., Canals, M., 2002. Slope failures on the flanks of the western Canary Islands. Earth-Sci Rev 57, 1-35.

Mathisen, M.E., Vondra, C.F., 1983. The fluvial and pyroclastic deposits of the Cagayan Basin, northern Luzon, Philippines—An example of non-marine volcaniclastic sedimentation in an interarc basin. Sedimentology 30, 369-392.

Matsumoto, T., Tappin, D.R., Party, S.O.S., 2003. Possible coseismic large-scale landslide off the northern coast of Papua New Guinea in July 1998: Geophysical and geological results from SOS cruises. Pure Appl Geophys 160, 1923-1943.

McAdoo, B.G., Pratson, L.F., Orange, D.L., 2000. Submarine landslide geomorphology, US continental slope. Mar Geol 169, 103-136.

McAdoo, B.G., Watts, P., 2004. Tsunami hazard from submarine landslides on the Oregon continental slope. Mar Geol 203, 235-245.

McHugh, C.M., Seeber, L., Braudy, N., Cormier, M.-H., Davis, M.B., Diebold, J.B., Dieudonne, N., Douilly, R., Gulick, S.P.S., Hornbach, M.J., 2011. Offshore sedimentary effects of the 12 January 2010 Haiti earthquake. Geology 39, 723-726.

Mei, W., Xie, S.P., 2016. Intensification of landfalling typhoons over the northwest Pacific since the late 1970s. Nat Geosci 9, 753-757.

Melles, M., Kuhn, G., 1993. Sub-bottom profiling and sedimentological studies in the southern Weddell Sea, Antarctica: evidence for large-scale erosional/depositional processes. Deep Sea Research Part I: Oceanographic Research Papers 40, 739-760.

Meunier, P., Hovius, N., Haines, A.J., 2007. Regional patterns of earthquake-triggered landslides and their relation to ground motion. Geophys Res Lett 34.

Mienert, J., Posewang, J., Baumann, M., 1998. Gas hydrates along the northeastern Atlantic margin: possible hydrate-bound margin instabilities and possible release of methane. Geological Society, London, Special Publications 137, 275-291.

Mienert, J., Vanneste, M., Bunz, S., Andreassen, K., Haflidason, H., Sejrup, H.P., 2005. Ocean warming and gas hydrate stability on the mid-Norwegian margin at the Storegga Slide. Mar Petrol Geol 22, 233-244.

Milliman, J.D., Farnsworth, K.L., 2011. River discharge to the coastal ocean: a global synthesis. Cambridge University Press.

Milliman, J.D., Meade, R.H., 1983. World-wide delivery of river sediment to the oceans. The Journal of Geology, 1-21.

Milliman, J.D., Syvitski, J.P.M., 1992. Geomorphic Tectonic Control of Sediment Discharge to the Ocean - the Importance of Small Mountainous Rivers. J Geol 100, 525-544.

Milne, J., 1897a. Sub-Oceanic Changes. The Geographical Journal 10, 129-146.

Milne, J., 1897b. Sub-Oceanic Changes (Continued). The Geographical Journal 10, 259-285.

Moernaut, J., Van Daele, M., Heirman, K., Fontijn, K., Strasser, M., Pino, M., Urrutia, R., De Batist, M., 2014. Lacustrine turbidites as a tool for quantitative earthquake reconstruction: New evidence for a variable rupture mode in south central Chile. Journal of Geophysical Research: Solid Earth 119, 1607-1633.

Moernaut, J., Van Daele, M., Strasser, M., Clare, M.A., Heirman, K., Viel, M., Cardenas, J., Kilian, R., de Guevara, B.L., Pino, M., 2015. Lacustrine turbidites produced by surficial slope sediment remobilization: a mechanism for continuous and sensitive turbidite paleoseismic records. Mar Geol.

Montalto, A., Vinciguerra, S., Menza, S., Patane, G., 1996. Recent seismicity of Mount Etna: implications for flank instability. Geological Society, London, Special Publications 110, 169-177.

Montelli, A., Gulick, S.P.S., Worthington, L.L., Mix, A., Davies-Walczak, M., Zellers, S.D., Jaeger, J.M., 2017. Late Quaternary glacial dynamics and sedimentation variability in the Bering Trough, Gulf of Alaska. Geology, G38836. 38831.

Mori, N., Yasuda, T., Mase, H., Tom, T., Oku, Y., 2010. Projection of extreme wave climate change under global warming. Hydrological Research Letters 4, 15-19.

Mosher, D.C., Moran, K., Hiscott, R.N., 1994. Late Quaternary Sediment, Sediment Mass-Flow Processes and Slope Stability on the Scotian Slope, Canada. Sedimentology 41, 1039-1061.

Mosher, D.C., Piper, D.J.W., Campbell, D.C., Jenner, K.A., 2004. Near-surface geology and sediment-failure geohazards of the central Scotian Slope. AAPG bulletin 88, 703-723.

Mosher, D.C., Piper, D.J.W., Vilks, G.V., Aksu, A.E., Fader, G.B., 1989. Evidence for Wisconsinan glaciations in the Verrill Canyon area, Scotian Slope. Quaternary Res 31, 27-40.

Mudelsee, M., Schulz, M., 1997. The Mid-Pleistocene climate transition: onset of 100 ka cycle lags ice volume build-up by 280 ka. Earth and Planetary Science Letters 151, 117-123.

Mudelsee, M., Stattegger, K., 1997. Exploring the structure of the mid-Pleistocene revolution with advanced methods of time-series analysis. Geologische Rundschau 86, 499-511.

Mugford, R.I., Dowdeswell, J.A., 2010. Modeling iceberg-rafted sedimentation in high-latitude fjord environments. Journal of Geophysical Research: Earth Surface 115.

Mulder, T., Moran, K., 1995. Relationship among Submarine Instabilities, Sea-Level Variations, and the Presence of an Ice-Sheet on the Continental-Shelf - an Example from the Verrill Canyon Area, Scotian Shelf. Paleoceanography 10, 137-154.

Mulder, T., Syvitski, J.P.M., 1995. Turbidity currents generated at river mouths during exceptional discharges to the world oceans. The Journal of Geology, 285-299.

Mulder, T., Syvitski, J.P.M., Migeon, S., Faugeres, J.-C., Savoye, B., 2003. Marine hyperpycnal flows: initiation, behavior and related deposits. A review. Mar Petrol Geol 20, 861-882.

Müller, J., Massé, G., Stein, R., Belt, S.T., 2009. Variability of sea-ice conditions in the Fram Strait over the past 30,000 years. Nat Geosci 2, 772-776.

Müller, J., Stein, R., 2014. High-resolution record of late glacial and deglacial sea ice changes in Fram Strait corroborates ice–ocean interactions during abrupt climate shifts. Earth and Planetary Science Letters 403, 446-455.

Murray-Wallace, C.V., 2002. Pleistocene coastal stratigraphy, sea-level highstands and neotectonism of the southern Australian passive continental margin—a review. Journal of Quaternary Science 17, 469-489.

Myhre, A.M., Thiede, J., Firth, J.V., 1995. 1. North Atlantic-Arctic Gateways, in: Myhre, A.M., Thiede, J., Firth, J.V., et al. (Eds.), Proceedings Ocean Drilling Program Initial Reports, vol. 151.

Nakajima, T., Kanai, Y., 2000. Sedimentary features of seismoturbidites triggered by the 1983 and older historical earthquakes in the eastern margin of the Japan Sea. Sediment Geol 135, 1-19.

Nam, S.-I., Stein, R., Grobe, H., Hubberten, H., 1995. Late Quaternary glacial-interglacial changes in sediment composition at the East Greenland continental margin and their paleoceanographic implications. Mar Geol 122, 243-262.

Nam, S.I., Stein, R.A., 1999. Late Quaternary variations in sediment accumulation rates and their paleoenvironmental implications: a case study from the East Greenland continental margin, Retrospective Collection. Trans Tech Publ, p. 223.

Nanayama, F., Furukawa, R., Shigeno, K., Makino, A., Soeda, Y., Igarashi, Y., 2007. Nine unusually large tsunami deposits from the past 4000 years at Kiritappu marsh along the southern Kuril Trench. Sediment Geol 200, 275-294.

Nash, I.F.J., Burnett, C., Smith, R., 2014. Middle East India Deepwater Pipeline (MEIDP) crossing of the Indus Fan, Offshore Technology Conference. Offshore Technology Conference.

Nelson, A.E., Smellie, J.L., Hambrey, M.J., Williams, M., Vautravers, M., Salzmann, U., McArthur, J.M., Regelous, M., 2009. Neogene glacigenic debris flows on James Ross Island, northern Antarctic Peninsula, and their implications for regional climate history. Quaternary Sci Rev 28, 3138-3160.

Nelson, A.R., Atwater, B.F., Bobrowsky, P.T., Bradley, L.-A., Clague, J.J., Carver, G.A., Darienzo, M.E., Grant, W.C., Krueger, H.W., Sparks, R.S.J., 1995. Radiocarbon evidence for extensive plate-boundary rupture about 300 years ago at the Cascadia subduction zone. Nature 378, 371 - 374.

Niemi, T.M., Ben-Avraham, Z., 1994. Evidence for Jericho earthquakes from slumped sediments of the Jordan River delta in the Dead Sea. Geology 22, 395-398.

Nitsche, F.O., Gohl, K., Vanneste, K., Miller, H., 1997. Seismic expression of glacially deposited sequences in the Bellingshausen and Amundsen Seas, West Antarctica, in: Barker, P.F., Cooper, A.K. (Eds.), Geology and Seismic Stratigraphy of the Antarctic Margin, pp. 95-108.

Noda, A., TuZino, T., Kanai, Y., Furukawa, R., Uchida, J., 2008. Paleoseismicity along the southern Kuril Trench deduced from submarine-fan turbidites. Mar Geol 254, 73-90.

Noormets, R., Dowdeswell, J.A., Larter, R.D., Ó Cofaigh, C., Evans, J., 2009. Morphology of the upper continental slope in the Bellingshausen and Amundsen Seas–Implications for sedimentary processes at the shelf edge of West Antarctica. Mar Geol 258, 100-114.

Nothold, H., 1998. Die Auswirkungen der" NorthEastWater"-Polynya auf die Sedimentation vor NO-Grönland und Untersuchungen zur Paläo-Ozeanographie seit dem Mittelweichsel= The

implication of the" NorthEastWater"-Polynya on the sedimentation by NE-Greenland and Late Quaternary Paleo-oceanic investigations. Berichte zur Polarforschung (Reports on Polar Research) 275.

Nygård, A., Haflidason, H., Sejrup, H.P., 2003. Morphology of a non-glacigenic debris flow lobe in the Helland Hansen area investigated with 3D seismic data, European Margin Sediment Dynamics. Springer, pp. 63-65.

Nygård, A., Sejrup, H.P., Haflidason, H., Bryn, P., 2005. The glacial North Sea Fan, southern Norwegian Margin: architecture and evolution from the upper continental slope to the deep-sea basin. Mar Petrol Geol 22, 71-84.

Nygård, A., Sejrup, H.P., Haflidason, H., Lekens, W.A.H., Clark, C.D., Bigg, G.R., 2007. Extreme sediment and ice discharge from marine-based ice streams: New evidence from the North Sea. Geology 35, 395-398.

O'Brien, P.E., Cooper, A.K., Florindo, F., Handwerger, D.A., Lavelle, M., Passchier, S., Pospichal, J.J., Quilty, P.G., Richter, C., Theissen, K.M., 2004. Prydz Channel Fan and the history of extreme ice advances in Prydz Bay, Proceedings of the Ocean Drilling Program, Scientific Results, pp. 1-32.

O'Brien, P.E., Goodwin, I., Forsberg, C.-F., Cooper, A.K., Whitehead, J., 2007. Late Neogene ice drainage changes in Prydz Bay, East Antarctica and the interaction of Antarctic ice sheet evolution and climate. Palaeogeography, Palaeoclimatology, Palaeoecology 245, 390-410.

O'brien, P.E., Harris, P.T., 1996. Patterns of glacial erosion and deposition in Prydz Bay and the past behaviour of the Lambert Glacier, Papers and Proceedings of the Royal Society of Tasmania, pp. 79-85.

O'Leary, D.W., 1991. Structure and morphology of submarine slab slides: clues to origin and behavior. Marine Georesources & Geotechnology 10, 53-69.

Ó Cofaigh, C., Andrews, J.T., Jennings, A.E., Dowdeswell, J.A., Hogan, K.A., Kilfeather, A.A., Sheldon, C., 2013. Glacimarine lithofacies, provenance and depositional processes on a West Greenland trough-mouth fan. Journal of Quaternary Science 28, 13-26.

Ó Cofaigh, C., Dowdeswell, J.A., Evans, J., Kenyon, N.H., Taylor, J., Mienert, J., Wilken, M., 2004. Timing and significance of glacially influenced mass-wasting in the submarine channels of the Greenland Basin. Mar Geol 207, 39-54.

Ó Cofaigh, C., Dowdeswell, J.A., Evans, J., Larter, R.D., 2008. Geological constraints on Antarctic palaeo-ice-stream retreat. Earth Surf Proc Land 33, 513-525.

Ó Cofaigh, C., Dowdeswell, J.A., Kenyon, N.H., 2006. Geophysical investigations of a high-latitude submarine channel system and associated channel-mouth lobe in the Lofoten Basin, polar North Atlantic. Mar Geol 226, 41-50.

Ó Cofaigh, C., Larter, R.D., Dowdeswell, J.A., Hillenbrand, C.D., Pudsey, C.J., Evans, J., Morris, P., 2005. Flow of the West Antarctic Ice Sheet on the continental margin of the Bellingshausen Sea at the Last Glacial Maximum. Journal of Geophysical Research: Solid Earth 110.

Ó Cofaigh, C., Taylor, J., Dowdeswell, J.A., Pudsey, C.J., 2003. Palaeo-ice streams, trough mouth fans and high-latitude continental slope sedimentation. Boreas 32, 37-55.

Olsen, J., van der Borg, K., Bergstrøm, B., Sveian, H., Lauritzen, S.-E., Hansen, G., 2001a. AMS radiocarbon dating of glacigenic sediments with low organic carbon content - an important tool for reconstructing the glacial variations in Norway. Norwegian Journal of Geology 2, 59-92.

Olsen, L., Sveian, H., Bergstrøm, B., 2001b. Rapid adjustments of the western part of the Scandinavian Iee Sheet during the Mid and late Weichselian. Norwegian Journal of Geology 2, 93-117.

Ottesen, D., Dowdeswell, J.A., 2006. Assemblages of submarine landforms produced by tidewater glaciers in Svalbard. Journal of Geophysical Research: Earth Surface (2003–2012) 111.

Ottesen, D., Dowdeswell, J.A., Bugge, T., 2014. Morphology, sedimentary infill and depositional environments of the Early Quaternary North Sea Basin (56°–62°N). Mar Petrol Geol 56, 123-146.

Ottesen, D., Dowdeswell, J.A., Landvik, J.Y., Mienert, J., 2007. Dynamics of the Late Weichselian ice sheet on Svalbard inferred from high-resolution sea-floor morphology. Boreas 36, 286-306.

Ottesen, D., Dowdeswell, J.A., Rise, L., 2005. Submarine landforms and the reconstruction of fast-flowing ice streams within a large Quaternary ice sheet: The 2500-km-long Norwegian-Svalbard margin (57–80 N). Geological Society of America Bulletin 117, 1033-1050.

Ottesen, D., Dowdeswell, J.A., Rise, L., Bugge, T., 2012. Large-scale development of the mid-Norwegian shelf over the last three million years and potential for hydrocarbon reservoirs in glacial sediments. Geological Society, London, Special Publications 368, 53-73.

Ottesen, D., Rise, L., Rokoengen, K., 2001. Glacial processes and large-scale morphology on the mid-Norwegian continental shelf. Norwegian Petroleum Society Special Publications 10, 441-449.

Owen, L.A., Kamp, U., Khattak, G.A., Harp, E.L., Keefer, D.K., Bauer, M.A., 2008. Landslides triggered by the 8 October 2005 Kashmir earthquake. Geomorphology 94, 1-9.

Owen, M., Day, S., Maslin, M., 2007. Late Pleistocene submarine mass movements: occurrence and causes. Quaternary Sci Rev 26, 958-978.

Özener, P.T., Özaydın, K., Berilgen, M.M., 2009. Investigation of liquefaction and pore water pressure development in layered sands. Bulletin of Earthquake Engineering 7, 199-219.

Palanques, A., Puig, P., Guillén, J., de Madron, X.D., Latasa, M., Scharek, R., Martín, J., Salat, J., 2011. Effects of storm events on the shelf-to-basin sediment transport in the southwestern end of the Gulf of Lions (Northwestern Mediterranean). Natural Hazards & Earth System Sciences 11.

Palanques, A., Puig, P., Latasa, M., Scharek, R., 2009. Deep sediment transport induced by storms and dense shelf-water cascading in the northwestern Mediterranean basin. Deep Sea Research Part I: Oceanographic Research Papers 56, 425-434.

Parker, E.J., Traverso, C.M., Giudice, T.D., Evans, T., Moore, R., 2009. Geohazard Risk Assessment - Vulnerability of Subsea Structures to Geohazards - Risk Implications, Proceedings of the Offshore Technology Conference, 20090, Houston, Texas.

Parker, E.J., Traverso, C.M., Moore, R., Evans, T., Usher, N., 2008. Evaluation of landslide impact on deepwater submarine pipelines, Offshore Technology Conference. Offshore Technology Conference.

Parsons, J.D., Bush, J.W.M., Syvitski, J.P.M., 2001. Hyperpycnal plume formation from riverine outflows with small sediment concentrations. Sedimentology 48, 465-478.

Passchier, S., O'Brien, P.E., Damuth, J.E., Januszczak, N., Handwerger, D.A., Whitehead, J.M., 2003. Pliocene–Pleistocene glaciomarine sedimentation in eastern Prydz Bay and development of the Prydz trough-mouth fan, ODP Sites 1166 and 1167, East Antarctica. Mar Geol 199, 279-305.

Patterson, M., 1974. Oceanographic data from hurricane Camille, Offshore Technology Conference. Offshore Technology Conference, pp. 781 - 790.

Patton, H., Andreassen, K., Bjarnadóttir, L.R., Dowdeswell, J.A., Winsborrow, M.C.M., Noormets, R., Polyak, L., Auriac, A., Hubbard, A., 2015. Geophysical constraints on the dynamics and retreat of the Barents Sea Ice Sheet as a palaeo-benchmark for models of marine ice-sheet deglaciation. Rev Geophys 53, 1051-1098.

Patton, H., Hubbard, A., Andreassen, K., Winsborrow, M., Stroeven, A.P., 2016. The build-up, configuration, and dynamical sensitivity of the Eurasian ice-sheet complex to Late Weichselian climatic and oceanic forcing. Quaternary Sci Rev 153, 97-121.

Patton, J.R., Goldfinger, C., Morey, A.E., Romsos, C., Black, B., Djadjadihardja, Y., 2013. Seismoturbidite record as preserved at core sites at the Cascadia and Sumatra–Andaman subduction zones. Nat. Hazards Earth Syst. Sci 13, 833 - 867.

Paull, C.K., Buelow, W.J., Ussler, W., Borowski, W.S., 1996. Increased continental-margin slumping frequency during sea-level lowstands above gas hydrate-bearing sediments. Geology 24, 143-146.

Paull, C.K., Ussler III, W., Greene, H.G., Keaten, R., Mitts, P., Barry, J., 2002. Caught in the act: the 20 December 2001 gravity flow event in Monterey Canyon. Geo-Mar Lett 22, 227-232.

Paull, C.K., Ussler, W., Holbrook, W.S., 2007. Assessing methane release from the colossal Storegga submarine landslide. Geophys Res Lett 34.

Pausata, F.S.R., Li, C., Wettstein, J., Kageyama, M., Nisancioglu, K.H., 2011. The key role of topography in altering North Atlantic atmospheric circulation during the last glacial period. Climate of the Past 7, 1089-1101.

Pecher, I.A., Henrys, S.A., Ellis, S., Chiswell, S.M., Kukowski, N., 2005. Erosion of the seafloor at the top of the gas hydrate stability zone on the Hikurangi Margin, New Zealand. Geophys Res Lett 32.

Pedrosa, M.T., Camerlenghi, A., De Mol, B., Urgeles, R., Rebesco, M., Lucchi, R.G., 2011. Seabed morphology and shallow sedimentary structure of the Storfjorden and Kveithola trough-mouth fans (north west Barents Sea). Mar Geol 286, 65-81.

Peduzzi, P., Chatenoux, B., Dao, H., De Bono, A., Herold, C., Kossin, J., Mouton, F., Nordbeck, O., 2012. Global trends in tropical cyclone risk. Nature Clim. Change 2, 289-294.

Piper, D.J.W., 1988. Glaciomarine sedimentation on the continental slope off eastern Canada. Geoscience Canada 15.

Piper, D.J.W., 2005. Late Cenozoic evolution of the continental margin of eastern Canada. Norsk geologisk tidsskrift 85, 305.

Piper, D.J.W., Aksu, A.E., 1987. The source and origin of the 1929 grand banks turbidity current inferred from sediment budgets. Geo-Mar Lett 7, 177-182.

Piper, D.J.W., Campbell, D.C., 2005. Quaternary geology of Flemish Pass and its application to geohazard evaluation for hydrocarbon development. GAC Special Paper 43, 29-43.

Piper, D.J.W., Campbell, D.C., Mosher, D.C., 2016. Mid-latitude complex trough-mouth fans, Laurentian and Northeast fans, eastern Canada. Geological Society, London, Memoirs 46, 363-364.

Piper, D.J.W., Cochonat, P., Morrison, M.L., 1999. The sequence of events around the epicentre of the 1929 Grand Banks earthquake: initiation of debris flows and turbidity current inferred from sidescan sonar. Sedimentology 46, 79-97.

Piper, D.J.W., Deptuck, M.E., Mosher, D.C., Hughes Clarke, J.E., Migeon, S., 2012. Erosional and depositional features of glacial meltwater discharges on the eastern Canadian continental margin.

Applications of the Principles of Seismic Geomorphology to Continental Slope and Base-of-slope Systems: Case Studies from Seafloor and Near-Seafloor Analogues. Edited by BE Prather, ME Deptuck, D. Mohrig, B. van Hoorn, and R. Wynn. Society for Sedimentary Geology (SEPM), Special Publications 99, 61-80.

Piper, D.J.W., Ingram, S., 2003. Major Quaternary sediment failures on the east Scotian Rise, eastern Canada. Natural Resources Canada, Geological Survey of Canada.

Piper, D.J.W., Mosher, D.C., Gauley, B.-J., Jenner, K., Campbell, D.C., 2003. The chronology and recurrence of submarine mass movements on the continental slope off southeastern Canada, Adv Nat Tech Haz Res. Springer, pp. 299-306.

Piper, D.J.W., Mudie, P.J., Aksu, A.E., Skene, K.I., 1994. A 1 Ma record of sediment flux south of the Grand Banks used to infer the development of glaciation in southeastern Canada. Quaternary Sci Rev 13, 23-37.

Piper, D.J.W., Normark, W.R., 2009. Processes that initiate turbidity currents and their influence on turbidites: a marine geology perspective. Journal of Sedimentary Research 79, 347-362.

Piper, D.J.W., Savoye, B., 1993. Processes of late Quaternary turbidity current flow and deposition on the Var deep-sea fan, north-west Mediterranean Sea. Sedimentology 40, 557-582.

Piper, D.J.W., Shaw, J., Skene, K.I., 2007. Stratigraphic and sedimentological evidence for late Wisconsinan sub-glacial outburst floods to Laurentian Fan. Palaeogeography, Palaeoclimatology, Palaeoecology 246, 101-119.

Pope, E.L., Talling, P.J., Carter, L., 2017. Which earthquakes trigger damaging submarine mass movements: Insights from a global record of submarine cable breaks? Mar Geol 348, 131-146.

Pope, E.L., Talling, P.J., Hunt, J.E., Dowdeswell, J.A., Allin, J.R., Cartigny, M.J.B., Long, D., Mozzato, A., Stanford, J.D., Tappin, D.R., Watts, M., 2016. Long-term record of Barents Sea Ice Sheet advance to the shelf edge from a 140,000 year record. Quaternary Sci Rev 150, 55-66.

Pope, E.L., Talling, P.J., Urlaub, M., Hunt, J.E., Clare, M.A., Challenor, P., 2015. Are large submarine landslides temporally random or do uncertainties in available age constraints make it impossible to tell? Mar Geol 369, 19-33.

Pouderoux, H., Lamarche, G., Proust, J.-N., 2012. Building an 18 000-year-long paleo-earthquake record from detailed deep-sea turbidite characterisation in Poverty Bay, New Zealand. Nat. Hazards Earth Syst. Sci 12, 2077-2101.

Pouderoux, H., Proust, J.-N., Lamarche, G., 2014. Submarine paleoseismology of the northern Hikurangi subduction margin of New Zealand as deduced from Turbidite record since 16 ka. Quaternary Sci Rev 84, 116-131.

Powell, R.D., 1990. Glacimarine processes at grounding-line fans and their growth to ice-contact deltas. Geological Society, London, Special Publications 53, 53-73.

Powell, R.D., Domack, E., 1995. Modern glaciomarine environments. Glacial environments 1, 445-486.

Prior, D.B., Coleman, J.M., Bornhold, B.D., 1982. Results of a known seafloor instability event. Geo-Mar Lett 2, 117-122.

Prior, D.B., Suhayda, J.N., Lu, N.-Z., Bornhold, B.D., Keller, G.H., Wiseman, W.J., Wright, L.D., Yang, Z.-S., 1989. Storm wave reactivation of a submarine landslide. Nature 341, 47-50.

Pudsey, C.J., Camerlenghi, A., 1998. Glacial–interglacial deposition on a sediment drift on the Pacific margin of the Antarctic Peninsula. Antarctic Science 10, 286-308.

Puig, P., Ogston, A.S., Mullenbach, B.L., Nittrouer, C.A., Parsons, J.D., Sternberg, R.W., 2004. Storm-induced sediment gravity flows at the head of the Eel submarine canyon, northern California margin. Journal of Geophysical Research: Oceans 109.

Puig, P., Palanques, A., Orange, D.L., Lastras, G., Canals, M., 2008. Dense shelf water cascades and sedimentary furrow formation in the Cap de Creus Canyon, northwestern Mediterranean Sea. Continental Shelf Research 28, 2017-2030.

Quincey, D.J., Luckman, A., Benn, D.I., 2009. Quantification of Everest region glacier velocities between 1992 and 2002, using satellite radar interferometry and feature tracking. J Glaciol 55, 596-606.

Quinn, P.E., Diederichs, M.S., Rowe, R.K., Hutchinson, D.J., 2012. Development of progressive failure in sensitive clay slopes. Canadian Geotechnical Journal 49, 782-795.

Ramsey, C.B., 1998. Probability and dating. Radiocarbon 40, 461-474.

Ramsey, L.A., Hovius, N., Lague, D., Liu, C.S., 2006. Topographic characteristics of the submarine Taiwan orogen. Journal of Geophysical Research: Earth Surface (2003–2012) 111.

Rasmussen, E., Fjeldskaar, W., 1996. Quantification of the Pliocene-Pleistocene erosion of the Barents Sea from present-day bathymetry. Global and Planetary Change 12, 119-133.

Rasmussen, T.L., Thomsen, E., Kuijpers, A., Wastegård, S., 2003. Late warming and early cooling of the sea surface in the Nordic seas during MIS 5e (Eemian Interglacial). Quaternary Sci Rev 22, 809-821.

Rasmussen, T.L., Thomsen, E., Ślubowska, M.A., Jessen, S., Solheim, A., Koç, N., 2007. Paleoceanographic evolution of the SW Svalbard margin (76 N) since 20,000 14 C yr BP. Quaternary Res 67, 100-114.

Rasmussen, T.L., Van Weering, T.C.E., Labeyrie, L., 1997. Climatic instability, ice sheets and ocean dynamics at high northern latitudes during the last glacial period (58-10 KA BP). Quaternary Sci Rev 16, 71-80.

Ratzov, G., Cattaneo, A., Babonneau, N., Déverchère, J., Yelles, K., Bracene, R., Courboulex, F., 2015. Holocene turbidites record earthquake supercycles at a slow-rate plate boundary. Geology 43, 331-334.

Rauscher, K.F., 2010. The Reliability of Global Undersea Communications Cable Infrastructure (ROGUCCI) Report. IEEE.

Raymo, M.E., Nisancioglu, K.H., 2003. The 41 kyr world: Milankovitch's other unsolved mystery. Paleoceanography 18.

Raymo, M.E., Ruddiman, W.F., 1992. Tectonic forcing of late Cenozoic climate. Nature 359, 117-122.

Rebesco, M., Liu, Y., Camerlenghi, A., Winsborrow, M., Laberg, J.S., Caburlotto, A., Diviacco, P., Accettella, D., Sauli, C., Wardell, N., 2011. Deglaciation of the western margin of the Barents Sea Ice Sheet—a swath bathymetric and sub-bottom seismic study from the Kveithola Trough. Mar Geol 279, 141-147.

Rebesco, M., Pedrosa, M.T., Camerlenghi, A., Lucchi, R.G., Sauli, C., De Mol, B., Madrussani, G., Urgeles, R., Rossi, G., Böhm, G., 2012. One million years of climatic generated landslide events on the northwestern Barents Sea continental margin, Adv Nat Tech Haz Res. Springer, pp. 747-756.

Reeder, M.S., Rothwell, R.G., Stow, D.A.V., 2000. Influence of sea level and basin physiography on emplacement of the late Pleistocene Herodotus Basin Megaturbidite, SE Mediterranean Sea. Mar Petrol Geol 17, 199-218.

Reeder, M.S., Stow, D.A.V., Rothwell, R.G., 2002. Late Quaternary turbidite input into the east Mediterranean basin: new radiocarbon constraints on climate and sea-level control. Geological Society, London, Special Publications 191, 267-278.

Reimer, P.J., Bard, E., Bayliss, A., Beck, J.W., Blackwell, P.G., Ramsey, C.B., Buck, C.E., Cheng, H., Edwards, R.L., Friedrich, M., 2013. IntCal13 and Marine13 radiocarbon age calibration curves 0–50,000 years cal BP. Radiocarbon 55, 1869-1887.

Richter, T.O., Lassen, S., van Weering, T.C.E., De Haas, H., 2001. Magnetic susceptibility patterns and provenance of ice-rafted material at Feni Drift, Rockall Trough: implications for the history of the British–Irish ice sheet. Mar Geol 173, 37-54.

Rise, L., Bøe, R., Riis, F., Bellec, V.K., Laberg, J.S., Eidvin, T., Elvenes, S., Thorsnes, T., 2013. The Lofoten-Vesterålen continental margin, North Norway: Canyons and mass-movement activity. Mar Petrol Geol 45, 134-149.

Rise, L., Chand, S., Haflidason, H., L'Heureux, J.S., Hjelstuen, B.O., Bellec, V., Longva, O., Brendryen, J., Vanneste, M., Bøe, R., 2012. Investigations of Slides at the Upper Continental Slope Off Vesterålen, North Norway, in: Yamada, Y., Kawamura, K., Ikehara, K., Ogawa, Y., Urgeles, R., Mosher, D., Chaytor, J., Strasser, M. (Eds.), Adv Nat Tech Haz Res. Springer Netherlands, pp. 167-176.

Rise, L., Ottesen, D., Berg, K., Lundin, E., 2005. Large-scale development of the mid-Norwegian margin during the last 3 million years. Mar Petrol Geol 22, 33-44.

Rokoengen, K., Rise, L., Bryn, P., Frengstad, B., Gustavsen, B., Nygaard, E., Sættem, J., 1995. Upper Cenozoic stratigraphy on the mid-Norwegian continental shelf. Norsk Geologisk Tidsskrift 75, 88-104.

Romans, B.W., Castelltort, S., Covault, J.A., Fildani, A., Walsh, J.P., 2016. Environmental signal propagation in sedimentary systems across timescales. Earth-Sci Rev 153, 7-29.

Rothwell, R.G., Hoogakker, B., Thomson, J., Croudace, I.W., Frenz, M., 2006. Turbidite emplacement on the southern Balearic Abyssal Plain (western Mediterranean Sea) during Marine Isotope Stages 1–3: an application of ITRAX XRF scanning of sediment cores to lithostratigraphic analysis. Geological Society, London, Special Publications 267, 79-98.

Rothwell, R.G., Thomson, J., Kähler, G., 1998. Low-sea-level emplacement of a very large Late Pleistocene 'megaturbidite'in the western Mediterranean Sea. Nature 392, 377-380.

Ruffman, A., 2001. Potential for large-scale submarine slope failure and tsunami generation along the US mid-Atlantic coast: Comment. Geology 29, 967-967.

Sackett, D.L., Rosenberg, W., Gray, J.A., Haynes, R.B., Richardson, W.S., 1996. Evidence based medicine: what it is and what it isn't. Bmj 312, 71-72.

Sættem, J., Bugge, T., Fanavoll, S., Goll, R.M., Mørk, A., Mørk, M.B.E., Smelror, M., Verdenius, J.G., 1994. Cenozoic margin development and erosion of the Barents Sea: Core evidence from southwest of Bjørnøya. Mar Geol 118, 257-281.

Sættem, J., Poole, D.A.R., Ellingsen, L., Sejrup, H.P., 1992. Glacial geology of outer Bjørnøyrenna, southwestern Barents Sea. Mar Geol 103, 15-51.

SAGE, 2010. Deepwater Pipeline Energy Corridor from teh Gulf region to India, Petrotech, November 3 2010, New Dehli.

Scheuer, C., Gohl, K., Larter, R.D., Rebesco, M., Udintsev, G., 2006. Variability in Cenozoic sedimentation along the continental rise of the Bellingshausen Sea, West Antarctica. Mar Geol 227, 279-298.

Schoof, C.G., 2007. Ice sheet grounding line dynamics: Steady states, stability, and hysteresis. Journal of Geophysical Research: Earth Surface (2003–2012) 112.

Scordilis, E.M., 2006. Empirical global relations converting M S and m b to moment magnitude. Journal of Seismology 10, 225-236.

Scott, R.F., Zuckerman, K.A., 1972. Sandblows and liquefaction in the great Alaska earthquake of 1964. Engineering Publication 1606, 170-189.

Seed, H.B., Idriss, I.M., 1971. Simplified procedure for evaluating soil liquefaction potential. Journal of Soil Mechanics & Foundations Div 97, 1249 - 1273.

Seed, H.B., Rahman, M.S., 1978. Wave-induced pore pressure in relation to ocean floor stability of cohesionless soils. Marine Georesources & Geotechnology 3, 123-150.

Sejrup, H.P., Aarseth, I., Haflidason, H., Løvlie, R., Bratten, Å., Tjøstheim, G., Forsberg, C.F., Ellingsen, K.L., 1995. Quaternary of the Norwegian Channel: glaciation history and palaeoceanography. Norwegian Journal of Geology 75, 65-87.

Sejrup, H.P., Haflidason, H., Aarseth, I., King, E.L., Forsberg, C.F., Long, D., Rokoengen, K., 1994. Late Weichselian glaciation history of the northern North Sea. Boreas-International Journal of Quaternary Research 23, 1-13.

Sejrup, H.P., Haflidason, H., Hjelstuen, B.I., Nygard, A., Bryn, P., Lien, R., 2004. Pleistocene development of the SE Nordic seas margin. Mar Geol 213, 169-200.

Sejrup, H.P., Hjelstuen, B.O., Dahlgren, K.I.T., Haflidason, H., Kuijpers, A., Nygård, A., Praeg, D., Stoker, M.S., Vorren, T.O., 2005. Pleistocene glacial history of the NW European continental margin. Mar Petrol Geol 22, 1111-1129.

Sejrup, H.P., King, E.L., Aarseth, I., Haflidason, H., Elverhøi, A., 1996. Quaternary erosion and depositional processes: western Norwegian fjords, Norwegian Channel and North Sea Fan. Geological Society, London, Special Publications 117, 187-202.

Sejrup, H.P., Larsen, E., Haflidason, H., Berstad, I.M., Hjelstuen, B.O., Jonsdottir, H.E., King, E.L., Landvik, J., Longva, O., Nygård, A., Ottesen, D., Raunholm, S., Rise, L., Stalsberg, K., 2003. Configuration, history and impact of the Norwegian Channel Ice Stream. Boreas 32, 18-36.

Sejrup, H.P., Larsen, E., Landvik, J., King, E.L., Haflidason, H., Nesje, A., 2000. Quaternary glaciations in southern Fennoscandia: evidence from southwestern Norway and the northern North Sea region. Quaternary Sci Rev 19, 667-685.

Sejrup, H.P., Nagy, J., Brigham-Grette, J., 1989. Foraminiferal stratigraphy and amino acid geochronology of Quaternary sediments in the Norwegian Channel, northern North Sea. Norsk geologisk tidsskrift 69, 111-124.

Shanmugam, G., 2008. Deep-water bottom currents and their deposits. Developments in sedimentology 60, 59-81.

Shirai, M., Omura, A., Wakabayashi, T., Uchida, J., Ogami, T., 2010. Depositional age and triggering event of turbidites in the western Kumano Trough, central Japan during the last ca. 100years. Mar Geol 271, 225-235.

Si, H., Midorikawa, S., 1999. New attenuation relationships for peak ground acceleration and velocity considering effects of fault type and site condition. Journal of structural and construction engineering, 63-70.

Siegert, M.J., Dowdeswell, J.A., Hald, M., Svendsen, J.-I., 2001. Modelling the Eurasian Ice Sheet through a full (Weichselian) glacial cycle. Global and Planetary Change 31, 367-385.

Siegert, M.J., Marsiat, I., 2001. Numerical reconstructions of LGM climate across the Eurasian Arctic. Quaternary Sci Rev 20, 1595-1605.

Smith, D.E., Harrison, S., Jordan, J.T., 2013. Sea level rise and submarine mass failures on open continental margins. Quaternary Sci Rev 82, 93-103.

Smith, D.P., Kvitek, R., Iampietro, P.J., Wong, K., 2007. Twenty-nine months of geomorphic change in upper Monterey Canyon (2002–2005). Mar Geol 236, 79-94.

Solheim, A., Andersen, E.S., Elverhøi, A., Fiedler, A., 1996. Late Cenozoic depositional history of the western Svalbard continental shelf, controlled by subsidence and climate. Global and Planetary Change 12, 135-148.

Solheim, A., Berg, K., Forsberg, C.F., Bryn, P., 2005a. The Storegga Slide complex: repetitive large scale sliding with similar cause and development. Mar Petrol Geol 22, 97-107.

Solheim, A., Bryn, P., Sejrup, H.P., Mienert, J., Berg, K., 2005b. Ormen Lange—an integrated study for the safe development of a deep-water gas field within the Storegga Slide Complex, NE Atlantic continental margin; executive summary. Mar Petrol Geol 22, 1-9.

Solheim, A., Faleide, J.I., Andersen, E.S., Elverhøi, A., Forsberg, C.F., Vanneste, K., Uenzelmann-Neben, G., Channell, J.E.T., 1998. Late Cenozoic seismic stratigraphy and glacial geological development of the East Greenland and Svalbard–Barents Sea continental margins. Quaternary Sci Rev 17, 155-184.

Solignac, S., Seidenkrantz, M.-S., Jessen, C., Kuijpers, A., Gunvald, A.K., Olsen, J., 2011. Late-Holocene sea-surface conditions offshore Newfoundland based on dinoflagellate cysts. The Holocene 21, 539-552.

Sonoyama, T., Wang, F., Honda, M., Kuwada, Y., 2013. Experimental Study on the Influence of Cable Diameters on the Impact Forces Caused by Submarine Landslide, Progress of Geo-Disaster Mitigation Technology in Asia. Springer, pp. 491-501.

Sornette, D., 2009. Dragon-kings, black swans and the prediction of crises. arXiv preprint arXiv:0907.4290.

Spiegler, D., Jansen, E., 1989. Planktonic foraminifer biostratigraphy of Norwegian Sea sediments: ODP Leg 104, Proceedings of the Ocean Drilling Program, Scientific Results. TX (Ocean Drilling Program) College Station, pp. 681-696.

Spielhagen, R.F., Baumann, K.-H., Erlenkeuser, H., Nowaczyk, N.R., Nørgaard-Pedersen, N., Vogt, C., Weiel, D., 2004. Arctic Ocean deep-sea record of northern Eurasian ice sheet history. Quaternary Sci Rev 23, 1455-1483.

St. John, K.E., Krissek, L.A., 2002. The late Miocene to Pleistocene ice-rafting history of southeast Greenland. Boreas 31, 28-35.

Stein, R., Grobe, H., Hubberten, H., Marienfeld, P., Nam, S., 1993. Latest Pleistocene to Holocene changes in glaciomarine sedimentation in Scoresby Sund and along the adjacent East Greenland Continental Margin: Preliminary results. Geo-Mar Lett 13, 9-16.

Stein, R., Nam, S.-I., Grobe, H., Hubberten, H., 1996. Late Quaternary glacial history and short-term ice-rafted debris fluctuations along the East Greenland continental margin. Geological Society, London, Special Publications 111, 135-151.

Stewart, M.A., Lonergan, L., Hampson, G., 2013. 3D seismic analysis of buried tunnel valleys in the central North Sea: morphology, cross-cutting generations and glacial history. Quaternary Sci Rev 72, 1-17.

Stigall, J., Dugan, B., 2010. Overpressure and earthquake initiated slope failure in the Ursa region, northern Gulf of Mexico. J Geophys Res-Sol Ea 115.

Stocker, T.F., 2014. Climate change 2013: the physical science basis: Working Group I contribution to the Fifth assessment report of the Intergovernmental Panel on Climate Change. Cambridge University Press.

Stone, G.W., Liu, B., Pepper, D.A., Wang, P., 2004. The importance of extratropical and tropical cyclones on the short-term evolution of barrier islands along the northern Gulf of Mexico, USA. Mar Geol 210, 63-78.

Straneo, F., Hamilton, G.S., Sutherland, D.A., Stearns, L.A., Davidson, F., Hammill, M.O., Stenson, G.B., Rosing-Asvid, A., 2010. Rapid circulation of warm subtropical waters in a major glacial fjord in East Greenland. Nat Geosci 3, 182-186.

Strasser, M., Anselmetti, F.S., Fäh, D., Giardini, D., Schnellmann, M., 2006. Magnitudes and source areas of large prehistoric northern Alpine earthquakes revealed by slope failures in lakes. Geology 34, 1005-1008.

Strasser, M., Kölling, M., dos Santos Ferreira, C., Fink, H.G., Fujiwara, T., Henkel, S., Ikehara, K., Kanamatsu, T., Kawamura, K., Kodaira, S., 2013. A slump in the trench: Tracking the impact of the 2011 Tohoku-Oki earthquake. Geology 41, 935-938.

STRATAGEM, P., 2002. The Neogene stratigraphy of the glaciated European margin from Lofoten to Porcupine. A product of the EC-supported STRATAGEM project, p. 75.

Strozyk, F., Strasser, M., Förster, A., Kopf, A., Huhn, K., 2010. Slope failure repetition in active margin environments: constraints from submarine landslides in the Hellenic fore arc, eastern Mediterranean. Journal of Geophysical Research: Solid Earth (1978–2012) 115.

Su, C.-C., Tseng, J.-Y., Hsu, H.-H., Chiang, C.-S., Yu, H.-S., Lin, S., Liu, J.T., 2012. Records of submarine natural hazards off SW Taiwan. Geological Society, London, Special Publications 361, 41-60.

Sugi, M., Murakami, H., Yoshimura, J., 2009. A reduction in global tropical cyclone frequency due to global warming. Sola 5, 164-167.

Sullivan, M.C., Cowen, R.K., Able, K.W., Fahay, M.P., 2003. Effects of anthropogenic and natural disturbance on a recently settled continental shelf flatfish. Marine Ecology Progress Series 260, 237-253.

Sultan, N., Cochonat, P., Canals, M., Cattaneo, A., Dennielou, B., Haflidason, H., Laberg, J.S., Long, D., Mienert, J., Trincardi, F., Urgeles, R., Vorren, T.O., Wilson, C., 2004. Triggering mechanisms of slope instability processes and sediment failures on continental margins: a geotechnical approach. Mar Geol 213, 291-321.

Sumner, E.J., Siti, M.I., McNeill, L.C., Talling, P.J., Henstock, T.J., Wynn, R.B., Djajadihardja, Y.S., Permana, H., 2013. Can turbidites be used to reconstruct a paleoearthquake record for the central Sumatran margin? Geology 41, 763-766.

Svendsen, J.I., Alexanderson, H., Astakhov, V.I., Demidov, I., Dowdeswell, J.A., Funder, S., Gataullin, V., Henriksen, M., Hjort, C., Houmark-Nielsen, M., 2004a. Late Quaternary ice sheet history of northern Eurasia. Quaternary Sci Rev 23, 1229-1271.

Svendsen, J.I., Astakhov, V.I., Bolshiyanov, D.Y., Demidov, I., Dowdeswell, J.A., Gataullin, V., Hjort, C., Hubberten, H.W., Larsen, E., Mangerud, J., 1999. Maximum extent of the Eurasian ice sheets in the Barents and Kara Sea region during the Weichselian. Boreas 28, 234-242.

Svendsen, J.I., Briner, J.P., Mangerud, J., Young, N.E., 2015. Early break-up of the norwegian channel ice stream during the last glacial maximum. Quaternary Sci Rev 107, 231-242.

Svendsen, J.I., Gataullin, V., Mangerud, J., Polyak, L., 2004b. The glacial history of the Barents and Kara Sea region. Developments in Quaternary Sciences 2, 369-378.

Swan, A.R.H., Sandilands, M., 1995. Introduction to geological data analysis. Blackwell Science, Oxford ; Cambridge, Mass., USA.

Symons, W.O., Sumner, E.J., Paull, C.K., Cartigny, M.J.B., Xu, J.P., Maier, K.L., Lorenson, T.D., Talling, P.J., 2017. A new model for turbidity current behavior based on integration of flow monitoring and precision coring in a submarine canyon. Geology 45, 367-370.

Synolakis, C.E., Bardet, J.P., Borrero, J.C., Davies, H.L., Okal, E.A., Silver, E.A., Sweet, S., Tappin, D.R., 2002. The slump origin of the 1998 Papua New Guinea Tsunami. P Roy Soc a-Math Phy 458, 763-789.

Talling, P.J., 2014. On the triggers, resulting flow types and frequencies of subaqueous sediment density flows in different settings. Mar Geol 352, 155-182.

Talling, P.J., Allin, J., Armitage, D.A., Arnott, R.W.C., Cartigny, M.J.B., Clare, M.A., Felletti, F., Covault, J.A., Girardclos, S., Hansen, E., Hill, P., Hiscott, R.N., Hogg, A., Hughes-Clarke, J., Jobe, Z., Malgesini, G., Mozzato, A., Naruse, H., Parkinson, S., Peel, F., Piper, D.J.W., Pope, E., Postma, G., Rowley, P., Sguazzini, A., Stevenson, C.J., Sumner, E.J., Sylvester, Z., Watts, C., Xu, J.P., 2015. Key Future Directions For Research On Turbidity Currents and Their Deposits. Journal of Sedimentary Research 85, 153-169.

Talling, P.J., Clare, M.A., Urlaub, M., Pope, E., Hunt, J.E., Watt, S.F.L., 2014. Large Submarine Landslides on Continental Slopes. Oceanography 27, 32.

Talling, P.J., Masson, D.G., Sumner, E.J., Malgesini, G., 2012. Subaqueous sediment density flows: Depositional processes and deposit types. Sedimentology 59, 1937-2003.

Talling, P.J., Paull, C.K., Piper, D.J.W., 2013. How are subaqueous sediment density flows triggered, what is their internal structure and how does it evolve? Direct observations from monitoring of active flows. Earth-Sci Rev 125, 244-287.

Talling, P.J., Wynn, R.B., Masson, D.G., Frenz, M., Cronin, B.T., Schiebel, R., Akhmetzhanov, A.M., Dallmeier-Tiessen, S., Benetti, S., Weaver, P.P.E., Georgiopoulou, A., Zuhlsdorff, C., Amy, L.A., 2007. Onset of submarine debris flow deposition far from original giant landslide. Nature 450, 541-544.

Talwani, M., Udintsev, G.B., White, S.M., 1976. Introduction and explanatory notes, leg 38, deep sea drilling project. Initial Reports DSDP 38.

Tappin, D.R., 2010. Submarine mass failures as tsunami sources: their climate control. Philos T R Soc A 368, 2417-2434.

Tappin, D.R., Grilli, S.T., Harris, J.C., Geller, R.J., Masterlark, T., Kirby, J.T., Shi, F., Ma, G., Thingbaijam, K.K.S., Mai, P.M., 2014. Did a submarine landslide contribute to the 2011 Tohoku tsunami? Mar Geol 357, 344-361.

Tappin, D.R., Watts, P., Grilli, S.T., 2008. The Papua New Guinea tsunami of 17 July 1998: anatomy of a catastrophic event. Nat Hazard Earth Sys 8, 243-266.

Tappin, D.R., Watts, P., McMurtry, G.M., Lafoy, Y., Matsumoto, T., 2001. The Sissano, Papua New Guinea tsunami of July 1998 - offshore evidence on the source mechanism. Mar Geol 175, 1-23.

Taylor, J., Dowdeswell, J.A., Kenyon, N.H., Ó Cofaigh, C., 2002a. Late Quaternary architecture of trough-mouth fans: debris flows and suspended sediments on the Norwegian margin. Geological Society, London, Special Publications 203, 55-71.

Taylor, J., Dowdeswell, J.A., Siegert, M.J., 2002b. Late Weichselian depositional processes, fluxes, and sediment volumes on the margins of the Norwegian Sea (62–75 N). Mar Geol 188, 61-77.

ten Brink, U.S., Chaytor, J.D., Geist, E.L., Brothers, D.S., Andrews, B.D., 2014. Assessment of tsunami hazard to the US Atlantic margin. Mar Geol 353, 31-54.

Thiede, J., Eldholm, O., Taylor, E., 1989. Variability of Cenozoic Norwegian-Greenland Sea paleoceanography and northern hemisphere paleoclimate, Proceedings of the Ocean Drilling Program, Scientific Results, pp. 1067-1118.

Thiede, J., Winkler, A., Wolf-Welling, T.C.W., Eldholm, O., Myhre, A.M., Baumann, K.-H., Henrich, R., Stein, R., 1998. Late Cenozoic history of the polar North Atlantic: results from ocean drilling. Quaternary Sci Rev 17, 185-208.

Thomas, S., Hooper, J., Clare, M.A., 2010. Constraining geohazards to the past: Impact assessment of submarine mass movements on seabed developments, Adv Nat Tech Haz Res. Springer, pp. 387-398.

Tinti, S., Armigliato, A., Manucci, A., Pagnoni, G., Zaniboni, F., Yalçiner, A.C., Altinok, Y., 2006. The generating mechanisms of the August 17, 1999 Izmit Bay (Turkey) tsunami: Regional (tectonic) and local (mass instabilities) causes. Mar Geol 225, 311-330.

Tripsanas, E.K., Piper, D.J.W., 2008. Glaciogenic debris-flow deposits of Orphan Basin, offshore eastern Canada: sedimentological and rheological properties, origin, and relationship to meltwater discharge. Journal of Sedimentary Research 78, 724-744.

Tulaczyk, S., Kamb, W.B., Engelhardt, H.F., 2000. Basal mechanics of Ice Stream B, west Antarctica: 2. Undrained plastic bed model. Journal of Geophysical Research: Solid Earth 105, 483-494.

Tveranger, J., Houmark-Nielsen, M., Løvberg, K., Mangerud, J., 1994. Eemian-Weichselian stratigraphy of the Flakkerhuk ridge, southern Jameson Land, East Greenland. Boreas 23, 359-384.

Tziperman, E., Gildor, H., 2003. On the mid-Pleistocene transition to 100-kyr glacial cycles and the asymmetry between glaciation and deglaciation times. Paleoceanography 18.

Urciuoli, G., Picarelli, L., Leroueil, S., 2007. Local soil failure before general slope failure. Geotechnical and Geological Engineering 25, 103-122.

Urlaub, M., Talling, P.J., Clare, M.A., 2014. Sea-level-induced seismicity and submarine landslide occurrence: Comment. Geology 42, e337.

Urlaub, M., Talling, P.J., Masson, D.G., 2013. Timing and frequency of large submarine landslides: implications for understanding triggers and future geohazard. Quaternary Sci Rev 72, 63-82.

Urlaub, M., Zervos, A., Talling, P.J., Masson, D.G., Clayton, C.I., 2012. How Do ~2° Slopes Fail in Areas of Slow Sedimentation? A Sensitivity Study on the Influence of Accumulation Rate and Permeability on Submarine Slope Stability, in: Yamada, Y., Kawamura, K., Ikehara, K., Ogawa, Y., Urgeles, R., Mosher, D., Chaytor, J., Strasser, M. (Eds.), Adv Nat Tech Haz Res. Springer Netherlands, pp. 277-287.

van Rooij, M.J.W., Nash, B.A., Rajaraman, S., Holden, J.G., 2013. A fractal approach to dynamic inference and distribution analysis. Frontiers in physiology 4.

Vanneste, K., Uenzelmann-Neben, G., Miller, H., 1995. Seismic evidence for long-term history of glaciation on central East Greenland shelf south of Scoresby Sund. Geo-Mar Lett 15, 63-70.

Vanneste, M., Mienert, J., Bünz, S., 2006. The Hinlopen Slide: A giant, submarine slope failure on the northern Svalbard margin, Arctic Ocean. Earth and Planetary Science Letters 245, 373-388.

Vanoudheusden, E., Sultan, N., Cochonat, P., 2004. Mechanical behaviour of unsaturated marine sediments: experimental and theoretical approaches. Mar Geol 213, 323-342.

Vogt, C., Knies, J., Spielhagen, R.F., Stein, R., 2001. Detailed mineralogical evidence for two nearly identical glacial/deglacial cycles and Atlantic water advection to the Arctic Ocean during the last 90,000 years. Global and Planetary Change 31, 23-44.

Völker, D., Scholz, F., Geersen, J., 2011. Analysis of submarine landsliding in the rupture area of the 27 February 2010 Maule earthquake, Central Chile. Mar Geol 288, 79-89.

Vorren, T.O., Laberg, J.S., 1997. Trough mouth fans—palaeoclimate and ice-sheet monitors. Quaternary Sci Rev 16, 865-881.

Vorren, T.O., Laberg, J.S., Blaume, F., Dowdeswell, J.A., Kenyon, N.H., Mienert, J., Rumohr, J., Werner, F., 1998. The Norwegian Greenland Sea continental margins: Morphology and late Quaternary sedimentary processes and environment. Quaternary Sci Rev 17, 273-302.

Vorren, T.O., Landvik, J.Y., Andreassen, K., Laberg, J.S., 2011. Glacial history of the Barents Sea region. Quaternary Glaciations—Extent and Chronology—A Closer Look, Dev. in Quat. Sci, 361-372.

Vorren, T.O., Lebesbye, E., Andreassen, K., Larsen, K.-B., 1989. Glacigenic sediments on a passive continental margin as exemplified by the Barents Sea. Mar Geol 85, 251-272.

Vorren, T.O., Lebesbye, E., Larsen, K.B., 1990. Geometry and genesis of the glacigenic sediments in the southern Barents Sea. Geological Society, London, Special Publications 53, 269-288.

Vorren, T.O., Plassen, L.I.V., 2002. Deglaciation and palaeoclimate of the Andfjord-Vågsfjord area, North Norway. Boreas 31, 97-125.

Vorren, T.O., Richardsen, G., Knutsen, S.-M., Henriksen, E., 1991. Cenozoic erosion and sedimentation in the western Barents Sea. Mar Petrol Geol 8, 317-340.

Waelbroeck, C., Labeyrie, L., Michel, E., Duplessy, J.C., McManus, J.F., Lambeck, K., Balbon, E., Labracherie, M., 2002. Sea-level and deep water temperature changes derived from benthic foraminifera isotopic records. Quaternary Sci Rev 21, 295-305.

Wald, D.J., Lin, K.-W., Quitoriano, V., 2008. Quantifying and qualifying USGS ShakeMap uncertainty, US Geological Survey Open-File Report 2008 - 1238. Geological Survey (US), Golden, CO, p. 27.

Wald, D.J., Quitoriano, V., Heaton, T.H., Kanamori, H., Scrivner, C.W., Worden, C.B., 1999. TriNet "ShakeMaps": Rapid generation of peak ground motion and intensity maps for earthquakes in southern California. Earthquake Spectra 15, 537-555.

Wald, D.J., Worden, B.C., Quitoriano, V., Pankow, K.L., 2005. ShakeMap manual: technical manual, user's guide, and software guide, US Geological Survey, Reston, VA, p. 132.

Watt, S.F.L., Talling, P.J., Hunt, J.E., 2014. New insights into the emplacement dynamics of volcanic island landslides. Oceanography 27, 46-57.

Watts, M., Talling, P., Hunt, J., Xuan, C., van Peer, T., 2016. A new date for a large pre-Holocene Storegga Slide, EGU General Assembly Conference Abstracts, p. 17055.

Waythomas, C.F., Watts, P., 2003. Numerical simulation of tsunami generation by pryoclastic flow at Aniakchak Volcano, Alaska. Geophys Res Lett 30.

Waythomas, C.F., Watts, P., Walder, J.S., 2006. Numerical simulation of tsunami generation by cold volcanic mass flows at Augustine Volcano, Alaska. Natural Hazards & Earth System Sciences 6.

Weaver, P.P.E., Kuijpers, A., 1983. Climatic control of turbidite deposition on the Madeira Abyssal Plain.

Weaver, P.P.E., Rothwell, R.G., Ebbing, J., Gunn, D., Hunter, P.M., 1992. Correlation, frequency of emplacement and source directions of megaturbidites on the Madeira Abyssal Plain. Mar Geol 109, 1-20.

Weber, M.E., Bonani, G., Fütterer, K.D., 1994. Sedimentation processes within channel-ridge systems, southeastern Weddell Sea, Antarctica. Paleoceanography 9, 1027-1048.

Wellner, J.S., Lowe, A.L., Shipp, S.S., Anderson, J.B., 2001. Distribution of glacial geomorphic features on the Antarctic continental shelf and correlation with substrate: implications for ice behavior. J Glaciol 47, 397-411.

Wells, D.L., Coppersmith, K.J., 1994. New empirical relationships among magnitude, rupture length, rupture width, rupture area, and surface displacement. B Seismol Soc Am 84, 974-1002.

Wetzel, A., 1984. Bioturbation in deep-sea fine-grained sediments: influence of sediment texture, turbidite frequency and rates of environmental change. Geological Society, London, Special Publications 15, 595-608.

Whillans, I.M., Bentley, C.R., Van der Veen, C.J., 2001. Ice streams B and C. The West Antarctic Ice Sheet: Behavior and Environment, 257-281.

Wilken, M., Mienert, J., 2006. Submarine glacigenic debris flows, deep-sea channels and past ice-stream behaviour of the East Greenland continental margin. Quaternary Sci Rev 25, 784-810.

Williams, J.R., 1969. Flood routing with variable travel time or variable storage coefficients. Transactions of the ASAE 12, 100-0103.

Wilt, G.G., 2015. A Study of Delta Collapse Caused Turbidity Current Cable Failures. , International Cable Protection Committee Plenary, Enhanced Submarine Cable Security and Co-operation in Balance with the Environment, Hong Kong, China.

Winkelmann, D., Jokat, W., Jensen, L., Schenke, H.-W., 2010. Submarine end moraines on the continental shelf off NE Greenland–Implications for Lateglacial dynamics. Quaternary Sci Rev 29, 1069-1077.

Winkler, A., Wolf-Welling, T., Stattegger, K., Thiede, J., 2002. Clay mineral sedimentation in high northern latitude deep-sea basins since the Middle Miocene (ODP Leg 151, NAAG). International Journal of Earth Sciences 91, 133-148.

Winsborrow, M.C.M., Andreassen, K., Corner, G.D., Laberg, J.S., 2010. Deglaciation of a marine-based ice sheet: Late Weichselian palaeo-ice dynamics and retreat in the southern Barents Sea reconstructed from onshore and offshore glacial geomorphology. Quaternary Sci Rev 29, 424-442.

Winsborrow, M.C.M., Stokes, C.R., Andreassen, K., 2012. Ice-stream flow switching during deglaciation of the southwestern Barents Sea. Geological Society of America Bulletin 124, 275-290.

Wolf-Welling, T.C.W., Cremer, M., O'Connell, S., Winkler, A., Thiede, J., 1996. Cenozoic Arctic gateway paleoclimate variability: Indications from changes in coarse-fraction composition, Proceedings of the Ocean Drilling Program. Scientific Results. Ocean Drilling Program, pp. 515-567.

Woo, M.K., McCann, B.S., 1994. Climatic variability, climatic change, runoff, and suspended sediment regimes in northern Canada. Physical Geography 15, 201-226.

Woods, R., Sivapalan, M., 1999. A synthesis of space-time variability in storm response: Rainfall, runoff generation, and routing. Water Resour Res 35, 2469-2485.

Wright, S.G., Rathje, E.M., 2003. Triggering mechanisms of slope instability and their relationship to earthquakes and tsunamis. Pure Appl Geophys 160, 1865-1877.

Xu, J.P., Sequeiros, O.E., Noble, M.A., 2014. Sediment concentrations, flow conditions, and downstream evolution of two turbidity currents, Monterey Canyon, USA. Deep Sea Research Part I: Oceanographic Research Papers 89, 11 - 34.

Zachos, J., Pagani, M., Sloan, L., Thomas, E., Billups, K., 2001. Trends, rhythms, and aberrations in global climate 65 Ma to present. Science 292, 686-693.

Zhang, M., Huang, Y., Bao, Y., 2015. The mechanism of shallow submarine landslides triggered by storm surge. Nat Hazards, 1-11.

Ziegler, P.A., 1990. Geological atlas of western and central Europe. Geological Society of London.